THE UNIVERSITY
of EDINBURGH

Molecular Modelling Approaches to Phase Equilibria in Facilitated Transport Membranes

by

Odin Kvam

presented for the degree of

Doctor of Philosophy

The University of Edinburgh

2020

Declaration

I declare that this thesis has been composed solely by myself and that it has not been submitted, in whole or in part, in any previous application for a degree. Except where stated otherwise by reference or acknowledgement, the work presented is entirely my own.

Odin Kvam

August 31, 2020

Abstract

Facilitated transport membranes (FTM) are a promising new class of materials for CO_2-selective gas separation, with potential for application to post-combustion carbon capture and sequestration. FTM separation takes advantage of the chemical reactions of CO_2 to increase throughput and selectivity, with potential for reducing costs and improving purity in the resulting gas streams. However, the process performance of FTM separation relies on material properties, determined by a complex chain of dependencies including polymer composition, water absorption, reactivity, and temperature, with the underlying physical processes not being fully understood. The development of new FTM materials is in turn limited by a lack of quantitative models and poor understanding of the microscopic mechanisms of FTM separation. This motivates the development of new theory and molecular models for estimating process performance and thermodynamic behaviour in this important class of materials.

Unlike simple fluids, FTM systems exhibit multiple complex features which have limited the application of existing model frameworks. In this work, three key aspects of facilitated transport membranes are examined in order to build a predictive model of thermodynamics and phase equilibrium processes in FTM systems: (i) Thermodynamics of polymer melts and vapour-liquid equilibrium in polymer solutions are approached by both molecular simulation and theoretical models, in order to characterise the behaviour of polyvinylamine, a prototypical FTM polymer. Simulation of oligomers based on a TraPPE-UA molecular model are found to produce good quality ρpT data for common polymers, and a hybrid simulation / equation of state approach is proposed for predicting polymer properties. By substituting experimental measurement with molecular simulation, equation of state models are obtained with PC-SAFT even where the real polymer is thermally unstable or experimentally inaccessible. (ii) The aqueous-organic electrolyte solution originating from amine-CO_2 is considered based on theoretical and simulation approaches, with significant shortcomings found in current models. New molecular parameters are proposed for aliphatic ammonium chlorides and bicarbonate, optimized against experimental phase equilibrium data, allowing CO_2 solubility in aqueous amine systems to be simulated at varying stages of absorption. (iii) The reactive aspects of CO_2 absorption in aqueous amine solutions is examined in light of literature approaches. A new hybrid methodology is proposed, using infinite dilution experimental data in combination with molecular simulation utilizing the newly optimised molecular models.

Together, advancements in the three aspects outlined above permit description of facilitated transport membranes by molecular simulation, and in turn parametrisation of equation of state models for reactive polyamine systems. The knowledge gained for polymer-solvent systems, electrolytes, and reactive gas absorption allow prediction of material properties and process performance of FTM polymers. Here, the quaternary system PVAm - H_2O - CO_2 - N_2 is examined as a prototypical post-combustion FTM system, in order to chart the dependence of process performance on operating conditions. These advances inform future application of associating equations of state to amine-based facilitated transport membranes in particular, as well as the wider field of reactive electrolyte systems.

Lay Summary

Separation of gases using membranes has a proven track record in existing industry applications, and has in recent years been suggested as a possible solution to capture and sequestration of anthropogenic CO_2 from combustion processes. In the European Union Horizon 2020 framework, capture and sequestration of CO_2 is recognised as an important step towards meeting environmental emission targets in Europe and worldwide. Membrane-based separation technology has the potential for reducing investment and operating costs for CO_2 capture and sequestration. However, the performance of membrane separation is limited by available membrane materials available and their suitability for different separation processes.

A promising class of membrane materials for CO_2 separation is facilitated transport membranes (FTM). FTM separation takes advantage of the chemical reactions of CO_2 to increase throughput and selectivity, in turn reducing costs and improving purity in the resulting gas streams. However, the process performance of FTM materials rely on a complex chain of dependencies including polymer composition, water absorption, reactivity, and temperature, with the underlying physical processes not being fully understood. The development of new FTM materials is in turn limited by the limited knowledge of underlying microscopic processes governing FTM separation.

Molecular models are often used as a vehicle to study microscopic processes, in order to better understand complex systems which are not readily studied by experimental means. Molecular models also enable the prediction of key physical properties. A wide range of approaches with different levels of detail exist, developed for the study of specific systems. However, the diverse physical phenomena of FTM materials have caused these systems to until now go without a suitable model for representing physical properties. This work investigates how best to represent facilitated transport membranes using molecular models, and develops a predictive approach for the separation performance of FTM materials under typical post-combustion conditions. To deconvolute the different processes in FTM separation, molecular models for a sequence of model systems are considered in turn.

Firstly, we consider the polymer species making up typical FTM materials. These compounds absorb water upon contact with humidity, swelling to as much as twice their initial weight, with the added water content being essential for improved process performance. Using molecular simulation, properties of both pure polymer systems and polymer-water solutions are investigated, including a prototypical FTM polymer.

The simulation data are in turn used to construct analytical thermodynamic models for polymer systems and polymer-water solutions. Through this approach, properties of new polymer compounds are readily predicted and can be explored under a wide range of process conditions.

Secondly, the absorption of CO_2 in FTM materials generates charged electrolyte species. The properties of electrolytes differ considerably from CO_2 in the gas phase, and influence overall system behaviour. While establishing molecular models for electrolytes in FTM systems, significant weaknesses in existing models for organic electrolyte compounds are identified. By considering thermodynamic properties of real electrolyte solutions, we develop new molecular models for the key species involved in CO_2 absorption. These models allow organic electrolyte solutions to be studied with higher confidence, including FTM compounds together with a wide range of solvent mixtures.

Third, the chemical reactions responsible for enhanced separation of CO_2 in FTM membranes are considered. Through the formation of an acid-base equilibrium, CO_2 is absorbed at far greater quantities than volatile gases such as N_2. Using the previously developed models for polymers and electrolyte compounds, a new approach to predicting reaction equilibrium in fluid systems is described and tested for CO_2 absorption in a mixed solvent. Further, analytical approaches to representing reactive systems are reviewed with parameters developed for use together with a prototypical FTM polymer.

Finally, the models developed based on each of the three categories above are combined to give a unified framework for predicting properties of FTM materials. By considering the dependence of the key properties gas solubility and transport on process conditions, a map is generated for the likely process performance of the prototypical FTM polymer as a function of temperature and humidity. The model is found to over-predict process performance, but correctly identifies the relative performance between different gases and is close in magnitude to experimental values. This provides a first view of FTM process performance predicted from molecular models.

The knowledge gained from this work in part pertains to each of the three model systems discussed above, and in part to the FTM systems as a whole: a unified and predictive molecular model for these systems is possible, given a thorough treatment of each constituent element. Having a pathway to predict process performance in this novel class of materials unlocks new strategies for material development, as well as aiding application of FTM separation within the area of carbon capture and sequestration.

Contents

List of Symbols and Constants

Symbol	SI Unit	Meaning
P_i	$\mathrm{mol\,m^{-1}\,s^{-1}\,Pa^{-1}}$	membrane permeability
α_j^i	-	membrane selectivity
J_i	$\mathrm{mol\,m^{-2}\,s^{-1}}$	membrane flux
σ	nm	particle size
ϵ	$\mathrm{kJ\,mol^{-1}}$	particle interaction energy
m	-	chain length
Γ	metre^3	phase space coordinate
U	$\mathrm{kJ\,mol^{-1}}$	potential energy
v	$\mathrm{m\,s^{-1}}$	velocity
t	s	time
F	$\mathrm{kg\,m\,s^{-2}}$	force
A	$\mathrm{kJ\,mol^{-1}}$	Helmholtz free energy
T	K	temperature
p	Pa	pressure
μ	$\mathrm{kJ\,mol^{-1}}$	chemical potential
a	-	thermodynamic activity
ϕ	$\mathrm{J\,C^{-1}}$	electrostatic potential
ϵ_r	-	relative permittivity

Constant	Unit	Value	Meaning
N_A	$\mathrm{mol^{-1}}$	6.02214×10^{23}	Avogadro constant
R	$\mathrm{kJ\,mol^{-1}\,K^{-1}}$	8.31446×10^{-3}	gas constant
ϵ_0	$\mathrm{C\,V^{-1}\,m^{-1}}$	8.85419×10^{-12}	vacuum permittivity

Chapter 1

Introduction

1.1 Gas Separation Membranes: Applications and Opportunities

Separation and purification of gas streams is an essential operation in process engineering, with particular importance for the energy sector [1, 2]. Multiple competing separation technologies are available depending on the specific application, including liquid absorption [3], cryogenic distillation [4], temperature- or pressure-swing adsorption [5, 6], and membrane separation [7, 8, 9]. Membrane-based gas separation selectively extracts either products or pollutants from a feed stream as a direct gas-to-gas process, resulting in purified gas ready for further processing. Gas separation membranes are found in a wide range of applications. In biogas refining, membranes are used to separate CH_4 or H_2 from predominantly CO_2 after the fermentation process [10]. For natural gas sweetening, membranes are used to remove CO_2 or H_2S from a stream containing a mixture of hydrocarbons [1]. Membranes are used to produce enriched air for medical applications without the need for high-pressure gas cylinders [11], by separating O_2 from atmospheric air on a continuous basis. Conversely, membrane separation can be used to generate a nitrogen-rich atmosphere [12], as illustrated in figure 1.1 for a commercial fuel tank inert gas generating system.

A key advantage of membrane-based separation is the single-phase gas-to-gas operation. Competing technologies, such as liquid-phase absorption or cryogenic distillation, rely on energy- and process-intensive phase changes to achieve separation. This gives membranes the potential of significant advantages over conventional separation processes – for desalination, membrane-based separation only consumes one-tenth the energy of the corresponding thermal evaporation-condensation processes [13]. Transitioning to membrane-based separation technology is also an avenue for process intensification [14], due to the simple operation, low energy cost, and small footprint of membrane processes [7, 8]. These features make membranes an attractive alternative for future generations of efficient and sustainable separation technology.

A more recent application for gas separation is the capture of CO_2 from post-combustion flue gas streams, as a step towards combating increasing anthropogenic emissions of climate gases. Membrane-based sepa-

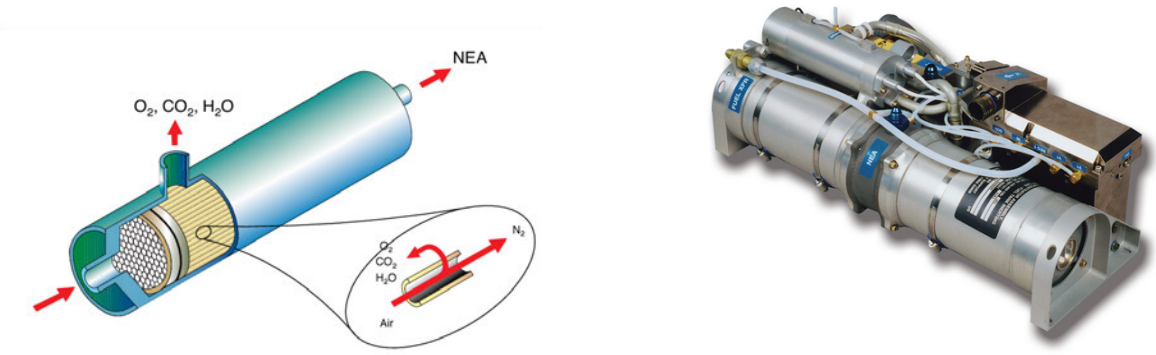

Figure 1.1: Membrane separation module for nitrogen enriched atmosphere (NEA) generation. Left: Diagrammatic representation of a hollow-fibre membrane module for NEA generation, reproduced from Reynolds et al. [12]. Right: Commercial on-board inert gas generating system by Cobham Mission Systems [19].

ration of CO_2 has already seen successful applications within natural gas and biogas treatment [1, 10], and were quickly proposed as a likely solution for post-combustion CO_2 capture [15, 16]. Membrane separation technology is relatively easy to retrofit for CO_2-intense processes such as power plants and cement production [17], making it a feasible option for conversion of existing energy infrastructure to carbon-neutral energy production. Capture of CO_2 from post-combustion flue gases was recognized by the European Commission through the Horizon 2020 work programme [18], calling for further research on carbon capture and storage technologies targeting commercial applications.

In order to be commercially viable, membrane-based CO_2 separation must both meet purity and recovery specifications, and be competitive on implementation and operating costs relative to state-of-the-art separation technology. Due the fundamental thermodynamic advantages of single-phase separation, the potential for significant energy savings is present. However, membranes are reliant on polymers with sufficiently good material properties to achieve efficient separation: both throughput per unit area and separation factor vary over several orders of magnitude depending on the membrane material used. To provide a competitive alternative for CO_2 capture, application-specific materials must be developed that are suited to post-combustion conditions and have adequate separation performance.

Material development in turn requires knowledge of the underlying processes and relationships governing separation performance [7]. While some of the relationships governing membrane separation performance have been uncovered [20], there is no consensus predictive model for estimating membrane separation performance and material properties from polymer composition. This is particularly true for facilitated transport membranes [21, 22], a class of materials leveraging the chemical reactions of CO_2 in order to achieve significantly enhanced separation performance.

Molecular modelling approaches makes it possible to study the underlying processes of membrane separation for existing or novel polymer compounds, and at arbitrary physical conditions. In this work, a new predictive modelling approach is developed for gas separation membranes. Firstly, we show that polymer material properties are readily characterised based on molecular simulation, allowing optimisation of analytical

models for polymer behaviour. Secondly, the solution thermodynamics of facilitated transport systems are considered, and new models for reaction products found in facilitated transport membranes are developed. Third, we describe the chemical reactions involved in CO_2 absorption in a new thermodynamic framework, allowing combination of experimental data and simulation results. Finally, the results from each of these aspects are integrated using an analytical model, allowing exploration of membrane properties for different compositions and under varying physical conditions.

The remainder of this chapter will review the fundamentals of membrane separation, introduce the fundamentals of CO_2 facilitated transport, and define the research aims and strategies of this work. Prevailing macroscopic models for facilitated transport are presented, revealing no clear alternative for predictive modelling of separation performance. The shortcomings of existing macroscopic models motivate the use of molecular models to investigate the underlying phenomena driving CO_2 separation in this class of membrane materials. By considering the essential features of facilitated transport, we identify likely modelling approaches and analogous chemical systems, stepping stones towards a more robust theory for this important class of materials.

1.2 Membrane Operating Principles and Facilitated Transport

Gas separation membranes are thin films of typically micrometre thickness, often combined with a porous supporting structure to improve mechanical robustness [7]. For commercial applications membranes are collated in modules to drastically increase effective surface area per unit volume, with hollow fibre [23] or spiral-wound [24] configurations being most commonly adopted. The performance of membrane gas separation processes depends on a number of factors [7], including the following.

- Module and process design, determining the operating conditions for the separation process.
- Module configuration and construction, defining flow regimes and internal pressure drop gradients.
- Membrane manufacture and thickness, determining the achievable permeance.
- Material properties, defining the permeability and selectivity ratio of the membrane.

These aspects together determine the throughput, separation factor, and energy consumption of the process. Of the above factors, material properties in particular represents a fundamental limit to the performance of membrane separation – membrane manufacture, module construction and process design can be improved incrementally, while advances in material properties are discontinuous and reliant on the discovery of new material families. The key material properties for membrane gas separation processes are permeability P_i, describing the throughput of a gas species i in response to an applied pressure differential, and selectivity α^i_j, describing the relative permeability between species i and j in the gas stream. A comparison of membrane material families for separation of CO_2 / N_2 gas mixtures is shown in figure 1.2. Separation of CO_2 from N_2

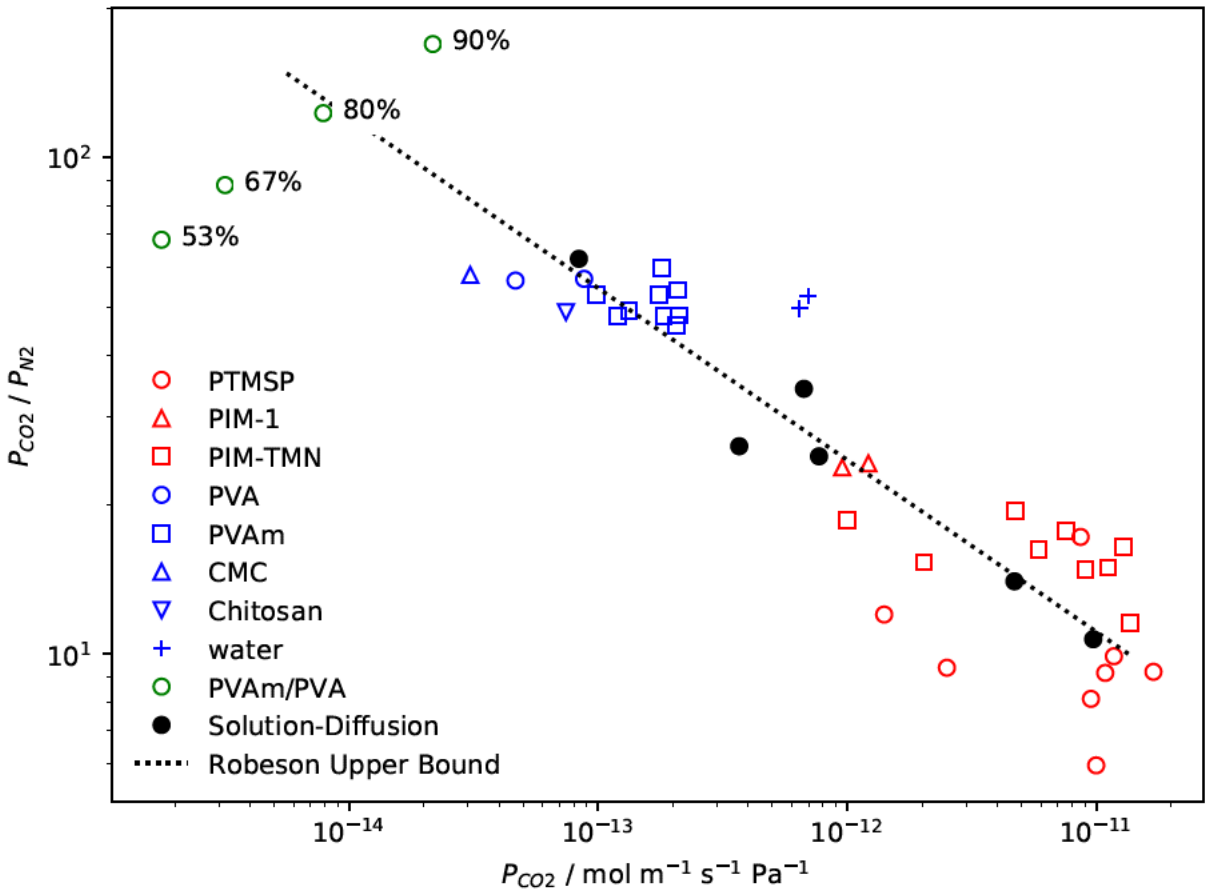

Figure 1.2: Permeability and selectivity for CO_2 / N_2 separation membranes. Black filled circles show conventional solution-diffusion membranes, while the dotted line indicates the empirical upper bound reported by Robeson [26] for this class of compounds. Red open symbols show high porosity materials, including polymer of intrinsic microporosity (PIM); PIM-TMN reported by Rose et al. [27] and PIM-1, poly(1-trimethylsilyl-1-propyne) (PTMSP) reported by Lau et al. [28]. Blue open symbols show hydrogel membranes reported by Liu et al [29], together with estimated separation performance for a hypothetical liquid water membrane. Green open circles show permeability of a PVAm/PVA hybrid membrane, calculated from the experimental data reported by Deng et al. [30], with the annotation indicating relative humidity of the feed gas.

is the primary point of comparison for carbon capture from flue gas, with a typically CO_2 content of 10% - 20% and a variable amount of H_2O contained in the flue gas stream [25].

To understand the dependence between material properties and membrane performance, it is informative to consider the operating principles of membrane gas separation. Unlike porous filtration media, gas separation membranes are dense structures [7]. Molecular transport through conventional gas separation membranes is explained by the solution-diffusion model [7, 21, 22], characterising the permeability P_i for a given gas by its solubility S_i in the membrane matrix times its transport diffusivity D_i,

$$P_i = S_i D_i \tag{1.1}$$

relating material properties to the separation performance observed in a membrane module. Since gas dissolves into the body of the membrane, transport in solution-diffusion membranes is conventional diffusion driven by

the chemical potential gradient across the thickness of the membrane, as opposed to Knudsen diffusion [31] or configurational diffusion [32] sometimes seen in microporous membranes or other filtration media.

The measured flux through a membrane module is in turn dependent on the membrane thickness l and partial pressure drop Δp_i across the membrane, given by the relationship

$$J_i = P_i \frac{\Delta p_i}{l} \tag{1.2}$$

connecting the material properties in equation 1.1 to the observable permeance of a membrane module given a certain construction and process conditions. Permeance describes the overall throughput of gas per unit area of the membrane, with high permeance membranes permitting a larger throughput of gas thus reducing the required membrane surface area for a given process.

Further to permeability, gas separation performance is determined by the selectivity of a membrane. Selectivity describes the capacity of a membrane to enriches one component over another from the feed stream. It is defined by the pairwise permeability ratio between species,

$$\alpha_j^i = \frac{P_i}{P_j} \tag{1.3}$$

and is the fundamental operating principle of membranes as a separation process. Commercial separation membranes are often targeted towards a specific pair of species, such as O_2 / N_2 for oxygen production from air, or CO_2 / CH_4 for natural gas sweetening.

The optimal gas separation membrane has both high permeability and high selectivity, resulting in both high throughput and purity of the desired product. In practice, membranes can rarely obtain good performance both for permeability and selectivity at the same time, creating a Pareto front of materials with different material properties. This trade-off in permeability and selectivity is known as the Robeson upper bound [33, 34, 26], illustrated in figure 1.2 for conventional solution-diffusion membranes.

A possible route to circumvent the Robeson upper bound is to employ material families with permeation mechanisms operating outside the conventional solution-diffusion regime. One such mechanism is that of multiple parallel routes of permeation: if a species can traverse the membrane through multiple pathways, the permeability of that species may be selectively enhanced, improving both permeability and selectivity. This category of materials are known as facilitated transport membranes [21, 22], and have seen significant adoption for CO_2-selective gas separation. CO_2 facilitated transport membranes comprise molecular amine-functionalized polymer or molecular amine species. In the presence of humidity, CO_2 reacts with amines to form carbonic acid derivatives and other reaction products, which may permeate the membrane in parallel with molecular CO_2. Figure 1.3 illustrates this general principle: molecular CO_2 traverses the membrane through conventional solution-diffusion mass transport, while reacted species permeate with assistance from membrane chemical groups. In figure 1.2, the permeability and selectivity of the facilitated transport membrane reported

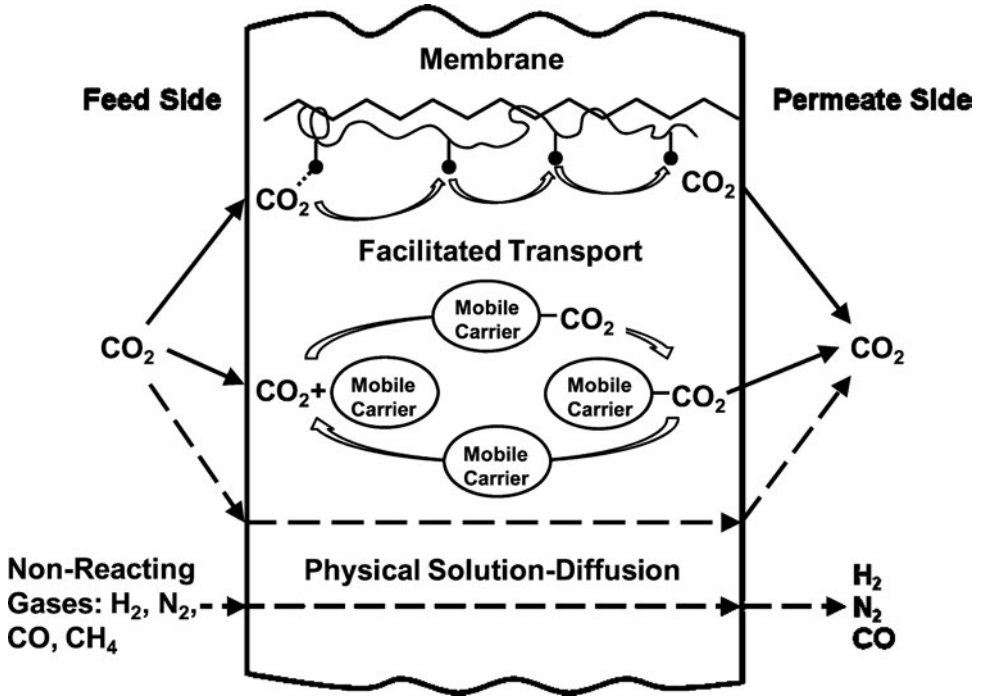

Figure 1.3: Transport modes in CO_2 facilitated transport membranes. Non-reacting gases permeate through physical solution-diffusion mode of transport, while CO_2 permeates through a combination of solution-diffusion and facilitated transport modes. Figure from Zhao and Ho [36].

by Deng et al. [30] is indicated. Separation performance is highly dependent on relative humidity, with both permeability and selectivity for CO_2 increasing as the hygroscopic membrane absorbs up to 100% of its own mass in water [35]. This allows the Robeson upper bound to be exceeded in the case of 90% relative humidity, suggesting facilitated transport membranes is a class of materials with potential to improve performance and enable new applications within the area of CO_2 separation.

The development of facilitated transport membranes for post-combustion CO_2 separation has seen renewed interest in recent years due to the rapid rise of anthropogenic emissions and their impact on global climate and environmental health. Feasibility studies by Matsumiya et al. [15] and Hussain and Hägg [16] indicate that facilitated transport membranes have the potential for significant cost savings and improved separation performance relative to conventional liquid-phase separation technology. A recent design study by Han and Ho [37] highlighted the potential for facilitated transport membranes in post-combustion carbon capture applications, estimating a capture cost of USD 41.7 per tonne CO_2 based on existing technology. In a review of membrane gas separation applications, Ding [25] estimates a capture cost for CO_2 / N_2 based on facilitated transport membranes as low as 27 EUR per tonne CO_2, compared against 55 EUR per tonne CO_2 for conventional liquid-phase separation [25]. The potential of facilitated transport membranes motivated the research initiative NANOMEMC^2 (NanoMaterials Enhanced Membranes for Carbon Capture)* targeting development of next-generation commercial membrane materials, with the objective "*to fully develop the potential of membranes in the selective capture of CO_2 from gaseous emissions, increasing the efficiency of*

*Project website: `https://www.nanomemc2.eu`

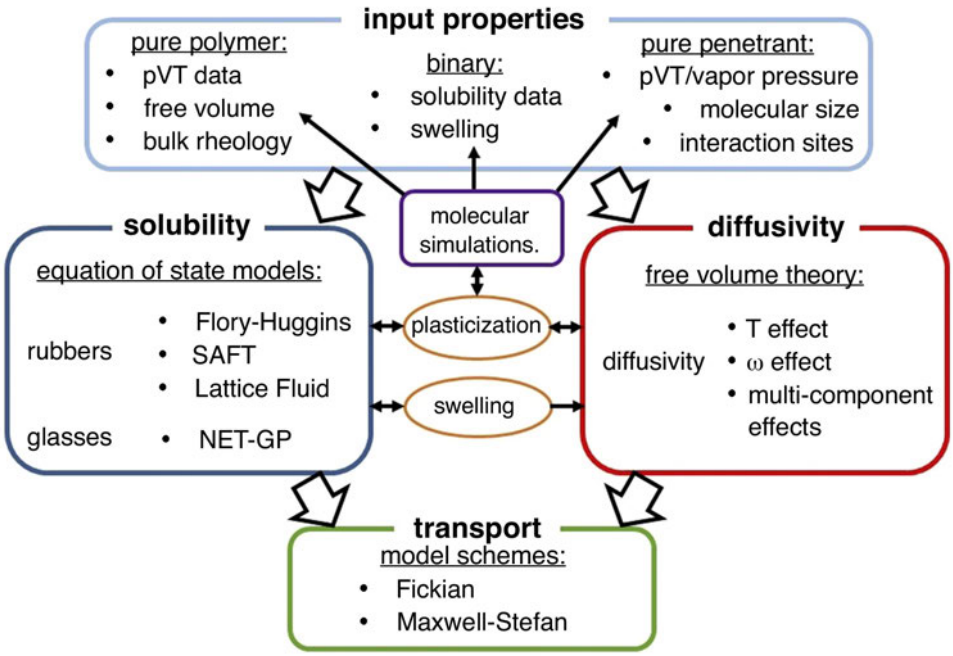

Figure 1.4: Data sources, modelling frameworks, and mass transport models for employed for studying solution-diffusion membranes. For solubility models, polymer pVT (equivalently ρpT) data together with binary polymer solution data are used to optimise equation of state models. Molecular simulation fulfils a complementary role to experimental data, allowing characterisation of systems or conditions where experimental measurements are not available. Figure from Minelli and Sarti [40].

the capture step, and reducing the overall CCS [carbon capture and sequestration] cost below the value of 40 EUR/tonne of CO_2 avoided" [38].

Despite years of development, the material properties and underlying molecular mechanisms for facilitated transport membranes remain poorly understood. Optimisation of membrane composition and operating parameters such as temperature, pressure, and humidity are critical to the efficient operation of membrane separation processes [37], and would be aided by improved models for vapour-liquid equilibrium and diffusive transport. Further, material design for CO_2 selective membranes is largely exploratory in nature, and would benefit from methods of intelligent design as seen for liquid-phase separation technology [39].

1.3 Models for CO_2 Facilitated Transport

Models for gas separation membranes span a wide range of scales, from plant design and optimisation, through membrane module operation, to membrane material properties and microscopic description. For conventional gas separation membranes, Minelli and Sarti [40] recently described successful approaches to representing mass transport for multi-scale modelling of gas separation membranes. Key to each modelling approach is the representation of solubility and (transport) diffusion, the two coefficients in equation 1.1, with a range of models available for each coefficient. Figure 1.4 summarizes the input data, modelling frameworks, and resulting transport models available for conventional solution-diffusion membranes.

The primary discrepancy between the approaches outlined in figure 1.4 and facilitated transport membranes is the reactive solubility seen for CO_2. Commonly employed equation of state models for polymer systems are poorly suited for describing reactive solubility. Additionally, the dependence of separation performance on relative humidity indicated in figure 1.2 is not seen for conventional solution-diffusion membranes, indicating a more complex interdependence in the polymer - H_2O - CO_2 ternary system. Membrane swelling and plasticization upon absorption of water is also likely to alter the diffusivity of gas species, as seen e.g. for cellulose acetate-based gas separation membranes [41] and perfluorosulfonate ion-exchange membranes [42].

The differences in both solubility and transport modes mean that models developed for conventional solution-diffusion mass transport cannot be directly applied to facilitated transport membranes. Multiple alternative models have been proposed, aiming to incorporate the reactive transport path through the membrane. In two recent reviews of facilitated transport membranes for CO_2 separation, Rafiq et al. [21] and Tong and Ho [22] suggest the same general expression for transport through a facilitated transport system, following Fick's law for both solution-diffusion and facilitated modes of transport;

$$\boldsymbol{J} = -D_{\text{solute}} \nabla C_{\text{solute}} - D_{\text{complex}} \nabla C_{\text{complex}} \tag{1.4}$$

where $\boldsymbol{J}$ is the flux, D_i is the diffusivity, and ∇C_i is the local concentration gradient of the permeating species in the system. Equation 1.4 applies to a particular membrane composition, and assumes the chemical potential gradient is proportional to concentration. The labels *solute* and *complex* refers to molecular and reacted forms of the gas species, indicating their parallel contribution to overall transport. The comprehensive review by Rea et al. [43] details further macroscopic models for transport in solvent and polymer facilitated transport systems.

1.4 Motivation and Objectives

While the macroscopic models outlined above provide some intuition and means to express mass transport in facilitated transport membranes, equation 1.4 and similar approaches do not provide a predictive model for correlating or predicting concentration or diffusion constants. New and improved models are needed to describe the separation performance of facilitated transport membranes in response to temperature, pressure, humidity, and membrane composition.

Solubility in hydrated facilitated transport membranes in many ways resembles CO_2 solubility in aqueous amines or alkanolamines. In a review of solvent chemistry and absorption capacity, Bernhardsen and Knuutila [44] identify alkanolamines as the largest group of solvents employed for CO_2 separation, with a wide range of chemistries available for optimisation of specific separation processes. The chemical environment of aqueous alkanolamine solutions clearly resembles that of the PVA/PVAm facilitated transport membrane reported by Deng et al. [30]. Hence, modelling approaches used for CO_2 absorption in aqueous amines is a

natural starting point for facilitated transport membranes.

This work aims to establish a molecular modelling approach for facilitated transport membranes which provides quantitative prediction of physical and reactive solubility for gases relevant to CO_2 capture. The aim of a predictive molecular modelling approach is supported by the following objectives.

- Identify a representative equation of state for describing polymer hydration and develop parameters for facilitated transport membrane polymer, exemplified by polyvinyl amine (PVAm).
- Assess the likely CO_2 reaction products in PVAm facilitated transport membranes, and develop molecular models suitable for describing vapour-liquid equilibrium in the resulting electrolyte solutions.
- Develop a framework for combining molecular simulation with empirical data to predict composition in reactive absorption systems, illustrated by CO_2 absorption in aqueous MDEA solution.
- Combine the equation of state model for hydrated PVAm with the reaction model tested on MDEA solutions, in order to predict absorption in a prototypical facilitated transport membrane.

The above objectives target solubility in facilitated transport membranes, pertaining to the concentration gradients of equation 1.4. While this work will centre on the thermodynamic properties of facilitated transport membranes, kinetic properties are also key for predicting overall transport rates. For diffusion constants in facilitated transport membranes, work by Fayon and Sarkisov [45] indicates multiple diffusion regimes separated by a threshold in water content, similar to that seen for cellulose acetate-based membranes [41]. Due to the ongoing research into diffusion regimes and transport in polymer membranes, predictive models for diffusion constants will not be an objective of this work.

1.5 Approaches to Molecular Modelling

Facilitated transport membranes are complex fluid systems, comprising multiple elements which individually require specialised theory. The primary areas are: (i) polymer solutions and vapour-liquid equilibrium in these systems; (ii) electrolyte systems where both solvent and solutes have organic character, and the resulting solution activities; (iii) reaction equilibrium in aqueous-organic electrolyte solvents, describing the reactive absorption of CO_2 in response to applied vapour pressures. These three areas of theory come together to describe the thermodynamics of gas solubility in facilitated transport membranes. To develop an integrated model comprising the three aspects outlined above, we require modelling tools beyond any one approach or theory. Molecular simulation can provide significant predictive power for vapour-liquid equilibrium in fluid systems, as shown in our previous work [46], but faces challenges with statistical precision and accuracy when generating predictions of physical quantities for polymer systems due to the long time scales in these systems. Equations of state which are commonly used to study polymer-solvent systems and vapour-liquid equilibrium,

MODEL DESCRIPTION	SOLUTION V-L-E	POLYMER RHO-P-T	POLYMER SOLUTIONS	ELECTROLYTE SOLUTIONS	REACTION SYSTEMS
Lattice EoS	Limited Precision		Limited Precision		
Molecular EoS					
Continuum Electrostatics				Dilute solution, empirical	
Electrolyte EoS	As molecular EoS	As molecular EoS	As molecular EoS	Limited range of compositions	
Activity Coefficent	Empirical correlation			Empirical correlation	Empirical correlation
SAFT		Parameter regression	Parameter regression		Limited reaction types
Molecular Simulation		Convergence limited	Convergence limited	Model dependent	With empirical reaction data

Figure 1.5: Modelling approaches for physical phenomena in facilitated transport membranes. For each modelling approach, suitability within each area is indicated by colour. Green: high suitability, good agreement with experimental behaviour and no significant technical challenges. Orange: medium suitability, reasonable agreement with experimental behaviour and only minor technical technical challenges. Red: poor suitability, significant deviations from experimental behaviour or unacceptably high statistical uncertainty in numerical predictions.

have limited predictive power when faced with reactions and aqueous-organic electrolyte solutions, as we have explored for CO_2 absorption in aqueous amine solutions [47]. Conventional aqueous-phase reaction models, relying on assumptions of dilute solution behaviour, require empirical correction factors which are cumbersome to obtain for multi-component systems.

The body of this work is structured by the three theoretical areas identified above; polymer solutions, electrolyte solutions, and reaction systems. For each area, appropriate modelling frameworks are discussed together with their theoretical basis, informing the model choices for facilitated transport membranes. Both molecular simulation and analytical models are considered and found to complement each other, allowing description of systems at previously unexplored compositions and conditions.

1.5.1 Models of Polymers and Polymer Solutions

Polymers are linear or branched chains of monomeric units, comprising a backbone of repeating covalent bonds. Chain length and backbone chemistry in polymer systems greatly influence phase behaviour, kinetics, and mechanical properties. These properties can be further modified through the introduction of chemical functionality, making polymers attractive for application-specific material design and optimisation.

Chapter 3 details selected modelling approaches for polymer systems. Lattice-based theory is introduced using the Sanchez-Lacombe equation of state [48, 49, 50] as an example of a framework employed to characterise polymer ρpT behaviour and phase behaviour of polymer solutions. Statistically associating fluid theory and contemporary molecular equations of state are discussed, and the PC-SAFT equation of state [51, 52, 53] introduced as a general modelling framework suitable for a variety of fluid systems.

Both the equation of state approach and molecular simulation are compared against ρpT behaviour in real polymer systems. While the former provides an excellent data regression framework with fast numerical solutions, the latter provides good predictive power for chemically novel or physically uncharacterised systems. Combining the two methods, models for polyethylene oxide (PEO) and polyvinyl alcohol (PVA) are regressed against molecular simulation data and compared against experimental values. The same approach permits regression of parameters for polyvinyl amine (PVAm), for which there are no available experimental data. By considering a combination of volumetric properties and absorption isotherms in polymer-water systems, binary polymer-water interaction parameters are optimised for each polymer.

1.5.2 Models of Electrolyte Solutions

Electrolyte solutions are mixtures of neutral solvent with ionic species such as salts, creating electrically conductive liquids. Facilitated transport membranes generate electrolyte species upon absorption of CO_2. Chapter 4 starts by reviewing fundamentals of continuum electrolyte solution theory, tying solution thermodynamics properties to solvent permittivity. Born and Debye-Hückel theory is discussed in the context of ions and solvent of increasing complexity, and high-concentration systems are shown to diverge considerably from the behaviour predicted by continuum solvation models. Recent efforts to augment molecular equations of state with continuum solution theory are discussed, with different approaches exemplified by the ePC-SAFT [54, 55] and eCPA [56, 57, 58, 59] models.

Further, we review recent advances in molecular simulation of electrolyte solutions based on explicit molecular models. Molecular simulation has the advantage of not requiring prior knowledge of solvent permittivity, as well as a more fine-grained representation of electrolyte shape and chemical structure. While other analytical approaches such as the work of Maribo-Mogensen et al. [59] also can be used to predict mixed solvent permittivity, this requires significant assumptions or prior knowledge of geometric structure in mixed solvent systems. Further, we assess common optimisation targets for electrolyte model development, and identify phase equilibrium simulations as a significant weakness of most existing models. A new objective function targeting liquid density and osmotic coefficients is specified.

Using liquid density and solvent activities as optimisation targets, new molecular models for alkylammonium halides are developed by optimising halide ion parameters. We show that correct liquid density and solvent activity can be obtained based on classical integer charge models, allowing simulation of vapour-liquid electrolyte systems. Building further on the proposed alkylammonium parameters, a model for bicarbonate

is developed based on a combination of experimental vapour-liquid data and *ab initio* structural data. In combination, the new models for organic ammonium and bicarbonate allow simulation of reaction products in amine - H_2O - CO_2 ternary systems.

1.5.3 Models of Reactive Systems

The reactive absorption of CO_2 in facilitated transport membranes closely resembles that of aqueous amines, which are far better characterised experimentally. In chapter 5, aqueous amine systems are used as a chemical analogue to develop modelling approaches for reactive CO_2 absorption in facilitated transport membranes. The absorption mechanisms of CO_2 in aqueous amine systems belong to the category of rapid equilibrium reactions, where system composition is a response to CO_2 partial pressure together with other physical parameters. We present a thermodynamic framework for equilibrium reaction systems, relating activities and reaction free energy to system composition, allowing equilibrium speciation to be calculated based on activities obtained through molecular models.

Using literature models for polymer and water, together with parameters for organic amines developed in chapter 3 and models for alkylammonium bicarbonate developed in chapter 4, amine - H_2O - CO_2 systems are simulated at varying levels of CO_2 absorption. Predictions for methane solubility in the ternary system are found to be in good quantitative agreement with experimental values, indicating physical solubility is well described by the molecular model. By measuring the activity of each species in solution, a reaction equilibrium is calculated allowing absorption isotherms to be predicted for the well-characterised MDEA - H_2O - CO_2 system. Comparison with literature absorption data shows reasonable qualitative agreement with experimental values.

The integration of reactive absorption data with equation of state models is considered through a survey of recent studies of reactive CO_2 absorption. Statistically associating fluid theory is found to give an acceptable representation of reactive absorption. In chapter 5, this approach is combined with the equation of state models developed in chapter 3, giving an integrated predictive model for facilitated transport membranes. Trends for reactive and physical solubility are explored as functions of temperature and relative humidity.

1.5.4 Application to Facilitated Transport Membranes

Combining the approaches to polymer, electrolyte, and reaction systems outlined above, each column indicated in figure 1.5 can be described with sufficient accuracy to provide an integrated model for reactive CO_2 absorption in hydrated polymers. In chapter 6, the molecular models developed in chapters 3, 4, and 5 are combined to make predictions for the thermodynamic properties of facilitated transport membranes under a variety of process conditions. We consider hydrated PVAm, the CO_2-selective polymer investigated by Deng et al. [30].

Using the molecular model, we predict absorption of N_2 and CO_2 for variable temperature and relative

humidity, offering quantitative predictions for gas solubility as used in equation 1.1. By comparing the solubility ratio of the two gases, the solubility-selectivity is confirmed as the explanation for the high selectivity observed in figure 1.2. However, solubility alone does not permit comparison with permeability data for process performance.

To provide more versatile predictions of process performance, a simple qualitative model for diffusion in polymer solution is used to calculate speculative estimate of diffusion constants for equation 1.1. These are combined with predicted gas solubility to estimate permeability of CO_2 and N_2 in hydrated PVAm over a range of process conditions relevant to post-combustion carbon capture.

Further, molecular simulation with the molecular models from 3 and 4 is used to provide a qualitative view of the facilitated transport membrane system. Close association of the bicarbonate ion with one or two protonated amine groups in PVAm suggests a 'stepping' process for transport in the resulting electrolyte solution, where bicarbonate can rapidly walk along or between the PVAm polymer strands to traverse the membrane.

Finally, in chapter 7 we close by providing an overview of the key developments and contributions to knowledge made in this project. We comment on the application of results from this work to process optimisation and material development for facilitated transport membranes, and identify promising avenues for future work building on the models and methodology developed here.

Chapter 2

Methodology

2.1 Overview

This chapter details the methodology used for evaluating thermodynamic properties in model fluids, either through molecular simulation or analytical equations of state. Model fluids are simplified representations of real systems such as polymer solutions based on their thermodynamic properties, providing a means to explore and understand their behaviour over a wide range of conditions. The interactions of model fluids in this work are based on the premise of additive two-body potentials, describing the strength of interaction between pairs of particles as a function of distance. Although both molecular simulation and equations of state operate on this principle, the two approaches differ in the potentials functions used, the treatment of electrostatic and dispersion interactions, and most significantly, the methods used for evaluating the thermodynamic functions resulting from the molecular description. This makes molecular simulation and equations of state complementary approaches in the study of fluid systems.

The two classes of model fluids employed in this work can be described as follows: classical molecular simulation is based on explicit representations of molecular geometries and interaction potentials, aiming to reproduce the physical forces acting between real molecules. Molecular equations of state are frameworks for correlating fluid properties based on model parameters, typically describing size, interaction strength, and chain lengths, together with an association model for bond formation. The selection of these models is in part justified in this chapter, with further detail and development of model parameters both for molecular simulation and equations of state detailed in subsequent chapters. Figure 2.1 compares the representation of ethanol in each of the two approaches: for molecular simulation, the molecular shape together with distribution of charges describes its interactions with nearby fluid particles. For associating equations of state, molecules have a chain length, size, and interaction strength, but no distinct shape, and strong interactions (e.g. hydrogen bonding) are described using association sites.

In the section 2.2, a general description of classical molecular simulation is presented, detailing interaction

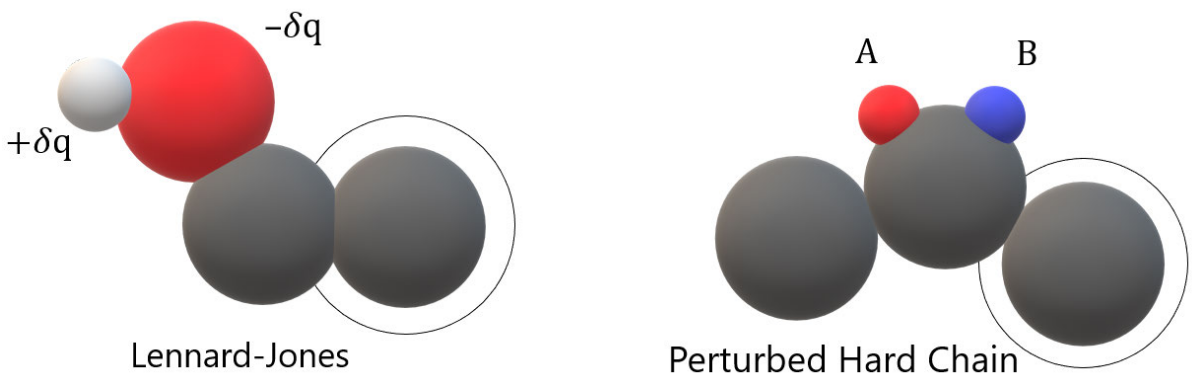

Figure 2.1: Model fluid representations of ethanol. Left panel: United-atom molecular simulation, with partial charges $\pm\delta q$ used to represent the electrostatic potential of the molecule, and dispersion interactions are described by a Lennard-Jones potential. Ethanol has a geometry with bond lengths and angles resembling that of the real molecule. Right panel: Associating equation of state, with intermolecular interactions described in a mean-field sense using a perturbed hard chain potential. Associating sites, indicated by A and B, form strong directional interactions corresponding e.g. to hydrogen bonding seen for alcohol compounds.

potentials, equations of motion, and coupling of the macroscopic observables temperature and pressure to microscopic properties of molecular systems. These methods are used for simulation of molecular systems in the isothermal-isobaric ensemble, and permit measurement of properties such as molar volumes, expansivity, and compressibility. Further, section 2.2 provides a brief derivation of thermodynamic perturbation theory in the context of small-molecule solvation in condensed liquid systems. Perturbation theory is used to calculate free energy differences between thermodynamic states, in turn allowing properties such as solvation free energy, Henry's law constants, and solution activities to be determined. Practical challenges regarding correlation times and the statistics of ensemble averaging are discussed in the context of polymer systems, together with an overview of the replica-exchange accelerated sampling technique.

Equations of state are introduced in section 2.4 as a complementary method to molecular simulation, providing analytical expressions of the Helmholtz free energy of a mean-field interacting fluid. Equations of state have the significant advantage of providing numerically exact solutions to thermodynamic functions for the given model, as well as being orders of magnitude faster to evaluate. Standard thermodynamic relations, connecting Helmholtz free energy with thermodynamic observables such as pressure and enthalpy, are presented as a general path to calculating phase equilibria and compositions in fluid system. Examples of the lattice fluid and statistically associating fluid theory (SAFT) equation of state families are given in the form of the Sanchez-Lacombe and perturbed-chain SAFT (PC-SAFT) equations of state. By comparing vapour-liquid coexistence curves for a selection of solvents, the performance of three- and five-parameter Sancehz-Lacombe and PC-SAFT equations of state are evaluated relative to high-precision multi-parameter equations of state correlated to multiple independent data sets for dimethyl ether [60], methanol [61], and water [62].

2.2 Molecular Simulation

2.2.1 System Hamiltonian

The properties of classical molecular systems are governed by analytical interaction potentials, describing the inter- and intramolecular forces acting between particles in the system as a function of their positions. Intermolecular potentials describe the interaction energy between molecules, and comprise electrostatic and dispersion interactions, while intramolecular potentials describe the internal energy based on molecular geometry. Together, inter- and intramolecular potentials define the instantaneous potential energy of a molecular system, and implicitly, the Helmholtz free energy for a given thermodynamic state. Interaction potentials together with kinetic energy due to translation together comprise the system Hamiltonian $\mathcal{H}$, representing the total energy of the system,

$$\mathcal{H} = E^{\mathrm{kin}} + U^{\mathrm{pot}} \tag{2.1}$$

where the potential energy U^{pot} contains all pairwise potential interactions in the system. In equation 2.1, kinetic energy E^{kin} is defined per mole of systems as

$$E^{\mathrm{kin}} = \sum_i \frac{p_i^2}{2m_i} \tag{2.2}$$

for a system of particles i and where m_i and p_i is the particle mass and momentum, respectively. The Hamiltonian defines the time-propagation of the system state Γ, comprising positions q_i and momenta p_i for all particles in the system. In turn, the system Helmholtz free energy is a result of U^{pot} alone and independent of time-propagation, delineating the thermodynamic and kinetic properties of a system.

In classical molecular simulation, the forces acting on particles in a fluid system are calculated from interaction potentials between two or more particles. Each potential is emulates a real physical interaction such as the electrostatic potential or quantum mechanical bond-angle energy. The potential energy surface U^{pot} normally comprises van der Waals, Coulomb, bond, angle, and dihedral potentials,

$$U^{\mathrm{pot}} = U^{\mathrm{vdW}} + U^{\mathrm{Coul}} + U^{\mathrm{bond}} + U^{\mathrm{angle}} + U^{\mathrm{dihedral}} \tag{2.3}$$

with each potential energy contribution a function of the system coordinates. The system potential defined over phase space Γ limits the available states for a given system and thermal energy, with Γ_m denoting the available phase space volume for a given state m, containing all energetically accessible combinations of particle positions and momenta. The probability of visiting a particular state is in turn given by the Boltzmann distribution,

$$P(\Gamma) = \frac{1}{Q_m} \exp\left[\frac{-U^{\mathrm{pot}}(\Gamma)}{RT}\right] \tag{2.4}$$

with Q_m being the configurational partition function of the system in state m. The configurational partition

function is in turn an integral over all possible states for the system. In the case of a system of N identical particles and constant volume,

$$Q_m = \frac{1}{N!h^{3N}} \int_{\Gamma_m} \exp\left[\frac{-U_m}{RT}\right] \mathrm{d}\Gamma \tag{2.5}$$

where h is Planck's constant. The partition function will be revisited in section 2.3 for the calculation of free energy between different states.

2.2.2 van der Waals Interactions

Short-ranged intermolecular forces originate from quantum mechanical electronic effects, comprising repulsion due to Pauli exclusion of electronic orbitals, and attraction due to London dispersion forces originating from induced-dipole interactions. These short-ranged effects are collectively referred to as van der Waals interactions, and describe the interaction potential between uncharged particles such as noble gases [63].

Classical molecular systems represent van der Waals interactions using explicit pairwise functions of the separation r between particles, describing both short-ranged repulsion and long-range attraction. Perhaps the most widely employed description for van der Waals interactions is the 12-6 or Lennard-Jones potential [64, 65],

$$U^{\mathrm{LJ}} = 4\epsilon \left[\left(\frac{\sigma}{r}\right)^{12} - \left(\frac{\sigma}{r}\right)^{6}\right] \tag{2.6}$$

where ϵ is the magnitude of the potential energy minimum and σ is the contact distance at which the potential interaction is zero. Alternatives to equation 2.6 include the three-parameter Buckingham potential [66],

$$U^{\mathrm{Buckingham}} = A \left[\exp[-Br] - \left(\frac{\sigma}{r}\right)^{6}\right] \tag{2.7}$$

and four-parameter Mie potential [67],

$$U^{\mathrm{Mie}} = \frac{A}{A-B}\left(\frac{A}{B}\right)^{B/(A-B)} \epsilon \left[\left(\frac{\sigma}{r}\right)^{A} - \left(\frac{\sigma}{r}\right)^{B}\right] \tag{2.8}$$

where A and B in equations 2.7 and 2.8 are generalized parameters. The Mie potential reverts to the Lennard-Jones potential for $A = 12$ and $B = 6$, but gives additional flexibility to the scaling of attractive and repulsive components.

In this work, the Lennard-Jones potential is employed for van der Waals interactions, largely to maintain compatibility with existing molecular models of organic molecules as detailed in chapters 3 and 4. Equation 2.6 is used for calculation of short-ranged dispersion interactions, while a mean-field tail correction is applied for long-range interactions [68].

For unlike species, the parameters ϵ and σ for interactions between particles i and j are determined by the Lorentz-Berthelot combining rules,

$$\epsilon = \sqrt{\epsilon_i \epsilon_j} \tag{2.9}$$

$$\sigma = (\sigma_i + \sigma_j)/2 \tag{2.10}$$

where the subscripts indicate particle-specific parameters. The Lorentz-Berthelot combining rules have been criticized for overestimating the energy parameter ϵ for unlike particles based on comparison with noble gas experiments [69]. However, use of non-Lorentz-Berthelot combining rules in molecular simulation has been explored by e.g. Rouha and Nezbeda [70] and Moučka and Nezbeda [71] for alcohol-water mixtures, and were found to provide limited benefit in the description of excess molar volumes. While mixture properties may be modulated by variations in combining rules, there is no simple alternative providing quantitative agreement for generic fluid mixtures.

2.2.3 Electrostatic Interactions

Electrostatic forces in molecular simulation are determined based on fixed partial charges q_i assigned to each particle. Electrostatic interactions are normally calculated according to the Coulomb potential,

$$U^{\mathrm{Coul}} = \frac{1}{4\pi\epsilon_0}\frac{q_i q_j}{r} \tag{2.11}$$

where ϵ_0 is the vacuum permittivity. Long-range effects are particularly significant in systems with anisotropy or long-range structure, including electrolyte solutions. Unlike the Lennard-Jones potential, there is no simple correction accounting for long-range electrostatic interactions. Instead, long-range electrostatic interactions are calculated using an Ewald summation method [72] with the conventional periodic boundary conditions. The use of Ewald summation for long-range interactions requires an additional factor of $1 - \mathrm{erf}(\beta r)$ for the Coulomb potential in equation 2.11, where β is a weighting between direct- and reciprocal space sums. The smooth particle-mesh method of Darden [73] is employed for Ewald summation, with further detail provided in section 2.5.

2.2.4 Bonded Interactions

While van der Waals and electrostatic interactions describe the intermolecular interactions of molecules, the intramolecular bond, angle and dihedral interactions are described by bonded interaction potentials. These intramolecular degrees of freedom govern the shape and flexibility of polyatomic molecules. Unlike intermolecular potentials, bonded interactions can be functions of more than two particles. Each potential describes the energy penalty for deviating from the minimum-energy conformation, emulating the quantum mechanical energy of different configurational states.

Bond angles describe the angle θ between three consecutively bonded atoms. The bond angle interaction is defined by a harmonic potential,

$$U^{\mathrm{angle}} = k_\theta(\theta - \theta_0)^2 \tag{2.12}$$

with force constant k_θ and equilibrium angle θ_0. Dihedral angles describe the angle ϕ between intersecting planes defined by four consecutively bonded atoms, and often denoted 1-4 interactions. Unlike bond angles, dihedral angles can have multiple symmetrical minimum-energy conformations depending on molecular symmetry. In this work a three-term cosine expansion is employed for dihedral potentials,

$$U^{\text{dihedral}} = C_1(1 + \cos(\phi)) + C_2(1 - \cos(2\phi)) + C_3(1 + \cos(3\phi)) \tag{2.13}$$

suitable for the one-, two- and three-fold bond symmetry seen for most organic molecules.

Bond lengths, while flexible in real molecules and often represented as a harmonic bonded potential, are constrained to a fixed distance for all species in this work. Forces on bonded atoms are propagated using the linear constraint solver described by Hess et al. [74, 75].

2.2.5 Equations of Motion and Weak Coupling Algorithms

In molecular dynamics simulation, the system state is propagated by mimicking the natural time evolution of the microscopic system using the classical interaction potentials described in sections 4.6.3 - 2.2.4. Forces are calculated using the Hamiltonian equation of motion,

$$\frac{d\mathbf{p}}{dt} = -\frac{d\mathcal{H}}{d\mathbf{q}} \tag{2.14}$$

where the variables $\mathbf{p}$ and $\mathbf{q}$ comprise the positions and momenta of all particles in the system. Straightforward application of equation 2.14 results in the microcanonical ensemble with fixed particle count, density, and total system energy. Since physically observable quantities typically are obtained at fixed temperature and pressure rather than fixed energy and volume, it is convenient to modify equation 2.14 to reflect coupling of the simulated microscopic system to external temperature and pressure regulators.

Temperature is the macroscopic observable corresponding to kinetic energy in the simulated system. While kinetic energy is an instantaneous property, temperature is an average property of the simulated ensemble. By sampling kinetic energy, temperature can be calculated as

$$T = \frac{2}{RN_{\text{df}}} \left\langle E^{\text{kin}} \right\rangle \tag{2.15}$$

where N_{df} is the number of degrees of freedom in the system, calculated as $N_{\text{df}} = 3N - N_{\text{c}}$ for a system of N particles and N_{c} constraints. In equation 2.15, the angled brackets indicate an ensemble average over the simulated states. To maintain kinetic energy fluctuations corresponding to a target temperature T, a thermostat algorithm is incorporated in the equations of motion. Here, the Langevin equation as described by van Gunsteren et al. [76] is used for this purpose. By introducing a stochastic force $\mathbf{R}$ and coefficient of friction γ acting on all particles in the system, kinetic energy can be modulated using the modified equation

of motion

$$\frac{d\mathbf{p}}{dt} = -\frac{d\mathcal{H}}{d\mathbf{q}} + \frac{\mathbf{R}}{m} - \gamma\frac{\mathbf{p}}{m} \tag{2.16}$$

where m is the particle mass. The stochastic force is Gaussian distributed and must satisfy $\langle \mathbf{R}^2 \rangle = 6m\gamma RT$ in order to maintain the correct Boltzmann distribution of energies [76, 77]. Equation 2.16 is known as the Langevin equation of motion, and ensures sampling of the system degrees of freedom even in cases where particles are entirely non-interactive (as is encountered when simulating decoupled states for free energy perturbation, see section 2.3). However, due to the stochastic nature of the random force $\mathcal{R}$ the equation of motion is irreversible, unlike the time-reversible nature of purely Newtonian systems. This system description in equation 2.16 is adopted for all constant-temperature simulations in this work.

Similar to temperature, the system pressure is a macroscopic observable corresponding to the difference between kinetic energy and the virial Ξ,

$$p = \frac{2}{3V}\left\langle E^{\mathrm{kin}} - \Xi \right\rangle \tag{2.17}$$

where the virial is defined as

$$\Xi = \frac{1}{2}\sum_{ij} r_{ij}\frac{dU_{ij}}{dr_{ij}} \tag{2.18}$$

and the sum over ij comprises all pairwise particle interactions with separation $\mathbf{r}_{ij}$ and interaction potential U_{ij}. A barostat is employed to maintain fluctuations around a target pressure p, in practice modulated by scaling the system volume V. Here, the Parrinello-Rahman barostat [78, 79] is employed with the extensions of Nosé and Klein [80]. For a cubic simulation cell, the system diameter b is coupled to an equation of motion as

$$\frac{d^2b}{dt^2} = \frac{b}{W}(p - p_0) \tag{2.19}$$

where the coupling strength parameter W determines the time period of oscillation around the target pressure p_0. Equation 2.19 together with the Langevin equation of motion (equation 2.16) permit simulation at constant temperature and pressure. This system description is adopted for all simulations in the isothermal-isobaric ensemble in this work.

2.3 Perturbation Theory

The free energy difference between thermodynamic states is a foundational concept within the area of equilibrium thermodynamics, governing phase and reaction equilibria. The free energy difference $\Delta_{mn}A$ can be expressed as the ratio of the partition functions of the two states m and n,

$$\Delta_{mn}A = -RT\ln\frac{Q_n}{Q_m} \tag{2.20}$$

where the configurational partition function Q_m is defined in equation 2.5. To estimate the free energy difference of a state n that is not too dissimilar to m, we need a way of estimating Q_n based on our knowledge of Q_m. To evaluate the fraction Q_n/Q_m in equation 2.20 we can write

$$\frac{Q_n}{Q_m} = \frac{\int_{\Gamma_n} \exp\left[\frac{-U_m - \Delta_{mn}U}{RT}\right] \mathrm{d}\Gamma}{\int_{\Gamma_m} \exp\left[\frac{-U_m}{RT}\right] \mathrm{d}\Gamma} \tag{2.21}$$

where U_m is the potential energy of state m evaluated at Γ, and $\Delta_{mn}U$ is the corresponding energy difference $U_n - U_m$. Then, if the available phase space volume $\Gamma_n \approx \Gamma_m$, the fraction Q_n/Q_m simplifies to

$$\frac{Q_n}{Q_m} = \int_{\Gamma_n} \exp\left[\frac{-\Delta_{mn}U}{RT}\right] \mathrm{d}\Gamma \tag{2.22}$$

which by insertion in equation 2.20 gives an estimate of the free energy difference $\Delta_{mn}A$. While $\Gamma_n \approx \Gamma_m$ may initially seem like a drastic approximation, the differences between Γ_n and Γ_m are found for sparsely occupied states, provided the differences in U_m and U_n are small: Changes to the available phase space occurs for configurations that have sufficiently high potential energies to be thermally inaccessible, which in turn means these configurations carry little weight in the partition function. As long as the frequently visited configurations of both m and n are accessible in simulation, the approximations in equation 2.22 hold.

In practice, partition function integrals for anything but the simplest of systems are infeasible to evaluate analytically and must instead be estimated by simulation. However, the same free energy expression applies, with Q_n/Q_m instead estimated by an ensemble average,

$$\Delta_{mn}A = -RT \ln \left\langle \exp\left[-\frac{\Delta_{mn}U}{RT}\right] \right\rangle_m \tag{2.23}$$

where $\Delta_{mn}U \equiv U_n - U_m$ and the angled brackets denotes an exponential average for samples taken from state m for both potential functions U_m and U_n. Equation 2.23 was introduced by Zwanzig [81], and forms the core for later developments in the area of free energy perturbation theory [82]. It gives a practical recipe for estimating free energy differences by sampling the configurational states of the system of interest, and comparing the resulting potential energy differences.

2.3.1 Widom Insertion

The free energy relation in equation 2.23 has straightforward applications to molecular systems, where U can be evaluated exactly for a given state coordinate Γ. Perhaps the simplest implementation is the Widom insertion method for evaluating excess chemical potential μ^{ex}, typically used for calculating solubility of small volatile species in liquids or porous materials [68]. The Widom insertion method measures the the excess chemical potential of a particle, equal to the free energy difference of the particle relative to the ideal gas

reference state, where all particle positions and orientations are equally likely. Using the simulation framework outlined in section 2.2, the combined particle + condensed phase system may be simulated with all interactions switched off for the test particle. Given a suitable stochastic temperature coupling algorithm, the particle would drift randomly in space. For insertion into a liquid, the excess chemical potential is equal to the solvation free energy $\Delta_{\mathrm{solv}}A$, and may be calculated using equation 2.23 as

$$\Delta_{\mathrm{solv}}A = -RT \ln \left\langle \exp\left[-\frac{\Delta_{\mathrm{solv}}U}{RT}\right]\right\rangle_{\mathrm{IG}} \tag{2.24}$$

where IG indicates that the test particle energies are sampled from the ideal gas state. In this case, $\Delta_{\mathrm{solv}}A$ corresponds to the excess chemical potential μ^{ex}, and can be used to calculate Henry's law solubility constants K_H. Henry's law constant describes molal concentration in the condensed phase at the temperature and mechanical pressure of interest, in response to partial pressure of a species in an ideal (i.e. non-interacting) gas phase. K_H is calculated as

$$K_H = \frac{1}{RT}\exp\left[-\frac{\Delta_{\mathrm{solv}}A}{RT}\right] \tag{2.25}$$

for a given value of $\Delta_{\mathrm{solv}}A$ calculated at temperature T. In practice, the Widom insertion method can be used in a much more efficient manner by generating the condensed phase ensemble first, and subsequently sampling $\Delta_{mn}U$ by insertion of the test particle at randomly chosen coordinates.

2.3.2 Bennett Acceptance Ratio and other Estimators

The exponential equality in equation 2.23 forms the basis of thermodynamic perturbation theory, and is generally applicable to any modification to the system Hamiltonian. However, it is not the most efficient estimator for free energy differences, and in particular produces poor statistics for systems with few but energetically favourable configurations [83], such as particle insertion in dense systems.

The minimum-variance estimator for free energy perturbations was derived by Bennett [84], with key steps given below. The key development is introduction of a weight function W in equation 2.20,

$$\Delta_{mn}A = -RT \ln \frac{\langle WQ_n\rangle_m}{\langle WQ_m\rangle_n} \tag{2.26}$$

such that sampled Hamiltonian differences can be rescaled to give a lower variance estimate for the free energy difference. Bennett demonstrates [84] that the minimum variance weight function for a free energy perturbation sampled from both states m, n is given by

$$W(\Gamma) = C'\left(\frac{Q_m}{n_m}\exp\left[\frac{-U_n}{RT}\right] + \frac{Q_n}{n_n}\exp\left[\frac{-U_m}{RT}\right]\right)^{-1} \tag{2.27}$$

where n_m, n_n are the number of samples obtained from each state and C' is a constant. Substituting

equation 2.27 into equation 2.26 gives the free energy estimate as

$$\Delta_{mn}G - C = -RT \ln \frac{\langle f(U_m - U_n + C)\rangle_m}{\langle f(U_n - U_m - C)\rangle_n} \tag{2.28}$$

where $f(U) = 1/(1+\exp\left[\frac{U}{RT}\right])$ is the Fermi-Dirac distribution. Bennet shows through variational calculus [84] that the minimum-variance value of the constant in equation 2.28 is $C = \Delta_{mn}G + RT\ln(n_m/n_n)$, containing the to-be-estimated quantity $\Delta_{mn}G$. Insertion into equation 2.28 and rearranging gives

$$0 = \frac{1}{1 + \left\langle \exp\left[\frac{\Delta_{mn}U}{RT} - \frac{\Delta_{mn}G}{RT} + \ln\frac{n_m}{n_n}\right]\right\rangle_m} - \frac{1}{1 + \left\langle \exp\left[\frac{\Delta_{nm}U}{RT} + \frac{\Delta_{mn}G}{RT} + \ln\frac{n_n}{n_m}\right]\right\rangle_n} \tag{2.29}$$

which must be solved iteratively for $\Delta_{mn}G$. Equation 2.29 is known as the Bennett acceptance ratio, and is commonly utilized for calculation of free energy differences from equilibrium states.

Other alternatives to equation 2.23 include thermodynamic integration [85] as well as non-equilibrium work [86] methods, both relying on gradual change to the λ-coordinate of the system Hamiltonian during the course of a simulation. A further development of this λ dynamics [87], where the λ-coordinate is treated as a dynamic variable and incorporated into the phase space volume Γ. A similar principle is used for expanded ensemble simulation [88], utilized in our previous study of solubility in mixed solvents for improved convergence [46]. Independent comparisons of free energy estimators conducted by Shirts and Pande [83] and Bruckner and Buresch [89] both conclude the Bennett acceptance ratio is the most efficient estimator for free energy perturbations, and it is used for all free energy perturbations in this work.

2.3.3 Hamiltonian Perturbations and Soft-Core Scaling

The potential energy difference in equation 2.20 describes some change in the description of the system from state m to state n, reflected in changes to the Hamiltonian of each state. In practice, the change between states is specified by adjusting the underlying interaction potentials of the system, governed by a thermodynamic parameter λ describing the degree of transition from one state to the next. For a perturbation to the Lennard-Jones potential (equation 2.6) and Coulomb potential (equation 2.11) we may write

$$\mathcal{H} = E^{\mathrm{kin}} + U^{\mathrm{LJ}}(\lambda) + U^{\mathrm{Coul}}(\lambda) + U^{\mathrm{angle}} + U^{\mathrm{dihedral}} \tag{2.30}$$

where different values of λ corresponding to different states of the system. Note that relative to equation 2.1, U^{vdW} has been replaced by U^{LJ} and U^{bond} is omitted due to the use of fixed bond lengths. It is customary to select interaction potentials such that $\lambda = 0$ and $\lambda = 1$ produce the two end states of interest. A simple example of such a potential is given by

$$U(\lambda) = \lambda U_m + (1 - \lambda)U_n \tag{2.31}$$

describing simple linear interpolation between states m and n. For perturbations with relatively small changes to the system Hamiltonian, a simple linear interpolation as shown in equation 2.31 provides sufficient overlap between states. This is typically the case for Coulomb interactions provided dispersion interactions are maintained constant [90], as the repulsive dispersion interaction prevents the system from reaching any singularities in the Coulomb potential.

For dispersion interactions based on the Lennard-Jones potential, linear interpolation provides poor thermodynamic overlap when considering particle insertion in dense systems. The singularity in equation 2.6 at $r = 0$ creates a 'goalpost effect': no matter the value of λ, there is always a region δr around the particle which remains inaccessible as the interaction potential exceeds the thermal energy in the system. This leads to a discontinuity in the phase space Γ, resulting in poor thermodynamic overlap close to the decoupled state and large uncertainties in the resulting free energy estimates.

To circumvent the singularity near $r = 0$ for dispersion interactions, a soft-core expression is used to modify the conventional Lennard-Jones potential. A fixed term is added to the numerators of the Lennard-Jones potential to limit the magnitude of the repulsive interaction. The resulting potential is

$$U_{mn}^{\mathrm{LJ-SC}}(\lambda) = (1-\lambda)^a 4\epsilon_m \left[\left(\frac{\sigma_m^c}{\alpha\lambda^b\sigma_m^c + r^c} \right)^{12/c} - \left(\frac{\sigma_m^c}{\alpha\lambda^b\sigma_m^c + r^c} \right)^{6/c} \right] + \lambda^a 4\epsilon_n \left[\left(\frac{\sigma_n^c}{\alpha(1-\lambda)^b\sigma_n^c + r^c} \right)^{12/c} - \left(\frac{\sigma_n^c}{\alpha(1-\lambda)^b\sigma_n^c + r^c} \right)^{6/c} \right] \quad (2.32)$$

where α is a scaling factor determining the soft-core diameter, and the exponents a, b, and c adjust the shape of the soft-core potential. Note that equation 2.32 simplifies to equation 2.6 at the end points of λ equal to 0 or 1 regardless of choice of parameters.

The purpose of introducing soft-core scaling of dispersion interactions in free energy perturbation calculations is to increase the thermodynamic overlap of states where a particle is being 'grown' from nothing in a condensed-phase system. The choice of α, a, b, and c in equation 2.32 will result in different and potentially system-specific differences in the thermodynamic overlap obtained. This problem has been been investigated by Pham and Shirts [91, 92] for the case of small-molecule solvation in water, by evaluating the thermodynamic distance between states described by a different parameter combinations. In practice, the resulting pathway is only weakly system-dependent, with useful discernible trends based on commonly encountered systems. The authors conclude a pathway of $a = 1$, $b = 1$, $c = 48$ (1-1-48) is optimal for solvation of small molecules such as methane in water.

Unfortunately, the $c = 48$ exponent places additional demands on the numerical precision of particle coordinates during simulation, requiring the use of double precision floating point operations. Double precision operations in turn increases computational expense by 20% - 100% [93]. For this reason, the somewhat higher variance but more numerically stable 1-1-6 pathway is employed in this work. As shown by Pham and Shirts [91], the 1-1-6 pathway has lower variance than the other commonly used 4-1-6 and 1-2-6 soft-core

potentials. The scaling factor α is set to 0.5 as suggested by Steinbrecher et al. [90], while σ in the soft-core expression is calculated from Lorentz-Berthelot mixing rules with an added floor of 0.3 nm,

$$\sigma = \max \begin{cases} (\sigma_i + \sigma_j)/2 \\ 0.3\,\text{nm} \end{cases} \tag{2.33}$$

where the atom indices i, j may differ between states m and n, for instance with conversion between a methyl and ethyl group.

Further to the choice of soft-core potentials, the specific λ schedule for traversing the free energy landscape must be determined. Several iterative schemes have been proposed for optimising λ pathways, aiming to evenly separate intermediate states resulting in lower overall variance. Here, we assess systems on a case-by-case basis, with linear λ pathways employed unless otherwise noted.

2.3.4 Accelerated Sampling Techniques

Simulation of molecular systems requires careful treatment of weak coupling algorithms and monitoring of system energy to ensure the correct ensemble of equilibrium states are obtained, rather than trapped metastable states. This is particularly true for polymer systems, where chain relaxation can be hindered by large energy barriers. A multitude of enhanced sampling methods have been developed to accelerate convergence and reduce correlation times in such systems, which can be broadly categorized as mean force biasing, non-Boltzmann sampling, and parallel exchange methods [94]. Methods belonging to the categories of mean force biasing and non-Boltzmann sampling aim to drive the system state away from a locally favoured equilibrium, for instance for studying targeted transitions between protein conformations [95] or ligand binding processes [96].

For polymer-solvent systems there are no clearly defined end-states, unlike those observed in the preceding two examples. Rather, the objective for accelerated sampling is to decrease correlation times between system configurations over the course of the simulation. Hence, any accelerated sampling technique must conform to the correct isothermal-isobaric ensemble while providing an appreciable computational efficiency for polymer systems.

The replica exchange method [97, 98, 99], also known as parallel tempering, is of particular interest for the simulation of polymer systems where condensed-phase properties at multiple temperature points are considered. Replica exchange accelerates simulations through the exchange of system configurations at different temperatures: By propagating kinetically trapped high-energy configurations towards high-temperature systems, the higher thermal energy is used to accelerate exploration of new system states. Hence, energy barriers which may have indefinitely trapped a low-temperature system in a small pocket of configurational space can be efficiently overcome.

The exchange of system configurations in the replica exchange method is a form of Monte Carlo simulation, with proposed exchanges accepted or rejected depending on system enthalpy, comprising internal energy and pressure-volume work, to maintain the detailed balance condition. In the isobaric-isothermal ensemble, the exchange probability between two states m and n is [100]

$$P_{ij} = \min \begin{cases} 1 \\ \exp\left[\frac{U_m - U_n}{RT_m} - \frac{U_m - U_n}{RT_n} + \frac{p_m(V_m - V_n)}{RT_m} - \frac{p_n(V_m - V_n)}{RT_n}\right] \end{cases} \tag{2.34}$$

where U, V are instantaneous potentials and volumes for each system, and p, T are the target pressures and temperatures. As the potential energies in equation 2.34 are extensive quantities, the systems should not be too large in order to maintain reasonable exchange probabilities.

The computational cost of replica exchange scales linearly with the number of replicas. Further, replicas cannot be too widely spaced in temperature to ensure reasonable exchange probabilities, nor too closely spaced else there is too little spread in temperatures to reap any acceleration effect. For polymer systems, the temperatures investigated should cover the phase diagram well into the melt phase where there is rapid structural change. While there is a substantial added computational cost of replica exchange, this is largely recouped by the added temperature range for sampling.

2.4 Equations of State

Equations of state provide a exact descriptions of fluid systems through analytical expressions for Helmholtz free energy as a function of molar density and temperature. From the Helmholtz free energy and its derivatives, all other thermodynamic properties can be determined. Since analytical expressions can be solved efficiently and precisely at arbitrary physical conditions, equations of state are powerful correlative tools for describing the properties of model fluid systems and extrapolating behaviour in one region of phase space to another.

This section describes the construction of molecular equations of state for solvents, polymers, and polymer-solvent systems, together with thermodynamic relations employed for calculating derived thermodynamic properties. The Sanchez-Lacombe [48, 49] and PC-SAFT [51, 52, 53] equations of state are employed as examples of respectively lattice-based and associating equations of state, two categories which have been widely employed in the study of fluid systems including polymers and their solutions.

The molecular parameters employed in equations of state are non-geometric, containing limited information about the shape and connectivity of molecular species, illustrated in figure 2.1. Hence, molecular equations of state are a further abstraction from real fluids than that seen for molecular simulation in section 2.2. Some notion of the molecular structure can nonetheless be identified by the segment number (chain-like character), interaction energy, and volume parameters of molecular equations of state. Association interactions, detailed in section 2.4.3, give further character to the specific interactions of the molecule, but remain abstracted from

molecular geometry.

2.4.1 Standard Thermodynamic Relations

Where molecular simulation employs 'computer experiments' to estimate observable properties from molecular systems, equations of state derive thermodynamic properties directly from the expression of Helmholtz free energy through thermodynamic relations. All equations of state may be formulated as a description of Helmholtz free energy A as a function of molar densities ρ_i and temperature T. Thermodynamic properties such as pressure and chemical potentials are readily obtained as partial derivatives of system Helmholtz free energy with respect to these fundamental variables.

The relationships between Helmholtz free energy and thermodynamic quantities are universal, and are readily applied to any equation of state model. Here, we use the thermodynamic relations and solution strategies from Quiñones-Cisneros and Deiters [101], employing the Helmholtz free energy density as primary thermodynamic potential. The advantage of using Helmholtz free energy density as thermodynamic potential is the use of molar densities as primary variables, replacing mole fractions and density (or molar quantity and volume) simplifying the resulting expressions and reducing computational cost for evaluation [101] of thermodynamic properties. Chemical potential for a species i is calculated from Helmholtz free energy as

$$\mu_i = \left(\frac{\partial A\rho}{\partial \rho_i}\right)_{\rho_j,T} \tag{2.35}$$

which is numerically faster to evaluate using the partially differentiated expression

$$\mu_i = A + \rho\left(\frac{\partial A}{\partial \rho_i}\right)_{\rho_j,T} \tag{2.36}$$

where the partial derivatives in both cases are performed at constant molar densities of species $j \neq i$ and temperature. Gibbs free energy may be calculated by summation of chemical potentials for all species in the system,

$$G = \frac{1}{\rho}\sum_i \rho_i \mu_i \tag{2.37}$$

which allows the mechanical pressure to be calculated using the definition of Gibbs free energy, $G = A + p/\rho$. Inserting equations 2.37 and 2.36 into the definition of Gibbs free energy, pressure is given as

$$p = -A\rho + \sum_i \rho_i \left(\frac{\partial A\rho}{\partial \rho_i}\right)_{\rho_j,T} \tag{2.38}$$

which simplifies to

$$p = \rho\sum_i \rho_i \left(\frac{\partial A}{\partial \rho_i}\right)_{\rho_j,T} \tag{2.39}$$

which for a single-component system reduces to the simple relation $p = \rho^2 \partial A/\partial\rho$. Further thermodynamic

relations give the system entropy S as the negative change of free energy with temperature,

$$S = -\frac{\partial A}{\partial T} \tag{2.40}$$

allowing the enthalpy H, the sum of internal energy and pressure-work, to be calculated as

$$H = G + TS \tag{2.41}$$

with G and S as defined above. These relations are used for evaluation of thermodynamic potentials, as well as determination of phase equilibrium, for equations of state in this work.

As noted for molecular simulations, experimental data typically refers to isothermal-isobaric conditions at a prescribed mechanical pressure. For phase coexistence calculations, care must be taken to specify phase coexistence in a consistent manner to the actual experiments performed, in order to obtain meaningful comparisons of model predictions with experiment. Equal chemical potentials, or 'chemical pressure', is required for each species in addition to mechanical pressure. For excess chemical potentials and other excess properties, the ideal gas contribution should first be subtracted. The above thermodynamic relations form the basis of phase calculations in this work. For example, simultaneous physical and chemical equilibrium between vapour and liquid phases (denoted by $'$ and $''$) is defined by

$$P' = P'', \quad T' = T'', \quad \mu_i' = \mu_i'' \tag{2.42}$$

satisfied for all species i considered volatile in the system. To allow efficient generation of thermodynamic expressions for mixtures of arbitrary compositions and constraints, this work represents equations of state using the open source SymPy library [102] for symbolic mathematics, as will be detailed in section 2.5. Expressions for pressures and chemical potentials are first generated using SymPy, which through the relationships in equation 2.42 define a system of equations describing the two-phase system. This equation system is solved based using an appropriate SciPy optimization routine. Using this approach, properties of any equation of state model are readily obtained provided a description of Helmholtz free energy.

2.4.2 Lattice Fluid Theory

The lattice fluid approach is founded on a description of fluid systems as chain-like molecules arranged on a regular grid, where intermolecular interactions are represented by nearest-neighbour interactions. Pioneering work on lattice fluids was done by Guggenheim, Flory and Huggins, initially in the context of polymer-solvent systems but later expanded to generic fluids. The Flory-Huggins theory of polymer solutions will be revisited in chapter 3.

A re-formulation of lattice fluid theory as a general equation of state was proposed by Sanchez and

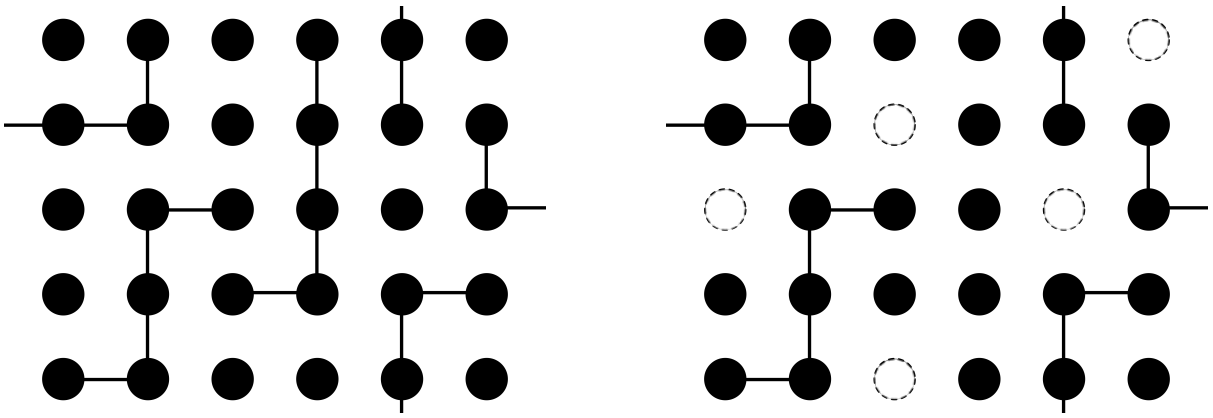

Figure 2.2: The Flory-Huggins and Sanchez-Lacombe lattice fluid models for polymer solutions. In the Flory-Huggins model (left panel), each species is represented as a chain-like molecule arranged on an imagined lattice, with the solvent occupying all interstitial sites. The Sanchez-Lacombe model (right panel) has an additional entropic contribution from the inclusion of vacant lattice sites.

Lacombe [48, 49, 50]. In the Sanchez-Lacombe equation of state, molecules are described by three parameters: their segment number r, close-packed monomer volume ν, and pairwise interaction energy ϵ. In addition, lattice vacancies are incorporated in the lattice to confer compressibility to the liquid phase. Figure 2.2 illustration the Flory-Huggins and Sanchez-Lacombe lattice fluids for a mixture of solvents.

The original derivation of the Sanchez-Lacombe equation of state is in terms of Gibbs free energy, with pressure p and temperature T as explicit variables [48, 49]. For pressure-explicit equations of state, density is calculated as a dependent variable for a given temperature and pressure, unlike the density-explicit Helmholtz free energy formulation described in section 2.4. Below, a brief derivation of the Sanchez-Lacombe equation of state is given following the development of the authors [48, 49], but expressed in terms of Helmholtz free energy with temperature and density as explicit variables. From the resulting expression, pressure and other thermodynamic properties can be readily calculated using the thermodynamic relations in section 2.4.1, illustrating the connection between the system partition function, Helmholtz free energy, and macroscopic observables.

For the lattice fluid, the system partition function may be described by the number of near-neighbour connections made in the fluid, contributing to the residual system energy E, and the number of permutations which result in this energy, denoted $\Omega(E)$ or the density of states. The Helmholtz free energy of a fluid mixture is related to these quantities through the configurational partition function, defined as

$$A = -RT \ln \sum_{E} \Omega(E) \exp\left[-\frac{E}{RT}\right] \tag{2.43}$$

where the sum over E counts all possible energy states available to the system. For a lattice fluid, expressions for Ω and E can be obtained as functions of N_0, the number of lattice vacancies in the system [48]. Consider a system of r-mers and vacancies, as illustrated in figure 2.2. The total number of lattice sites N_r given by

the number of lattice vacancies N_0 plus the sum of sites occupied by each species,

$$N_r = N_0 + \sum_i r_i N_i \tag{2.44}$$

distributed randomly on the lattice. If each nearest-neighbour interaction carries the same mean-field interaction energy, the total energy of the system is described by the number of non-bonded nearest-neighbour interactions,

$$E = -\sum_{ij} \frac{r_i r_j N_i N_j}{N_r} \epsilon^*_{ij} \tag{2.45}$$

where ϵ^*_{ij} is the per-segment interaction energy. For unary systems $\epsilon^*_{ii} = \epsilon^*$ is a model parameter, while for binary and higher order systems ϵ^*_{ij} is obtained using the mixing rules from Sanchez and Lacombe [50]. The number of possible states Ω at a given composition and number of vacancies N_0 is the number of possible arrangements of the r-mers on the lattice. The solution by Guggenheim [103] is expanded by Lacombe and Sanchez [49] for a mixture of holes and r-mers, with solution

$$\Omega = \frac{N_r!}{\prod_i N_i!} \left(\frac{N_q!}{N_r!}\right)^{z/2} \prod_i \left(\frac{\delta_i}{\sigma_i}\right)^{N_i} \tag{2.46}$$

where z is the coordination number of the lattice, and δ_i and σ_i are flexibility and symmetry parameters for each species describing intramolecular degrees of freedom. In equation 2.46, N_q is defined by $N_q = [(z-2)N_r + 2N_0 + 2\sum_i N_i]/z$, with $zN_q/2$ equal to the number of non-bonded pairs. In the limit of large z (i.e. infinite grid resolution) the limiting value of Ω can be found using Stirling's approximation as [48]

$$\lim_{z\to\infty} \Omega = \left(\frac{N_0}{N_r}\right)^{N_0} \prod_i \left(\frac{\omega_i N_r}{r_i N_i}\right)^{N_i} \tag{2.47}$$

where $\omega = \delta r/(\sigma \exp[r-1])$ is a constant value representing the number of possible intramolecular configurations for each species, which cancels in the calculation of residual thermodynamic properties.

With the expressions for Ω and E in equations 2.45 and 2.47 both being functions of the number of lattice vacancies, the sum over energies in equation 2.43 can be replaced by a sum over N_0. The multinomial distribution for Ω can in turn be approximated by its maximum term for systems of large N_r, found by minimizing the free energy based on the generic expression in equation 2.47. The resulting expression for A is

$$A = -r\epsilon^*\rho + r\epsilon^* T \left[(1/\rho - 1)\ln(1-\rho) + \frac{1}{r}\ln(\rho) + \sum_i \frac{\phi_i}{r_i} \ln\frac{\phi_i}{\omega_i}\right] \tag{2.48}$$

where the molar density is defined as $\rho = 1/(Nr\nu^*)$, the close-packed volume fraction ϕ is given by

$$\phi_i = \frac{r_i N_i}{\sum_i r_i N_i} \tag{2.49}$$

and the model parameters r, ϵ^* and ν^* for multi-component systems are given by the revised mixing rules by Sanchez and Lacombe [50]. Equation 2.48 corresponds to equation 23b from Lacombe and Sanchez [49] for the Gibbs free energy. The parameters δ and σ are left undefined as the constant ω_i in equation 2.48 does not influence derivatives of the Helmholtz free energy.

Based on equation 2.48, molecular parameters can be regressed for polymers and solvents from their physical behaviour. For pure solvents, the vapour-liquid coexistence curve is typically used for parameter regression [48], covering temperatures, pressures, and liquid densities from the triple point to the critical point. In figure 2.3, the vapour liquid-coexistence curve for dimethylether is shown, using molecular parameters regressed from experimental data using the procedure recommended by Sancehez and Lacombe [48]. For polymers, ρpT data at elevated pressure and temperatures can be used [50], provided the polymer is in either the rubber or melt (liquid) state.

The lattice fluid approach, and Sanchez-Lacombe equation of state in particular, does well for systems of isotropic chains, such as aliphatic hydrocarbonds and most polymers. Conversely, compounds forming associations such as hydrogen bonds represent a particularly challenging class of solvents for the lattice fluid models. The assumption of mean-field nearest-neighbour interactions is central to the development of lattice fluid models, and is incongruent with the strong directional bonding seen in e.g. liquid alcohols and water. In figure 2.3, experimental vapour-liquid coexistence curves for dimethylether and methanol – chemical analogues without and with hydrogen bonding character, respectively – are compared against model fluids for the same compounds based on equations of state. Additionally, simulated vapour-liquid coexistence points for the TraPPE-UA molecular model are shown for each compound, as reported by Stubbs et al. [104] for dimethylether and Chen et al. [105] for methanol. The critical points are estimated from simulation data using the law of rectilinear diameters [106] with scaling exponents 0.325 and 0.28, respectively [104, 105]. Chen et al. [105] note use of a scaling exponent other than the Ising value of 0.325 due to the scaling law for polar compounds, an effect also observed in real fluids [107].

The accuracy of the Sanchez-Lacombe equation of state is seen to worsen from dimethylether to methanol, with significant deviations for liquid and critical densities. As mean-field equations of state, both the Sanchez-Lacombe and PCSAFT models predict scaling exponents that are too large, hence producing a more rounded shape near the critical point. Further, the molecular representation of methanol corresponds to a long-chain compound with $r = 10.73$, at odds with the chemical structure of the compound. This long-chain representation is a result of the Sanchez-Lacombe equation of state compensating for hydrogen bond formation in the real liquid. It is evident that the lattice fluid model has significant limitations in the representation of fluids with hydrogen bonding interactions.

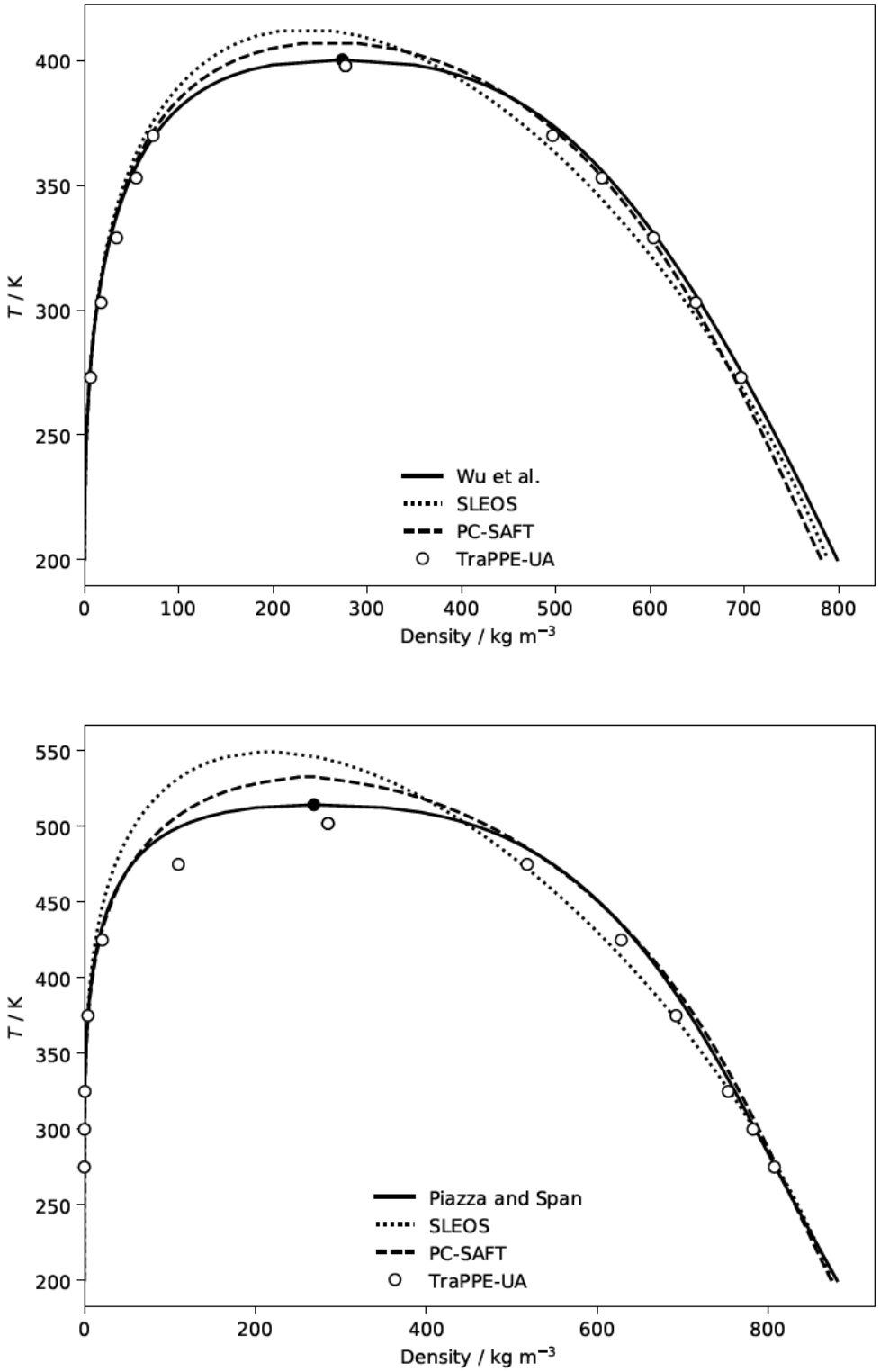

Figure 2.3: Vapour-liquid coexistence curves for dimethylether (top panel) and methanol (bottom panel) from 200 K to the critical point. Solid lines corresponds to the experimental correlations by Wu et al. [60] and Piazza and Span [61], with the filled circle indicating the critical point. Dotted lines indicate the Sanchez-Lacombe equation of state (SLEOS), with dimethylether parameters $r = 7.26$, $\epsilon^* = 3.226\,\mathrm{kJ\,mol^{-1}}$, $\nu^* = 7.302\,\mathrm{cm^3\,mol^{-1}}$, and methanol parameters from Sanchez and Lacombe [48]. Dashed lines indicates PC-SAFT with parameters from Gross and Sadowski [51]. Open circles indicate values for the TraPPE-UA model as reported by Stubbs et al. [104] for dimethylether and Chen et al. [105] for alcohols.

2.4.3 Statistically Associating Fluid Theory

The fluid properties of compounds forming hydrogen bonds and other strong interactions requires a different approach than the mean-field interactions of lattice fluid models. A more suitable model for describing such compounds is statistically associating fluid theory (SAFT), developed by Chapman et al. [108, 109]. SAFT builds on the work of Wertheim [110, 111, 112, 113, 114, 115], describing bonding of fluids with highly directional attractive forces. In SAFT, molecular species are described by their size, length, and mean-field interactions as for lattice fluids, but additionally by their capacity to form strong interactions (e.g. dimers) with other molecules. This allows the free energy of interactions such as hydrogen bonding to be accounted in a similar manner to the formation of chemical bonds.

The implementation of SAFT as an equation of state relies on an accurate description of a reference fluid, followed by one or more modifications to the interaction potential of the reference fluid implemented as perturbation terms. In the original work by Chapman et al. [108, 109] the hard sphere fluid reported by Carnahan and Starling [116] was used as reference. Perturbations to the reference fluid describing chain formation, dispersion interactions, and association interactions are added to give the overall Helmholtz free energy,

$$A = A^{\mathrm{id}} + A^{\mathrm{ref}} + A^{\mathrm{disp}} + A^{\mathrm{assoc}} \tag{2.50}$$

where the dispersion (disp) and association (assoc) terms rely on the radial distribution function of the underlying reference fluid (ref). The ideal contribution (id) is independent of implementation details, given by

$$A^{\mathrm{id}} = \sum_i \frac{\rho_i}{\rho} \ln\left(\frac{\rho_i}{\rho^\circ}\right) \tag{2.51}$$

where ρ° is the unit concentration. Equation 2.51 omits an additive constant accounting for the internal free energy of the molecules, similar to the parameter ω_i in equation 2.48. These internal degrees of freedom are assumed not to contribute to the observable thermodynamic properties of the system, in other words only intermolecular interactions are considered for the residual contributions to equation 2.50.

The association term A^{assoc} in equation 2.50 describes the Helmholtz free energy of directional bonding in the model fluid, as a function of bond formation. For a species with association sites* A and B on species i and j, the quantities X_{A_i} and X_{B_j} denotes the fraction of association sites *not* bonded in the system for the respective site and species. As shown by Michelsen and Hendriks [117], A^{assoc} can be expressed as

$$\frac{A^{\mathrm{assoc}}}{RT} = \sum_i \rho_i \sum_{A_i} (\ln X_{A_i} - X_{A_i} + 1) - \sum_i \sum_j \frac{\rho_i \rho_j}{\rho} \sum_{A_i} \sum_{B_j} X_{A_i} X_{B_j} \Delta^{A_i B_j} \tag{2.52}$$

with the added condition that

$$\frac{\partial A^{\mathrm{assoc}}}{\partial X_{A_i}} = 0 \tag{2.53}$$

*Note the use of non-italicised labels for association sites to distinguish from Helmholtz free energy.

for all X_{A_i}, i.e. that the bonding through association is at a stationary point with respect to free energy for all association sites. Equation 2.52 describes the law of mass action, governing the equilibrium of competing interactions of different interaction strength. The factor $\Delta^{A_iB_j}$ in equation 2.52 describes interaction strength between sites A and B on molecules i and j, and is of the form

$$\Delta^{A_iB_j} = g_{ij}(d)\kappa^{A_iB_j}\left[\exp\left(\epsilon^{A_iB_j}/k_BT\right) - 1\right] \tag{2.54}$$

with parameters κ^{AB} and ϵ^{AB} denoting interaction volume and interaction energy, respectively. Hence, SAFT equations of state require five parameters: three parameters for the reference fluid size, chain, and dispersion interactions, and two additional parameters for each association interaction.

Contributions from the reference fluid and dispersion interactions in equation 2.50 will depend on the potential employed in developing the equation of state. A number of approaches have been adopted, such as square-well potentials for the SAFT equation of state by Huang et al. [118, 119] and perturbed-chain PC-SAFT by Gross and Sadowski [51, 52], the Lennard-Jones potential in equation 2.6 for soft-SAFT developed by Blas and Vega [120, 121], or the Mie potential in equation 2.8 for variable-range SAFT-VR Mie by Lafitte et al. [122].

Each of these variants of SAFT builds on the same assumptions of thermodynamic behaviour, and has been employed to study a variety of complex fluid systems. The principal differentiating factor between SAFT equations of state is the balance of computational efficiency against sophistication. In a review of equations of state for carbon-capture applications, Diamantonis et al. [123] find PC-SAFT to perform particularly well for prediction of system behaviour without binary interaction parameters. Perez et al. [124] find similar performance for PC-SAFT and SAFT-VR-Mie in a comparison of equations of state for carbon capture applications.

2.4.4 PC-SAFT

In this work, perturbed-chain statistically associating fluid theory (PC-SAFT) [51, 52, 53] is employed as a general thermodynamic framework for the description of polymer, solvent, and solute species. The PC-SAFT equation of state is well suited for the representation of polymer systems [53], and shows good predictive capacity in the description of their solutions [125]. PC-SAFT performs well for modelling compounds relevant for carbon capture and sequestration applications [126], including CO_2 and H_2O which are central to the present study. In figure 2.3, the performance of PC-SAFT is compared against the Sanchez-Lacombe equation of state for vapour-liquid coexistence curves in dimethylether and methanol. The PC-SAFT model fluid improves the description of liquid states as well as the critical behaviour of both fluids. In figure 2.4, a similar comparison is made for water using parameters from Diamantonis and Economou [127], with the PC-SAFT model showing better performance both for liquid density and in the critical region. However, both equation

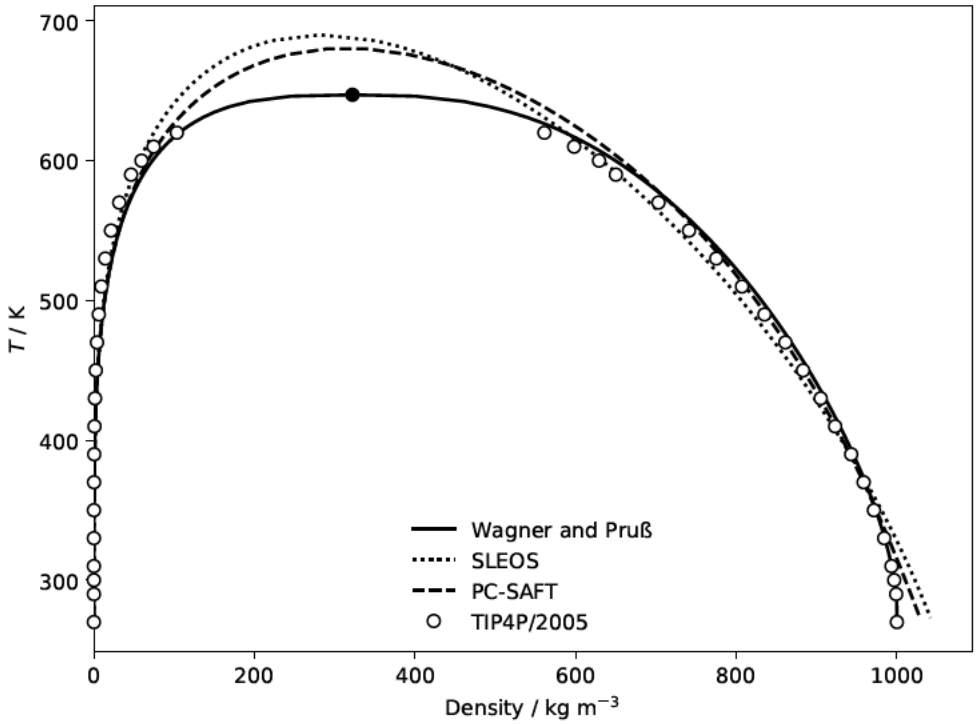

Figure 2.4: Vapour-liquid coexistence curve of water from 273 K to the critical point. Solid line corresponds to the experimental correlation by Wagner and Pruß [62] with the filled circle indicating the critical point. Dashed line indicates PC-SAFT with parameters from Diamantonis and Economou [127]. Dotted line indicates the Sanchez-Lacombe equation of state with parameters from Sanchez and Lacombe [48]. Open circles indicate simulated values for the TIP4P/2005 model as reported by Vega and Abascal [129].

of state models fail to reproduce the low-temperature density maximum of water. Conversely, molecular simulation with the TIP4P/2005 model [128, 129] produces near-quantitative agreement with experimental liquid densities along the saturation curve.

The PC-SAFT equation of state follows the perturbation-based approach described in equation 2.50, adopting the same hard-sphere-chain reference fluid as the SAFT equation of state described by Chapman et al. [108, 109]. Expressed in Helmholtz free energy, the reference fluid contribution to equation 2.50 is

$$A^{\mathrm{ref}} = \sum_i \frac{\rho_i}{\rho} \left[m_i A^{\mathrm{hs}} - (m_i - 1) \ln g_{ii}^{\mathrm{hs}} \right] \tag{2.55}$$

where the Helmholtz free energy A^{hs} and radial distribution function g^{hs} refers to the hard-sphere system described by Boublik [130] and Mansoori et al. [131]. Hard spheres are analytically more tractable than soft particles, and is used as the reference fluid, while further interactions described as perturbations to the hard-sphere fluid. Hence, any further interactions build on the assumption of hard spheres, which is a reasonable assumption for molecular systems. The hard-sphere Helmholtz free energy A^{hs} in equation 2.55 is given by

$$A^{\mathrm{hs}} = \frac{1}{\zeta_0} \left[\frac{3\zeta_1\zeta_2}{1-\zeta_3} + \frac{\zeta_2^3}{\zeta_3(1-\zeta_3)^2} + \left(\frac{\zeta_2^3}{\zeta_3^2} - \zeta_0 \right) \ln(1-\zeta_3) \right] \tag{2.56}$$

while the generic hard-sphere radial distribution function g_{ij}^{hs} for species i, j with segment diameters d_i and d_j given by

$$g_{ij}^{\mathrm{hs}} = \frac{1}{1-\zeta_3} + \frac{d_i d_j}{d_i + d_j}\frac{3\zeta_2}{(1-\zeta_3)^2} + \left(\frac{d_i d_j}{d_i + d_j}\right)^2 \frac{2\zeta_2^2}{(1-\zeta_3)^3} \tag{2.57}$$

at contact distance for the hard spheres. In equations 2.56 and 2.57, ζ_n is defined by

$$\zeta_n = \frac{\pi}{6}\sum_i \frac{\rho_i m_i d_i^n}{\rho} \tag{2.58}$$

for species i with exponent n equal to 0, 1, 2 or 3. The reference fluid system described by equations 2.55 - 2.58 is athermal, without interaction energies or other temperature-dependent parameters. This is modified by the introduction of a temperature dependence in the species-specific segment diameter d_i in equations 2.56, 2.57 and 2.58, given by

$$d_i = \sigma_i \left[1 - 0.12\exp\left(\frac{-3\epsilon_i}{k_B T}\right)\right] \tag{2.59}$$

describing the temperature-dependent effective collision diameter of the square-well hard-sphere system [51] as a function of size parameter σ and well depth ϵ. Equation 2.59 accounts for the decrease in effective particle size with the addition of interaction energy.

To bring the equation of state from non-interacting hard spheres to a system of interacting particles, a square-well interaction potential is used. The dispersion contribution to the Helmholtz free energy is based on Barker and Henderson perturbation theory [132] for the square-well potential with first- and second-order contributions. The Helmholtz free energy from dispersion interactions A^{disp} is given by

$$A^{\mathrm{disp}} = -2\pi I_1 \sum_i \sum_j \frac{\rho_i \rho_j}{\rho} m_i m_j \sigma_{ij}^3 \left(\frac{\epsilon_{ij}}{k_B T}\right) - \pi m C_1 I_2 \sum_i \sum_j \frac{\rho_i \rho_j}{\rho} m_i m_j \sigma_{ij}^3 \left(\frac{\epsilon_{ij}}{k_B T}\right)^2 \tag{2.60}$$

where I_1 and I_2 are integrals over the radial distribution function g_{ij}^{hc}. Unlike the hard-sphere system, no analytical solution to the hard-chain radial distribution function is available, and it is instead approximated as

$$I_1 = \int_1^\infty u(\mathbf{r}) g_{ij}^{\mathrm{hc}}(\mathbf{r}) \mathbf{r}^2 \,\mathrm{d}\mathbf{r} \approx \sum_{i=0}^{6} a_i(m)\eta^i \tag{2.61}$$

and

$$I_2 = \frac{\partial}{\partial \rho}\left[\rho \int_1^\infty u(\mathbf{r})^2 g_{ij}^{\mathrm{hc}}(\mathbf{r}) \mathbf{r}^2 \,\mathrm{d}\mathbf{r}\right] \approx \sum_{i=0}^{6} b_i(m)\eta^i \tag{2.62}$$

with the coefficients a_i and a_b regressed against molecular simulation data. Values for a_i and b_i can be found in Table 1 of Gross and Sadowski [51]. The factor C_1 in equation 2.60 is the hard-chain fluid compressibility [51], given by

$$C_1 = 1 + m\frac{8\eta - 2\eta^2}{(1-\eta)^4} + (1-m)\frac{20\eta - 27\eta^2 + 12\eta^3 - 2\eta^4}{(1-\eta)^2(2-\eta)^2} \tag{2.63}$$

where η in equations 2.61, 2.62, and 2.63 is the packing fraction, $\eta \equiv \zeta_3$. The reference and dispersion

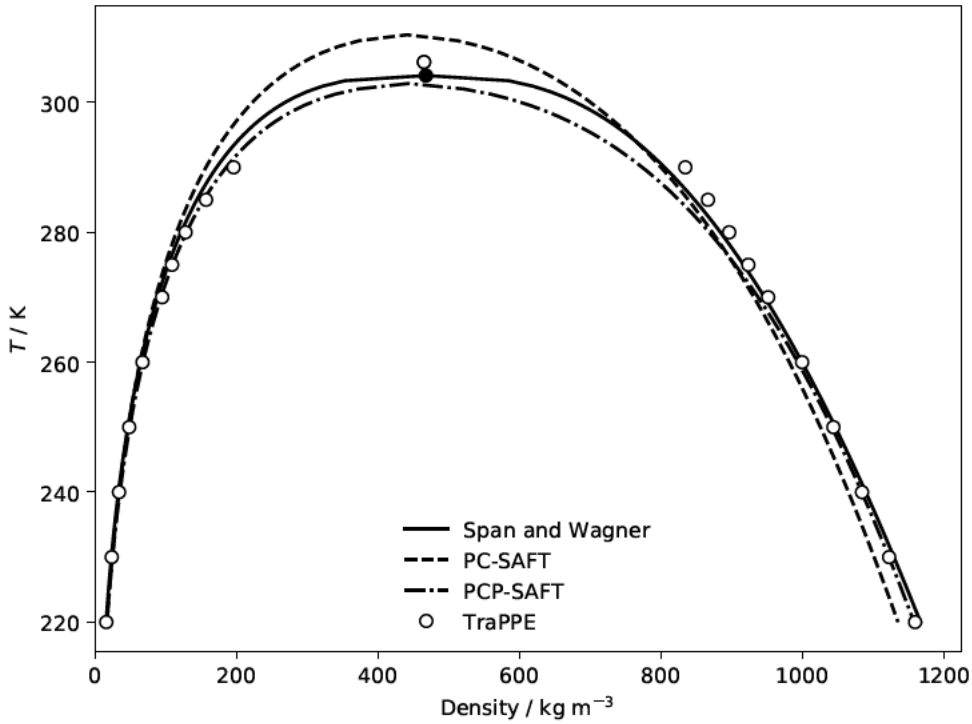

Figure 2.5: Vapour-liquid coexistence curve for CO_2 from 220 K to the critical point. Solid line corresponds to the experimental correlation by Span and Wagner [136] with the filled circle indicating the critical point. Dashed line indicates PC-SAFT with parameters from Gross and Sadowski [51]. Dash-dotted line indicates the PCP-SAFT equation of state with parameters from Gross [133]. Open circles indicate simulated values for the TraPPE model as reported by Potoff and Siepmann [137].

energies given by equations 2.55 and 2.60 are sufficient to describe non-associating molecules. For associating molecules, the conventional SAFT framework is used as described by equation 2.52, representing bonding for different combinations of species and association sites.

Extensions to the PC-SAFT equation of state have been made through the description of multipolar moments. Similar to the electrostatic interaction between formal charges described for molecular simulation, long-range interactions between polar molecules contribute to the system Helmholtz free energy. Gross [133] introduced a quadrupole-quadrupole term A^{QQ} regressed against simulation data for homonuclear Lennard-Jones dimers with point quadrupole moments, similar to the approximate integrals in equations 2.61 and 2.62. As shown in figure 2.5, the quadrupole-quadrupole interaction improves the model performance for CO_2 compared against PC-SAFT, with the largest improvement seen in the critical region. Similarly, a dipolar-dipolar energy contribution A^{DD} was introduced by Gross and Vrabec [134], and dipolar-quadrupolar energy contribution A^{DQ} by Vrabec and Gross [135]. Each multipolar moment requires one additional parameter for the molecular species, increasing both the data required for parameterisation and computational expense of the model.

The multipolar interactions described by PCP-SAFT can in some cases overlap with the association interactions described by the SAFT framework in equation 2.52. This is for example the case with water, which carries strong dipolar and quadrupolar moments whilst exhibiting strong hydrogen bonding behaviour.

As equation 2.50 relies on orthogonal contributions from each free energy component, it is unclear how species can be assigned both strong multipolar and associative character without double-counting interactions due to the similarity of association and directional polar interactions. In a study including H_2S-H_2O and CO_2-H_2O binary systems, Tang and Gross [138] argue that water should be modelled as an associative species without multipole moments, while CO_2 and H_2S should retain their multipole character. The authors find excellent agreement for phase equilibria in the two systems.

Nonetheless, a modified PCP-SAFT equation of state has been proposed for water by Ahmed et al. [139], incorporating a three-parameter temperature-correlated hard-core diameter replacing equation 2.59 and a dipolar fraction parameter delineating dipolar and associative contributions. While the expansion of equation of state contributions to equation 2.50 offers additional parameter space for complex systems, doing so is difficult to justify if putting the physical realism of the model at risk. Hence, the conventional PC-SAFT equation of state is employed in this work. Further refinements to the PC-SAFT equation of state include electrolyte contributions due to long-range electrostatic interactions between charged species. These free energy contributions will be discussed in chapter 4.

2.5 Implementation Details

Through sections 2.2 - 2.4, frameworks for molecular simulation and equation of state descriptions of fluid systems have been outlined allowing the construction of models for polymers and other compounds related to facilitated transport membranes. In order to use these frameworks for modelling of fluid systems, the framework implementations must also be considered. The practical considerations pertaining to implementation of molecular simulation and equation of state models differ considerably, as the former relies on efficient stochastic sampling of simple function with hundreds of free variables, and the latter with efficient solution strategies for functions with a handful of free variables but elaborate analytical expressions.

2.5.1 Molecular Simulation

The description of interactions potentials and simulation methods in sections 2.2 and 2.3 establish the physical basis for molecular simulation, yet the details of how this system description is interpreted differs depending on software implementation. In this work, the GROMACS software package [93] version 2018.8 is used for all molecular simulation. A leapfrog integrator with time step 0.2 fs is used to integrate the equation of motion described in section 2.2.5. The Lennard-Jones potential from equation 2.6 and Coulomb potential from equation 2.11 are truncated at 1.2 nm. As noted in sections 2.2.2 and 2.2.3, a mean-field correction is employed for long-range Lennard-Jones interactions and the smooth particle-mesh Ewald method of Darden [73] is used for long-range electrostatics. A grid spacing of 0.1 nm and cubic cardinal-B spline interpolation [140] is used for calculating the reciprocal space sum for the particle-mesh Ewald method. For weak coupling algorithms as

described in section 2.2.5, a temperature coupling time constant of 2 ps and pressure coupling time constant of 5 ps are employed according to their respective GROMACS implementations [93]. Examples of GROMACS parameter files are provided in appendix A.

For free energy calculations (section 2.3) and accelerated sampling (section 2.3.4, multiple states are evaluated in a single simulation. Free energy calculations are carried out using the Bennett acceptance ratio method. For soft core scaling described by equation 2.32, the 1-1-6 pathway is employed with scaling factor $\alpha = 0.5$ and soft-core parameter $\sigma = 0.3$ nm. Unless otherwise noted, a 21-state λ schedule is employed for particle insertion, with the Lennard-Jones and Coulomb potentials switched independently and a λ spacing of 0.1 between states. For accelerated sampling, the replica exchange method described by equation 2.34 is used, as illustrated in figure 2.6. Exchange between neighbouring systems is attempted every 100 ps.

Further to the software implementation details and parameters described above, evaluation of thermodynamic averages from molecular simulation requires careful consideration of system size, time scale, and ensuring the system ensemble sampled corresponds to true thermal equilibrium. All systems considered in this work are isotropic, and a cubic simulation box with periodic boundary conditions [93] is employed for representing the bulk fluid. As there is some influence of finite-size effects in the simulation of electrolyte solutions [141], a fixed system diameter of approximately 3.2 nm is employed for all simulations. For pure water, this corresponds to 1070 molecules. Particle numbers in mixed solvent and electrolyte systems are adjusted to yield consistent system sizes, with further detail provided in subsequent chapters.

For estimation of simulation time scales and ensuring convergence to true thermodynamic equilibrium, the method of Chodera [142] for automatic equilibration detection is employed. This approach takes advantage of the fact that correlation times tend to be long in a system progressing towards equilibrium, and relatively shorter once the system is fluctuating around equilibrium. By maximizing the number of statistically uncorrelated samples, the initial period of system equilibration can be discarded. This approach is illustrated in figure 2.6. Similarly, the total simulated time for simulations is chosen based on the observed correlation time of the system. Total system energy, comprising interaction potentials, kinetic energy, and pressure-volume work, is used as the observable for monitoring system correlation times.

2.5.2 Equations of State

The implementation of equations of state for phase equilibrium calculations describes how to solve equation 2.42 for two or more phases. Unlike molecular simulation where thermodynamic observables are estimated by averages, equations of state give exact numerical solutions (to within the precision of the data types used for calculation). Hence, for equations of state there is no consideration to statistical convergence, but rather ensuring efficient evaluation of Helmholtz free energy and its derivative thermodynamic functions presented in section 2.4.1.

In order to efficiently evaluate thermodynamic functions for a variety of systems and equations of state,

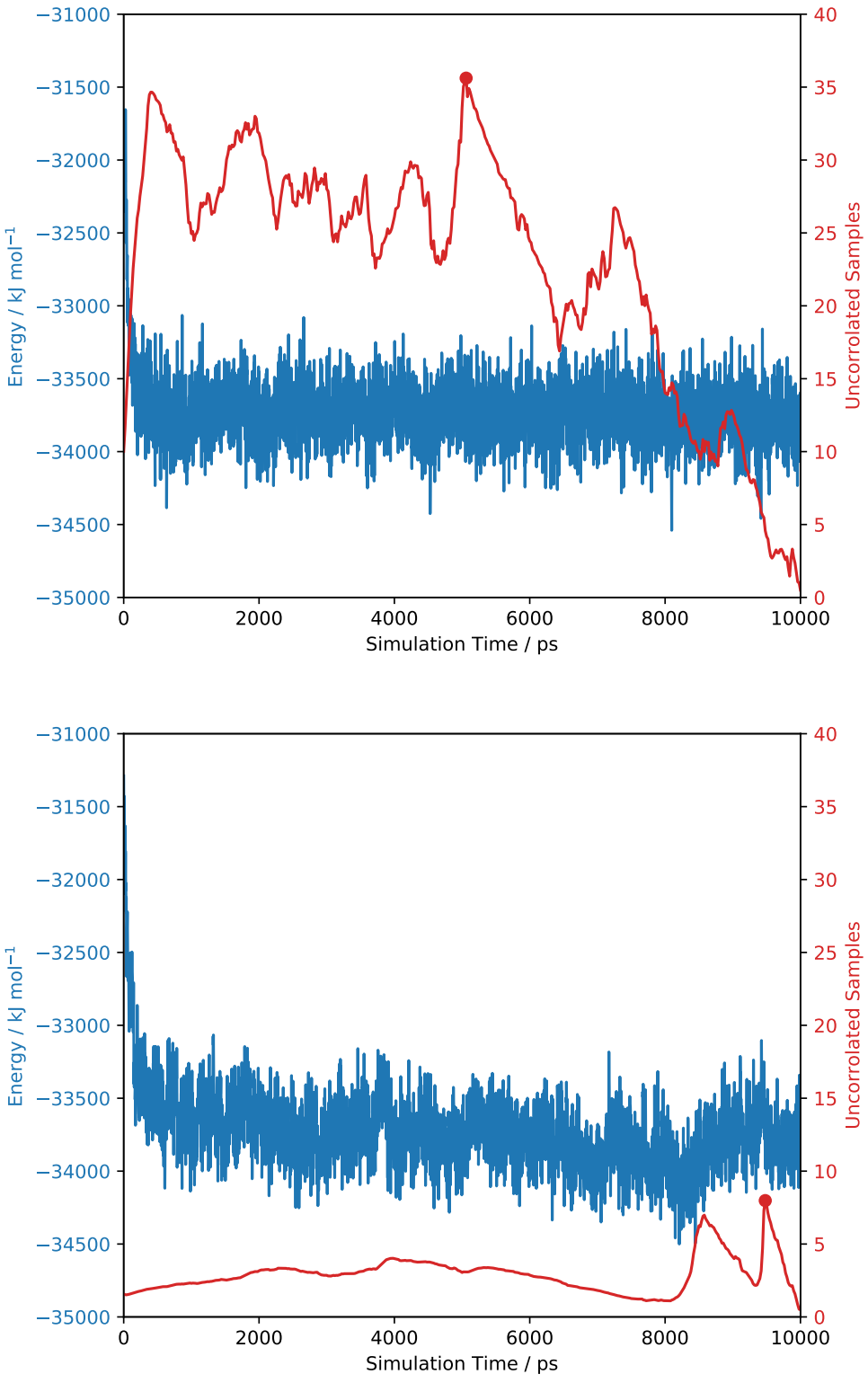

Figure 2.6: Equilibration of total system energy and corresponding statistically uncorrelated samples for simulations of polyethylene oxide oligomers in water (0.2 water mass fraction) at 298 K. Top panel: replica exchange molecular dynamics, showing a maximum of 36 uncorrelated samples after 5 ns of simulation. Bottom panel: conventional molecular dynamics, showing a maximum of 8 uncorrelated samples after 9.5 ns of simulation. The maximum in uncorrelated samples occurring at the tail end of the simulation suggests incomplete convergence towards thermodynamic equilibrium. Further detail of the molecular models used is given in chapter 3.

a generic equation of state solver was implemented in Python using the SymPy [102], NumPy [143], and SciPy [144] libraries. The equation of state is implemented using an object-oriented approach, where each state contains a number of species with molecular parameters attached as object attributes. The Helmholtz free energy expression $A(T, \rho_i)$ is dynamically updated according to system composition. Arbitrary constraints may be enforced through SymPy expressions, with a commonly encountered example being $T' = T''$, $p' = p''$, and $\mu_i' = \mu_i''$ for a two-phase system at the vapor-liquid equilibrium line.

Through differentiation using SymPy symbolic variables T and ρ_i, thermodynamic functions from section 2.4.1 are calculated on-the-fly according to the current system composition. For determination of state points through constraints, the symbolic constraint functions are converted to NumPy functions and solved with a multivariate numerical root finder using the Powell method [144]. A reasonable initial guess of the system states is required, obtained from experimental or simulation data as available. The implementation strategy is illustrated in figure 2.7.

2.6 Summary

In this chapter, frameworks for representing fluid systems have been presented based on molecular simulation and molecular equations of state. In both cases, these frameworks use model fluids represented by molecular parameters describing the interactions of species in the system. The use of model fluids allow description of complex system under arbitrary physical conditions, in turn permitting investigation into the thermodynamic properties which may be inaccessible or impractical to study using experimental methods. In this work, model fluids will provide a means to investigate facilitated transport membranes and related systems.

A general system description was provided for molecular simulation, imitating the geometries and interactions of real compounds. Molecular simulation represents a general and predictive framework for representing fluid systems, provided molecular interactions can be represented by classical interaction potentials. The functional forms used for interaction potentials were presented in sections 2.2.2 - 2.2.4, modelled after quantum mechanical interaction energies. Methods for simulation in the isothermal-isobaric ensemble were reviewed in section 2.2.5, which will be used for simulation of fluid systems in chapters 3 - 6. Molecular simulation can also be used for free energy calculations, with sections 2.3 - 2.3.2 presenting the principles of perturbation theory together with soft-core scaling of dispersion potentials and the Bennett acceptance ratio estimator for free energies, which will be used in chapters 4 and 5 to calculate solvent activity and gas solubility in fluid systems.

In contrast to the stochastic nature of molecular simulation, molecular equations of state provide an analytical mean-field description of fluid interactions and the resulting Helmholtz free energy. Molecular equations of state represent a further simplification of model fluids relative to molecular simulation, but come with the advantage of exact solutions and significantly reduced computational expense. In section 2.4.1,

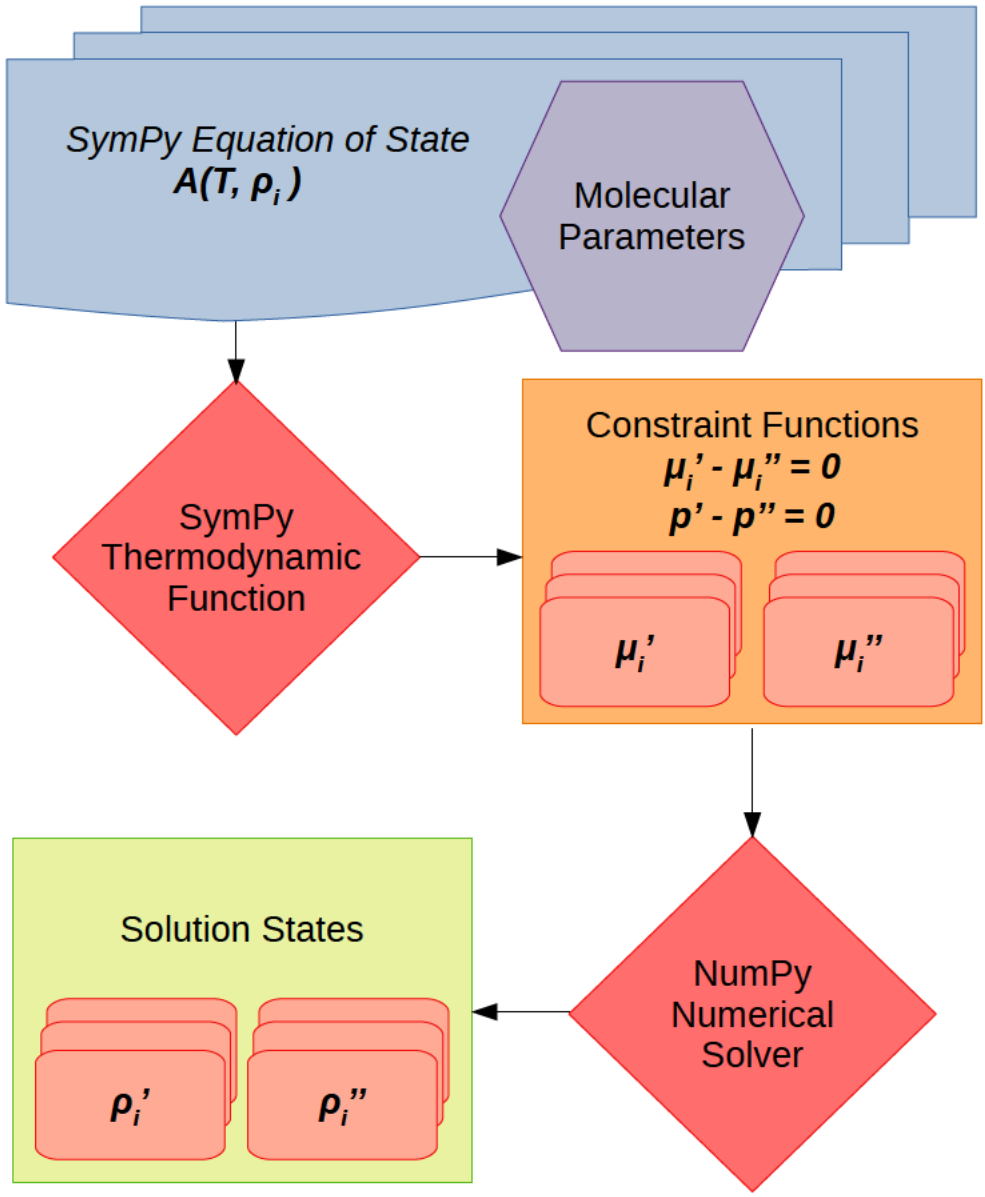

Figure 2.7: Implementation strategy for object-oriented equation of state solver. The Helmholtz free energy expression is generated using SymPy symbolic expressions based on system composition and associated molecular parameters. Symbolic differentiation is used to generate constraint functions, according to the phase equilibrium considered. Examples of chemical potential and pressure are shown, but any constraints may be enforced, connecting an arbitrary number of phases. The constraints are converted to NumPy functions and solved using a multivariate root finder to yield the solution states.

the Helmholtz free energy of molecular equations of state is connected to other thermodynamic functions, allowing calculation of observable properties for model fluids. Two molecular equations of state, based on the lattice fluid and SAFT theories, are presented in sections 2.4.2 - 2.4.4 together with comparisons of their performance in representing small-molecule solvents at saturation conditions. Based on its performance for solvents together with extensive use for polymer systems in literature, the PC-SAFT equation of state is adopted for use together with molecular simulation in subsequent chapters, describing polymer systems in chapter 3 and a variety of aqueous-organic fluid mixtures in the remaining chapters.

Chapter 3

Models of Polymers and Polymer-Water Solutions

3.1 Overview

This chapter examines the properties of polymers and their interactions with water, with the objective of establishing a predictive modelling approach for hydrophilic polymers and their aqueous solutions. Molecular simulation is used in combination with the PC-SAFT equation of state to develop model parameters for the well-understood polymers polyethylene oxide (PEO) and polyvinyl alcohol (PVA). The same approach is employed for prediction of solution properties of aqueous polyvinylamine (PVAm), allowing model parameters to be generated for the description of polymer-water systems encountered in facilitated transport membranes, where experimental data are lacking.

In order to build representative models for polymers, the phase behaviour and physical properties of pure polymer systems are first reviewed in section 3.2. Pure polymer ρpT behaviour is discussed in the context of the glass-rubber and rubber-melt transitions frequently encountered in polymer systems. The thermodynamics of polymer solutions are introduced together with the notion of upper and lower critical solutions temperatures. The classical Flory-Huggins model of polymer solutions is used to illustrate solubility as a function of polymer-solvent interaction strength.

Next, literature approaches to molecular simulation of pure polymer and polymer-solvent systems are reviewed in section 3.3, ranging from detailed atomistic models to coarse-grained representations of polymer beads. Key findings from molecular simulation include the slow diffusive dynamics of polymer-solvent systems, together with the importance of solvent-polymer hydrogen bonding in typical aqueous polymer solutions. A selection of available model parameters is considered in section 3.3.1, with the TraPPE-UA model chosen as a suitable compromise between molecular detail and accuracy in reproducing physical data for small molecules.

Additional parameters for the TraPPE-UA model, describing amine torsional interactions, are developed in section 3.3.2 on the basis of *ab initio* data for small-molecule amines to permit the representation of polyamines seen in facilitated transport membranes.

In section 3.4, the TraPPE-UA polymer models are used to simulate pure polymer ρpT behaviour for PEO, PVA, and PVAm over a wide range of temperatures and pressures. The simulated data are compared against experimental ρpT data for PEO and PVA, and used to regress molecular parameters for each of the three polymers. The hybrid molecular simulation / equation of state approach is found to have comparable accuracy with parameter regression from experimental data. However, glass-rubber and rubber-melt transitions are not observed in the simulation data for any of the polymers.

Further, polymer-water systems are simulated for PEO, PVA, and PVAm, producing liquid densities across a wide range of compositions and temperatures. For PEO, simulated solution densities and the resulting equation of state model are in good agreement with experimental sources. Aqueous PVA does not show the same conformity, due to a gradual experimental transition to the glass state that is not captured by either of the molecular models. PVAm is found to behave similarly to PEO, mirroring the similarities between small-molecule amine and ether compounds.

This chapter demonstrates that molecular simulation ρpT data can be used in a manner similar to experimental measurements, or as a complementary source of data, for the development of equation of state parameters. In order to provide sufficient accuracy for engineering applications, the models developed from molecular simulation should show consistent qualitative behaviour with experiment, and offer quantitative accuracy comparable with the tolerances of the application. For facilitated transport membranes, water activity and corresponding hydration levels is a primary parameter determining process performance. Based on water absorption characteristics [145] a solvent activity within 10% is deemed acceptable for a predictive model.

Using molecular simulation as an alternative data source allows prediction of thermodynamic properties where experimental data are unavailable, exemplified by PVAm found in facilitated transport membranes. The parameters developed in this chapter form the basis of polymer-water systems studied in chapter 6, detailing reactive absorption in PVAm.

3.2 Polymer and Polymer Solution Thermodynamics

The thermodynamic properties of polymers are determined by their chemical structure, chain length, and degree of branching or cross-linking between chains. Depending on the rigidity of the polymer and strength of monomer-monomer interactions, polymers can be dense or porous, have a rigid or flexible structure, and high or low melting points. Most polymers can exist in multiple states depending on temperature, pressure, and chain length, and undergo rapid changes in thermal expansivity and other properties at the transition temperature. While these states have different thermodynamic properties, they are not necessarily separate

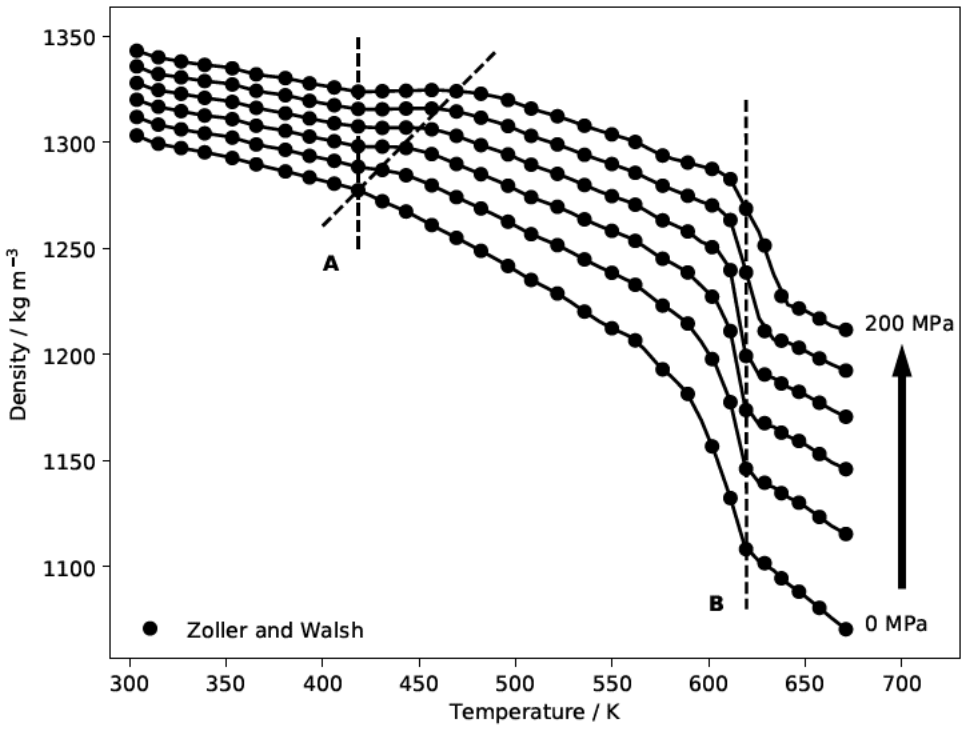

Figure 3.1: Glass-rubber and rubber-melt transitions in polyether ether ketone determined from ρpT behaviour. Solid symbols indicate experimental data from Zoller and Walsh [146] for isobars at 0 MPa, 40 MPa, 80 MPa, 120 MPa, 160 MPa, and 200 MPa, with higher pressures corresponding to higher densities as indicated. Solid lines are to guide the eye. **A**: The vertical dashed line indicates T_g, the zero-pressure glass-rubber transition temperature. The diagonal dashed line indicates the beginning of the melt phase. **B**: The vertical dashed line indicates T_m, the zero-pressure rubber-melt transition temperature.

phases for the material, and transitions can be somewhat dispersed in temperature. Figure 3.1 illustrates the different states of typically encountered by polymers, by displaying density isobars for polyether ether ketone (PEEK) over a wide range of temperatures and pressures.

At low temperature, polymers occupy a glassy or semi-crystalline state [147, 148] with solid-like properties. The polymer is brittle and exhibits limited hysteresis upon deformation. The glassy state is shown for PEEK figure 3.1 in the temperature range 300 K - 420 K. Some polymers incorporate crystalline regions in the glassy phase, as seen for microcrystalline cellulose [149]. High-permeability gas separation membranes are commonly in the glassy state [9, 26], with high-permeability polymers often showing poor packing efficiency which creates sufficient mobility for gas species to permeate through the membrane.

With increasing temperature many polymers enter a more flexible rubber state. The resulting materials are sometimes denoted elastomers. The rubber state is elastic rather than brittle, and is characterised by a rapid increase in thermal expansivity near the glass-rubber transition temperature. The rubber state is also more compressible than the glassy state. The glass-rubber transition is illustrated in figure 3.1 for PEEK at 420 K. Rather than a clean transition from one state to the other, the glass-rubber transition may involve a sequence of metastable states where material properties gradually change, as seen for PEEK along high-pressure isobars.

The rubber state is commonly explained by the tube model [150] of elasticity. In the tube model, each

polymer chain is confined by interactions with surrounding chains, constraining its movement. The polymer can wiggle free from any given tube - termed reptation [151] - but the timescale of this process scales with the energy of the chain constraints. As thermal energy RT increases, these constraints no longer limit available polymer configrations and the timescale of polymer movement reduces drastically.

At high temperatures, polymers melt to form a liquid phase. The melt phase is normally significantly lower in density than the glass or rubber states. Unlike crystalline solids, the melting process is a continuous transition, as seen in figure 3.1 for PEEK near the melting temperature of 620 K. In the melt phase, the polymer behaves like a liquid with no elasticity or hysteresis upon deformation.

Further to the glass, rubber, and melt phases described above, some polymers encounter a nematic mesophase, and many polymer mixtures exhibit complex phase behaviour [152]. These states, although interesting in their own right and relevant to the construction of gas separation membranes using co-polymer or hybrid membranes, will not be discussed further here.

Like solvents, polymers also readily form mixtures with compounds of similar chemical character. The properties of polymer-solvent systems vary widely depending on the compounds involved, ranging from supercritical polystyrene-CO_2 used for closed-cell polystyrene foam extrusion, to polyethyelene oxide-water used as a biomedical drug delivery agent [153]. Here, we are interested in polymer solutions, due to their importance for hydration phenomena observed in facilitated transport membranes [30, 35]. Similar to solvents, polymer-solvent mixtures can either be continuously soluble or form a two-phase system depending on physical conditions. In figure 3.2, the phase diagram of polystyrene-acetone is shown to illustrate typical features of polymer-solvent phase behaviour.

The phase diagram of polymer-solvent systems can be grouped into three regions. At low temperatures, polymer-solvent mixtures form polymer-rich and polymer-lean phases. Solubility in this region is determined by the strength of polymer-solvent interactions [155]: for systems where solvent-solvent interactions are energetically favourable, a limited amount of polymer can be dissolved. As temperature increases, so does the entropic contribution to polymer solvation, increasing solubility. Above the upper critical solution temperature (UCST), all polymer-solvent compositions form a continuous phase. The two-phase envelope and UCST can be observed for the 4800 g mol^{-1} and 10 300 g mol^{-1} polymer fractions in the lower portion of figure 3.2. For the lower molecular weight polymer, the entropic contribution is greater and so the UCST occurs at a lower temperature.

At high temperatures, entropic contributions to polymer solvation become dominant, driven by the thermal expansion of polymer and solvent compounds [154]. For polymer-solvent mixtures with large differences in thermal expansivity, the system undergoes a second phase separation once it reaches the lower critical solution temperature (LCST). This can be seen for the 4800 g mol^{-1} and 10 300 g mol^{-1} polymer fractions in the upper portion of figure 3.2. The LCST for the lower molecular weight polymer occurs at a higher temperature due to the increase in expansivity [154].

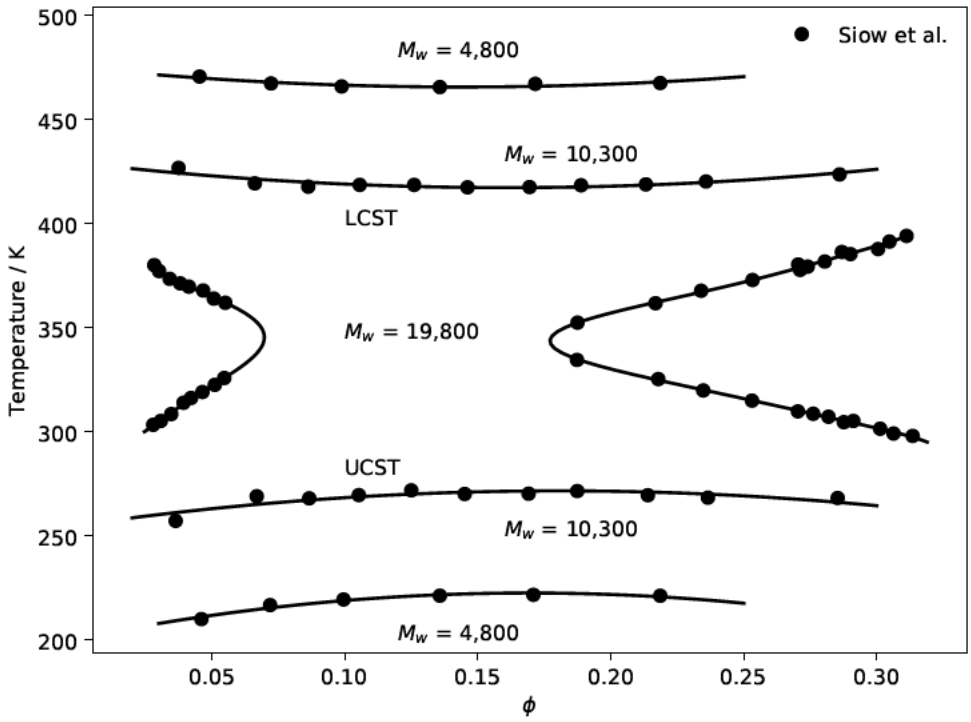

Figure 3.2: Polystyrene-acetone phase diagram as a function of temperature and solvent volume fraction. Solid symbols indicate experimental values from Siow et al. [154] at saturated vapour pressures. Solid lines are a guide to the eye. At molecular weights of 4800 g mol^{-1} and 10 300 g mol^{-1}, the solution forms continuous UCST and LCST curves. At 19 800 g mol^{-1} the two curves merge to create an hourglass-like contour, with intermediate solvent volume fraction systems always forming binary phases.

For certain solvents and polymer chain lengths, the UCST and LCST may join to form an hourglass-shaped phase diagram. These polymers never fully dissolve, despite significant solubility in their respective phases. This phenomenon is seen in figure 3.2 for 19 800 g mol^{-1} polystyrene-acetone solutions. Hence, the phase behaviour of polymer-solvent systems is sensitive to chain length, with short-chain polymer generally being more soluble and across a wider range of temperatures. This is important for the construction of hybrid polymer membranes, where the hydrophilic layer should resist dissolution in order to avoid structural damage. It also informs the simulation of polymer-solvent systems, where short-chain polymer is more likely to remain soluble over a wider range of conditions.

3.2.1 Solvent Activity in Polymer Solutions

The polystyrene-acetone mixtures examined in figure 3.2 illustrates the phase behaviour of polymer-solvent systems, but does not aid in determining the solvent activity in these systems. Solvent activity a_s is defined for a given temperature as

$$\ln a_i = \frac{\mu_i - \mu_i^\circ}{RT} \tag{3.1}$$

where μ_i° is the chemical potential at the chosen reference state. Unless otherwise noted, the neat solvent at saturation pressure is chosen as the reference state here.

To determine vapour-liquid water absorption in facilitated transport membranes, we need to describe the polymer-solvent composition as a function of solvent activity. The lattice fluid description of polymers, described in section 2.4.2, was the first model to provide a quantitative explanation of solvent activity in polymer solutions. Flory [156] and Huggins [157] each developed a theoretical description for the free energy of mixing in these systems. Flory-Huggins theory is based on a chain-like description of polymer-solvent systems, where each molecule occupies a fixed number of lattice sites as illustrated in figure 2.2. Upon mixing, the two species will populate the lattice according to their concentration and chain length. The resulting entropy change for polymer-solvent solutions is calculated combinatorially based on the lattice site fraction ϕ occupied by each species, given by

$$\phi_i = \frac{r_i N_i}{\sum_j r_j N_j} \tag{3.2}$$

where r denotes the number of sites occupied by a molecule and N is the number of molecules. For an athermal system where the energy of polymer-solvent interactions is the same as for each individual species, the Gibbs energy of mixing is purely entropic:

$$\frac{\Delta G}{RT} = -\frac{\Delta S}{R} = \sum_i N_i \ln \phi_i \tag{3.3}$$

which reduces to the ideal entropy of mixing in the case of $r_i = 1$ for all species.

Flory-Huggins theory may be used for describing mixtures of e.g. aliphatic polymers with aliphatic solvents, but has limited application to polymer-solvent systems where interaction energies between unlike species vary. To remedy this deficiency, a second-order semiempirical correction to equation 3.3 can be used:

$$\frac{\Delta G}{RT} = \sum_i N_i \ln \phi_i + \sum_{ij} \chi_{ij} \phi_i \phi_j (r_i N_i + r_j N_j) \tag{3.4}$$

where the Flory-Huggins binary interaction parameter χ_{ij} encodes the strength of interactions between unlike species relative to those of like species. This adjustable parameter allows regression of solvent-polymer interaction strength against experimental data, for example based on solvent activity in polymer-solvent mixtures. In figure 3.3, solvent activity in polystyrene-toluene and polystyrene-butanone solutions is plotted as a function of solvent weight fraction, and correlated using equation 3.4. Toluene and polystyrene both comprise the aromatic benzene group, while butanone has a polar ketone group. The polystyrene-toluene system has $\chi = 0.43$, while polystyrene-butanone has $\chi = 0.69$, indicating greater differences between polymer-solvent interactions. Hence, toluene is more readily absorbed by polystyrene, resulting in a greater solvent weight fraction for a given activity compared against butanone.

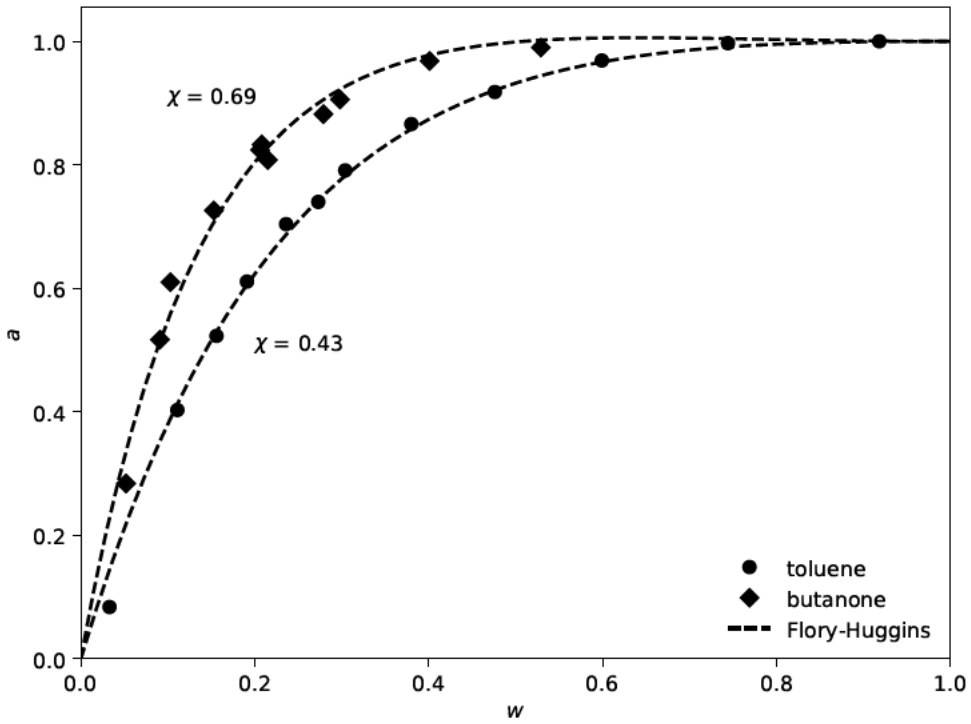

Figure 3.3: Solvent activity as a function of solvent weight fraction for polystyrene-toluene and polystyrene-butanone solutions. Experimental values from Bawn et al. [158] for $M_w = 290\,\mathrm{kg\,mol^{-1}}$ polystyrene at 298.15 K and 101.325 kPa. Dashed lines indicate solvent activity correlated using equation 3.4 with r = 2785 calculated from the unit formula of polystyrene. Values for χ are regressed against experimental data for each solvent using a least-squares approach.

3.3 Simulation of Polymers and Polymer Solutions

Simulation of polymers and polymer-solvent systems has received continual interest since the early works of Ryckaert and Bellemans [159, 160], and Rapaport [161, 162] on short-chain aliphatic polymers. Practical applications of polymer molecular simulation are largely limited by inefficient sampling of configurational space and the long correlation times in these systems. The systems accessible through molecular simulation can to a certain extent be extended through the use of coarse-grained models, illustrated in figure 3.4.

Significant progress was made by de Pablo et al. [163] for molecular simulation of polymer melts and rubbers using Monte Carlo algorithms through the development of the continuum configurational bias algorithm. Continuum configurational bias spontaneously re-grows polymer chains during a simulation. These 'unphysical' moves allow torsional energy barriers to be overcome at faster rates. However, both Monte Carlo and molecular dynamics approaches are used to study polymer systems, provided configurational degrees of freedom can be sampled in an efficient manner. Compared with Monte Carlo approaches, molecular dynamics has the benefit of also providing kinetic data. A detailed investigation in the use of molecular dynamics to obtain structural and kinetic properties of pure polymer systems was made by Brodeck et al. [164], simulating polyethylene oxide in the melt phase ($T = 375\,\mathrm{K}$) using a fully atomistic model. Both structural and kinetic properties were found to be in good agreement with experimental quasielastic neutron scattering data.

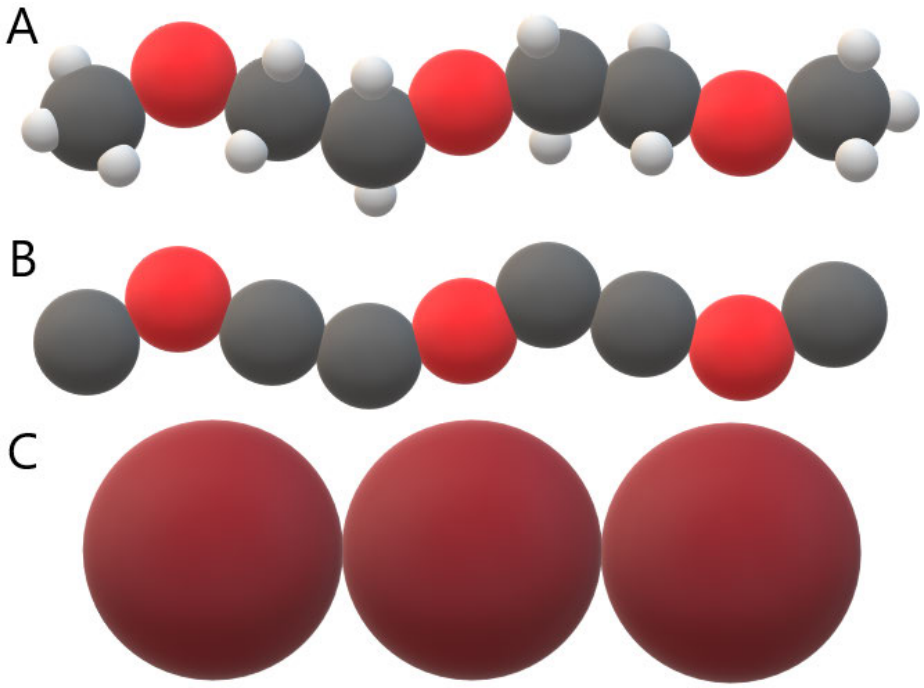

Figure 3.4: Schematic comparison of molecular model resolutions, exemplified by a polyethylene oxide (PEO) oligomer. A: Fully atomistic molecular model, e.g. OPLS-AA. B: United-atom model with hydrocarbon groups represented by a single site, e.g. TraPPE-UA. C: Coarse-grained model with each monomer unit represented by a single site, e.g. Martini force field.

Conversely, experimental ρpT data for polymer melts may be used to optimise interaction potentials for molecular models. This has been explored e.g. for linear alkanes by Widmann et al. [165] using a united atom model and Krishna Pant et al. [166] with an anisotropic united atom model. Rosi-Schwartz and Mitchell [167] additionally incorporated neutron scattering data to optimise bond lengths and angles for polyethylene. Coarse-grained representations are often developed based on the iterative Boltzmann inversion technique [168].

Simulation of polymer-solute systems and polymer solutions faces similar challenges as for polymer melts. By employing the continuum configurational bias method together with Widom insertion as outlined in section 2.3.1, de Pablo et al. [169] estimated solubility constants for small hydrocarbons in polyethylene, obtaining good agreement with experimental values. A later study by van der Vegt [170] considered solubility of chloroform in swollen polydimethylsiloxane, employing a thermodynamic perturbation approach similar to that presented in section 2.3.2. Sorption of CO_2 in polystyrene, and resulting glass-rubber transition, has been studied using molecular simulation by van der Vegt [171], with phase equilibrium calculated based on the Widom insertion technique. Spyriouni et al. [172] later studied the same system using a direct particle deletion method, the inverse process of Widom insertion.

In a recent review of simulation approaches to sorption and diffusion in glassy polymers, Vergadou and Theodorou [173] highlight both Monte Carlo and molecular dynamics as valid methods for studying these systems. The authors stress the importance of multi-scale approaches due to the complexity of polymer

systems, suggesting a combination of coarse-grained and atomistic models. Comparison between experimental data, simulation, and theoretical frameworks has been done e.g. by Dodd and Theodoru [174] for polyethylene, finding good agreement between simulation and experiment.

Multiple authors have simulated aqueous-polymer and alcohol-polymer solutions with emphasis on structural and dynamic properties. Müller-Plathe and van Gunsteren [175] studied the solvation of polyvinyl alcohol in water and ethanol, finding preferential hydrogen bonding between the polymer chain and water. Müller-Plathe [176] later simulated water-PVA and ethanol-PVA solutions to study the diffusion properties of pervaporation membranes, finding random-walk dynamics dominating at high water content, transitioning to a site hopping mechanism at high polymer content. A Mackie-Meares lattice model [177, 178] was found to explain the diffusive mechanics across a wide range of water contents, with the solvent diffusion constant D related to the bulk diffusion constant D° by

$$D = D^\circ \left(\frac{1-\phi}{1+\phi} \right)^2 \tag{3.5}$$

where ϕ is the polymer lattice site fraction, corresponding to volume fraction for non-lattice systems. Further to the slow limiting diffusivity in polymer, there is significant evidence of anomalous diffusive behaviour occuring at small timescales in these systems, reported by Müller-Plathe et al. [179] for gases in polyisobutane. Anomalous diffusion regimes originate from the different length scales encountered in polymer-solvent systems: since solvent rearrangement occurs on a much smaller timescale than chain conformational changes, overall diffusive mechanics are a combination of fast and slow degrees of freedom.

Transport in aqueous polymer systems has more recently been studied by Fayon and Sarkisov [45], reporting similar anomalous diffusion regimes for solvent transport in partially protonated PVAm using a fully atomistic model. Similar behaviour was found by Gusev et al. [180] for diffusion of small gases in polycarbonate and polyisobutylene, and underlines the long timescales required for simulating polymer-solvent systems without accelerated sampling techniques. A review of polymer-solvent diffusion by Amsden [181] concluded that most polymer-solvent systems can be described by an obstruction scaling model,

$$D = D^\circ \exp\left[-\pi \left(\frac{r_\mathrm{s} + r_\mathrm{f}}{\kappa/\phi + 2r_\mathrm{f}} \right)^2 \right] \tag{3.6}$$

where r_s is the solvent radius, r_f is the polymer chain radius, and κ is a polymer-specific adjustable parameter. In both equation 3.5 and 3.6, solvent diffusion is dramatically reduced as polymer content increases.

Further to structural and kinetic properties, molecular simulation may be used to predict solubility and solvation effects in polymer solutions. However, a limited number of studies report solubility in polymer solutions based on molecular simulation, and there is no consensus method for obtaining this property. Solubility of water in polymers was investigated by Nick and Suter [182] for PVA and polycarbonate using a combined Widom insertion and thermodynamic integration approach. While this method allowed the authors

to distinguish between the hydration behaviour of the two polymers, quantitative agreement with experimental systems was limited. The thermodynamics of the PVA-water system was investigated by molecular simulation by Wu [183], finding a lowering of glass transition temperatures in the binary system consistent with experimental values. PVA-water was found to be miscible for the temperatures considered, matching the experimentally observed behaviour [184]. Simulations of water and ethanol sorption in PVA were performed by Qiao et al. [185], investigating the optimal conditions for ethanol dehydration. Molecular simulation can also be used to investigate structural modifications. Chiessi et al. [186] simulated PVA hydrogel (polymer volume fraction of 0.12), finding that cross-linking had essentially no significant impact on system behaviour.

Hydrogen bonding is central to the polymer hydration phenomena seen in hydrophilic polymers. Dormidontova [187] used a combined simulation and experimental approach to study hydrogen bonding in PEO-water mixtures, finding hydrogen bond strength could explain the closed-loop upper/lower critical solution temperatures (UCST/LCST) of this system. Similar systems were considered qualitatively by Zhang et al. [188], investigating swelling of ternary PVA mixtures with water and ethanol. PVA was found to preferentially associate with water rather than ethanol, helping explain the selectivity of PVA for water-ethanol pervaporation.

Simulation of polymer and polymer-solvent systems is a complex field of study due to the long correlations of these systems in both space and time. Care must be taken to ensure proper sampling of their configurational states, and accelerated sampling techniques are frequently employed to aid the convergence of thermodynamic properties. This is also reflected in the interaction potentials used for polymer systems, with coarse-grained representations allowing larger systems or longer timescales to be studied.

3.3.1 Classical Models of Polymer Systems

In the previous section, we considered a selection of molecular simulation approaches to polymer systems as well as their solutions, covering a broad range of systems and properties. This section further elaborates on the interaction potentials used for molecular simulation of polymers, their construction, and their suitability for describing the thermodynamics of pure polymer and polymer solutions.

Classical molecular models allow simulation of a wide range of systems, and have long seen application for studying polymers. The early works of Ryckaert and Bellemans [159, 160] used a united-atom model to characterise n-alkanes, giving a first molecular view of thermodynamic and kinetic properties in these systems. A more refined molecular model, now known as optimised potentials for liquid simulations (OPLS) was developed by Jorgensen et al. [189], providing parameters for branched, unsaturated, and aromatic hydrocarbons based on liquid densities and heats of vaporization. A large number of refinements for united-atom models have been developed since. The model by Berger et al. [190] was optimised for lipid bilayers in organic systems. Toxvaerd [191] proposed an anisotropic adjustment to better represent methylene groups, giving improved agreement for vapour pressures. A further refinement was proposed by Ungerer et al. [192], with improvements to liquid densities, vapour pressures, and enthalpies of vaporization over a wide temperature

range. This family of potentials is known as anisotropic united atom (AUA), and has a number of extensions including alcohols [193], ethers [194], amines [195, 196], and alkanolamines [197].

The OPLS model was itself developed by the original group of authors to include chemical functionality for amides [198], oxygen- [199, 200] and sulfur-containing [201] compounds, and an all-atom implementation [202] (OPLS-AA) with explicit hydrogen atoms covering a wide range of chemical functionalities including amines [203]. Later refinements have centred on biomolecular simulation, such as revised torsional parameters for peptides [204], better transferability of long-chain hydrocarbons [205] for lipid bilayers, and improved descriptions of nucleosides and nucleotides [206].

While the OPLS models are reasonably accurate for condensed-phase properties and biological systems, phase equilibrium properties are not always well represented. A comparison of saturation properties for alkanes and alcohols by Martin [207] showed OPLS-AA reproduced experimental saturation properties within 1% for less than half the cases considered. The family of tranferable potentials for phase equilibria (TraPPE) is a series of refinements of OPLS models to better capture phase equilibria in organic compounds including alkanes [208, 209, 210], unsaturated compounds [211], alcohols [105] and other oxygen compounds [104], nitrogen-containing compounds (including amines) [212], sulfur-containing compounds [213], heterocyclic compounds [214], and a large number of compound-specific models. The TraPPE family of potentials exists both as explicit hydrogen and united-atom models, and have shown good transferability to mixed systems.

Other notable molecular models include the general Amber force field [215] (GAFF) and Groningen molecular simulation (GROMOS) force field [216, 217, 218], developed primarily for the study of biomolecular systems such as lipids and proteins. While these have undergone substantial development, targeting condensed-phase properties does not necessarily produce good models for phase equilibria, as observed e.g. for the OPLS models.

Further coarse-graining of molecular models is common, especially for the study of large biomolecular and polymer systems. The Martini force field [219] is perhaps most commonly used, employing a four-to-one coarse graining ratio (approximately four heavy atoms are represented by each model particle). Polymer species including polyethylene oxide (PEO) [220, 221] have been parameterised for use within the Martini framework using a coarse-grained representation illustrated in figure 3.4, showing that excellent agreement can be obtained for liquid density in polymer-water systems. However, vapour-liquid simulations do not directly translate to this approach due to the coarse-graining of solvent molecules, and hydration patterns around strongly interacting species such as electrolytes are not described in sufficient resolution to describe e.g. hydrogen bonding and ion solvation.

For simulations of systems relevant to facilitated transport membranes there are multiple criteria for the polymer model used. The properties of the polymer itself, its interaction with water, and the ternary and higher-order systems formed through gas absorption are all important for creating a thermodynamic system resembling the real material. Hence, the polymer model should satisfy the following.

- Accurately describe polymer ρPT behaviour in the melt (liquid) phase, to ensure the polymer cohesive energy is correctly described and consistent with equation of state representations.

- Reproduce the phase behaviour of polymer-water mixtures governing the absorption isotherms of water in polymer observed in facilitated transport membranes.

- Represent polymer-solute interactions in a realistic manner for ternary systems (e.g. polymer-water-CO_2), providing a means to estimate ternary solubility and assess anisotropic solvation effects in these higher order systems.

The families of molecular models described above were evaluated according to these criteria based on literature sources for each model. TraPPE was found to give the most universal coverage of fluid phase properties for the compounds of interest, primarily aliphatic polymers, polar substituents (in particular amines), and gas molecules relevant to separation including CO_2 and N_2. Proprietary molecular models, such as condensed-phase optimized molecular potential for atomistic simulation studies [222] (COMPASS) and polymer consistent force field [223, 224, 225, 226, 227] (PCFF) were not considered.

While the TraPPE model reviewed above shows good performance for condensed-phase properties of many organic compounds and small molecules, not all molecular parameters are available from literature sources. In particular, only hydrogen-explicit parameters have been reported for dihedral potentials in amines [212]. For hydrogen bonding compounds such as amines, alkyl groups may reasonably be approximated by a united atom representation (figure 3.4 B), while amine groups are represented with explicit hydrogen atoms. This is the same approach as Chen et al. [105] employ for the TraPPE united-atom representation of alcohols: non-polar alkyl groups are represented by a single interaction site, while substituents are presented in full atomistic detail to capture hydrogen bonding interactions. To employ this approach to organic amines, new amine torsional parameters developed for the united atom approach are required.

3.3.2 Development of Amine Torsional Parameters

The representation of amine chemical groups by classical molecular models has been the subject of considerable investigation [228, 229, 230, 231, 203], in large part due to the unusual solvation pattern of methylated ammonia compounds. Solubility of organic compounds is expected to reduce with increasing methylation due to the hydrophobicity of alkyl groups, with the anticipated sequence in order of solubility $NH_3 > MeNH_2 > Me_2NH > Me_3N$. Instead, the singly substituted methylamine is most soluble, with overall sequence $MeNH_2 > NH_3 \approx Me_2NH > Me_3N$. More recently Hesske and Gloe [232] studied the ammonia and methylamine hydration using Car-Parrinello molecular dynamics, finding the main difference between the compounds to be in the structure of the first hydration shell. This indicates amine hydration relies on cooperative effects rather than being the product of individual water-amine interactions.

Dihedral	C_0 / kJ mol^{-1}	C_1 / kJ mol^{-1}	C_2 / kJ mol^{-1}	C_3 / kJ mol^{-1}	Source
C-C-C-N	0	2.9519	-0.5670	6.5794	[208]
C-C-C-N	0	1.5602	-0.0317	9.0564	This work
C-C-N-H	1.3875	0.6050	-1.5300	2.8050	This work
C-C-N-C	-2.2240	7.3567	-4.5099	5.6552	This work

Table 3.1: Dihedral potential parameters for aliphatic amines described by the TraPPE-UA model, for use with the dihedral potential in equation 3.7. Parameters for nitrogen-containing dihedral potentials are regressed against *ab initio* torsional energies of small-molecule aliphatic amines. For details, see the text and figures 3.5 and 3.6.

Rizzo and Jorgensen [203] proposed the first classical molecular model to correctly capture the hydration energies of the methylamine series, showing that the effect resulted from the specific hydration pattern formed around each compound. The model showed good transferability to other organic amines within the OPLS-AA framework [203]. Later, Oostenbrink et al. [233] showed that a united-atom approach could also be used for the organic amines with good results, as part of the GROMOS 53A6 parameter set. The TraPPE parameter set for amines [212] is based on the model of Rizzo and Jorgensen [203] with charges and dispersion parameters re-optimised to reproduce vapour-liquid coexistence curves of $MeNH_2$, Me_2NH, and Me_3N. Since the model does not employ scaled 1-4 interactions (unlike OPLS-AA), torsional parameters for the TraPPE-EH model were re-fitted from the OPLS-AA potential. A four-parameter dihedral potential was employed [212],

$$U^{\mathrm{dihedral}} = C_0 + C_1(1 + \cos(\phi)) + C_2(1 - \cos(2\phi)) + C_3(1 + \cos(3\phi)) \tag{3.7}$$

where U^{dihedral} is the potential energy for two atoms with dihedral angle ϕ, and C_0, C_1, C_2, and C_3 are adjustable parameters. The parameter C_0 is included in order to normalize the lowest energy dihedral angle to zero, but has no impact on the rotational distribution.

In this work, the TraPPE-UA model is employed for polymer chains to improve computational efficiency in high particle count systems. The model is partially coarse grained, with hydrogen atoms included for polar groups including amines, following the TraPPE-UA model for alcohols by Chen et al. [105]. However, the amine torsional parameters from the explicit hydrogen model by Wick et al. [212] do not yield the correct dihedral distributions when applied to amines with a united atom carbon chain. Hence, new torsional parameters were fitted using the form in equation 3.7, using the same methodology as the OPLS model on which the TraPPE amine model is built. Development of the individual nitrogen-containing dihedral potentials are described below, with the resulting torsional parameters reported in table 3.1.

The C-C-C-N dihedral potential was fitted based on *ab initio* torsional energies at the 6-31G* level from Maxwell et al. [234], the same torsional profiles used to parameterise OPLS-AA. A comparison of the resulting cosine expansion is shown in the top panel of figure 3.5. The earlier values by Allinger et al. [235] at the 4-31G level appear consistent with those of Maxwell et al. [234], with both being calculated based on propylamine.

For the C-C-N-H dihedral potential the analytical function by Zeroka et al. [236] was used, based on *ab*

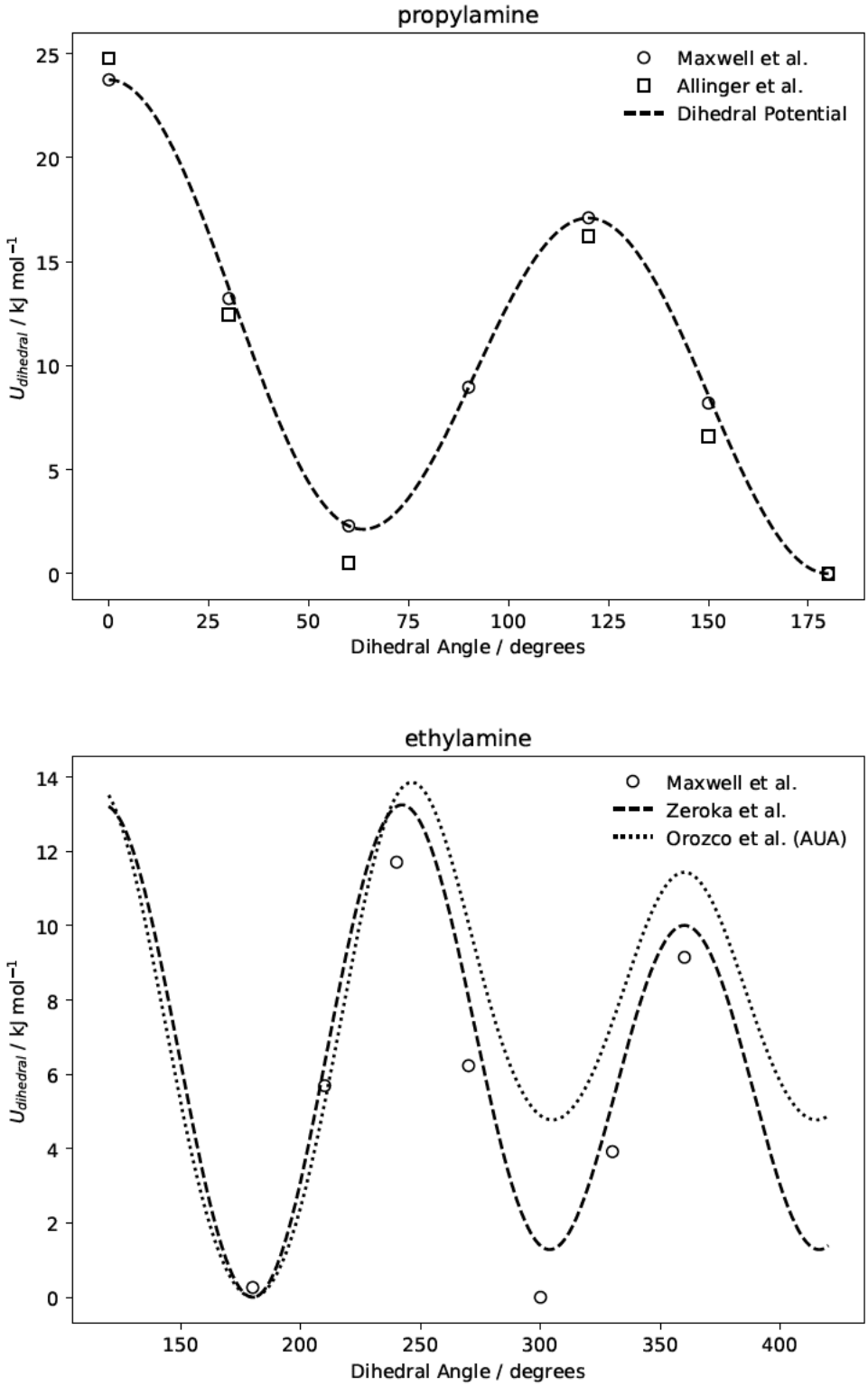

Figure 3.5: Torsional energies for aliphatic amines from *ab initio* calculations and dihedral potentials. Top panel: Propylamine torsional energy described by a single C-C-C-N dihedral potential, compared against energies from Maxwell et al. [234] and Allinger et al. [235]. Bottom panel: Ethylamine torsional energy described by two C-C-N-H dihedral potentials as reported by Zeroka et al. [236], compared against energies from Maxwell et al. [234]. The dihedral potential of AUA [195] is shown for comparison.

initio torsional energies of ethylamine at the 6-311G** level. The resulting cosine expansion is shown in the bottom panel of figure 3.5. Note that the dihedral angle shown is that of the nitrogen lone pair, assumed to be at 120° from each hydrogen, with the resulting torsional potential being the sum of the C-C-N-H potentials with a phase shift of 120°. The expression is found to be in reasonable agreement with the values from Maxwell et al. [234]. However, the potential from Zeroka et al. [236] identifies the 180° conformation (nitrogen lone pair *trans* to the methyl group) as the lowest energy. This is supported by the AUA model by Orozco et al. [195], albeit with some difference in the relative energy of the two conformers. The AUA model is fitted against density functional theory calculations of ethylamine, although no potential energies were reported by the authors.

The C-C-N-C dihedral potential can be parameterised either based on the secondary amine (e.g. ethylmethylamine) or tertiary amine (e.g. dimethylethylamine). Torsional energies for ethylmethylamine at the 4-31G level have been reported by Allinger et al. [235] and Batista de Carvalho and Teixeira-Dias [237], but requires the inclusion of a C-C-N-H dihedral potential to account for the remaining amine hydrogen. Instead, the torsional energies for dimethylethylamine from Batista de Carvalho and Teixeira-Dias [238] at 6-31G* level are used. The resulting dihedral potential is shown in the top panel of figure 3.6. As for the C-C-N-H torsion fitted to ethylamine, the dihedral angle is that of the nitrogen lone pair with the two methyl groups shifted by $\pm$ 120°.

As a test of transferability, the dihedral potential for ethylmethylamine was calculated from the C-C-N-C and C-C-N-H dihedral potentials fitted above. Rotation around the central C-N bond in ethylmethylamine comprises both C-C-N-C and C-C-N-H torsional interactions, with a $\pm$ 120° phase shift between the two corresponding dihedral potentials. The dihedral potential resulting from one C-C-N-C and one C-C-N-H potential is in excellent agreement with torsional energies reported for *ab initio* calculations of ethylmethylamine [235, 237], as shown in figure 3.6. This illustrates the transferability of torsional interactions, and demonstrates the accuracy of the amine dihedral parameters in table 3.1 for organic amine compounds.

3.4 Prediction of Polymer ρpT Behaviour

The molecular models outlined so far allows description of the properties of fluid systems, including pure polymer and polymer-solvent systems, which help explain and predict phase behaviour relevant to polymer solvation. However, in order to be useful for property prediction in real systems, any molecular models must first be trained against physical data for the base species involved. For molecular simulation, the group contribution principle is readily applied as outlined in section 3.3: polymers are simply long-chain variants of their constituent monomers, and the behaviour of a given polymer is an emergent property accurately reflected in the molecular simulation.

For equation of state models, the molecular parameters of polymer species do not in general correspond

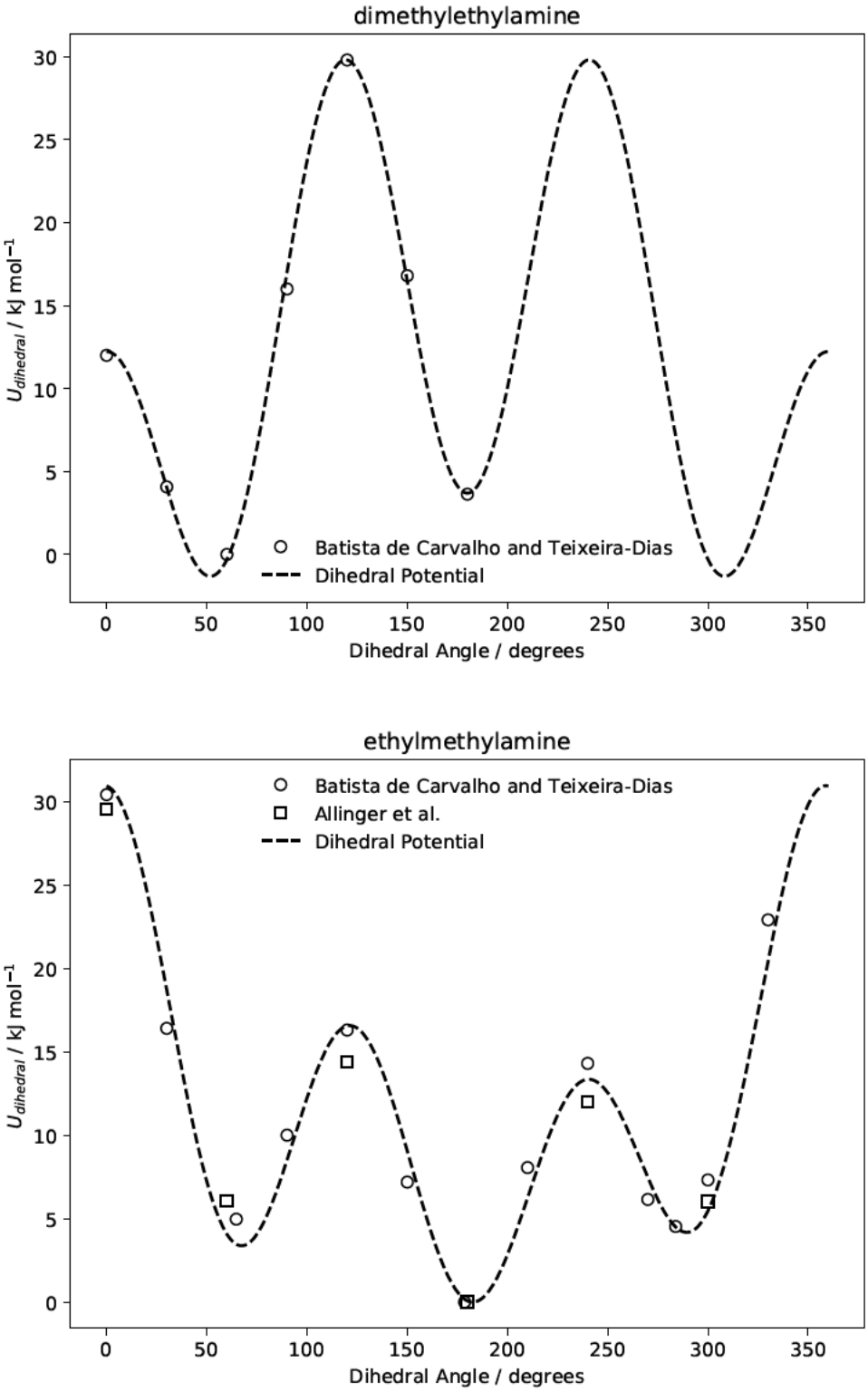

Figure 3.6: Torsional energies for aliphatic amines from *ab initio* calculations and dihedral potentials. Top panel: Dimethylethylamine torsional energy described by two C-C-N-C dihedral potentials, compared with the values from Batista de Carvalho and Teixeira-Dias [238]. Bottom panel: Ethylmethylamine torsional energy described by one C-C-N-H and one C-C-N-C dihedral potential. Comparison against the values Allinger et al. [235] and Batista de Carvalho and Teixeira-Dias [237] shows excellent transferability of the parameters developed from propylamine, ethylamine, and dimethylethylamine to the description of torsional energies in ethylmethylamine.

to a simple increase in the chain length parameter. Rather, all molecular parameters are modified to reflect the changing mean-field interactions of the polymer. Hence, experimental data for polymer systems are typically used directly to develop molecular parameters. In the construction of equation of state models the ρpT behaviour of polymers in the melt state is particularly relevant, as the three independent properties of (i) density, (ii) thermal expansivity, and (iii) compressibility are sufficient for regressing the three molecular parameters of the equation of state model. Additionally, ρpT data for most polymers can be readily obtained experimentally, with data for the glass, rubber, and melt phases available in literature for common polymers. Here we will use the data collections of Zoller and Walsh [146] and Wohlfarth [239]. Other polymers may not yet have been synthesised, be thermally unstable at temperatures corresponding to the melt phase, or otherwise be unsuitable for ρpT characterisation (such as the PIM family of polymers [240] occupying trapped metastable states). This includes polyvinylamine (PVAm), for which no experimental data are available.

Where experimental data are unavailable, molecular models may be used in a predictive manner based on the group contribution principle: the interactions of a chemical group are largely independent of its chemical connectivity with other groups. Polymer molecules are simply long chains of repeating monomer species. The group-contribution approach has seen wide adoption both for equations of state, e.g. by Peters et al. [241, 242] for PC-SAFT. The group contribution principle is also one of the fundamental assumptions of transferable models for molecular simulation, including the TraPPE model described in section 3.3. Polymers take the group contribution principle to its logical conclusion but utilizing parameters from small molecules to describe chains orders of magnitude larger. In this section, the predictive power of molecular simulation for polymer ρpT behaviour is tested by comparing simulated models of short-chain polymers, illustrated in figure 3.7, with real polymer melts. Further, simulation data are used to train PC-SAFT models for PEO, PVA, and PVAm, allowing efficient representation of these polymers in more complex fluid systems.

3.4.1 Polyethylene Oxide

Polyethylene oxide (PEO, also referred to as polyethylene glycol or PEG) is a straight-chain polyether with unit formula C_2H_4O as shown in figure 3.7. PEO has a wide range of uses including pharmaceutical applications, surface treatments, packaging, and as a preservative, largely due to its strongly hydrophilic character. PEO is soluble in water at ambient conditions [243], and can be used to regulate osmotic pressure in aqueous solution. PEO has seen considerable use in CO_2 separation membranes due to its water regulating activity [244], either as part of the polymer membrane [245] or as an additive [246]. However, poor mechanical properties and high propensity for crystallization means PEO is unsuitable as the base polymer for gas separation membranes.

The phase behaviour of PEO follows the expected pattern for weakly interacting straight-chain polymers, with a glass-rubber transition near ambient temperatures [146]. The rubber-melt transition of long-chain PEO occurs at 320 K - 340 K, but varies considerably with chain length [146]. Low molecular weight oligomers do not undergo the rubber-melt transition, instead showing a tendency of crystallizing [247] at temperatures

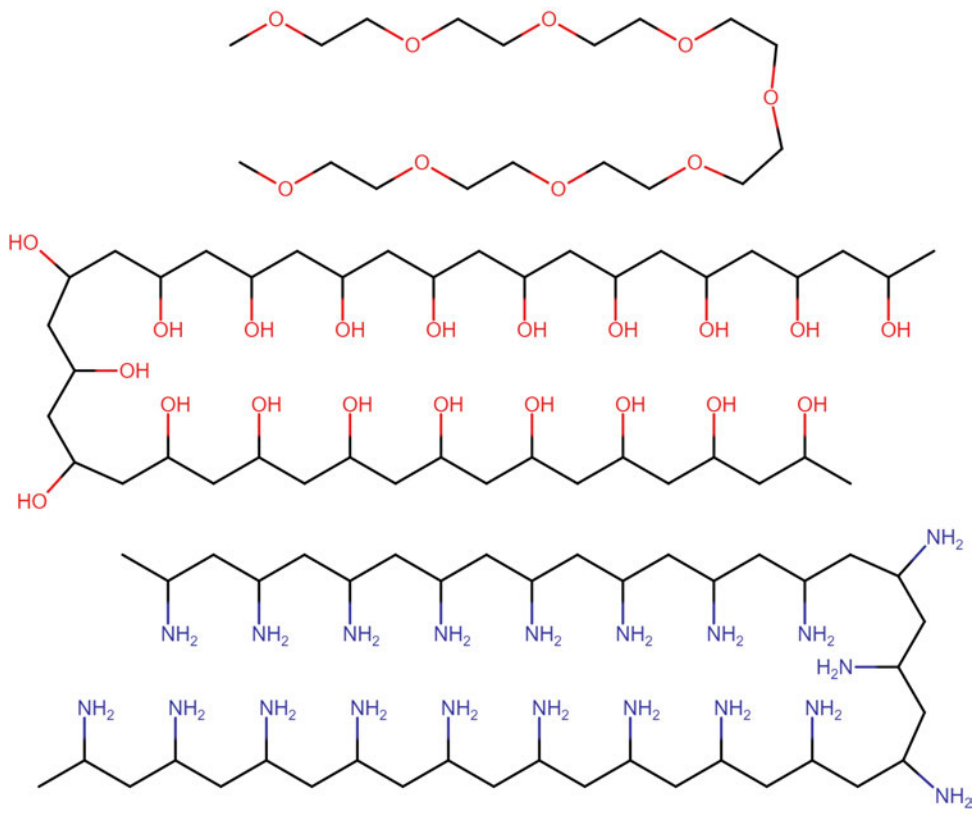

Figure 3.7: Chemical structures of short-chain polymer used for molecular simulation. Top panel: Polyethylene oxide (PEO). Middle panel: Polyvinyl alcohol (PVA). Bottom panel: Polyvinyl amine (PVAm). The polymers are in each case symmetrically capped with terminal methyl groups to limit tail effects.

below ambient, with the exact temperatures and conditions varying with chain length and monodispersity. Hence, rather than using long-chain PEO, separation membranes may be embedded with PEO oligomers to circumvent the problem of in-membrane crystalline regions as done by Shin et al. [246].

In order to establish a predictive modelling approach for hydrophilic polymers, PEO was selected as an initial test case. High-quality experimental ρpT data are available for both long- and short-chain PEO, and the phase transitions are well documented. While molecular simulation is limited to short-chain PEO due to computational constraints, the melt-phase properties are nearly identical for short- and long-chain polymer. Short-chain polymer also ensures the simulated system is in the melt phase, and accelerates convergence of ensemble averages. Three objectives were identified for the investigation of ρpT behaviour of PEO:

- Confirm the suitability of the PC-SAFT equation of state for representing polymer melt properties. Parameters for PEO have previously been reported by Peters et al. [241, 242] and Byun and Lee [248].
- Investigate the correspondence between experimental ρpT data and equivalent data generated by molecular simulation using the TraPPE-UA model.
- Optimise PC-SAFT molecular parameters for PEO based on simulated ρpT data using equation 3.8, determining the quantitative agreement between the hybrid simulation / equation of state approach and experimental data.

To generate ρpT data, PEO was simulated using the TraPPE-UA model for ethers [208, 104], using a system of 94 oligomers with chain length of 9 monomers. The oligomers used for molecular simulation have a molecular weight of $M_w = 398$ g mol^{-1}, within the range of low molecular weight PEO reported by Zoller and Walsh [146] ($M_w = 300 - 600$ g mol^{-1}). Simulations were performed for isobars at 0 MPa, 40 MPa, 80 MPa, 120 MPa, 160 MPa, and 200 MPa, across a temperature range of 373 K - 473 K. The systems were simulated for 20 ns using the replica-exchange method described in section 2.3. A comprehensive list of simulation parameters is given in appendix A. At the conditions considered, experimental PEO of this molecular weight does not undergo the melt-glass transition, with similar phase behaviour expected for the molecular model. However, as noted above ρpT behaviour is nearly identical to long-chain polymer above the melt transition, making it a representative system for optimising equation of state parameters. Finally, terminal groups of PEO oligomers have been shown to somewhat influence solution properties [187], with methyl-capped oligomers more closely resembling the behaviour of long-chain polymer. Hence, the model PEO was constructed with terminal methyl groups on both ends, as shown in figure 3.7.

The simulated ρpT data for PEO oligomers are shown in figure 3.8, with comparison against experimental values from Zoller and Walsh [146] and Wohlfarth [243] along the same isobars as noted above. Since short-chain PEO is used there is no rubber-melt transition, with the full temperature range considered corresponding to the melt phase. The simulated ρpT data are in excellent agreement with both experimental density and thermal expansivity along the 0 MPa and 40 MPa isobars. However, compressibility is somewhat high especially

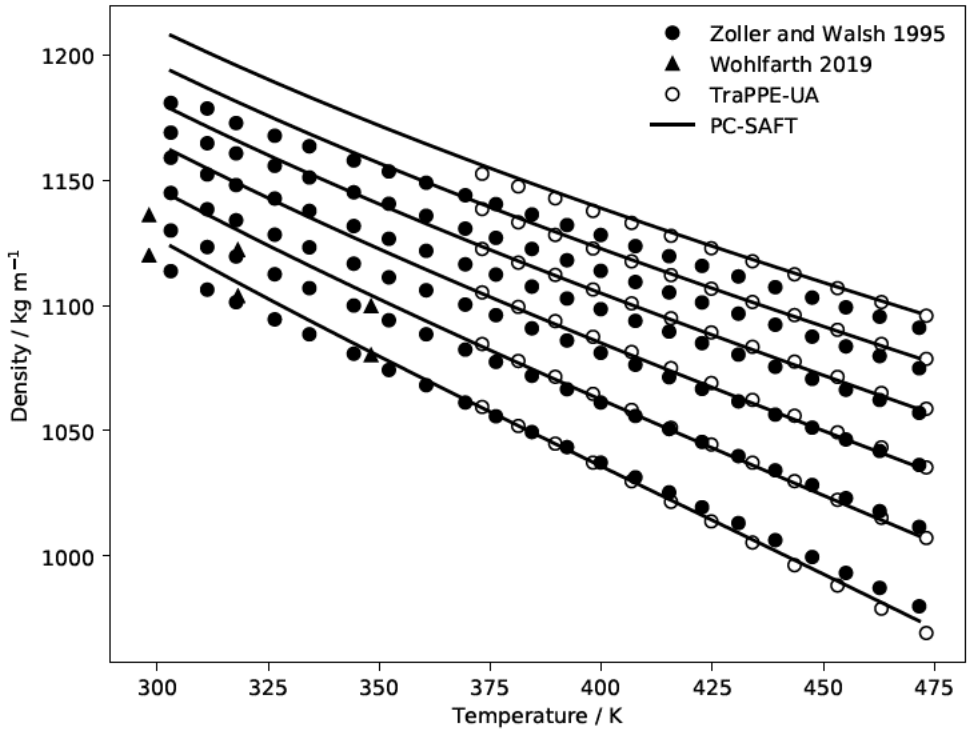

Figure 3.8: Polyethylene oxide ρpT behaviour for isobars at 0, 40, 80, 120, 160, and 200 MPa (increasing density). Solid symbols show experimental data by Zoller and Walsh [146] and Wohlfarth [239]. Open symbols show simulated values using the TraPPE-UA model as detailed in the text, with simulation uncertainties within the symbol size. Solid lines indicate PC-SAFT model regressed against simulation data, with resulting molecular parameters given in table 3.2.

at elevated pressures, leading to overestimation of melt density on the order of 1% at 200 MPa. Overall, the TraPPE-UA model appears to give an accurate representation of the experimental ρpT behaviour of PEO.

While the simulated data for PEO confirm the predictive capacity of molecular simulation, a further step is required on the path to developing a predictive equation of state model: the simulated ρpT must be used to optimise molecular parameters for the PC-SAFT equation of state. PEO is a non-associating polymer with hydrogen bond acceptors but no donors, and we expect a conventional three-parameter model as outlined in chapter 2 to work well, with molecular parameters σ, ϵ and chain length m. This parallels the polymer models developed by Gross and Sadowski [53] for non-associating polymers. PEO oligomers have also been studied by Nannan et al. [249] based on the PC-SAFT equation of state, who obtained good agreement with experimental values both for condensed-phase properties and vapour-liquid equilibrium without the need for association parameters.

In order to generate molecular parameters, numerical optimisation was performed by minimizing a least-squares objective function defined as

$$f(m,\sigma,\epsilon) = \sum_{p,T} \left(\frac{\rho^{\mathrm{EOS}}(m,\sigma,\epsilon) - \rho^{\mathrm{SIM}}}{\rho^{\mathrm{SIM}}} \right)^2 \tag{3.8}$$

where the sum over p, T iterates over all the physical conditions simulated, ρ^{SIM} is the average melt density

Polymer	M_w / g mol^{-1}	Unit Formula	σ / Å	ϵk_B^{-1} / K	m
PEO	44.05	C_2H_4O	2.9157	249.90	2.2373
PEO[1]	44.05	C_2H_4O	2.8824	257.73	2.3710
PEO[2]	44.05	C_2H_4O	3.5497	241.48	1.2731
PVA	44.05	C_2H_3OH	3.0090	403.47	1.9658
PVA[2]	44.05	C_2H_3OH	3.2993	302.2	1.5727
PVAm	43.07	$C_2H_3NH_2$	2.8427	285.33	2.4309

Table 3.2: Molecular parameters for polymers using the PC-SAFT equation of state. Parameters are regressed against simulated ρpT data as shown in figures 3.8, 3.9, and 3.10. [1]Parameters from the group-contribution approach of Peters et al. [241, 242]. [2]Parameters from Byun and Lee. [248]

estimated by molecular simulation, and $\rho\mathrm{EOS}$ is the melt density obtained by PC-SAFT for a given parameter combination m, σ, ϵ. The adaptive simplex algorithm described by Gao and Han [250] was employed for multi-parameter minimization with additional checks for convergence of the PC-SAFT equation of state at each iteration. The resulting molecular parameters are reported in table 3.2.

The combined molecular simulation / equation of state approach is shown with solid lines in figure 3.8, allowing comparison against both experimental and simulated ρpT data. The PC-SAFT model is in excellent agreement with simulated values for PEO melt density, as expected based on the parameter optimisation procedure above. The mean absolute deviation between the PC-SAFT model and simulation data for the temperature range 373 K - 473 K is 0.1%.

For comparison against experimental data, the low-temperature range down to 300 K was included to evaluate the predictive capacity of the model outside the temperature range of the optimisation data set. Unsurprisingly, the PC-SAFT model displays similar behaviour as the simulation data: low-pressure isobars are in good agreement with experimental data, while density in high-pressure systems is somewhat overestimated. Additionally, predictions outside the simulated range deteriorate somewhat, especially at high pressure. The mean absolute deviation between the PC-SAFT model and experimental ρpT data over full temperature range is 0.9%.

3.4.2 Polyvinyl Alcohol

Polyvinyl alcohol (PVA) is a straight-chain poly-alcohol with unit formula C_2H_4O, as shown in figure 3.7. PVA is used for a variety of industrial purposes including food packaging and paper production due to its solubility in water, thermal stability, and low cost of manufacture [251]. For gas separation purposes, PVA has been included as a component in a variety of membranes for CO_2 separation, including PVA-nanocellulose composite mebranes [252], PVA-PEO membranes [253] and PVA-PEO-silica mixed matrix membranes [254], as well as in the previously discussed amine-based facilitated transport membranes [30, 255, 256]. As a membrane component, PVA promotes water sorption, but unlike PEO it also has excellent physical properties [257, 258] and can be chemically crosslinked to further increase stability. This makes PVA well suited for membrane construction, and a good candidate for membranes applications where a hydrophilic character is

desired.

The behaviour of PVA is somewhat unusual compared to other carbon-backbone polymers. In figure 3.9, experimental ρpT behaviour for PVA is shown over the temperature interval 300 K - 550 K based on data from Zoller and Walsh [146] and Wohlfarth [239]. While the chain length for the ρpT data by Zoller and Walsh [146] in this case is unspecified, it is assumed to be for long-chain polymer. The long-chain PVA is a glassy polymer at ambient conditions, going through a relatively high-temperature glass-rubber transition near 350 K. However, the density change between the two phases is small, with the rubbery phase actually increasing in density under high-pressure conditions. The rubber-melt transition is near 500 K [146]. However, PVA is only thermally stable in the melt phase for a narrow temperature interval, and undergoes thermal decomposition near 540 K [259] making further data collection impossible. It is likely that experimental ρpT data in the interval 500 K-550 K also are of limited quality due to thermal degradation. Hence, experimental ρpT data are scarce for the melt phase, limiting the available range of experimental data for model regression.

Having seen good correspondence between simulated and experimental ρpT data for PEO, the same procedure used in section 3.4.1 was applied to PVA oligomers. This additionally gives information on the suitability of non-associating equations of state in describing hydrogen bonding polymers. PVA was simulated along isobars with pressures of 0 MPa, 40 MPa, 80 MPa, 120 MPa, 160 MPa and 200 MPa, and for 12 geometrically spaced temperature points over the range 450 K-550 K. These conditions overlap with the experimental ranges for the rubber-melt transition. The TraPPE-UA model for alcohols [208, 105] was used to describe the polymer, using a system of 40 PVA oligomers with chain length of 20 monomers, corresponding to an oligomer molecular weight of $M_w = 897$ g mol^{-1}. The systems were simulated for 20 ns using the replica-exchange method described in section 2.3. The resulting data are shown in figure 3.9.

The simulated values for polymer density are similar to those seen experimentally, but the trends with temperature deviate significantly from experimental both at high and low temperatures. Only immediately after the experimental rubber-melt transition do the simulated isobars for PVA show melt density and compressibility in agreement with those seen experimentally. At higher temperatures, the experimental melt density decreases sharply relative to the simulated values; however, given the instability of PVA at these conditions it is unclear whether this is a genuine extension of the melt phase behaviour or due to partial thermal decomposition for the experimental system. At lower temperatures, corresponding to the experimental rubber phase, the simulated polymer shows no sign of phase transitions. To investigate the lack of a rubber-melt transition, further sets of simulations were conducted at 12 temperature points over a lowered temperature range of 420 K-520 K. The resulting ρpT behaviour is consistent with that seen for the higher temperature range, showing no rubber-melt transition.

The absence of melt transition and divergence from experimental densities at high temperatures seen for simulated PVA systems has multiple likely causes: Firstly, polymer chain length is known to depress rubber-melt transition temperatures in experimental systems [146]. The 20-mer chains may simply be too

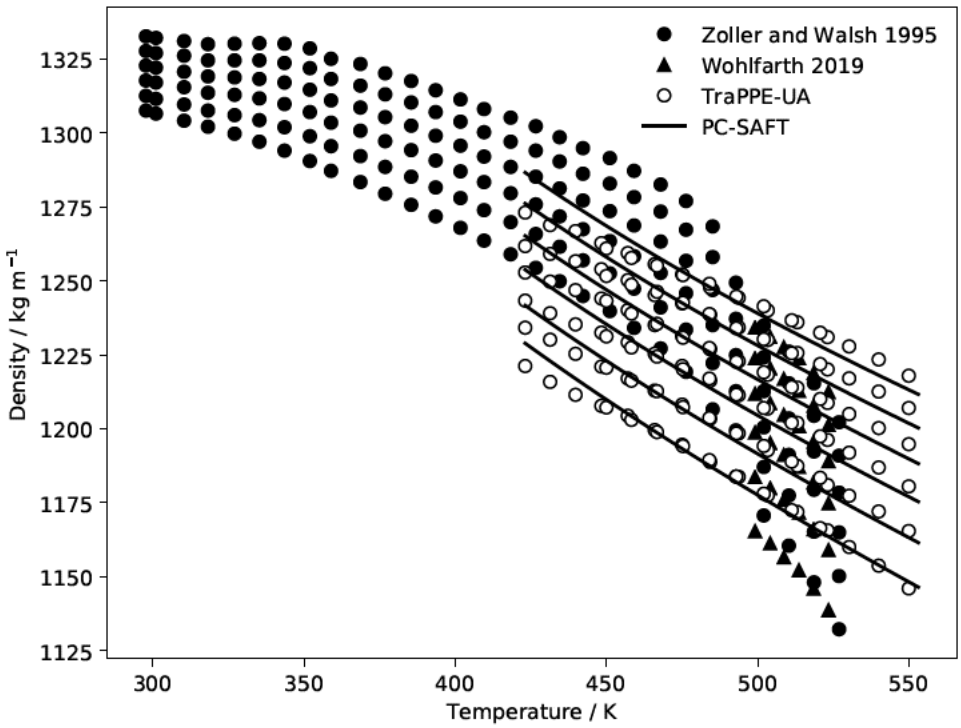

Figure 3.9: PVA ρpT behaviour for isobars at 0, 40, 80, 120, 160, and 200 MPa (increasing density). Solid symbols show experimental data by Zoller and Walsh [146] and Wohlfarth [239]. Open symbols show simulated values as detailed in the text, with simulation uncertainties within the symbol size. Solid lines indicate PC-SAFT model regressed against simulation data, with resulting molecular parameters given in table 3.2. The experimental melt transition near 500 K is not observed in the polymer simulation.

short to experience the rubber phase. Secondly, the thermodynamic properties of the TraPPE-UA model may not correspond well enough to the experimental system to correctly predict the rubber-melt transition. Third, the lack of a rubber-melt transition may be due to system-size effects, where polymer entanglement is weakened by the relatively small system size. Fourth, the rapid decrease in density observed near 540 K is uncharacteristic of polymer melts [146], suggesting a hypothetical thermally stable PVA would likely have a more flat density profile. Conversely, the TraPPE-UA model of PVA with fixed-length bonds is thermally stable under all conditions.

The simulated ρpT data for PVA form a basis on which to optimise molecular parameters for the PC-SAFT equation of state. However, the hydrogen bonding nature of PVA poses important questions regarding the representation of the polymer withing the PC-SAFT framework:

- SAFT is derived on the premise that molecules do not self-associate, a reasonable assumption for small molecules which are normally sterically restricted from doing so. Does this assumption hold for long-chain PVA, which forms numerous intra-chain bonds?
- Alcohols are normally modelled as two-site associating molecules, representing one hydrogen bond donor and one acceptor per alcohol group. How should PVA be represented?
- SAFT uses the molar density of the associating species to calculate Helmholtz free energies of association

(see equation 2.52). This implies significant changes in system thermodynamics between long-chain and infinite-chain polymer. How should this be resolved?

To incorporate association interactions in the model for PVA, we evaluated a modification to the association terms in equation 2.52 based on a per-monomer description of association;

$$\frac{A^{\text{assoc}}}{RT} = \sum_i \rho_i^* \sum_{A_i} (\ln X_{A_i} - X_{A_i} + 1) - \sum_i \sum_j \frac{\rho_i^* \rho_j^*}{\rho^*} \sum_{A_i} \sum_{B_j} X_{A_i} X_{B_j} \Delta^{A_i B_j} \tag{3.9}$$

where $\rho_i^* = \rho_i n_i$ is the monomer molar density rather than molecular molar density, for a polymer comprising n_i monomers. This assigns each monomer of a polymeric molecule as an independently associating entity, such that even infinitely long polymers (i.e., systems comprised of a single long polymer strand) show associative behaviour.

Two separate strategies were explored for optimising molecular parameters for PVA. Firstly, a conventional three-parameter description was used, similar to PEO described in the previous section. This approximates inter-chain association through the chain parameters m, σ and intra-chain association as part of the chain interaction energy parameter ϵ inherent to the PC-SAFT equation of state. Molecular parameters for this model were optimised based on the objective function in equation 3.8, and are listed in table 3.2. The resulting equation of state behaviour is indicated in figure 3.9 by solid lines. PC-SAFT shows acceptable agreement with molecular simulation data for the temperature and pressure ranges considered, albeit with slight deviations in density at lower temperatures.

Secondly, a five-parameter description was attempted, where monomer association is described by equation 3.9 and each monomer is assigned sites A, B following the association scheme for alcohols described in chapter 2. The additional associating parameters $\kappa_{AB}, \epsilon_{AB}$ were added as optimisation variables to the objective function in equation 3.8. However, the resulting molecular parameters failed to converge to physically reasonable solutions. This is likely due to the limited information content in ρpT data: the observed behaviour is well described by only three parameters (corresponding to density, thermal expansion, and compressibility), making optimisation with further parameters produce degenerate solutions.

Having explored both three-parameter and associating five-parameter representations of PVA, we opted for a conventional three-parameter model, incorporating alcohol hydrogen bonding as part of the mean-field description of the polymer. This also leaves room for the addition of cross-associating sites for e.g. interactions with water, which do not influence pure polymer ρpT behaviour.

3.4.3 Polyvinyl Amine

Polyvinyl amine (PVAm) is a straight-chain polyamine with unit formula $C_2H_3NH_2$ as shown in figure 3.7, and can be considered the amine chemical analogue of PVA. PVAm forms hydrogen bonds between amine groups in similar fashion to the alcohol. However, unlike PVA it is chemically reactive in solution, acting as a poly-

base [260] upon contact with water. This makes PVAm a chemically interesting and easily modifiable polymer for material development, offering many potential applications despite its relatively recent development on a commercial scale [261]. PVAm has the highest amine density of any polymer [262], making it an attractive compound for applications relying on amine functionality, including facilitated transport membranes. A number of facilitated transport membranes based on PVAm have been reported, with the largest available body of research being on PVA/PVAm membranes reported primarily by Hägg et al.[263, 264, 145, 30, 35, 265, 266, 267]. Other PVAm-based facilitated transport membranes include PVAm-polysulfone by Dong et al. [268] and amine-impregnated PVAm-polysulfone [269]. Mixed-matrix membranes have also been proposed based on PVAm, such as PVAm with hydrotalcite channels [270] or polyaniline nanorods [271], where the inclusion of microstructured material is meant to enhance diffusion and increase overall transport rates through the membrane.

The physical properties of PVAm are relatively poor, making defect-free thin film membranes hard to obtain. This may be overcome by the use of a supporting layer in composite membranes, chemical cross-linking, blending of PVAm with other polymers, or a combination thereof. The physical properties of PVAm also make it hard to characterise experimentally, and there are no reported ρpT data for pure PVAm. Purification of PVAm from the commercial salt form (Lupamin® 9095) to a non-protonated state also requires considerable experimental effort [272].

Despite the lack of ρpT data for PVAm and ambiguity around chemical protonation state, certain educated guesses can be made based on its chemical structure. Amines as chemical analogues of alcohols generally have a somewhat less dense liquid phase, owing to the reduced strength of the N-H hydrogen bond relative to O-H [273]. Following the same argument, we should also expect a rubber-glass transition temperature somewhat below 500 K, although it is unlikely to be observed for short-chain polymer.

In place of experimental data for PVAm, the same procedure as adopted for PEO and PVA was used to simulate ρpT for PVAm. Systems of 40 oligomers with chain length of 20 monomers were used to represent the polymer systems. The same isobars of 0 MPa, 40 MPa, 80 MPa, 120 MPa, 160 MPa and 200 MPa were simulated, with 14 geometrically spaced temperature points across the temperature range of 423 K - 553 K. The systems were simulated for 20 ns using the replica-exchange method described in section 2.3. This should give good coverage of the melt phase in a region where simulation data are likely to correspond well with experiment. The resulting data are shown in figure 3.10.

The simulated values for melt density are somewhat lower than those seen for PVA for the same temperatures, in line with our expectation based on chemical analogues. There is no discernible variation in thermal expansivity over the range studied. Following the same procedure as for PEO and PVA, the simulated ρpT values were used to optimise a three-parameter molecular model for the PC-SAFT equation of state, based on the objective function defined in equation 3.8. The resulting parameters are listed in table 3.2. It is worth noting the similarity of the molecular parameters obtained for PVAm to those previously obtained for PEO

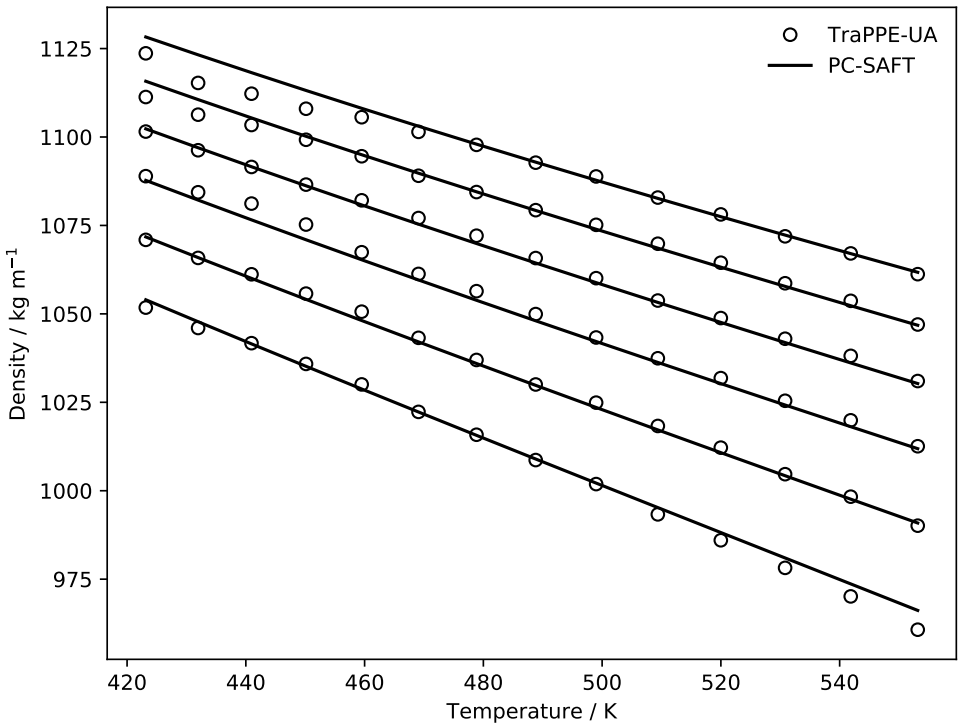

Figure 3.10: PVAm ρpT behaviour for isobars at 0, 40, 80, 120, 160, and 200 MPa (increasing density). Open symbols show simulated values as detailed in the text, with simulation uncertainties within the symbol size. Solid lines indicate PC-SAFT model regressed against simulation data, with resulting molecular parameters given in table 3.2.

and PVA. The interaction energy ϵ is somewhat larger than for PEO but not as great as for PVA, in line with the weakening hydrogen bond strength. The PC-SAFT model for PVAm has an absolute average deviation of 0.1% relative to simulation data, and appears reasonable based on the available evidence, although no experimental data are available at present to measure the agreement of ρpT behaviour.

3.5 Models for Polymer-Water Systems

There are a number of properties of binary polymer-solvent systems which may be experimentally characterised to obtain information about the thermodynamic behaviour of the mixture. The collection of aqueous polymer solutions by Wohlfarth [243] includes measurements of liquid-liquid equilibrium or cloud point curves, vapour-liquid equilibrium either through vapour pressure osmometry or by the isopeistic method, enthalpy change of solution, solution ρpT behaviour, freezing point depression and boiling point increase, as well as scattering data for characterising second virial coefficients. Polymer-solvent binary data are in turn used to correlate interaction parameters, as exemplified by the Flory-Huggins model in figure 3.3. For molecular equations of state, three strategies for representing polymer-solvent systems are commonly employed.

- The first approach is based on extrapolation from binary solvent mixtures. By characterising vapour-liquid equilibrium and saturated liquid densities in solvent mixtures with progressively longer chains, parameters for polymer-solvent systems may be obtained by extrapolation to infinite chain length. This

approach requires data for a well-characterised set of oligomers, and fails to account for e.g. long-chain entanglements and self-interactions [52].

- The second approach builds on polymer molecular parameters developed from ρpT behaviour of pure polymer. A binary interaction parameter k_{ij} is in turn regressed based on the binary polymer-solvent system. This approach has the advantage of requiring a limited amount of binary system data, as well as providing reasonable descriptions of the polymer-solvent system also under low-solvent conditions.

- The third approach employs data for polymer-solvent systems to directly correlate both molecular parameters for the polymer and the polymer-solvent binary interaction parameter. This approach can be expected to represent the binary system more accurately, but requires training data with sufficient information content to correlate four independent parameters (three molecular parameters for polymer, plus on binary interaction parameter). This approach was adopted by Gross and Sadowski [53] for characterising polymer-solvent systems, but is in practice limited to regression of two or three free parameters, depending on the available data. Remaining parameters (typically σ and k_{ij}) must be fixed on an *ad-hoc* basis.

Using the molecular models for PEO, PVA, and PVAm previously described together with the TIP4P/2005 model for water [128], polymer-water systems can be simulated at arbitrary composition to extract thermodynamic data. These simulated values can in turn be used to develop equation of state representations of the polymer-solvent system. However, certain practical constraints limit the type of data which may be reasonably obtained by molecular simulation, and hence which of the above approaches should be adopted.

Characterisation of cloud point curves, as shown in figure 3.2, is an experimentally slow processes requiring on the order of hours [274] for separation to occur. The long timescale makes characterisation of cloud point curves by molecular simulation challenging. Certain systems have nonetheless been characterised by molecular simulation, such as dilute solutions of N-isopropylacrylamide oligomers reported by Deshmukh et al. [275]. The authors found a distinct coil-globule transition for the molecular configuration of the oligomer chains at a lower critical solution temperature. However, behaviour near cloud-point curves is system-specific, and the suitability of molecular simulation for precise determination of cloud points is unclear.

Similarly, freezing processes occur on timescales too long for molecular simulation. Through the use of sophisticated seeding algorithms or phase coexistence methods [276] the freezing transition can be observed for water. However, the small system size of molecular simulation inhibits growth of crystalline structures, an effect which will be reinforced in polymer-solvent systems. These factors make molecular simulation unsuitable for characterisation of freezing point depression.

Unlike the two above phase transitions, polymer solution ρpT data can be readily obtained across a wide range of physical conditions. Through the use of accelerated sampling techniques, reliable ρpT data can be obtained at ambient conditions. Here, simulated ρpT data are used to correlate binary interaction parameters

of polymer-solvent systems, making use of the second approach listed above. A system composition of 50% polymer weight fraction is chosen for parameter correlation. The objective function for regression of binary interaction parameters is defined as

$$f(k_{ij}) = \sum_{w,T} \left(\frac{\rho^{\mathrm{PC-SAFT}} - \rho^{\mathrm{sim}}}{\rho^{\mathrm{sim}}} \right)^2 \tag{3.10}$$

where the sum over w, T covers the temperature range 298 K - 373 K for each polymer-solvent system. In the next sections, equation 3.10 is used in conjunction with simulated ρpT data to develop equation of state representations of PEO-water, PVA-water, and PVAm-water systems. Polymer-water systems are represented in PC-SAFT using the polymer parameters reported in table 3.2 together with the four-site water model of Diamantonis and Economou [127], as detailed for MDEA - H_2O solutions by CLeeton et al. [47].

Binary interaction parameters correlated from solution ρpT data are known to be less reliable for the representation of polymer-solvent phase equilibrium compared against using phase equilibrium data directly [52]. To assess the performance of the polymer-solvent equation of state representation for phase equilibrium, solvent activities for PEO-water and PVA-water are compared against experimental values.

3.5.1 Polyethylene Oxide - Water

PEO is a hydrophilic polymer, forming a liquid solution with water at high humidity. The hydration pattern of the ether group in PEO has been studied in detail by Raman scattering [277] and ultrasonic measurements [278], confirming a strong hydrogen bonding interaction with water. Each ether group is found experimentally to bond with one or two water molecules, depending on hydration level [277]. This pattern of interaction is replicated in molecular simulation, as illustrated in figure 3.11, with a large fraction of water molecules found to be doubly hydrogen bonded to PEO in a looped-chain structure. The association of water with PEO ether groups is the main driver for the hydrophilic character of PEO, which otherwise comprises hydrophobic aliphatic chains.

Thermodynamic properties of PEO-water solutions are available for a wide range of chain lengths, compositions, and physical conditions. Liquid densities of PEO-water solutions have been reported by numerous authors [279, 280, 281, 282, 283, 284, 285], with the values from Sadeghi et al. [286] and Eliassi and Modarress [287] used here. A detailed study of vapour-liquid equilibrium data was first reported by Herskowitz and Gottlieb [288] across the temperature range 293.15 K - 333.15 K. They found a group-contribution approach (UNIFAC, Herskowitz and Gottlieb [289]) dimethyl ether - water systems to only partially explain the water activities in PEO - water, likely owing to the association of water with the glycol ether group through hydrogen bonding. More recent results from Sadeghi and Shahebrahimi [290, 291] for the temperature range 298.15 K - 308.15 K, Sadeghi and Ziamajidi [292] for the temperature range 293.15 K - 318.15 K, and Zafarani-Moattar et al. [293] for the temperature range 298.15 K - 318.15 K are particularly well resolved for temperature and

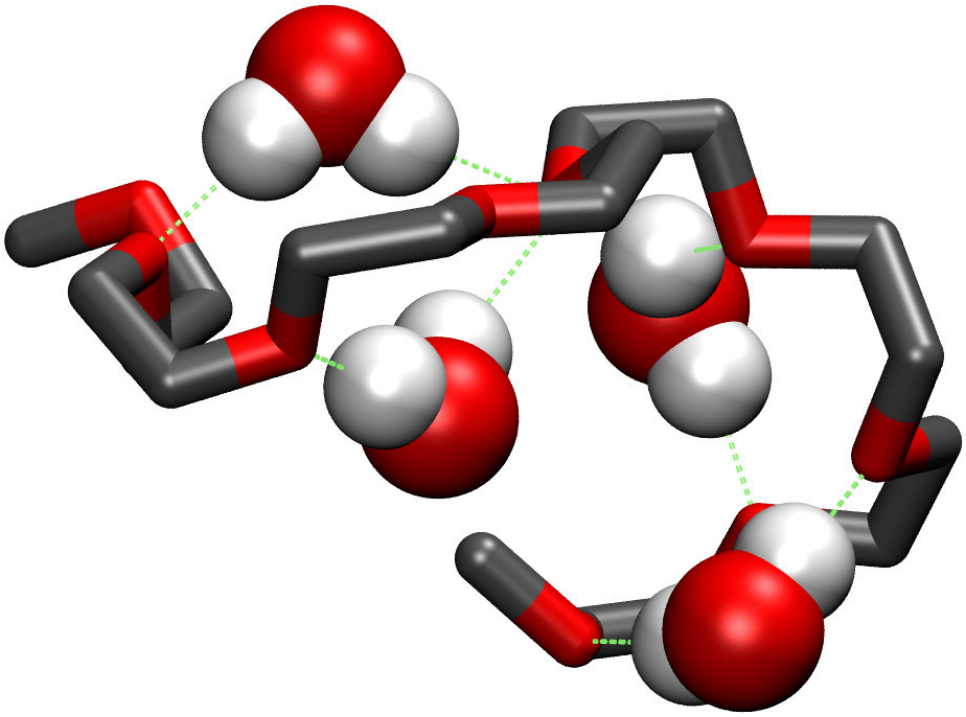

Figure 3.11: Looped-chain multiple hydrogen bonding of water to PEO oligomers in 0.5 water weight fraction solution. Hydrogen bonds are indicated by dashed green lines. Snapshot extracted from molecular simulation of 24 TraPPE-UA PEO oligomers and 535 TIP4P/2005 water molecules at 305.45 K.

water content, adding to the experimental data available for this system.

Solutions of PEO in water also display variations in activity with chain length, as investigated by Herskowitz and Gottlieb [288] and Ninni et al. [294]. They found solutions of short-chain PEO to have lower water activity for a fixed water mass fraction, consistent with the expectation from a lattice fluid model. By re-optimizing UNIFAC parameters for the PEO - water system, Ninni et al. [294] were able to obtain good agreement for water activity across temperatures and PEO chain lengths.

In order to develop equation of state parameters for the PEO-water system, molecular simulations of PEO-water solutions were performed with TraPPE-UE [104] PEO oligomers with chain length of 9 monomers ($M_w = 398.5\,\mathrm{g\,mol^{-1}}$) and TIP4P/2005 [128] water molecules. Particle numbers were chosen to give water weight fractions of 0.30, 0.40, 0.50, 0.60, 0.70, and 0.80, with a system diameter of approximately 3 nm. For each water weight fraction, eight systems at temperatures geometrically spaced in the range 298 K - 353 K were simulated in parallel using the replica exchange method detailed in section 2.3 for 20 ns. Liquid densities for the resulting 48 state points are reported in appendix B. In the upper panel of figure 3.12, simulated liquid densities for each composition at 298 K are compared against against experimental liquid densities of PEO-water mixtures [286, 287].

Liquid density from molecular simulation at 298 K gives excellent agreement with experimental values at 0.20 polymer weight fraction, and the trend with increasing concentration appears to be in line with the experimental data. Hence, it appears the PEO-water system is well described by the combination of

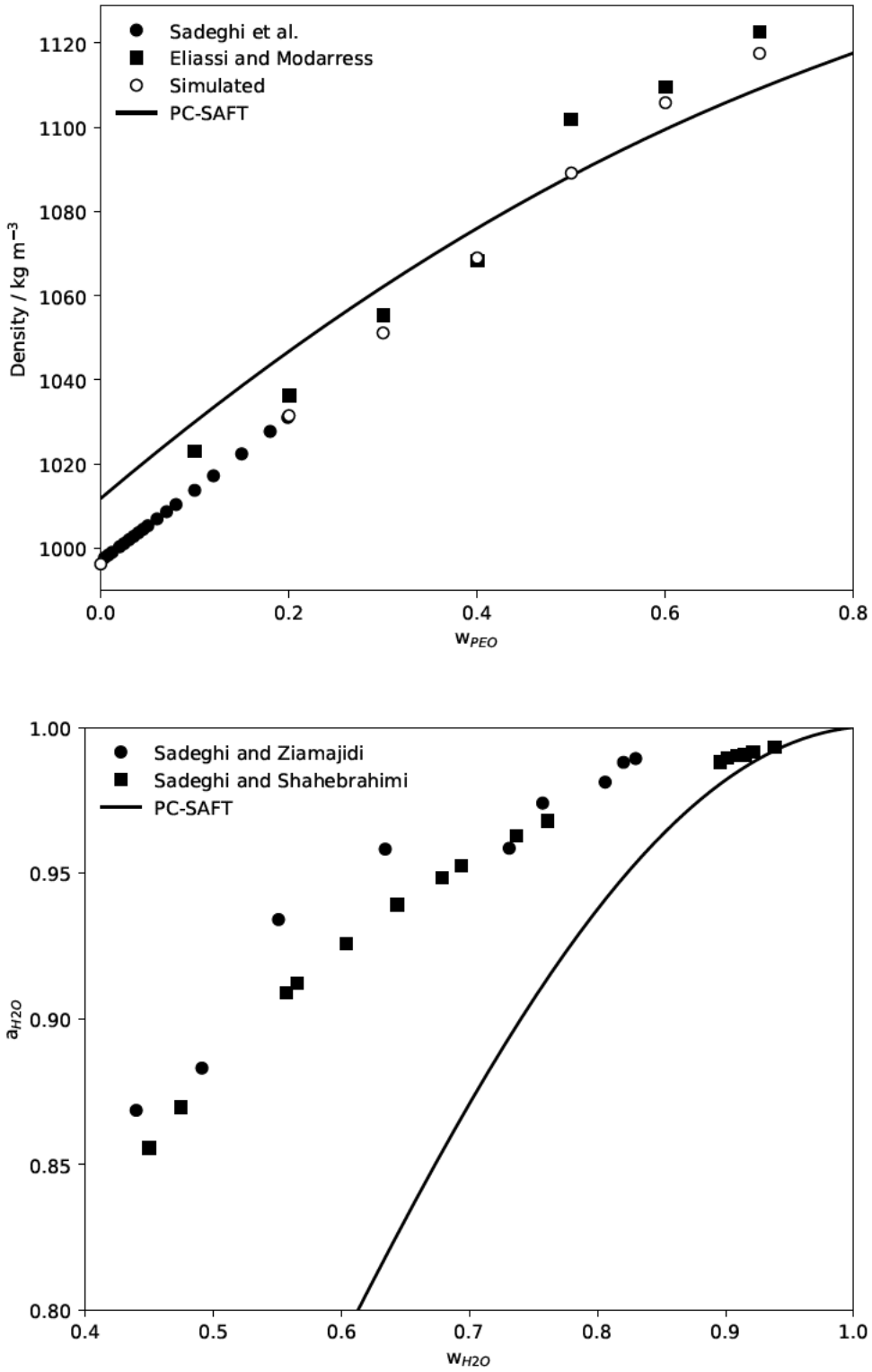

Figure 3.12: Liquid density and water activity in PEO-water solutions at 298 K. Solid line indicates PC-SAFT prediction based on the equation of state parameters in table 3.2, with k_{ij} = -0.1620 regressed against simulation data. Top panel: Liquid density as a function of polymer weight fraction. Solid circles indicate experimental values from Sadeghi et al. [286]. Solid squares indicate experimental values form Eliassi and Modarress [287]. Open circles indicate simulated liquid densities. Bottom panel: Water activity as a function of water weight fraction. Solid circles indicate experimental values from Sadeghi and Ziamajidi [295]. Solid squares indicate experimental values from Sadeghi and Shahebrahimi [291].

TraPPE-UA and TIP4P/2005 models described previously. In order to transfer the system description from molecular simulation to the PC-SAFT equation of state model, a binary interaction parameter $k_{ij} = -0.1620$ was correlated using the objective function in equation 3.10 based on liquid densities at the 48 simulated state points for PEO-water systems. Liquid densities from the resulting equation of state model at 298 K are shown in the upper panel of figure 3.12. As previously seen in figure 2.4, the water model by Diamantonis and Economou [126] overestimates water liquid density at low temperatures. Consequently, PEO-water liquid densities predicted by the PC-SAFT model are too high for water-rich systems. The mean absolute deviation between the PC-SAFT model and experimental densities from Eliassi and Modarress [287] is 0.8%.

Further to liquid densities, the equation of state representation for PEO-water allows prediction of water activities at prescribed system compositions and temperatures. In the lower panel of figure 3.12, water activities in PEO-water solutions at 298 K are compared against experimental values from Sadeghi and Ziamajidi [295] and Sadeghi and Shahebrahimi [291]. For water activities in the range 0.85 - 0.95, the PC-SAFT model overestimates the solution water content by 20% - 45%. While this is a considerable deviation, the PEO-water solution is correctly identified as miscible. Considering the sensitivity of polymer-solvent solutions to small variations in binary interaction parameter [53], we consider the simulation-developed PC-SAFT model to give a fair description of the overall system behaviour.

3.5.2 Polyvinyl Alcohol - Water

Similar to PEO, polyvinyl alcohol (PVA) is a hydrophilic polymer which readily absorbs water at high humidity. However, pure PVA is known to have micro-crystalline regions near ambient conditions, and there is conflicting evidence regarding the dissolution of these regions with increasing water content. Infrared spectroscopy and density measurements by Peppas [296] indicate the crystalline regions remain up to high water content. Conversely, Raman spectroscopy by Iwamoto et al. [297] and X-ray diffraction by Hodge et al. [298] indicate crystalline regions gradually dissolve upon absorption of water. Differences in the experimental timescales, as well as variations in the chemical composition of the polymer, are likely causes for the observed discrepancies. In the case of molecular simulation, the system size is insufficient for crystalline regions to emerge, so there is no ambiguity over micro-crystalline regions.

Solution densities for PVA-water systems have been reported by Eliassi and Modarress [287], Salabat and Mehrbad [284], and Molisso et al. [299]. Vapour-liquid equilibrium data for aqueous PVA solutions have also been reported by a number of authors. Kim et al. [300] measured water sorption using a gravimetric method at a temperature of 303 K. The resulting data, together with results from previous authors were used to fit parameters for Flory-Huggins model (see section 3.2.1) and UNIQUAC excess Gibbs energy models, together with multiple equation of state approaches including the Panayiotou and Vera [301] and Sanchez-Lacombe (see secton 2.4.2) lattice-fluid models. The authors found the Flory-Huggins model with a mean absolute deviation of 4.1% provided the best agreement with experimental values.

Striolo and Prausnitz [302] measured water absorption using a gravimetric method in the temperature range 343 K - 368 K. The results were fitted to a lattice fluid model by Hino et al. [303] for hydrogen bonding polymers, with varying levels agreement [302]. Palamara et al. [304] considered fully and partially hydrolyzed PVA and its solutions with water, methanol, and methyl acetate. Activity in PVA - water solutions was measured across the temperature range 363 K - 383 K. The authors used the Panayiotou and Vera equation of state [301] to correlate experimental results, finding good agreement for the conditions studied. However, only moderate water activities ($a_w < 0.3$) were considered. Csaki et al. [305] obtained water activity using a gel-deswelling method at 298 K, and interpreted the results based on the Flory-Huggins model. They found a concentration dependent interaction parameter χ_{ij} in the range 0.48 - 0.50 could fit the experimental data to good accuracy, but did not investigate temperature dependence in this system.

Cross-linking of PVA introduces additional elastic energy to the polymer, allowing the formation of hydrogels at high water content [306]. Hydrogels have different water absorption characteristics from regular polymer, with highly crosslinked polymer absorbing less readily. Although important for polymer membrane construction, cross linking is not considered further here in terms of its impact on polymer-water solutions.

As before, molecular simulation of PVA-water solutions was performed to develop equation of state parameters for the PVA-water system. PVA was represented with TraPPE-UA [105] PVA oligomers ($M_w = 897.1\,\mathrm{g\,mol^{-1}}$) and TIP4P/2005 [128] water molecules. Particle numbers were chosen to give water weight fractions of 0.3, 0.4, 0.5, 0.6, 0.7, and 0.8, with a system diameter of approximately 3 nm. Eight systems at geometrically spaced temperatures in the range 298.15 K - 353.15 K were simulated in parallel using the replica exchange method detailed in section 2.3 for 20 ns. Liquid densities for the resulting 48 state points are reported in appendix B. In figure 3.13, simulated liquid densities for each composition at 298 K are compared against against experimental liquid densities of PVA-water mixtures [287]. The experimental values are for long-chain PVA ($M_w = 15\,000\,\mathrm{g\,mol^{-1}}$), as no short-chain PVA-water solution data are available.

The simulated liquid densities at 298 K have a clear increasing trend with polymer content. This is in contrast to the experimental values for the same system, showing a moderate increase up to 0.70 PVA weight fraction and subsequent decrease as the system approaches pure polymer. This trend is due to the phase behaviour of PVA. As can be seen in figure 3.9, PVA is in the glassy state at 298 K. Hence, the liquid densities in figure 3.13 represent a transition from liquid water to glassy PVA. Conversely, the simulated liquid densities likely correspond to PVA in the melt phase. It is unclear to what extent the observed differences are due to the TraPPE-UA model employed or chain length dependence.

The PC-SAFT equation of state description is based on melt-phase data, and as such should be well suited to describing liquid densities seen in molecular simulation. Using the same approach as for PEO, a binary interaction parameter $k_{ij} = 0.0553$ was correlated using the objective function in equation 3.10 based on liquid densities at the 48 simulated state points for PVA-water systems. Liquid densities from the resulting equation of state model at 298.15 K are shown in figure 3.13. The PVA-water liquid densities predicted by the

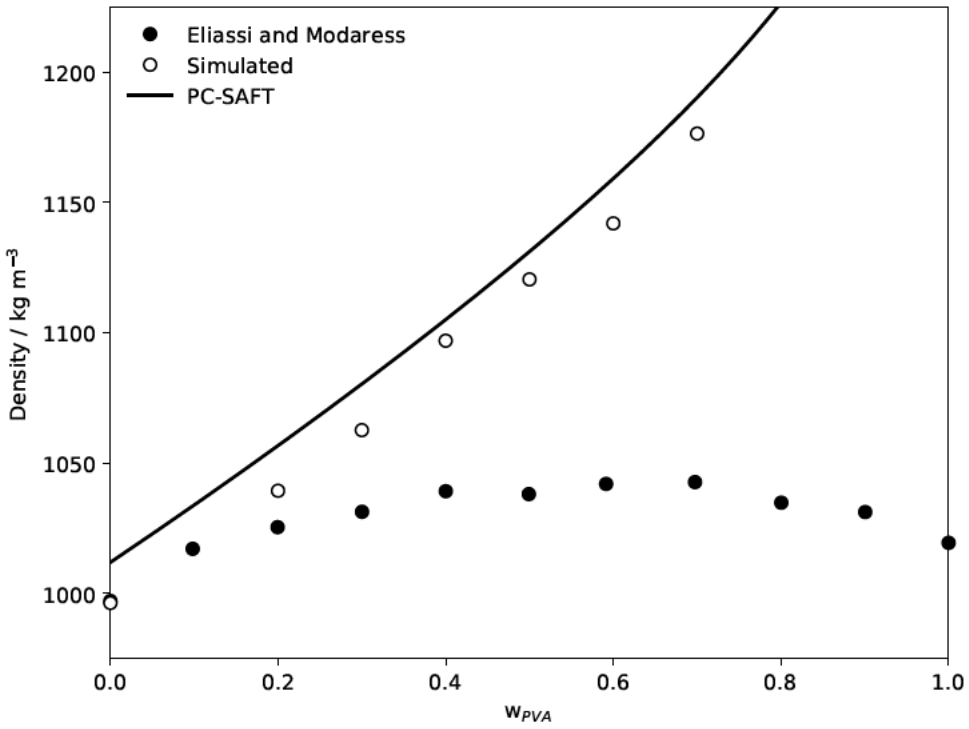

Figure 3.13: Polymer density as function of temperature for PEO-water solutions at 0.3, 0.4, 0.5, 0.6, 0.7, and 0.8 water weight fraction, from simulation with the TraPPE-UA and TIP4P/2005 models.

PC-SAFT model are elevated by approximately 1% relative to simulated values for all system compositions, owing to the increased density of the water model by Diamantonis and Economou [126]. Agreement with experimental densities from Eliassi and Modarress [287] is poor for the same reasons as considered for the simulated systems. Given the significant discrepancy from experimental data, we consider the simulation-developed PC-SAFT model to give a poor description of the overall system behaviour, although a comparison with short-chain PVA-water solution may reveal considerably better model performance.

3.5.3 Polyvinyl Amine - Water

Unlike the hydrophilic polymers discussed so far, polyvinyl amine (PVAm) is a protonatable compound with complex polybase properties in aqueous solution [260, 262]. Water absorption, and the resulting liquid solutions, will be influenced by both the protonation state of PVAm and the presence of balancing anions. In commercial solutions (e.g. Lupamin® 9095) the balancing ions will often be chloride, and the compound sometimes denoted as PVAm-HCl.

The hydration response of dilute PVAm to changes in pH has been investigated by Suh et al. [307], finding a dramatic increase in swelling in acidic solution (2000% relative to dry polymer volume, pH = 3) compared to neutral (pH = 7) or basic (pH = 11) conditions. Under acidic conditions PVAm is nearly fully protonated. The likely explanation of the enhanced swelling is based on the mutual repulsion of positively charged PVAm chains, producing an extended structure able to accommodate more water. Here, we consider aqueous solutions of PVAm in the neutral state in correspondence with the united-atom model used for pure

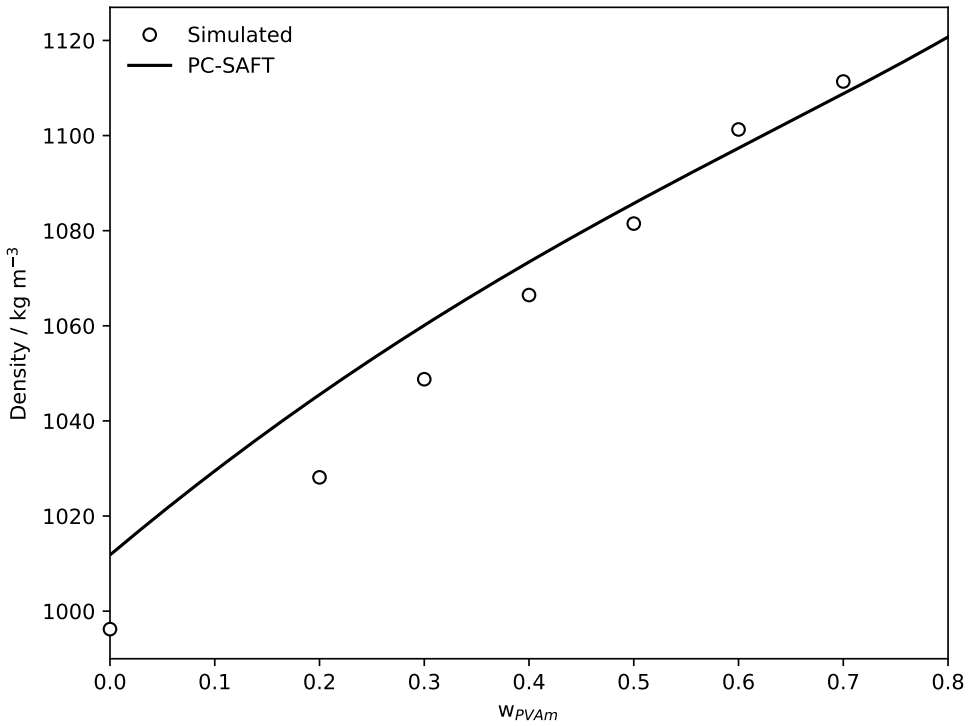

Figure 3.14: Polymer density as function of temperature for PVAm-water solutions at 0.3, 0.4, 0.5, 0.6, 0.7, and 0.8 water weight fraction, from simulation with the TraPPE-UA and TIP4P/2005 models. Apparent molar volumes for 0.3 water weight fraction systems are consistently higher than the more dilute systems, indicative of the system undergoing a phase transition at low water content.

polymer systems in order to develop equation of state parameters, despite this being a somewhat artificial construction.

Molecular simulation of PVAm-water solutions was performed using the modified TraPPE-UA model described in section 2.2 to construct PVAm oligomers ($M_w = 877.4\,\mathrm{g\,mol^{-1}}$), together with TIP4P/2005 [128] water molecules. Particle numbers were chosen to give water weight fractions of 0.3, 0.4, 0.5, 0.6, 0.7, and 0.8, and a system diameter of approximately 3 nm. For each water weight fraction, eight systems at temperatures geometrically spaced in the range 298.15 K - 353.15 K were simulated in parallel using the replica exchange method detailed in section 2.3 for 20 ns. Liquid densities for the resulting 48 state points are reported in appendix B. In figure 3.14, simulated liquid densities are shown for each composition at 298 K.

As for PEO and PVA, the simulated liquid densities at 298 K have a clear increasing trend with polymer content. The systems are nearly equal in density to PEO-water solutions in figure 3.12, mirroring the similar liquid densities seen for small-molecule amine and ether compounds. Using the same approach as for PEO and PVA, a binary interaction parameter $k_{ij} = -0.1336$ was correlated using the objective function in equation 3.10 based on liquid densities at the 48 simulated state points for PVAm-water systems. The binary interaction parameter is negative, similar to that for PEO-water, indicating strong binary polymer-water interactions. Liquid densities from the resulting equation of state model at 298.15 K are shown in figure 3.14. The PVAm-water liquid densities predicted by the PC-SAFT model are elevated by approximately 1% at low polymer content, but approach simulated densities with a mean average deviation of 0.4% for the

compositions shown. The parallels between the PC-SAFT models for PVAm and PEO are striking, with both molecular parameters and the polymer-water binary interaction parameter being similar. While no like-for-like comparison can be made against experimental data, the PC-SAFT model for PVAm appears to represent the solution properties of PVAm-water in a manner consistent with a highly absorbent and water-soluble polymer.

3.6 Summary

This chapter has detailed the development of molecular models for the polymers PEO, PVA, and PVAm together with their aqueous solutions. In order to identify the physical properties used for model development, thermodynamics of pure polymer and their solutions were first reviewed in section 3.2. Typical ρpT behaviour of polymers, showing glass-rubber and rubber-glass transitions, were illustrated by polyether ether ketone in figure 3.1, while polymer-solvent liquid-liquid phase behaviour and absorption isotherms were illustrated in figures 3.2 and 3.3, respectively.

Models for the molecular simulation of polymers and their solutions were reviewed in section 3.3, with the partially coarse-grained TraPPE-UA family of potentials identified as most suitable for systems where phase behaviour is of interest. PEO and PVA are both well described based on literature TraPPE-UA parameters [105, 104]. For PVAm, new dihedral potentials were developed in section 3.3.2, describing C-C-C-N, C-C-N-H, and C-C-N-C torsional interactions.

Using molecular simulation, the ρpT behaviour of PEO, PVA, and PVAm was characterised in section 3.4 for their respective melt phases. Simulated ρpT data were found to be in good agreement with experiment for PEO, with a mean average deviation of 0.1% in the temperature range 373 K - 473 K. For PVA, the experimental melt phase occurs close to the point of thermal degradation, so experimental data for the melt phase have limited reliability. However, simulated densities were nonetheless found to be close to experimental values for the temperature range 500 K-540 K. For PVAm, the simulation data show ρpT behaviour similar to that of PEO, although no experimental data are available for comparison.

The simulated ρpT data were used to develop PC-SAFT models for each of the three polymers, illustrated in figures 3.8, 3.9, and 3.10. The resulting molecular parameters were reported in table 3.2, and compared against PC-SAFT molecular parameters reported in literature based on experimental data for PEO and PVA. For PEO, where an unambiguous melt phase can be characterised experimentally, the PC-SAFT parameters developed from molecular simulation were found to be very close to the PC-SAFT parameters reported by Peters et al. [241, 242].

Continuing the approach of utilizing molecular simulation to characterise ρpT behaviour, the aqueous solutions of PEO, PVA, and PVAm were simulated using TraPPE-UA models in combination with the TIP4P/2005 [128] model for water over the temperature range 298 K - 353 K. From the resulting ρpT data, binary interaction parameters were developed for each polymer-water pair. In figures 3.12 - 3.14, both

molecular simulation data and the resulting PC-SAFT model behaviour were compared against experimental ρpT data, together with solution activities for PEO.

Overall, the hybrid molecular simulation / equation of state predictive approach was found to give good quantitative descriptions of pure polymer ρpT behaviour for the cases considered, and a reasonable qualitative representation of polymer-water systems. Liquid densities of PEO-water solutions were well represented, and the water activities in figure 3.12 indicate the solution is miscible. For PVA, the phase behaviour of the simulated system deviated from experimental behaviour, as shown in figure 3.13. However, this is likely due to chain length effects, and the simulation data are assumed to be representative for short-chain PVA solutions. For PVAm, the system behaviour was close to that of PEO, indicating a highly water-soluble polymer.

The proposed model for PVAm allows exploration of vapour-liquid equilibrium and gas solubility in the selective layer of facilitated transport membranes. However, for application to reactive CO_2 absorption, additional features of organic amine absorption must be understood. In chapter 4, the properties of organic electrolyte compounds are considered, and new models for alkylammonium and bicarbonate are developed for molecular simulation of their aqueous solutions. Chapter 5 details the processes governing reactive absorption, and how this process may be integrated with the equation of state model for PVAm described here. Finally, in chapter 6 the model for PVAm and PVAm - H_2O solutions developed here is applied to study reactive absorption of CO_2 and predict the performance of facilitated transport membranes under varying process conditions.

Chapter 4

Models of Electrolyte Solutions

4.1 Overview

Electrolytes are compounds which dissociate to form ionic species in solvent, producing electrically conductive solutions. The ionic species can either form from the electrolyte itself, as for sodium chloride, or be generated through a chemical reaction, as seen in absorption of CO_2 in aqueous amine solvents and facilitated transport membranes. Solvation of electrolytes influences the thermodynamic properties of solvents, electrolyte species, and the overall properties of solutions, such as density, heat capacity, and viscosity. In the context of phase equilibrium, electrolyte concentration modulates solvent and ion activity, as well as the solubility of other species. These effects may be understood by considering the ion-solvent and ion-ion forces acting in solution.

In this chapter, we begin by considering the physical behaviour of electrolyte solutions, spending some time developing the conventional Born and Debye-Hückel models of electrolyte solutions in sections 4.2 and 4.3. While these continuum models are presented in detail in other works, they serve as useful illustrations of the interactions governing thermodynamic behaviour in electrolyte solutions, and allow us to reflect on the reasons for failure of of classical theory in complex solutions. Empirical extensions to Debye-Hückel theory are also considered, exemplified by the Pitzer equation in section 4.4.

Building from the developments for polymer systems in chapter 3, the most straightforward molecular modelling approach for electrolyte solutions would be to use an equation of state description. This chapter examines commonly employed 'electrolyte' equations of state in section 4.5, reviewing the key differences in treatment of electrolytes between each approach. We first consider primitive models employing a continuum assumption for solvent permittivity, such as used in the conventional Debye-Hückel model. These models are seen to fail for complex fluid systems, motivating the use of more elaborate non-primitive approaches. Non-primitive models in the context of electrolyte solutions refers to explicit representation of solvent polarity, and representation of solution thermodynamic properties without evoking the dielectric constant. However, non-primitive models are found to be poorly developed for the polymer-solvent systems encountered in facilitated

transport membranes, necessitating the use of molecular simulation.

As an alternative to dielectric continuum and non-primitive theoretical approaches to electrolyte solutions, molecular simulation implicitly calculates the dielectric properties and ion-solvent interactions based on the constituent species of a system. In the second half of this chapter, electrolyte models for molecular simulation of alkylammonium, halide, and bicarbonate species are developed in order to build model parameters for facilitated transport membranes.

In section 4.6, literature approaches and models for simulation of electrolyte solutions are reviewed. Single-atom models make up the majority of past research efforts, with selected alkali halide models reviewed in section 4.6.1. Selection of target properties for electrolyte model development in the context of calculating fluid phase properties is discussed in section 4.6.2, alternative dispersion potentials in section 4.6.3, while consideration to non-integer charge models and the charge-scaling approach is given in section 4.6.4.

Using the identified best practices for electrolyte model development, section 4.8 develops molecular parameters for simulation of alkylammonium chloride solutions trained against experimental solvent activity data. Alkylmmonium parameters are constructed to be compatible with the TraPPE-UA model for organic amines developed in chapter 3, so that hydrated amine compounds can be represented in the protonated state when considering reactive systems in chapter 5 and facilitated transport membranes in chapter 6.

With a similar approach as for alkylammonium, molecular parameters are developed for bicarbonate in section 4.9, the primary anion expected for facilitated transport membranes. In combination, the new models provide an avenue for studying solutions of organic ammonium bicarbonate solutions, including a wide range of solutions important to CO_2 absorption applications. To test the transferability of the alkylammonium and bicarbonate models, water activity is predicted for tetramethylammonium bicarbonate solutions, and found to be in excellent agreement with experimental values.

4.2 Born Model

The simplest model of electrolyte solvation is that of spherical ions dissolved in a continuous dielectric solvent. Interactions between the ion and solvent are isotropic, and ions (of either charge) do not interact with each other in solution. The resulting free energy is described solely by the Coulomb potential for the ion, and corresponds to the energy required to 'charge up' the electric field in the surrounding dielectric medium to align with the ion in solution. For a fluid of permittivity ϵ, the electrostatic potential ψ at the boundary of a spherical ion with radius r_0 is

$$\psi(r_0) = \frac{\lambda}{4\pi\epsilon r_0} \tag{4.1}$$

for an ion with variable charge λ. Here, λ takes on values from 0 to q where q is the formal charge of the ion, equivalent to the thermodynamic perturbation approach described in subsection 2.3. The corresponding free energy A^{Born} can be found by integrating the work of charging up the ionic solute by adjusting λ from

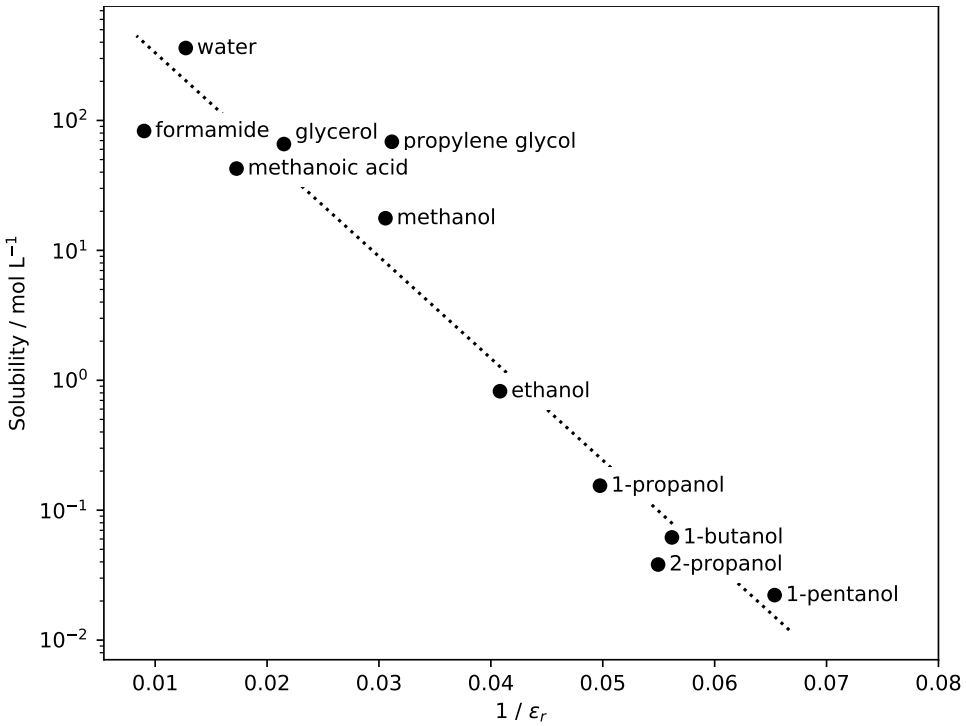

Figure 4.1: Solubility of sodium chloride at 298 K in hydrogen-bonding solvents with varying dielectric constants, with solid circles indicating experimental values reported by Burgess [309]. The dotted line shows scaling according to the Born model of ion solvation (equation 4.3) for solubility in similar solvents.

0 to q, with the resulting free energy

$$A^{\mathrm{Born}} = \int_0^q \psi \, \mathrm{d}\lambda = \frac{q^2}{8\pi\epsilon r_0} \tag{4.2}$$

for creating an ion in the dielectric medium. Note that free energies from continuum solvation models are often quoted as Gibbs free energy, although no pressure-work is incorporated in the model description. In practice, pressure-work in electrolyte solutions is negligible due to the small volume change of the liquid phase. Additionally, it has been argued by Atkins and MacDermott [308] that the work integral in equation 4.2 should be replaced by a summation due to the integer charges found in real systems, however as discussed in section 2.2 non-integer charges are readily used in the thermodynamic perturbation formalism. From equation 4.2, the free energy change for ion transfer between different solvents can be calculated. In the special case of ion transfer from a hypothetical vacuum state ($\epsilon = \epsilon_0$) into solvent, the free energy of solvation can be calculated as

$$\Delta_{\mathrm{solv}} A^{\mathrm{Born}} = -\frac{q^2}{8\pi\epsilon_0 r_0}\left(1 - \frac{1}{\epsilon_r}\right) \tag{4.3}$$

where ϵ_r is the relative permittivity of the solvent such that $\epsilon_r = \epsilon/\epsilon_0$. Equation 4.3 is known as the Born equation, and is the foundation of continuum electrostatics treatments of electrolyte solvation, and allows prediction of relative solublity between solvents of different permittivity.

To assess the applicability of the Born equation, figure 4.1 compares the solubility of sodium chloride

for solvents of varying relative permittivity. The Born equation predicts a logarithmic decrease in solubility with $1/\epsilon_r$, indicated by the dotted line. The experimental values show reasonable agreement with the Born equation over four orders of magnitude in solubility. However, in practice the assumptions of equation 4.3 only apply within a group of similar solvents: the effective ion radius r_0 is sensitive to changes in short-ranged ion-solvent interactions, resulting in large variations in solubility between chemically different solvents.

In addition to the lack of transferability between different solvents, a major shortcoming for the Born model of ion solvation is the lack of concentration dependence in the system description. Solvation free energy $\Delta_{\mathrm{solv}}A^{\mathrm{Born}}$ is fixed for a given solvent due to the assumption of no ion-ion interactions and the permittivity of the continuum solvent remaining constant. These are reasonable assumptions for very dilute systems, where ions do not encounter each other and the dielectric properties remain those of the bulk solvent.

As electrolyte concentration increases, the assumption of no ion-ion interactions breaks down due to long-range electrostatic interactions between ions. This stabilization of electrolyte species with increasing concentration causes a reduction in electrolyte activity coefficient, with a corresponding increase in solvent activity coefficient due to the Gibbs-Duhem equation. A successful theory setting out the relationship between electrolyte concentration and solution activities was first described by Debye and Hückel [310, 311].

4.3 Debye-Hückel Model

The Born model outlined above treats each ion as exclusively interacting with the surrounding solvent. To better account for solvent and electrolyte activities in solutions of higher concentration, long-range electrostatic forces between ions must be considered in addition to the Born energy described previously. The Debye-Hückel model [310, 311] of electrolyte solutions provides an analytical solution for systems away from infinite dilution. In order to provide a background for understanding the dominant forces in electrolyte solutions, a brief derivation of Debye-Hückel theory is given below. Further details of Debye-Hückel theory and its implications for electrolyte equations of state are discussed in further detail in the recent review by Kontegeorgis et al. [312].

Rather than treating the ion as solvated in an infinite electrostatic continuum, the Debye-Hückel model considers electrostatics in two regions. Firstly, the immediate environment of the ion will contribute a solvation energy similar to that of the Born model. No other ions occupy this space: it is within the distance of closest approach, a_0. The distance a_0 is separate from the ion radius r_0 in the Born model. Secondly, the more distant region will tend to be occupied by ions of opposite charge, attracted by long-range electrostatic forces. We are interested in the electrostatic potential ψ_i around the central ion. Within the distance of closest approach, we ignore the effects of external ions and the electrostatic potential is given by Laplace's equation,

$$\nabla^2\psi_i(\mathbf{r}) = 0, \qquad r \leq a_0. \tag{4.4}$$

Hence, the electrostatic potential is simply the electrostatic potential of the Born model (equation 4.1), up

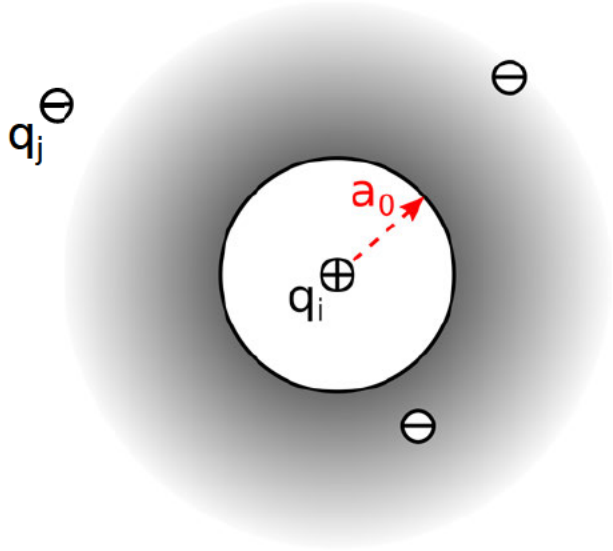

Figure 4.2: Point charges in electrostatic continuum. The Debye-Hückel model considers the mean field attraction of opposite charges around the central ion in addition to the solvation energy of the central ion in the surrounding continuum.

to an additive constant C_0

$$\psi_i(\mathbf{r}) = \frac{q_i}{4\pi\epsilon_0\epsilon_r r} + C_0, \qquad r \leq a_0 \tag{4.5}$$

where C_0 is left indeterminate for now. Outside the distance of closest approach, the effect of other charges on the electrostatic potential become important. In general, the electrostatic potential is related to the surrounding charge density $c_j(\mathbf{r})$ by the Poisson equation,

$$\nabla^2\psi_i(\mathbf{r}) = -\frac{c_j(\mathbf{r})}{\epsilon_0\epsilon_r} \tag{4.6}$$

whereby the problem becomes determining the charge density around the central ion. This may be solved in a mean field sense by considering the ion-ion radial distribution function $g_{ij}(\mathbf{r})$ and ignoring three-body effects, giving

$$c_i(\mathbf{r}) = \sum_j \rho_j q_j g_{ij}(\mathbf{r}) \tag{4.7}$$

with j summed over all oppositely charged species in solution. Continuing the mean field approach, the single-ion radial distribution function for an oppositely charged ion j in the electric field of i is approximated as the Boltzmann weighted electrostatic potential energy between ions i and j, allowing the charge density to be expressed as

$$c_i(\mathbf{r}) = \sum_j \rho_j q_j \exp\left[-\frac{q_j\psi_i(\mathbf{r})}{k_\mathrm{B}T}\right] \tag{4.8}$$

where $k_\mathrm{B}T$ is the thermal energy. The Boltzmann weighted distribution of ions in equation 4.8 is at the core of Debye-Hückel theory, providing an analytical mean-field solution to the system state. Expanding equation 4.8

to the first order in ψ_i around $\mathbf{r} = 0$ and substituting the resulting expression for c_i into equation 4.6 gives

$$\nabla^2\psi_i(\mathbf{r}) = -\frac{1}{\epsilon_0\epsilon_r}\sum_j \rho_j q_j \left[1 - \frac{q_j\psi_i(\mathbf{r})}{k_\mathrm{B}T}\right] \tag{4.9}$$

which together with the electroneutrality condition $\sum_i \rho_i q_i = 0$ gives an electrostatic potential in the region of ion-ion interactions described by

$$\nabla^2\psi_i(\mathbf{r}) = \frac{1}{\epsilon_0\epsilon_r k_\mathrm{B}T}\sum_j \rho_j q_j^2\psi_i(\mathbf{r}), \qquad r > a_0. \tag{4.10}$$

At this point we may define the Debye length κ^{-1} (with κ sometimes referred to as the inverse Debye screening length) as

$$\kappa^2 = \frac{1}{\epsilon_0\epsilon_r k_\mathrm{B}T}\sum_j \rho_j q_j^2 \tag{4.11}$$

allowing equation 4.10 to be written as

$$\nabla^2\psi_i(\mathbf{r}) = \kappa^2\psi_i(\mathbf{r}), \qquad r > a_0 \tag{4.12}$$

which can be recognized as the Helmholtz equation. Solutions to equation 4.12 are of the form

$$\psi_i(\mathbf{r}) = C_1\frac{e^{-\kappa r}}{r} + C_2\frac{e^{\kappa r}}{r} \tag{4.13}$$

where the constants C_1 and C_2 are determined by boundary conditions. For large r, the electrostatic force vanishes so we must have $C_2 = 0$. Further, at $r = a_0$ the value and gradient of ψ_i must be consistent between equations 4.5 and equation 4.13:

$$\psi_i(\mathbf{r})\Big|_{r\to a_0^-} = \psi_i(\mathbf{r})\Big|_{r\to a_0^+}, \qquad \frac{\mathrm{d}\psi_i(\mathbf{r})}{\mathrm{d}r}\Big|_{r\to a_0^-} = \frac{\mathrm{d}\psi_i(\mathbf{r})}{\mathrm{d}r}\Big|_{r\to a_0^+}. \tag{4.14}$$

These conditions give the values of constants C_0 (from equation 4.5) and C_1 as

$$C_0 = -\frac{q_i}{4\pi\epsilon_0\epsilon_r}\left(\frac{\kappa}{1+\kappa a_0}\right), \qquad C_1 = \frac{q_i}{4\pi\epsilon_0\epsilon_r}\left(\frac{e^{\kappa a_0}}{1+\kappa a_0}\right), \tag{4.15}$$

with either C_0 inserted into equation 4.5 or C_1 inserted into equation 4.13 at radius a_0 resulting in the same electrostatic potential. Simplifying the resulting expression, we obtain the electrostatic continuum potential adjusted for the Debye-Hückel energy:

$$\psi_i(r = a_0) = \frac{q_i}{4\pi\epsilon_0\epsilon_r r_0}\left(\frac{1}{1+\kappa a_0}\right). \tag{4.16}$$

The corresponding Helmholtz free energy can be found by a thermodynamic charging process for q_i, similar to the approach for the Born model,

$$A^{\mathrm{DH}} = \int_0^{q_i} \psi_i(\lambda)\,\mathrm{d}\lambda \tag{4.17}$$

with resulting Helmholtz free energy

$$A^{\mathrm{DH}} = -\frac{\kappa}{4\pi\epsilon_0\epsilon_r} q_i^2 \chi \tag{4.18}$$

where χ is

$$\chi = \frac{1}{(\kappa a_0)^3}\left[3/2 + \ln(1+\kappa a_0) - 2(1+\kappa a_0) + (1+\kappa a_0)^2/2\right] \tag{4.19}$$

using κ as defined in equation 4.11.

From equation 4.18 the chemical potentials of ion or solvent species can be obtained thorough equation 2.36. Many electrolyte equations of state employ the Debye-Hückel contribution A^{DH} in combination with a reference fluid Helmholtz free energy contribution to describe the thermodynamics of electrolyte solutions. In the case of associating equations of state, the resulting system description is a hybrid between molecular and continuum theory: association interactions are evaluated based on radial distribution functions, while Debye-Hückel interactions assume a fluid continuum for electrostatic properties.

The effect of long-range electrostatic interactions for electrolytes can be conveniently shown by considering activities in low concentration solutions. Conventionally, either the mean ionic activity coefficient $\gamma_\pm$ or the osmotic coefficient ϕ are used. The mean ionic activity coefficient is defined on molality basis as

$$\gamma_\pm = \frac{\mu_\pm - \mu_\pm^\circ}{RTm\nu M_s} \tag{4.20}$$

where m is the electrolyte molality, $\mu_\pm$ is the mean ionic chemical potential, and $\mu_\pm^\circ$ is the mean ionic chemical potential at a hypothetical reference state with concentration 1 molal and infinite dilution conditions. Similarly, the osmotic coefficient is defined on molality basis as

$$\phi = -\frac{\mu_s - \mu_s^\circ}{RTm\nu M_s} \tag{4.21}$$

where μ_s is the solvent chemical potential and μ_s° the chemical potential for the neat solvent. In equations 4.20 and 4.21, ν is the stoichiometric number of the electrolyte and M_s the molar mass of solvent.

For a single electrolyte solution the ion activity coefficient and osmotic coefficient are related through the Gibbs-Duhem equation [313], and may be calculated by integrating

$$\gamma_\pm = \phi - 1 - 2\int \frac{1-\phi}{\sqrt{m}}\,\mathrm{d}\sqrt{m} \tag{4.22}$$

The Debye-Hückel model only has a single adjustable parameters describing the ions, and no ion-specific parameters other than formal charge. As such it is a striking example of predictive theory in complex fluid

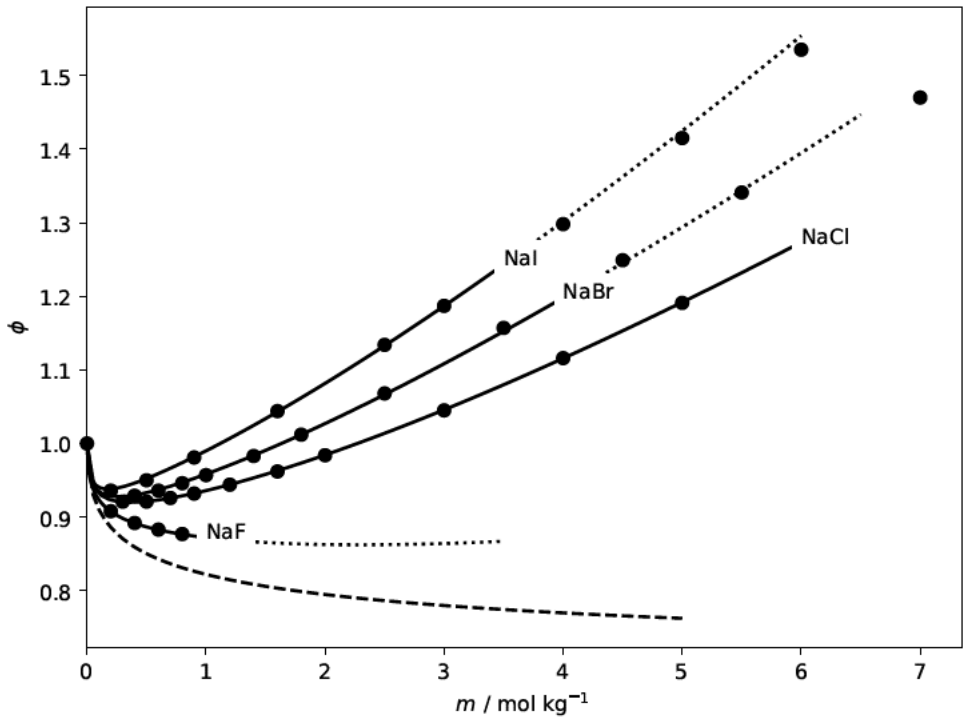

Figure 4.3: Osmotic coefficients as function of molality for the sodium halides in water at 298.15 K. Symbols indicate experimental values from Hamer and Wu [314] (only a subset of the data are shown for clarity). Solid lines indicate Pitzer model [315] using parameters from Pitzer and Mayorga [316], with dotted lines indicating extrapolation beyond model validity. The dashed line indicates limiting Debye-Hückel behaviour.

systems. The prediction of Debye-Hückel theory is shown in figure 4.3, comparing osmotic coefficients for a series of sodium halide salts in water. While the predicted osmotic coefficients are lower than experimental values for high-concentration systems, the limiting slope for each salt at low concentration ($m < 0.1$) converges to the same Debye-Hückel behaviour. This indicates that while treating ion-ion interactions in a mean field manner is acceptable for dilute solutions, systems with high concentrations require additional corrections to the treatment of electrostatics to capture experimental behaviour.

4.4 Pitzer and Other Empirical Models

While the Debye-Hückel theory presented above is well suited to represent electrolyte activity in dilute solutions, the behaviour of real electrolyte solutions rapidly diverges from theory with increasing concentration. The neglect of short-ranged ion-ion interactions becomes increasingly unphysical once concentration increases sufficiently for a significant number of near-neighbour interactions to take place. A number of extensions to Debye-Hückel theory have been proposed to account for the interactions of electrolyte solutions at moderate concentrations. The most widely used description is perhaps that of Pitzer et al. [315, 316, 317, 318, 319, 320], incorporating the effect of a repulsive hard core for ionic species. The Pitzer model for electrolyte solutions incorporates the following key assumptions.

- Solvent is treated as a dielectric continuum with constant permittivity.

- Solutes are treated as repulsive hard spheres, not permitting closer approach than the contact radius.
- Short-range ion-ion interactions are calculated from the second- and third-order virial coefficients.
- Long-range electrostatic interactions are calculated from the Debye-Hückel model.

The free energy formulation of the Pitzer model is presented here for reference, with a full derivation provided by Pitzer [315]. As for the Born and Debye-Hückel models, Pitzer uses Gibbs free energy to describe solution thermodynamics. Here, Helmholtz free energy is employed instead for compatibility with the general equation of state thermodynamic framework in section 2.4. For a solution of a single electrolyte MX the Helmholtz free energy is given by

$$\frac{A^{\mathrm{Pitzer}}}{RT} = -A_\phi \frac{4I}{b} \ln\left(1 + bI^{1/2}\right) + 2m^2 \nu_{\mathrm{M}} \nu_{\mathrm{X}} B^{\mathrm{G}} + 2m^3 (\nu_{\mathrm{M}} \nu_{\mathrm{X}})^{3/2} C^{\mathrm{G}} \tag{4.23}$$

where A_ϕ is the Debye-Hückel coefficient, I the ionic strength, b a solvent-specific constant set to 1.2, and ν is the stoichiometric number for each ion. B^{G} and C^{G} are electrolyte-specific terms, defined by

$$B^{\mathrm{G}} = \beta^{(0)} + \frac{2\beta^{(1)}}{\alpha^2 I}\left(1 - \exp\left[-\alpha I^{1/2}\right]\left(1 + \alpha I^{1/2}\right)\right) \tag{4.24}$$

where α is a solvent-specific constant typically set to 2, and

$$C^{\mathrm{G}} = \frac{C^\phi}{2} \tag{4.25}$$

where $\beta^{(0)}$, $\beta^{(1)}$, and C^ϕ are electrolyte-specific adjustable parameters. The parameters $\beta^{(0)}$ and $\beta^{(1)}$ define the second-order virial coefficient of the electrolyte pair, while C^ϕ defines the third-order virial coefficient which in many cases can be neglected in real electrolyte systems [315]. The Pitzer equation can be parameterised to give an accurate description of activity in simple electrolyte solutions up to a concentration of several molar, as shown in figure 4.3 for the sodium halides. With extensions for multi-valent ions, mixed electrolyte mixed solutions, and various solvents, Pitzer model is well suited for solutions of most simple ions.

For molecular species such as charged organic compounds, solute interactions often have more structure than the ion pairs formed by spherical electrolytes. These interactions may include directional bonding, formation of ion-solvent clusters, and regions of increased or decreased charge density. An extreme example of structured ion-ion interaction is the formation of micellar vesicles by salts of long-chain carboxylate acids, where ions of like charges nonetheless show cooperative behaviour.

The Pitzer model and other theories developed on similar premises fail when considering ions with more heterogeneous solute-solute interactions. This is the case for tetraalkylammonium chlorides, where solution activity shows increasingly complex behaviour with lengthening alkyl chains. Parameters for the Pitzer model fitted to alkylammonium chloride osmotic coefficients from Lindenbaum and Boyd [321] are reported in

Table 4.1: Pitzer coefficients for alkylammonium chlorides fitted to experimental osmotic coefficients from Lindenbaum and Boyd [321] for tetramethylammonium chloride (Me_4NCl), tetraethylammonium chloride (Et_4NCl), tetrapropylammonium chloride (Pr_4NCl), and tetrabutylammonioum chloride (Bu_4NCl). Limit of validity indicated by m, with coefficients fitted using least-squares regression up to this concentration.

electrolyte	$\beta^{(0)}$	$\beta^{(1)}$	C	m / mol kg^{-1}	RMSD
Me_4NCl	0.0654	−0.1752	−0.0001	6.0	0.005
Et_4NCl	0.0669	−0.1266	0.0089	4.5	0.004
Pr_4NCl	0.1293	−0.2904	0.0174	2.5	0.005
Bu_4NCl	0.2240	−0.3690	−0.0538	2.0	0.004

table 4.1.

A comparison of the Pitzer-Mayorga model against experimental osmotic coefficients for alkylammonium chloride systems is shown in Figure 4.4. At low concentration, each compound obeys the familiar Debye-Hückel slope. As concentration increases the osmotic coefficients of short-chain methylammonium and ethylammonium species are reasonably described by the Pitzer model, with an initial dip followed by monotonic increase. For the long-chain propylammonium and butylammonium species, osmotic coefficients instead level off and decline with increasing concentration, including a characteristic 'double dip' for tetrabutylammonium chloride. This indicates changes to the fluid structure beyond simply solvation and ion-ion interactions.

The changes to fluid structure and thermodynamics with increasing content of organic electrolytes do not follow the anticipated behaviour of electrolyte solutions, but rather resemble those seen in conventional fluid mixtures. This is expected, as the fluid mixture increasingly takes on the character of its organic components. This merger of electrolyte- and fluid mixture effects motivates the combination of electrolyte theory with an equation of state treatment for the fluid mixture, accounting both for long-range electrostatics and short-ranged fluid interactions as discussed in chapter 2. However, the continuum solvent assumption in electrolyte solution theory conflicts with the molecular- or lattice-based approaches outlined previously, leading to differing implementations of electrolyte equations of state.

A number of other extensions or modifications to Debye-Hückel theory have been proposed, such as the Davies equation [322] and specific ion interaction theory developed by Guggenheim and Turgeon [323]. In each case, post-Debye-Hückel theories are predominantly empirical in nature, and better suited as frameworks for data regression rather than predictive tools for complex electrolyte solutions. Indeed, the Pitzer model was shown by Rowland et al. [324] to perform similarly for most ions as a simple power law expansion in molality.

4.5 Electrolyte Equations of State

As ion concentration increases, the solvent content of an electrolyte solution decreases with concomitant changes to fluid properties. In the case of tetrabutylammonum bromide at 15 molal shown in figure 4.4, the electrolyte makes up 83% of the liquid mass. Similar changes in composition are expected for CO_2 absorption in aqueous amine solutions and facilitated transport membranes. Given the departure of fluid composition

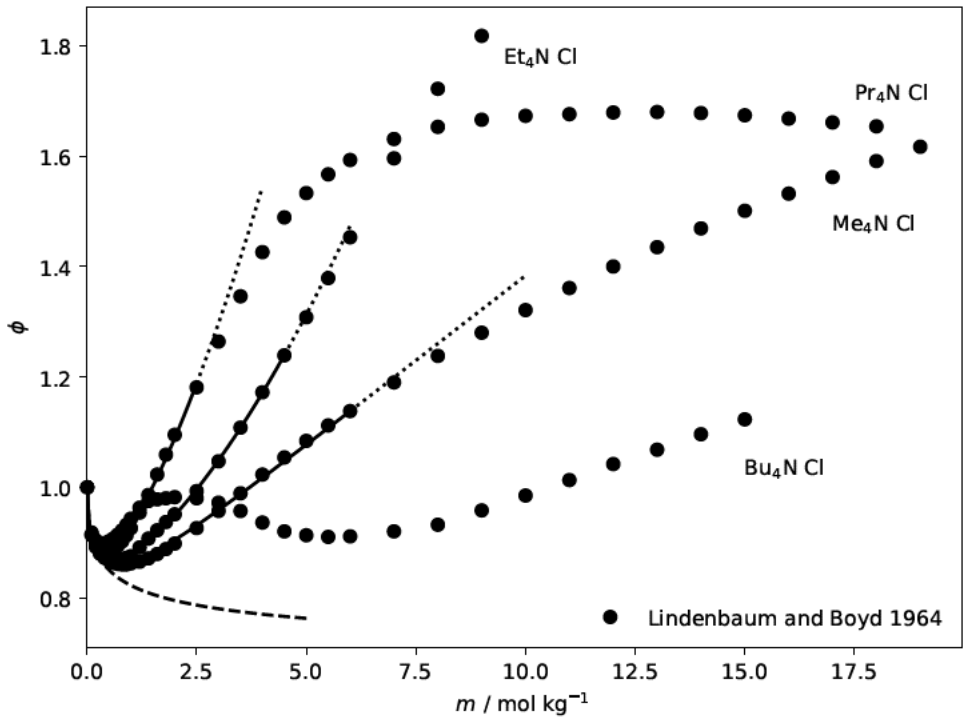

Figure 4.4: Osmotic coefficients as function of molality for alkylammonium chlorides in water at 298.15 K. Symbols indicate experimental values from Lindenbaum and Boyd [321]. Solid lines indicate Pitzer model [315] for Me_4NCl, Et_4NCl, and Pr_4NCl using parameters from table 4.1, with dotted lines showing extrapolation beyond model validity. For Bu_4NCl the model validity range is too small to be observed. The dashed line indicates limiting Debye-Hückel behaviour.

from the original solvent (water), it is unsurprising when properties in these systems fail to be captured by continuum electrolyte models: these are based on assumptions of an invariant solvent continuum and simplified spherical ions. A more rigorous molecular theory for fluid mixtures is required to describe changes to fluid thermodynamics with changing composition.

The properties of fluid mixtures described by molecular equations of state have been detailed in chapter 3, placing particular emphasis on aqueous-organic systems. Molecular theory in the form of associating equations of state has proven successful in representing, and to a large extent predicting, fluid properties for these systems. However, electrolyte solutions (and particularly molecular ions) have proven difficult to represent within the same framework. As a result, Debye-Hückel theory or refinements thereof have been employed in tandem with molecular equations of state. Since the Debye-Hückel model requires knowledge of solvent permittivity – a structural quantity which is only indirectly related to thermodynamic properties and Helmholtz free energy – further machinery is required to implement equation 4.18 for an equation of state. Practical application to fluid systems thus requires additional parameters describing permittivity and its variations with temperature, pressure, and composition including fluid mixtures and varying electrolyte concentration.

The most straightforward method of obtain permittivity is simply measuring it through experiment or by calculation from an empirical correlation. This approach diminishes the predictive capacity of the model particularly for solvent mixtures or high-molality solutions, where separate measurements would be required

for each system of interest. The electrolyte PC-SAFT (ePC-SAFT) model developed by Held et al. [54, 55] and many other electrolyte equations of state belong to this category, often denoted *primitive* models.

A variation of the continuum solvent approach has been proposed by Maribo-Mogensen et al. [56], employing a geometric model for estimating permittivity in conjunction with equation 4.18. This allows modelling of electrolyte solutions at varying conditions without the need for additional empirical data, as demonstrated for the eCPA model (see section 4.5.2). However, challenges remain for high-concentration and organic systems as illustrated in figure 4.4, where the assumptions for Debye-Hückel theory start breaking down.

A third option is abandoning the Debye-Hückel framework and utilizing a so-called *non-primitive* electrolyte equation of state, where solvent is represented as explicit dipolar species rather than a dielectric continuum. Each of the above approaches is discussed further in the following sections.

4.5.1 ePC-SAFT

The ePC-SAFT model developed by Cameretti et al. [325] and Held et al. [54, 55] combines the PC-SAFT equation of state presented in section 2.4 with the Debye-Hückel expression in equation 4.18 to describe Helmholtz free energy of electrolyte solutions with varying solvent composition. Short-ranged ion-ion interactions are neglected in the original ePC-SAFT model, while a later revision by Held et al. [326] includes these. Due to the continuum solvent assumption permittivity must be known for the solvent, with the original work by Cameretti et al. [325] employing the correlation by Floriano and Nascimento [327]. Weak electrolytes such as organic acids are treated using a conventional reaction equilibrium description through the law of mass action,

$$K_{\mathrm{eq}} = \prod_i a_i^{\nu} \tag{4.26}$$

where k_{eq} is the reaction equilibrium constant and ν are stoichiometric coefficients (see chapter 5 for a more detailed treatment of chemical reactions).

The ePC-SAFT equation of state has been applied to a broad spectrum of electrolyte systems relevant to CO_2 solubility in aqueous or aqueous-organic systems. Yan et al. [328] considered solubility of CO_2 in brines, finding good agreement with experimental liquid densities relative to five other equations of state. Held et al. [329] investigated electrolyte solution in water-alcohol mixtures, where ePC-SAFT was able to reproduce the complex composition dependencies of solvent activity in water-ethanol mixtures with a variety of electrolytes. Activity coefficients of electrolytes and solvent in water-urea mixtures were modelled by ePC-SAFT by Sadeghi et al. [330] with average deviations below 5%. Held et al. [331] considered water-amino acid mixtures in a similar study, finding correct sequencing of halide anions with respect to experimental activity.

For the case of CO_2 absorption, special attention has been given to solutions of N-methyldiethanolamine (MDEA) and the MDEA - H_2O - CO_2 ternary system. Uyan et al. [332] considered MDEA and CO_2 each as weakly dissociating electrolytes as proposed by Held et al. [55] and developed three-parameter temperature-

correlations for the resulting binary parameters. The resulting absorption isotherms had an average deviation of 22.9% over the composition ranges studied. Wangler et al. [333] later considered CO_2, H_2S and CH_4 absorption in the same system, with a reported average deviation of 19.7% again relying on temperature-correlated binary interaction parameters. More recently, Cleeton et al. [47] explored competitive absorption in the quaternary systems MDEA - H_2O - CO_2 - H_2S and MDEA - H_2O - CO_2 - CH_4 systems over a wider range of conditions, while employing temperature-invariant binary interaction parameters. The resulting average deviations ranged from 20.3% - 65.5% for data sets of increasing concentration, showing clear degradation of the ePC-SAFT model with increasing organic content, despite the MDEA - H_2O binary system being well represented across the full range of compositions. Unsurprisingly, electrolyte contributions based on constant permittivity break down when departing from the original solvent composition, likely due to changes in permittivity and ion-solvent interactions.

4.5.2 eCPA

The description of permittivity in neat or mixed solvents is intimately linked to microscopic structural organisation, and its prediction is a long-standing problem in the study of liquids. An early study of the connection between permittivity and the structure of liquids was conducted by Kirkwood [334, 335], considering systems of molecular dipoles. For a dipole with moment $\boldsymbol{\mu}$ (note the use of bold vector notation $\boldsymbol{\mu}$ to distinguish from chemical potential μ), the permittivity ϵ_r is given by [335]

$$\frac{(\epsilon_r - 1)(2\epsilon_r + 1)}{\epsilon_r} = \frac{\rho}{\epsilon_0 RT} g_{\mathrm{K}} \boldsymbol{\mu}^2 \tag{4.27}$$

where g_{K} is the Kirkwood g-factor, describing the microscopic alignment of dipoles to a local electric field. For a system of molecular dipoles surrounding a central molecule with dipole $\boldsymbol{\mu}$, the Kirkwood g-factor may be calculated as

$$g_{\mathrm{K}} = \frac{\langle \boldsymbol{\mu} \cdot \mathbf{M} \rangle}{\boldsymbol{\mu}^2}, \tag{4.28}$$

where $\mathbf{M}$ denotes the total dipole of the system including the central molecule. Note that calculation of g_K from any microscopic system assumes the system is large enough that alignement with the central dipole decays at the system boundaries.

As shown by equation 4.28 the Kirkwood g-factor and hence macroscopic dielectric properties are intimately connected with local geometry and alignement. Later work has expanded on the connection between the Kirkwood g-factor and molecular geometry, such as the permittivity in liquid acohols and water by Oster and Kirkwood [336]. Rather than being a static property, g_{K} varies strongly with the applied field frequency once the timescale becomes comparable to that of molecular rearrangement in the fluid (e.g. for optical processes). For equilibrium thermodynamic properties, the zero-frequency value of ϵ_r is conventionally used.

Extending equation 4.27 to mixtures and accounting for electronic polarizability due to induced dipole

moments, Maribo-Mogensen et al. [56] derive the relation

$$\frac{(\epsilon_r - \epsilon_\infty)(2\epsilon_r + \epsilon_\infty)}{\epsilon_r(\epsilon_\infty + 2)^2} = \frac{\rho}{9\epsilon_0 RT} \sum_i x_i g_{K,i} \boldsymbol{\mu}_i^2 \tag{4.29}$$

where the sum is over all species i in the system. The infinite-frequency electric permittivity ϵ_∞ in equation 4.29 is related to molecular polarizability $\alpha_{0,i}$ by the Clausius-Mossotti equation,

$$\frac{\epsilon_\infty - 1}{\epsilon_\infty + 2} = \frac{\rho}{3\epsilon_0} \sum_i x_i \alpha_{0,i} \tag{4.30}$$

suitable for systems of isotropic polarizability. Hence, both static and induced dipoles contribute to the overall electric permittivity of the fluid in equation 4.29. The value of $\alpha_{0,i}$ can be determined experimentally from the refractive index, estimated by quantum-mechanical calculations, or used as a free parameter in the correlation of ϵ_r for a material.

Following a geometric argument similar to that of Oster and Kirkwood [336], Maribo-Mogensen et al. [56] showed that local dipole alignment in an associating fluid mixture can be approximated based on molecular angles γ, θ and the strength of association between fluid components. The resulting expression for g_{K} around species i is [56]

$$g_{\mathrm{K},i} = 1 + \sum_j \left(\frac{\boldsymbol{\mu}_j^2}{\boldsymbol{\mu}_i^2} \right)^{1/2} \frac{z_{ij} P_{ij} \cos\gamma_{ij}}{P_i \cos\theta_{ij} + 1} \tag{4.31}$$

where z_{ij} is the coordination number of species j around species i, P_{ij} is the probability of an association interaction between the two species, and P_i is the probability of the association sites of species i being bonded to any species. Equation 4.31 in combination with equation 4.29 allows calculation of the permittivity of fluid mixtures, provided the parameters $\boldsymbol{\mu}$ and α_0 are known for each species and the geometric parameters z_{ij} γ_{ij}, θ_{ij} for each binary pair.

The electrolyte cubic-plus-association (eCPA) model developed by Maribo-Mogensen et al. [56, 57, 58, 59] combines the permittivity expression in equation 4.29 with statistically associating fluid theory, as outlined in chapter 2. The resulting equation of state allows estimation of permittivity and electrolyte contributions to the Helmholtz free energy, albeit at the cost of two additional species-specific parameters and three binary parameters. The eCPA equation of state has been applied to a variety of systems including organic electrolytes. Sun et al. [337] modelled the vapour-liquid properties of aqueous tetra-n-butyl ammonium halides, investigating activity and density up to electrolyte concentrations exceeding 10 molal. For tetrabutylammonium bromide the authors found average deviations of 9.2% and 7.7% for liquid density and saturation pressures, respectively. Gas solubility in alkylammonium salt solutions was considered by the same authors [338] using temperature-correlated solute-solvent binary interaction parameters, finding average deviations within 10% for N_2, CH_4, and CO_2. However, the qualitative behaviour for e.g. CH_4 solubility in tetraalkylammonum bromide was inconsistent with experimental trends.

The eCPA model is a well developed model for characterising complex electrolyte systems, with a geometric framework for estimating permittivity which bridges the gap between continuum and molecular solvent models. However, the eCPA equation of state is poorly suited for the study of polymer systems due to the use of a cubic equation of state as reference fluid. Additionally the eCPA approach is limited by the large number of parameters required for electrolyte solutions, including knowledge of solvent-solvent interaction angles for dipole projections between associating compounds.

4.5.3 Non-Primitive Models

Developments beyond Debye-Hückel and semiempirical theories are coined non-primitive models for ion solvation, in which solvent is typically represented as molecular dipoles rather than a dielectric continuum. The most commonly used non-primitive model is the mean-spherical approximation (MSA) developed by Percus and Yevick [339] and Lebowitz and Percus [340], where the system of ions and dipoles is represented as hard spheres. Blum et al. [341, 342, 343, 344] developed analytical solutions for the thermodynamic properties of the MSA system, based on ion-ion, ion-dipole, and dipole-dipole contributions to the system Helmholtz free energy. Due to its formulation for hard spheres, the MSA model can be applied in conjunction with associating equations of state based on the same hard-sphere assumptions, as first demonstrated by Liu et al. [345] for a range of electrolytes in aqueous solution. Lee and Kim [346] and later Herzog et al. [347] explored this combination for PC-SAFT, with the latter authors finding a significant improvement in the description of the water vapour-liquid coexistence envelope, together with good descriptions for activity coefficients of alkali halides up to the solubility limit. Only one adjustable parameter was regressed per ion, demonstrating the predictive power of the non-primitive approach relative to continuum solvation models. Other applications of the MSA model in combination with associating equations of state include by Li et al. [348] investigating ionic liquid solutions, Das et al. [349] comparing the results from MSA against Monte Carlo simulation of molecular systems, and Eriksen et al. [350] more recently implementing the MSA model in combination with the Mie potential shown in equation 2.8. However, the MSA model has seen little adoption for organic and chain-like systems, likely due to the differences between spherical dipole systems for which MSA was developed. Further work is needed to establish the applicability of MSA-based non-primitive equations of state for organic electrolyte and polyelectrolyte solutions.

4.6 Molecular Simulation of Electrolyte Solutions

The increasingly complex models described in section 4.5 demonstrate the need for molecular descriptions of both solvent and electrolyte species in order to represent solution thermodynamics. But even the non-primitive MSA model by Blum et al. [341, 342, 343, 344] is limited by its assumptions of uniform spherical dipoles and charges. Molecular simulation offers a more direct and flexible alternative for studying electrolyte solution

thermodynamics, by representing solvent and electrolytes as explicit molecular species.

Electrolyte model development for molecular simulation has largely been focused on monatomic ions, together with protonatable amino acid side chains for biomolecular simulation. The solvent studied has primarily been water, with some exceptions for e.g. alcohol solutions [351, 352] and solutions in water-methanol mixed solvent [353, 354, 355, 356]. Unsurprisingly, electrolytes are preferentially solvated by water in water-methanol mixtures, being an order of magnitude more soluble in this solvent as shown in figure 4.1.

Despite a significant interest in simulation of electrolyte solutions, the optimisation of ion model parameters has been hampered by certain challenges unique to electrolytes:

- To maintain charge neutrality, ions only appear in pairwise or higher combinations. Observable properties are hence characteristics of ion pairs rather than single species.

- Due to charge-transfer interactions with solvent, ion-ion interactions in solutions are significantly different from those in the crystalline state, which compared to the liquid phase is more readily studied e.g. by crystallographic methods.

- While the charge distribution in molecular species can be optimised, ions are typically assigned an integer charge. This reduces the number of parameters for model optimisation. Additionally, integer charges may not reflect the effective ion charge in solution due to charge transfer interactions.

In the next section, model development approaches and parameter optimisation is reviewed for a selection of alkali halide models, reflecting our rapidly developing understanding of ion-solvent interactions [357, 358]. While alkali halides are significantly simpler than the organic ions encountered in reactive CO_2 absorption, they serve as illustrative examples for challenges and successful strategies for electrolyte model development.

4.6.1 Alkali Halide Molecular Models

Alkali halides are inorganic electrolytes formed by a group 1 alkali metal and group 17 halogen. Ions of these compounds are both monatomic and carry a formal charge of one, making their solutions the conceptually least complex of real electrolytes. Further, solutions of commonly encountered alkali halides such as sodium chloride and potassium bromide are well characterised experimentally: Standard thermodynamic quantities including osmotic coefficients, ion activity coefficients, apparent molar volumes, and enthalpies of solution are available for a range of conditions. The properties of alkali halide solutions are somewhat similar, and reasonably described by semi-empirical continuum solvation models as shown in figure 4.1.

The thermophysical properties of alkali halide solutions result from a range of physical interactions. In dilute solution, ion solvation is dominated by short-ranged ion-solvent forces including charge transfer between solvent and solute molecules. These interactions are sufficiently strong to create a relatively stable inner solvation shell, giving rise to the coordination numbers seen experimentally for alkali halides [359]. The

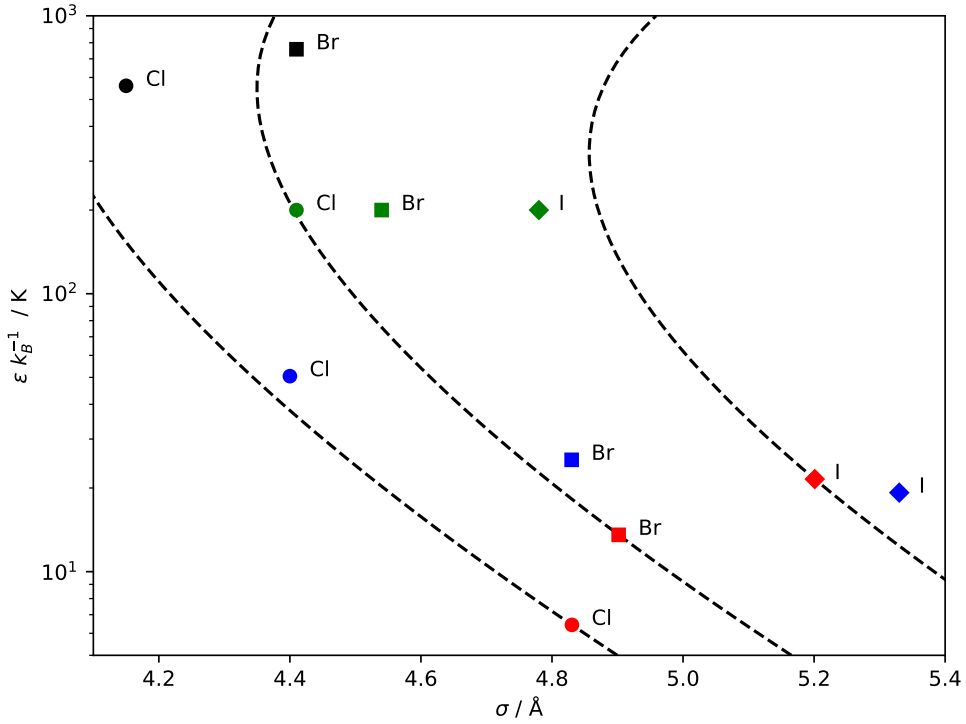

Figure 4.5: Parameter comparison for a selection of integer point-charge halide models with Lennard-Jones dispersion interactions reported in literature. Red: Joung and Cheatham [360, 361]; Blue: Horinek et al. [362], Green: Reiser et al. [363]. Symbol shape denotes chemical identity as indicated in the figure. Each model is developed for simulation with the SPC/E water model [364]. Dashed lines indicate contours of constant solvation free energy at infinite dilution as reported by Joung and Cheatham [360] at 298.15 K.

magnitude of dispersion interactions in alkali halide models varies significantly, as illustrated in figure 4.5 for chloride, bromide, and iodide models.

As concentration increases, ions of oppositely charged species compete with solvent for coordination sites. These ion-ion forces result in ion association pairs or higher-order complexes. Additional long-range electrostatic forces similar to those described in section 4.3 are observed at high concentrations. Hence, a molecular model aiming to describe alkali halide solutions at varying concentration should account for the following three classes of interactions.

- Short-range ion-solvent interactions, including charge transfer and hard core repulsion. These interactions make the primary contribution to solvation free energy, and corresponding to the r_0 parameter in the Born solvation energy from section 4.2.
- Short-range ion-ion interactions, responsible for effects such as Bjerrum pairs and cluster formation. Ion-ion interactions additionally determine the free energy of the crystalline state.
- Long-range electrostatic interactions, generating Debye-Hückel type behaviour as considered in sections 4.3 and 4.4. Long-range electrostatics are dependent on fluid permittivity.

It is worth noting that only the short-ranged ion-solvent and ion-ion interactions are expected to be sensitive to model parameters involving shape and short-ranged dispersion forces. Conversely, long-range electrostatic

interactions according to Debye-Hückel or similar theory are functions of ion charge and solvent dielectric properties, hence would depend only weakly on electrolyte model parameters.

The combination of geometric simplicity and ample experimental data for parameter regression makes alkali halides a natural starting point for building molecular models of electrolytes. Indeed, numerous models of alkali halides have been reported in literature attempting to capture properties of their aqueous solutions, crystal phase, or a combination thereof. Detailed reviews of pairwise potential models of alkali halides have been given elsewhere [357, 358] and will not be repeated here, but the most salient points of electrolyte model development and the current state-of-the-art bears mentioning in brief due to its relevance for organic ions.

4.6.2 Target properties

Similar to solvent and polymer molecular models, the development of electrolyte models requires good quality experimental data describing the system behaviour over a range of experimental conditions. However, unlike organic compounds, electrolyte species cannot be observed in a pure state, and the thermodynamic properties of their solutions must be seen in the context of solvent species. Similarly, electrolyte models are normally developed together with a particular solvent molecular model. Electrolyte model development is therefore an exercise in matching solution thermodynamics of the model solvent - solute system with experimental values.

For alkali halides, a wide range of target properties may be considered, mainly centring on liquid and solid states. The target properties should be chosen based on the intended purpose of the model. As pointed out by Nezbeda et al. [357], target properties should ideally be thermodynamic functions as a function of fundamental variables such as density and temperature. Helmholtz free energy and its derivatives are perhaps the most directly transferable thermodynamic functions for model development. However, changes in enthalpy or Gibbs free energy are more readily available experimentally. Target properties may also belong to more than one phase, such as crystal lattice ionic radii if developing a model intended to reproduce crystalline lattice parameters. Often, a combination of properties are used to avoid over-fitting of the model. In table 4.2, a series of physical properties used for alkali halide model development in the literature are listed together with examples of target property combinations from Joung and Cheatham [360, 361], Horinek et al. [362], and Reiser et al. [363]. For this work, solvent activity and solution density are adopted as target properties due to their direct connection to vapour-liquid absorption processes and strong connection to Helmholtz free energy. For bicarbonate model development (see section 4.9), solution structural properties are employed as an additional target property.

4.6.3 Dispersion Potentials

The short-ranged interactions of ions resemble those between strongly dipolar uncharged molecules such as water, comprising a repulsive core, attractive dispersion interactions, and electrostatic interactions varying with the local charge distribution, as elaborated in section 2.2. However, due to significant charge transfer

Table 4.2: Target properties for electrolyte models considered in this work. Filled circles indicate the property is used as an objective for training model parameters. Depending on the intended use of the model, a combination of liquid phase and solid phase properties may be appropriate, as used by Joung and Cheatham [360, 361]. For studies of transport phenomena, kinetic properties may be included as done by Reiser et al. [363]. This works targets solution activities and densities, similar to the training of solvent models for vapour-liquid coexistence.

Property	Phase	Concentration	Type	Joung and Cheatham [360, 361]	Horinek et al. [362]	Reiser et al. [363]	This work
Hydration free energy	liquid	infinite dilution	thermodynamic	•	•		
Hydration enthalpy	liquid	infinite dilution	thermodynamic				
Hydration entropy	liquid	infinite dilution	thermodynamic		•		
Liquid density	liquid	variable	thermodynamic				•
Solvent activity	liquid	variable	thermodynamic				•
Electrolyte activity	liquid	variable	thermodynamic				
Liquid structure	liquid	variable	structural		•	•	•
Diffusivity	liquid	variable	kinetic			•	
Viscosity	liquid	variable	kinetic				
Permittivity	liquid	variable	kinetic				
Enthalpy of solution	liquid, solid	variable	thermodynamic				
Limiting solubility	liquid, solid	saturation	thermodynamic				
Lattice parameters	solid	-	structural	•			
Lattice energy	solid	-	thermodynamic	•			
Ion-solvent clusters	gas	-	structural				

interactions between ions and solvent as part of the solvation process [365], the delineation of dispersion and electrostatic interactions is less clear-cut than for uncharged molecules. What is often denoted hard-core repulsion has is in reality some structure as a function of separation. For this reason, the use of dispersion potentials developed for uncharged molecules may not be directly transferable to electrolyte species creating a strongly polarized local charge distribution.

While the Lennard-Jones interaction potential discussed in the previous section is most commonly employed for electrolyte molecular simulation [357], a variety of alternative dispersion interaction potentials have been considered in the literature. Dispersion potentials are either based on *ab initio* ion-solvent interaction potentials or empirical approaches. An example of the former is the Born-Mayer-Huggins-Tosi-Fumi (BMHTF) potential [366, 367, 368, 369] described by

$$U^{\mathrm{BMHTF}}(r) = A \exp\left[-\frac{r}{r_0}\right] - \frac{B}{r^6} - \frac{C}{r^8} \tag{4.32}$$

with three energy parameters A, B, and C, together with r_0 describing the 'sharpness' of the repulsive core. The BMHTF potential has been of particular interest for electrolyte force field development, due to its flexibility in the description of short-ranged forces. Ferrario et al. [370] used the BMHTF potential to develop a model for aqueous potassium fluoride, targeting experimental chemical potentials in the liquid and crystal state using a thermodynamic integration approach. The authors obtained a limiting concentration of $17.9\,\mathrm{mol\,l^{-1}}$, compared to $24.4\,\mathrm{mol\,l^{-1}}$ for the experimental solution at ambient conditions. Solution liquid density was also reasonably described, without being targeted as part of the parameter optimisation process.

The approach of Ferrario et al. [370] was later employed by Sanz and Vega [371], who developed a model for sodium chloride based on the BMHTF potential. The authors later revisited the sodium chloride electrolyte system [372, 373] using multiple simulation approaches, finding significant differences in solubility depending on methodology. Other variations in dispersion potentials include the Buckingham potential (see equation 2.7), employed by e.g. Kiss and Baranyai [374] for alkali halide ions together with a polarizable Gaussian charge distribution. The generalized Mie potential (see equation 2.8) has yet to be investigated for molecular simulation of electrolyte solutions, but has been employed through the electrolyte SAFT-VR-Mie equation of state [350].

In each case, variations of ion dispersion interactions requires concomitant evaluation of ion-solvent interactions, and in most cases a solvent model described by the same interaction potential. Due to the importance of short-range ion-solvent interactions, electrolyte models have limited transferability, instead being developed for use with a specific solvent model [357, 358]. Due to the prevalence of the Lennard-Jones potential for molecular models of water, this has also been adopted as the *de-facto* standard for development and comparison of electrolyte models [357, 358].

As for uncharged species, mixing rules are applied to calculate dispersion interaction potentials between

unlike compounds, most commonly using Lorentz-Berthelot rules [357, 358] as defined in section 2.2. While the use of a geometric mixing rule for dispersion energy parameters is reasonably justified for long-range induced dipole interactions observed for uncharged molecules, its suitability for ion-solvent and ion-ion interactions has been questioned [357]. Using integer-charge Lennard-Jones potential models for sodium chloride, Weerasinghe and Smith [375] demonstrated that by scaling sodium-water dispersion interactions, coordination numbers of ion-water and ion-ion pairs could be reconciled with experimental observations. The Kirkwood-Buff-derived model of Gee et al. [359] employed a further variation, with geometric mixing rules and separately optimised ion-ion and ion-water dispersion interactions.

In this work Lennard-Jones dispersion interactions are assumed for all electrolyte species, together with conventional Lorentz-Berthelot combining rules. This ensures compatibility with preexisting models for both water and organic compounds, and no conclusive evidence has been found to support alternative potential functions.

4.6.4 Charge scaling

Models of electrolyte species are normally assigned integer charges, corresponding to the quantized elementary charges of protons and electrons in real ions. The continuum solvent models in sections 4.3 and 4.4 are similarly constructed on the principle of integer electrolyte charges. However, scaled charges in electrolyte solutions have seen use to better represent charge transfer processes since the early work of Jönsson et al. [376] on micelle formation. More recently, a formal argument for charge scaling has been presented by Leontyev and Stuchebrukhov [377, 378, 379, 380, 381] based on electronic polarizability, challenging the conventional wisdom of integer charges in molecular simulation of condensed systems.

Charge scaling approaches typically uses electrolyte total charge as a free model parameter, giving more flexibility to the optimisation of ion-solvent and ion-ion interactions. By scaling ion charges, the model effectively immitates a charge transfer effect, albeit with a constant magnitude optimised for a specific solvent. This primarily empirical approach has been employed by Kann and Skinner [382], finding a charge scaling factor of 0.94 for alkali halides in aqueous solution. Earlier work by Tainter et al. [383] using a similar approach found a charge scaling factor of 0.85. Charge scaling was also employed for the alkali halide models by Li and Wang [384, 385], using an adaptive force matching algorithm [386] in combination with *ab initio* simulation of electrolyte solutions, resulting in a scaling factor of 0.804. Charge scaling has also been used for development of electrolyte force fields which incorporate properties of the crystalline state within the optimisation targets. Fuentes-Azcatl and Barbosa [387] developed a model of sodium chloride targeting crystal density together with concentration-dependent solution density and permittivity, with a scaling factor of 0.885 found to produce good representations of both phases. A broader set of thermodynamic optimisation targets were studied by Benavides et al. [388], developing a sodium chloride model for use with the TIP4P/2005 water model. Benavides et al. [388] use a scaling factor of 0.85, following the work of Tainter et al. [383].

Further development by Zeron et al. [389] expands this model to include both uni- and bi-valent electrolyte species, retaining the same scaling factor in both cases.

While the models presented above employ charge scaling as a primarily empirical optimisation parameter, Leontyev and Stuchebrukhov [381] argue that the charge transfer processes, including molecular polarizability, should be understood as a combination of electronic and nuclear polarizability. Fast electronic effects should be treated separately from slow-moving nuclear charges. Electronic effects create a near-continuum dielectric medium, corresponding to the electronic polarizability of condensed-phase solvent molecules. Electronic polarizability is reasonably similar for most small molecules, with an electronic relative permittivity ϵ_r^{elec} near 2 proposed by Leontyev and Stuchebrukhov [381]. Typical solvent systems have a value of ϵ_r^{elec} in the range 1.7 - 2.2 [390]. To account for electronic permittivity nuclear charges should be scaled by a factor of $1/\sqrt{\epsilon_r^{\text{elec}}}$, corresponding to 0.67 - 0.77 across the above interval of permittivity. Within this 'electronic continuum' framework, all molecular charges - including partial charges in neutral molecules - should be scaled to reflect the electronic and nuclear electrostatics of molecular systems according to this approach. This argument has been tested for solvent systems by Jorge and Lue [391], finding significant improvements to solvent dielectric properties by charge scaling to account for electronic polarizability. The arguments presented by Leontyev and Stuchebrukhov [381] are convincing. However, literature molecular models for fluid simulations are not developed for use in electronic continuum simulation, and it remains unclear whether a full re-parameterisation would be required for solvents.

The varying charge scaling factors proposed above illustrate a fundamental weakness of classical models for simulation of electrolyte solutions: the charge transfer process is electronic in nature, while classical molecular simulation is based on nuclear degrees of freedom. The different scaling factors proposed for electrolyte models above reflect different compromises between thermodynamic properties - and the choice of solvent studied. Hence, model parameters become system-specific quantities. This makes scaled-charge electrolyte models poorly transferable to new solvent systems, particularly with differing charge-transfer interactions.

Additionally, the electronic continuum framework of Leontyev and Stuchebrukhov [381] suffers from a shortcoming of validated molecular models, particularly for organic solvents and vapour-liquid equilibrium simulations. It is also unclear how ϵ_r^{elec} should be resolved for systems comprising both liquid and vapour phases. Hence, conventional integer charges are assumed for the electrolyte species in this work.

4.7 Model Development Strategy

As argued in section 4.6.2, the target properties of existing electrolyte models largely focus on the liquid phase at infinite dilution. Conversely, the use of classical interaction potentials and integer charge electrolyte models to describe solvent activity in electrolyte systems is largely unexplored. In the next sections, the target properties from table 4.2 are used to develop molecular parameters for halides, alkylammonium, and

bicarbonate, the primary species required to represent reactive CO_2 absorption by organic amines. The model parameters are in each case numerically optimized in order to obtain models which can reproduce thermodynamic properties in real electrolyte solutions.

Parameter optimization is performed as a minimization of an objective function $f(C_i)$ describing the degree of agreement between physical properties in molecular simulation and those of target systems, and where C_i are model parameters (for example, σ and ϵ Lennard-Jones parameters) to be optimized. However, the objective function is a costly quantity to obtain as it must be evaluated by molecular simulation. For a single evaluation of solvent activity a set of 3 - 10 independent simulations are used, in order to obtain a numerical precision for $\Delta_{\mathrm{solv}}G$ of 0.1 kJ mol^{-1}. While this is considerably larger than experimental uncertainty of solvent activity in electrolyte solution, it is sufficient to allow a clear delineation of model performance between parameter sets. Given the computational expense of estimating properties, a polynomial expansion is used to approximate model properties in the region of likely solutions, based on a small set of trial models. This approach is illustrated in figure 4.5 for halide model development: trial solutions are shown as open symbols, while solid lines indicate contours of constant solvent activity and molar volume, based on local polynomial expansions. For each iteration of the optimisation, a new set of polynomial expansions are generated and the next proposed solution identified as the model parameters minimizing $f(C_i)$. The iterative procedure used for parameter optimization is illustrated in figure 4.7. In each case the objective function is formulated as a convex function with minimum at $f = 0$, i.e. when all model properties are in agreement with reference values. The iteration is continued until model properties agree with reference values to within statistical precision.

4.8 Alkylammonium Halide Model Development

Alkylammonium ions are organic compounds carrying a four-coordinated nitrogen cation. Primary, secondary, and tertiary alkylammonium act as conjugate acids in the presence of water, in rapid equilibrium with their uncharged amine equivalents. Conversely, quaternary alkylammonium ions are non-reactive and thus an important class of model species for investigating the fluid properties of charged organic compounds without the added complexity of reaction equilibria. Quaternary alkylammonium has served as model for solvation in biomolecular systems such as proteins, where charges are buried in the interior of the molecule [392] . Quaternary ammonium is also encountered in a range of room-temperature ionic liquids [393], with at least 31 commercially available alkylammonium-based ionic liquids [394].

Depending on the degree of substitution, we expect solute-solvent interactions for alkylammonium to range from largely hydrophobic (tetraalkylammonium) to largely hydrogen bonding (monoalkylammonium) in nature. The changing solute-solvent interactions between differently substituted alkylammonium ions results in divergent thermodynamic activity for high-concentration alkylammonium solutions, as shown in figure 4.8 for mono-, di-, tri-, and tetramethylammonium chloride.

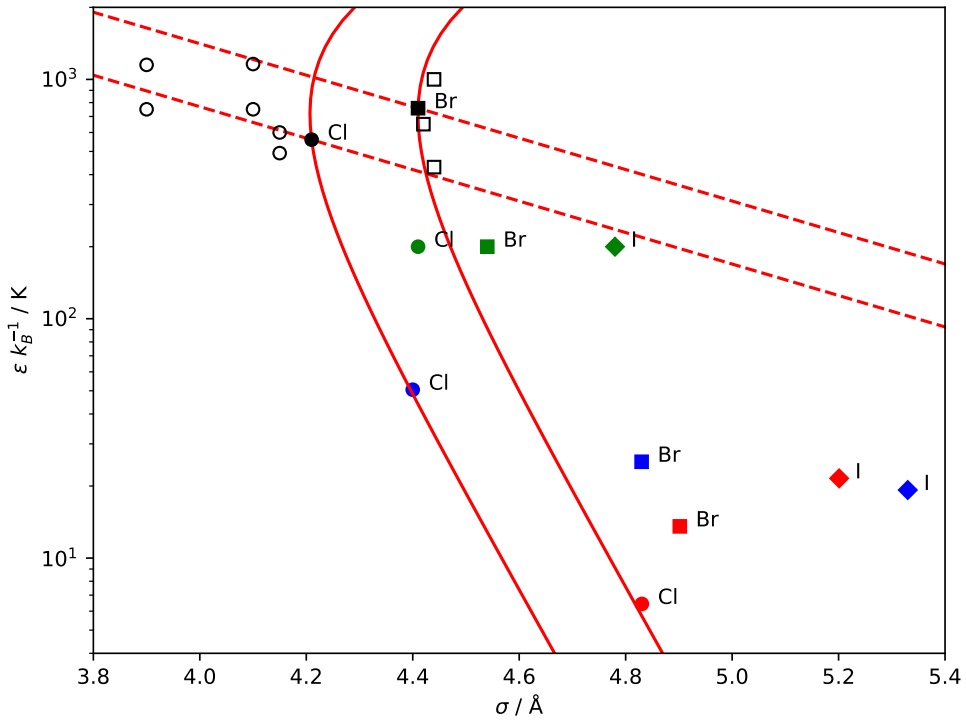

Figure 4.6: Parameter optimization for halide molecular parameters. The optimization targets of molar volume and solvent activity are approximated by local polynomal expansions: solid lines show contours of constant molar volume, while dashed lines show contours of constant solvent activity. The open symbols indicate trial models for chloride (circles) and bromide (squares), while the solid symbols indicate the final models as detailed in section 4.8. The coloured symbols indicate literature models for halides as detailed in figure 4.5.

Similar to the alkali halides, solvation of alkylammonium ions involves strong polar and charge transfer interactions through NH$\cdots$O hydrogen bond formation. However, solvation of the bulkier alkyl groups has been shown to follow a hydrophobic interaction pattern. Neutron diffraction characterisation of nitrogen-solvent radial distribution functions in aqueous tetramethylammonium chloride by Turner et al. [396, 397, 398] revealed no strong orientational effects of water around tetramethylammonium, with a single peak for both oxygen and hydrogen. In a later study Turner et al. [399] conclude water has an edge-on orientation around tetramethylammonium, characteristic for hydrophobic solvation. The interaction energy of the tetramethylammonium–water dimer has been estimated by *ab initio* calculations as approximately 42 kJ mol^{-1} [400, 401], although there is some variation with basis set. This compares with an estimated 103 kJ mol^{-1} for the NH$\cdots$O methylammonium–water dimer [402] and 84 kJ mol^{-1} for the chloride–water dimer [403].

In summary, a molecular model for alkylammonium solutions must account for both hydrophilic and hydrophobic solute-solvent interactions in order to reproduce the solvent activity behaviour observed in figure 4.8. Further to the interactions listed in section 4.6, the alkylammonium model should describe hydrophobic alkyl-solvent interactions as illustrated in figure 4.9, similar to those observed for alkanes in aqueous solutions.

When considering tetraalkylammonium ions, the interactions of the ions are simplified considerably due to the weak interactions of alkyl groups with solvent and other ions. Since the charge-carrying nitrogen is shielded by methyl groups, no strong ion-solvent or ion-ion interactions are observed. Models for alkyl

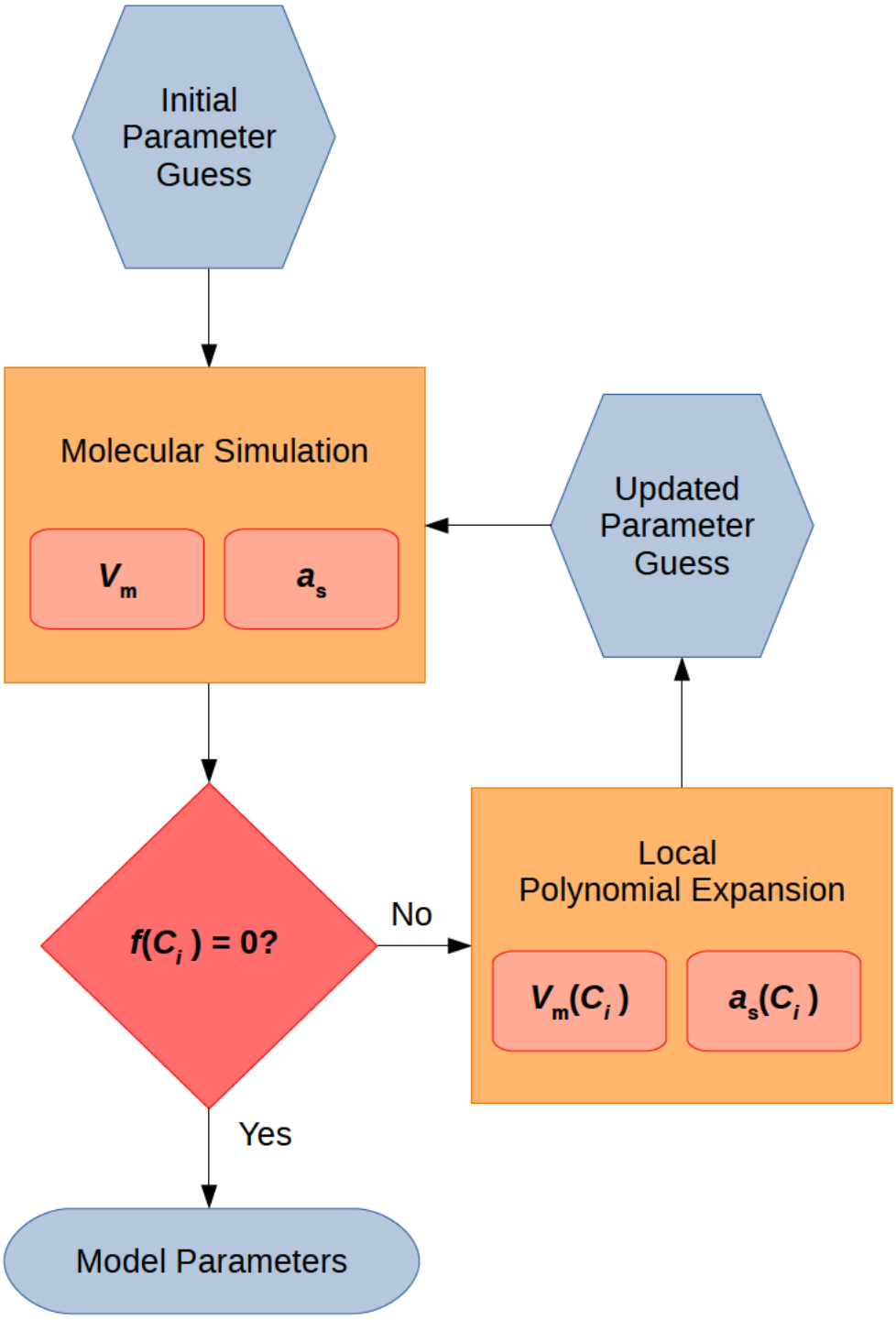

Figure 4.7: Iterative process for optimization of electrolyte molecular parameters. An initial set of parameters are evaluated by molecular simulation, allowing evaluation of the objective function and construction of local polynomial expansions for target properties. Polynomial expansions are used to identify the parameter set minimizing the objective function, which is used for the next round of iteration. Once the objective function has converged to within the statistical precision of simulation, the iteration is terminated.

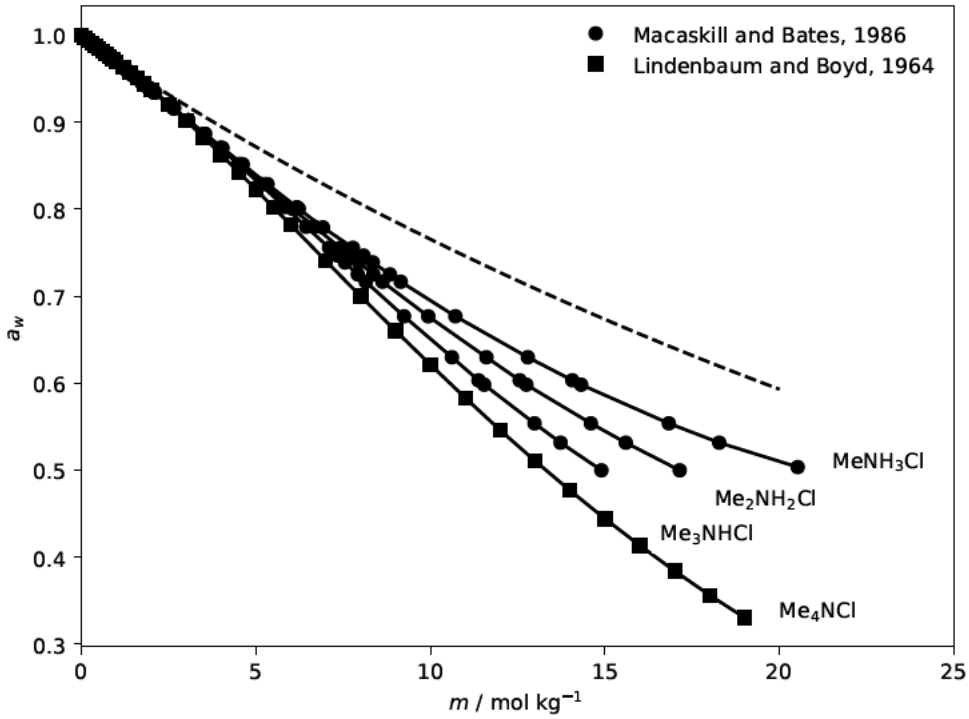

Figure 4.8: Solvent activity as function of molality for methylammonium chlorides in water at 298.15 K. Symbols indicate experimental values from Macaskill and Bates [395] for protonated alkylammonium species and Lindenbaum and Boyd [321] for quaternary alkylammonium. Solid lines connecting experimental symbols are a guide to the eye. The dashed line indicates limiting Debye-Hückel behaviour.

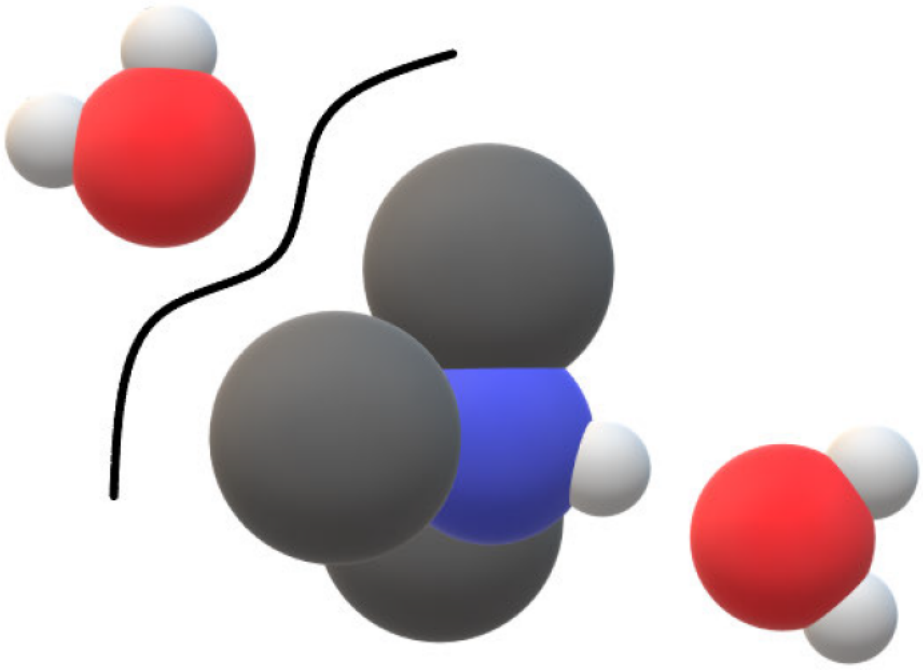

Figure 4.9: Model representation and solute-solvent interactions for the trimethylammonium ion, with united-atom representations of alkyl groups. Alkyl-water interactions have a primarily hydrophobic character [399], while NH···O forms a strong hydrogen bonding interaction [402]. For model parameters, see table 4.3.

chains together with dihedral potentials for C-C-N-C and C-C-C-N torsional interactions have already been established in chapter 3, allowing construction of realistic models for tetraalkylammonium species based on existing parameters. Similar approaches have previously been employed for simulation of tetraalkylammonium aqueous solutions [404, 405, 406, 407], relying on parameters for neutral organic molecules in combination with selected *ab-initio* data for bond lengths and charge distribution.

Existing simulation studies for alkylammonium solvation have largely focused on dilute systems, characterising ion-solvent interactions and limiting thermodynamic properties. However, as can be seen from figures 4.4 and 4.8 the experimentally accessible concentration range for alkylammonium halides extends to concentrations far outside the dilute regime. In the context of chemically reactive absorption in organic amine solvents, high concentrations are required to ensure a high total loading and working capacity of the fluid. Hence, it is essential for the development of alkylammonium models targeting industrial applications to make use of target properties across a range of conditions including the high concentration regime.

The chosen target properties of fluid density and solvent activity are both well characterised for alkylammonium halides across a wide range of concentrations. A comprehensive study of activities in aqueous mono-, di-, tri- and tetraalkylammonium chloride and bromide solutions was reported by Lindenbaum and Boyd [321]. MacAskill and Pethybridge [408] reported further data for mono-, di-, and trimethylammonium chloride and sulfate solutions. Bonner [409] questioned the integrity of earlier sources due to the significant volatility of mono-, di-, and trimethylammonium chloride, reporting a new set of osmotic coefficients for these compounds. In a later study, MacAskill and Bates [395] reported revised and extended osmotic coefficients for these compounds, which appear to be the most thoroughly vetted experimental data for methylammonium halide solution activities, and are shown in figure 4.8 together with the experimental data of Lindenbaum and Boyd [321] for tetramethylammonium chloride. These solvent activities were used for parameter optimisation in this work. As discussed in section 4.6 and our previous work [47], solvent activity in the dilute regime is dominated by Debye-Hückel effect and largely insensitive to the specific electrolyte. As such, solvent activity in the dilute regime has limited information content for the purpose of electrolyte model parameters, and only concentrations beyond 2 molal are considered for parameter optimisation in this work.

The liquid density of methylammonium solutions has also received considerable experimental interest. Lo-Surdo and Wirth [410] reported apparent partial molal volumes of tetraalkylammonium bromides and related species, observing regular trends with temperature and alkylammonium chain lengths. Leduc and Desnoyers [411] studied apparent partial molal volumes of tetrabutylammonium bromide and carboxylates, seeing evidence of the hydrophobic solute-solvent interactions discussed previously. Perron et al. [412] characterised volumes, heat capacities, and expansibilities of tetraalkylammonium halide solutions over the temperature range 273 K - 328 K, regressing their results to the analytical expression

$$V_\phi = V_\phi^\circ + A_\phi^{\mathrm{DH}}(\rho_s m)^{1/2} + B_\phi m + \mathcal{O}(m^2) \tag{4.33}$$

where A_ϕ^{DH} is the Debye-Hückel limiting slope and B_ϕ is an electrolyte-specific coefficient describing the dependence of apparent molar volume on short-range solute-solute interactions. Coefficients for equation 4.33 are reported in 5 K intervals [412] and the correlation is valid up to approximately 1 molal. These values are employed in this work, with apparent molal volumes evaluated from molecular simulation at concentrations of approximately 1 molal using the relationship

$$V_\phi = \frac{1}{m}\left(\frac{1}{\rho} - \frac{1}{\rho_{\mathrm{s}}}\right) + \frac{M}{\rho} \tag{4.34}$$

where m is the exact solution molality, ρ is the liquid density at m, ρ_{s} is the liquid density of the pure solvent, and M is the solute molar mass. Densities are obtained from molecular simulation based on the usual ensemble averages, with a comprehensive list of simulation parameters given in appendix A.

As outlined above, the optimization parameters for alkylammonium halides comprise Lennard-Jones potential parameters σ, ϵ for halides, together with hydrogen partial charge q_H for mono-, di-, and trialkylammonium. These parameters were treated as free variables and optimised using the objective function

$$f(\sigma, \epsilon, q_{\mathrm{H}}) = \left(\frac{V_{\mathrm{sim}}(m=1) - V_{\mathrm{exp}}(m=1)}{V_{\mathrm{exp}}(m=1)}\right)^2 + \sum_m \left(\frac{a_{\mathrm{sim}} - a_{\mathrm{exp}}}{a_{\mathrm{exp}}}\right)^2 \tag{4.35}$$

where V_{sim} and a_{sim} are obtained by molecular simulation using equations 4.34 and 5.18. The sum over molalities m ranges from 2 molal to approximately the point where a_{w} drops below 0.4, in 2 molal increments. Activity is referenced against the TIP4P/2005 model [128] at normal temperature and pressure. The minimum concentration of 2 molal for activity calculations was selected due to the low sensitivity of solvent activity to model parameters in the low-concentration region.

4.8.1 Tetraalkylammonium Model

The representation of alkylammonium ions using a pairwise potential model requires parameters for Lennard-Jones dispersion interactions, atomic partial charges, and geometric parameters describing bond lengths and angles, as described in section 2.2. In order to permit integration of organic ammonium groups into larger organic compounds, including partially protonated forms of PVAm, the parameters for alkylammonium face an additional constraint: the potential model should be as congruent as possible with parameters used for non-charged organic compounds. This facilitates transferrability of the model to e.g. long-chain butylammonium ions and multi-substituted organic amines such as alkanolamines. For this reason, the dispersion and bonded parameters of the TraPPE-UA model [208, 209] (previously used for unprotonated organic amines in PVAm) are adopted for describing alkyl groups. In table 4.3, non-bonded parameters are summarized for tetraalkylammonium species.

For the alkylammonium nitrogen multiple sets of dispersion parameters were evaluated for use, deriving from analogous primary, secondary, and tertiary amine compounds [212]. Perhaps unsurprisingly, the choice of

Table 4.3: Non-bonded parameters for simulation of alkylammonium halides in TIP4P/2005 [128]. Atom type is indicated in bold, with R denoting saturated organic substituents. Saturated alkyl dispersion parameters from the TraPPE-UA models for linear and branched alkanes [208, 209]. Nitrogen dispersion parameters based on TraPPE-EH model [212] for ternary amines. Hydrogen is represented with a partial charge but no disperson parameters, as done for aliphatic amines in chapter 3. Nitrogen partial charges are calculated to yield integer formal charges for the resulting ionic species.

type	σ / Å	ϵ / k_{B}^{-1}K	q / e	source
R–**N**$^+$–H_3	3.78	12	-0.810	[212], this work
R_2–**N**$^+$–H_2	3.78	12	-0.540	[212], this work
R_3–**N**$^+$–H	3.78	12	-0.270	[212], this work
R_4–**N**$^+$	3.78	12	0	[212], this work
N$^+$–**H**	0	0	+0.52	this work
N$^+$–**CH_3**	3.75	98	+ 0.25	[208, 209, 404]
N$^+$–**CH_2**–R	3.95	46	+ 0.25	[208, 209], this work
N$^+$–**CH**–R_2	4.68	10	+ 0.25	[208, 209], this work
N$^+$–**C**–R_3	6.4	0.5	+ 0.25	[208, 209], this work
Cl$^-$	4.21	560	- 1	this work
Br$^-$	4.41	758	- 1	this work

nitrogen dispersion interactions has no significant effect on the properties of tetralkylammonium, owing to the obstruction of the central nitrogen from interacting with surrounding solvent. Rather, the nitrogen dispersion interactions are important for modulating short-ranged NH$\cdots$O bonds of mono-, di-, and trialkylammonium in aqueous solution. Optimization of nitrogen dispersion parameters was for this reason performed as a secondary step, based on mono-, di-, and trimethylammonium solutions (see section 4.8.3).

As noted by Port and Pullman [400], there is some disagreement regarding the charge distribution of the tetraalkylammonium ion. Here, partial charges of +0.25 were assigned to each methyl group attached to alkylammonium, giving a residual zero charge on the central nitrogen in the case of tetramethylammonium, chosen in line with previously reported simulations of tetramethylammonium based on *ab initio* calculations [413, 404]. As with nitrogen dispersion parameters, ammonium hydrogen atom partial charges were optimized as a secondary step based on lower-order ammonium ions. For longer alkyl chains, the +0.25 charge was retained on the α carbon relative to alkylammonium, reflecting the localization of positive charge near the nitrogen atom [400].

4.8.2 Halide Model

As detailed in the previous section, alkylammonium is described as a tetrahedrally coordinated integer-charge model with TraPPE-UA parameters for the methyl groups. Conversely, halides are described as point-particles with a Lennard-Jones dispersion potential and integer negative charge. This leaves the halide dispersion parameters σ and ϵ as free optimisation variables. By varying σ and ϵ, solution density and solvent activity in alkylammonium halide solutions can be modulated to match experimentally observed solution properties.

Values for σ and ϵ for halide models reported in the literature fall into a broad range, as can be seen for chloride, bromide, and iodide models in figure 4.5. In particular, the ϵ parameter has been found to have

little influence on ion properties [363], likely due to the small magnitude of attractive dispersion interactions relative to electrostatic interactions. Instead, σ and ϵ in combination modulate the repulsion (r^{12}) term of the Lennard-Jones potential. For a given ion, σ corresponds approximately to the ionic radius, with Cl $<$ Br $<$ I as seen in figure 4.5. However, the attractive contribution of the Lennard-Jones potential nonetheless contributes to the total cohesive energy of the system, which becomes significant as ϵ increases in magnitude.

In combination with the tetramethylammonium model as described in section 4.8.1, σ and ϵ for chloride and bromide ions were optimised using the objective function in equation 4.35. Due to the computational cost of estimating solvent activity in aqueous tetramethylammonium a quadratic local function approximation was used, trained on the halide models of Joung and Cheatham [360, 361], Horinek et al. [362], Reiser et al. [363], together with additional trial halide models near the objective function minimum. The final model parameters are reported in table 4.3.

In figure 4.10, activities of water in tetramethylammonium chloride solution obtained from molecular simulation are compared against the experimental values reported by Lindenbaum and Boyd [321]. The models of Joung and Cheatham [360, 361] and Horinek et al. [362] both significantly underestimate water activity in tetramethylammonium chloride solution for concentrations over 2 molal, with respectively 10% and 14% mean average deviations calculated using linear interpolation of the experimental data. The model of Reiser et al. [363] performs somewhat better, with a mean average deviation of 5.2%. The proposed model parameters reduce the mean average deviation to 2.2%, well within the average statistical simulation uncertainty of 4.4%. Further, there is no indication of deteriorating model performance at high concentration.

4.8.3 Mono-, Di-, and Trialkylammmonium Models

Removal of methyl groups from tetramethylammonium produces a homologous sequence of alkylammonium ions with gradually changing solution properties, as illustrated in figure 4.8. The molecular model of alkylammonium chlorides should capture this progression in order to accurately reflect the solution thermodynamics of alkylammonium ions. With a fixed model for tetramethylammonium and chloride parameters already optimised, the remaining molecular parameters are those of the hydrogen atoms of the alkylammonium group, together with short-ranged nitrogen dispersion interactions.

Bonded parameters for hydrogen comprise bond length, bond angles, and torsional angles. Following the united-atom apprach for amines and alcohols, hydrogen is assigned charge but no Lennard-Jones dispersion interactions. For bond angles and dihedral interactions, we adopt the united-atom parameters for amines as detailed in chapter 3. For the nitrogen-hydrogen bond we use a fixed length of 0.101 nm, adopted from the OPLS model [413, 234, 202] on which TraPPE-UA is built. The electrostatic interactions of the ammonium group are determined both by the nitrogen-hydrogen bond lengths and atomic partial charges, and only one of these should be used as a free optimisation variable.

The alkylammonium hydrogen partial charge has been estimated in several *ab initio* studies; however,

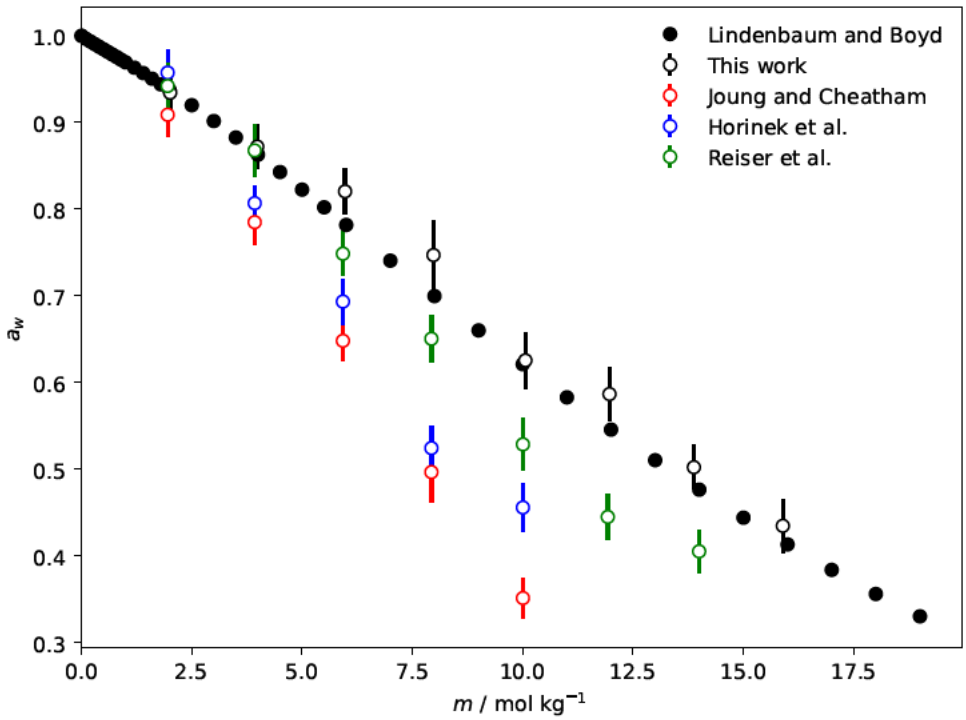

Figure 4.10: Water activity in aqueous tetramethylammonium chloride solutions at 298 K and 100 kPa. Solid circles indicate experimental values reported by Lindenbaum and Boyd [321]. Open symbols indicate simulated values using the tetramethylammonium model from table 4.3, in combination with chloride parameters from this work, Joung and Cheatham [360, 361], Horinek et al. [362], and Reiser et al. [363] as indicated. Error bars indicate standard deviations calculated from a minimum of three independent sets of simulations.

there is considerable disagreement between the reported values. Cremaschi and Simonetta [414] found values ranging from +0.325 to +0.472 in methylamine, depending on torsional angle. Jorgensen and Gao [413] found a value of +0.34 for the ground state conformation of the same molecule, while Wee et al. [402] reported a value of +0.471. Clearly, the charge distribution between nitrogen and hydrogen is sensitive to local geometry and the methodology applied. Further, the *ab initio* charge distribution does not necessarily reflect the properties of the alkylammonium-water complex, due to charge transfer occuring between oxygen lone pairs and the ammonium group [402]. Hence, hydrogen partial charge is left as a free optimization parameter to capture the experimental solvent activity curves from figure 4.8, with trial values in the range +0.3 to +0.5. The charge of each adjacent alkyl carbon is maintained at +0.25. The hydrogen charge was optimised using the objective function in equation 4.35, but leaving σ and ϵ fixed to the model parameters in table 4.3.

Further to the hydrogen partial charge, the nitrogen Lennard-Jones parameters influence the properties of protonated alkylammonium by modulating the distance of approach for solvent and anion species. However, a full three-variable optimisation of nitrogen Lennard-Jones parameters together with hydrogen partial charge requires additional target properties and exploration of a substantially larger parameter space, which was deemed out of scope for this work. Instead, the three sets of nitrogen parameters proposed for the TraPPE amine model [212] were each tested in conjunction with optimisation hydrogen partial charge. Only the

Lennard-Jones parameters for tertiary amines, listed in table 4.3, were found to give acceptable values for solvent activities together with apparent molar volumes across mono-, di-, and trimethylammonium species.

Similar to the optimisation of halide Lennard-Jones parameters, the optimised hydrogen partial charge was found using a quadratic local function approximation. The optimised hydrogen partial charge was determined as $+0.52$, somewhat higher than the estimates from *ab-initio* calculations. The resulting simulated water activities in solutions of mono-, di-, and trimethylammonium chloride solutions are shown in figures 4.11 and 4.12, and compared against experimental sources for the same systems.

The simulated water activities in protonated methylammonium chloride systems follow a similar behaviour as for tetramethylammonium chloride solutions. For dimethylammonium chloride and trimethylammonium chloride solutions, the model reproduces experimental solvent activity to within statistical uncertainty, with mean average deviations of 2.4% and 2.3%, respectively. The experimental values of MacAskill and Bates [395] are used for comparison. For methylammonium chloride agreement is somewhat worse, with a mean average deviation of 4.4%. Nonetheless the solvent activity in each alkylammonium chloride solution is captured to within statistical uncertainty, and with a precision that allows useful comparison of solutions of different concentration and chemical composition. For further improvement to the model, three-variable optimisation of nitrogen Lennard-Jones parameters together with hydrogen partial charges would allow more granular control of the short-ranged ion-solvent interactions, improving the description of hydrogen bond strength and hence overall solution thermodynamics.

4.9 Bicarbonate Model Development

The derivative species formed in reactive absorption of CO_2 involve carbonic acid, bicarbonate, carbonate, as well as carbamate and various transition state species, which will be discussed further in chapter 5. However, under typical working partial pressures of CO_2, bicarbonate is expected to be the primary species formed in solution for sterically hindered amines [415, 416], and the only free CO_2 species present in significant concentration. For this reason a realistic description of the bicarbonate ion is essential for a molecular model of amine – CO_2 solutions, and chemically reactive CO_2 absorption.

The bicarbonate ion HCO_3^- has a distorted trigonal-planar shape, with three oxygen atoms connecting to a central carbon atom and a single hydrogen attached, as indicated in figure 4.13. Most of the negative charge on the bicarbonate ion is localized near the two charge-carrying oxygen atoms, which form strong hydrogen bonds in aqueous solution [417]. Conversely, the hydrogen-carrying oxygen has a more neutral character, and neither it or the hydrogen appear to form hydrogen bonds with water [417].

The exact geometry of the bicarbonate ion has been determined by diffraction crystallography for e.g. sodium bicarbonate [418]. However, we should expect bicarbonate to behave somewhat differently as a hydrated ion in the liquid state. The geometry of bicarbonate in aqueous solution, together with radial

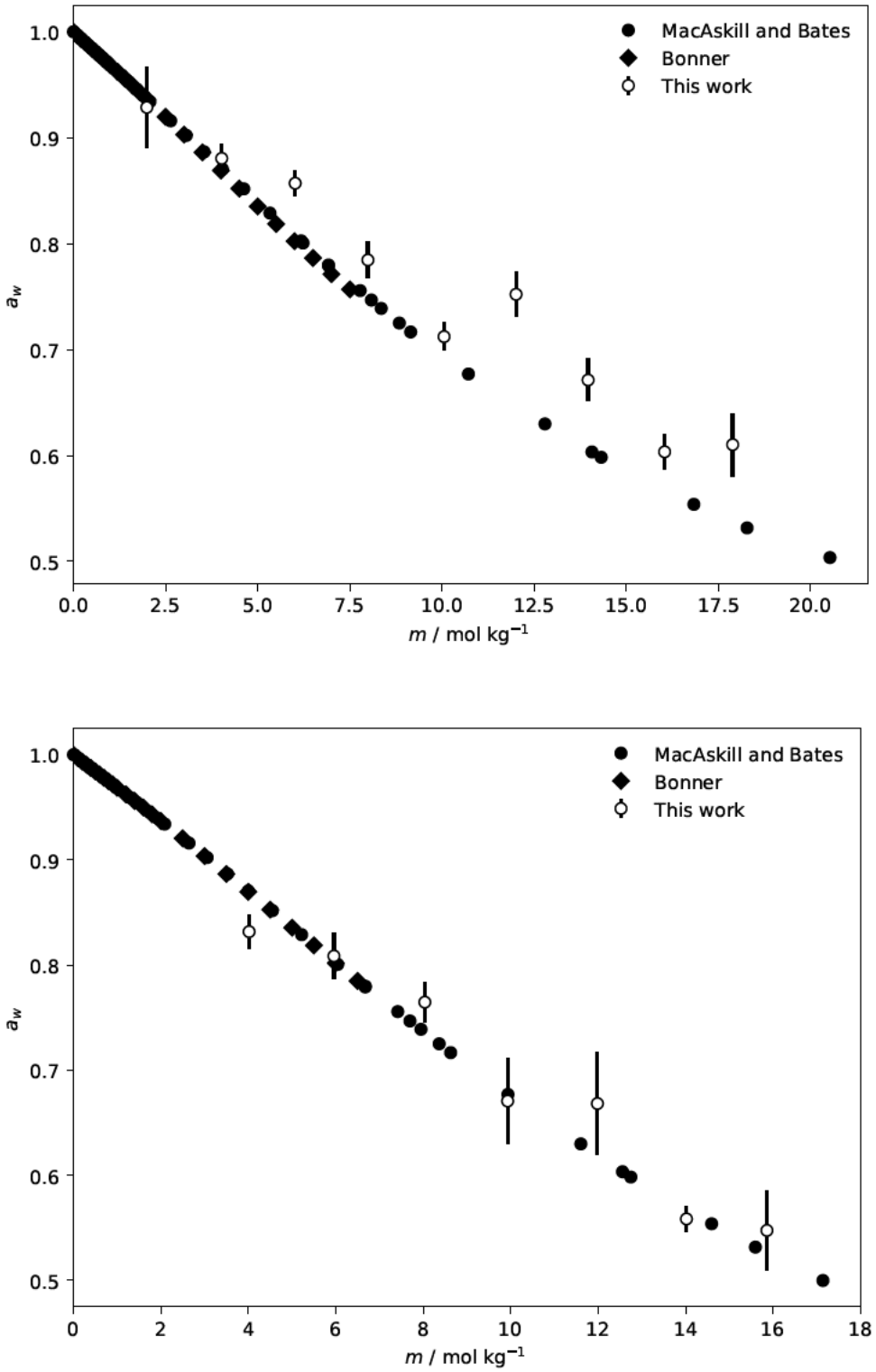

Figure 4.11: Water activity in aqueous methylammonium chloride (top panel) and dimethylammonium chloride (bottom panel) solutions at 298 K and 100 kPa. Solid symbols indicate experimental values, as reported by Lindenbaum and Boyd [395] and Bonner [409]. Open symbols indicate simulated values using the alkylammonium chloride model from table 4.3 developed in this work. Error bars indicate standard deviations calculated from independent sets of simulations.

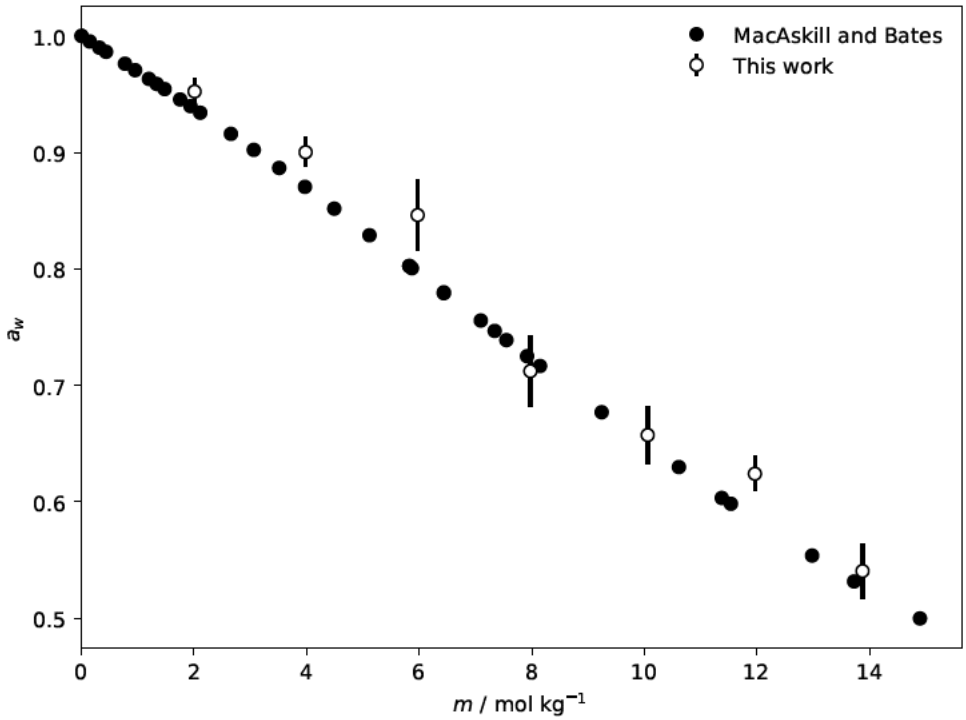

Figure 4.12: Water activity in aqueous trimethylammonium chloride solutions at 298 K and 100 kPa. Solid circles indicate experimental values as reported by MacAskill and Bates [395]. Open symbols indicate simulated values using the alkylammonium chloride model from table 4.3 developed in this work. Error bars indicate standard deviations calculated from independent sets of simulations.

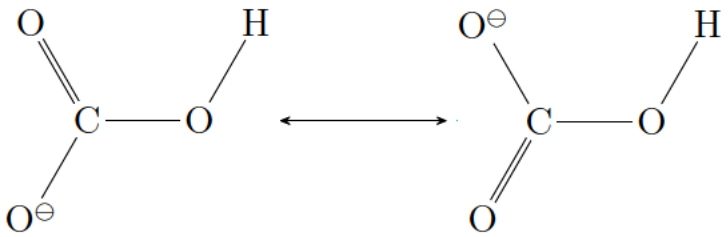

Figure 4.13: Mesomeric forms of the bicarbonate ion showing localization of the formal negative charge towards the two unprotonated (charge carrying) oxygen atoms. The carbon-oxygen bond length for the charge carrying oxygen atoms is approximately 0.1245 nm, a significant shortening relative to 0.1370 nm for the protonated oxygen [417]. This indicates increased electronic density in the region near the charge carrying oxygens.

distribution functions for the distribution of solvent molecules, has been characterised using *ab initio* methods by Vchirawongkwin et al. [417]. Bicarbonate, carbonic acid, and their dimers with water have also been studied using *ab initio* methods by George et al. [419] in vacuum conditions. Both in solution and vacuum conditions the bond connecting the central carbon to the hydrogen-carrying oxygen is elongated, with a bond length of 0.1370 nm reported by Vchirawongkwin et al. [417] and 0.1429 nm by George et al. [419]. This is in contrast to the short bonds connecting the charge-carrying oxygens to the central carbon, averaging respectively 0.1244 nm in solution [417] and 0.1245 nm in vacuum [419]. For comparison, the carbon-oxygen bond in the CO_2 molecule is 0.1162 nm [420].

The hydrogen atom of bicarbonate rapidly exchanges with water in aqueous solution [416], establishing a reaction equilibrium with carbonic acid (H_2CO_3) and carbonate (CO_3^{2-}). Additionally, molecular CO_2 is generated through the dehydration reaction of carbonic acid. The escape of CO_2 means most organic bicarbonate salts are volatile, in turn making reliable measurements of solution properties challenging. Tetraalkylammonium bicarbonate species are exceptions to this tendency since tetraalkylammonium ions do not participate in protonation reactions, unlike the salts formed by CO_2 with protonatable organic amines. Hence, tetraalkylammonium bicarbonate permits characterisation of thermodynamic properties of organic bicarbonate solutions, similar to those encountered in reactive CO_2 absorption applications.

The properties of tetraalkylammonium bicarbonate solutions are less well documented than salts of monatomic ions like the tetraalkylammonium halides, and pertain mainly to aqueous conditions at 298.15 K. The only available values for osmotic coefficients are reported by Abdel-Salam [421] for tetramethylammonium bicarbonate, measured using a dew point technique. For volumetric properties, the standard partial molar volumes of Marcus [422] can be used to calculate apparent molar volumes, with $V_{\mathrm{m}} = 28.9\,\mathrm{cm^3\,mol^{-1}}$ for bicarbonate and $V_{\mathrm{m}} = 84.1\,\mathrm{cm^3\,mol^{-1}}$ for tetramethylammonium giving a combined molar volume of $V_{\mathrm{m}} = 113\,\mathrm{cm^3\,mol^{-1}}$ for tetramethylammonum bicarbonate. Beyond aqueous properties, Levitin et al. [423] reports the phase properties of tetramethylammonium bicarbonate in methanol and water solutions at high pressures, while Yang et al. [424, 425] details the effect of tetramethylammonium bicarbonate on vapour-liquid equilibria in methanol – water and methanol – dimethyl carbonate solvent mixtures. These systems are interesting cases for exploring the interactions of bicarbonate with organic solvents, but are not considered further in the present work.

4.9.1 Bicarbonate Model

Similar to the model for alkylammonium ions, the representation of bicarbonate should be compatible with existing models for water, organic polymer, and alkylammonium ions relevant to the systems of interest for facilitated transport membranes. Conventional Lennard-Jones interaction parameters are employed for dispersion interactions, with hydrogen left without dispersion interactions as detailed for united-atom alcohols and amines in chapter 3. Bicarbonate is assumed to carry an integer charge of -1, with the two charge-

Table 4.4: Bonded parameters for the bicarbonate ion. Bond lengths and equilibrium angles assigned based on mean bond lengths and angles for hydrated bicarbonate from Vchirawongkwin et al. [417]. Force constants and dihedral parameters are adopted from the model of carboxylic acids by Kamath et al. [426], developed for compatibility with the united-atom TraPPE alkane model [208, 209].

bond	r_0 / Å			source
C–O	1.245			This work
C–OH	1.370			This work
O–H	0.960			This work
angle		θ_0 / °	k_θ / kJ mol^{-1} rad^{-2}	source
O–C–O		115	146.334	This work, [426]
O–C–OH		129	519.651	This work, [426]
C–O–H		107	335.071	This work, [426]
dihedral	C_0 / kJ mol^{-1}	C_1 / kJ mol^{-1}	C_2 / kJ mol^{-1}	source
O–C–O–H	31.219	5.238	-25.981	[426]

carrying oxygen atom assumed to carry most of the molecular charge. Further, these two oxygen atoms are treated as equivalent for all purposes, and the hydrogen atom is free to rotate around the H-O-C-O dihedral angles. The minor differences in geometry and charge distribution, reported by Vchirawongkwin et al. [417] and George et al. [419] between the oxygen atoms *cis* and *trans* relative to hydrogen, are too small to warrant separate sets of dispersion parameters and partial charges.

In developing a model for the intramolecular degrees of freedom of bicarbonate, the geometric parameters of existing united-atom molecular models for carboxylic acids [426], ketones [104], and esters [427] were compared to those reported for bicarbonate in aqueous solution [417]. The geometric parameters for carboxylic acids were in particular found to be quite close to those for bicarbonate. Hence, force constants for bond angle and dihedral potentials in carboxylic acids were adopted, in combination with equilibrium bond lengths and angles reported by Vchirawongkwin et al. [417]. The resulting non-bonded parameters employed for bicarbonate are listed in table 4.5.

As a five-atom molecule, bicarbonate has considerable flexibility in the distribution of charges, and as much as 9 free variables if both charge distribution and dispersion interactions for carbon and oxygen atoms are included (3 free partial charges + 3 sets of 2 dispersion interaction parameters for carbon, charge-carrying oxygen, and hydrogen-carrying oxygen). In order to avoid over-fitting based on the limited amount of data available, the oxygen dispersion parameters were fixed to those of the TraPPE-UA models for alcohols [105] and ketones [104] for hydrogen-carrying and charge-carrying oxygens, respectively; the same parameters used for the united-atom representation of carboxylic acids [426]. The non-bonded parameters of the bicarbonate ion are listed in table 4.5. The following five parameters were used for model optimisation.

- Charge-carrying oxygen partial charge (q_{O}).
- Hydrogen-carrying oxygen partial charge (q_{OH}).
- Hydrogen partial charge (q_{H}).
- Carbon size parameter (σ_{C}).

Table 4.5: Non-bonded parameters for the bicarbonate ion. Lennard-Jones parameters for oxygen atoms adopted from TraPPE-UA models for alcohols [105] and ketones [104]. Remaining parameters regressed against partial molar volume and radial distribution functions according to equation 4.36, with weights ω_V equal to 0.1, 1, and 10 for Trial Model 1, Trial Model 2, and the Final Model, respectively.

	Trial Model 1			Trial Model 2			Final Model		
atom	σ / Å	$\epsilon\ k_\mathrm{B}^{-1}$ / K	q / e	σ / Å	$\epsilon\ k_\mathrm{B}^{-1}$ / K	q / e	σ / Å	$\epsilon\ k_\mathrm{B}^{-1}$ / K	q / e
O	3.05	79	-0.620	3.05	79	-0.658	3.05	79	-0.661
OH	3.02	93	-0.479	3.02	93	-0.478	3.02	93	-0.518
H	0	0	0.226	0	0	0.242	0	0	0.233
C	5.58	47	0.493	5.27	42	0.552	4.94	44	0.607

- Carbon energy parameter (ϵ_C).

Due to the large number of free parameters, solvent activity was not chosen as a target property due to the significant computational expense of estimating this property. Rather, the standard partial molar volume of bicarbonate as reported by Marcus [422], $V_\mathrm{m} = 28.9\,\mathrm{cm^3\,mol^{-1}}$, was selected in combination with the integrated radial distribution functions reported by Vchirawongkwin et al. [417] for aqueous solution. In combination, this ensures that both liquid density and the strength of solute-solvent interactions are considered in the optimisation process. Radial distribution functions have the additional advantage of being atom-specific, allowing e.g. hydrogen bonding to be well resolved.

To optimise the bicarbonate model, the five parameters above were treated as free variables and adjusted to minimise an objective function, similar to the approach for alkylammonium halides in section 4.8. Based on the set of target properties outlined above, the objective function was defined as

$$\begin{aligned} f(q_\mathrm{O}, q_\mathrm{OH}, q_\mathrm{H}, \sigma_\mathrm{C}, \epsilon_\mathrm{C}) = \omega_V \left(\frac{V_\mathrm{m}^\mathrm{sim} - V_\mathrm{m}^\mathrm{exp}}{V_\mathrm{m}^\mathrm{exp}} \right)^2 \\ + \int_r \left(\frac{(g_\mathrm{H-O}^\mathrm{sim}(r) - g_\mathrm{H-O}^\mathrm{QM}(r)}{g_\mathrm{H-O}^\mathrm{QM}(r)} \right)^2 \mathrm{d}r + \int_r \left(\frac{(g_\mathrm{OH-O}^\mathrm{sim}(r) - g_\mathrm{OH-O}^\mathrm{QM}(r)}{g_\mathrm{OH-O}^\mathrm{QM}(r)} \right)^2 \mathrm{d}r \\ + \int_r \left(\frac{(g_\mathrm{O-O}^\mathrm{sim}(r) - g_\mathrm{O-O}^\mathrm{QM}(r)}{g_\mathrm{O-O}^\mathrm{QM}(r)} \right)^2 \mathrm{d}r + \int_r \left(\frac{(g_\mathrm{O-H}^\mathrm{sim}(r) - g_\mathrm{O-H}^\mathrm{QM}(r)}{g_\mathrm{O-H}^\mathrm{QM}(r)} \right)^2 \mathrm{d}r \end{aligned} \quad (4.36)$$

where $g_{i-j}(r)$ denotes the radial distribution function for bicarbonate atom i and water atom j. The superscripts sim and QM indicate respectively simulated values and the *ab initio* values from Vchirawongkwin et al. [417]. The integrals in equation 4.36 are approximated by sums over r up to the second peak of the radial distribution function, covering approximately the interval 0.2 nm - 0.6 nm. The weighting factor ω_V allows for adjustment of the relative importance of the volumetric and structural target properties. Three sets of non-bonded parameters were developed, corresponding to $\omega_V = 0.1$, $\omega_V = 1$, and $\omega_V = 10$, denoted 'Trial Model 1', Trial Model 2', and 'Final Model' in table 4.5, respectively.

A series of simulations were carried out where the parameters outlined above were allowed to vary and the resulting objective function evaluated. Each simulation was carried out at 298 K and 100 kPa, using a system size of approximately 3 nm. Bicarbonate was added at a concentration of 0.1 molal, giving approximately 500

water molecules per bicarbonate ion. No counter-ion was added to the solution, with the negative system charge instead removed by the Ewald summation method [93]. Each iteration comprised an initial 100 ps of simulation in the canonical ensemble, followed by 10 ns of simulation in the isothermal-isobaric ensemble, with V_{m} and g_{i-j} evaluated as averages from the isobaric-isothermal ensemble. A comprehensive list of simulation parameters is given in appendix A.

Minimization of the objective function was done using the adaptive simplex algorithm described by Gao and Han [250], as it does not require gradient information and is numerically stable with some amount of noise. The initial estimate for non-bonded model parameters was obtained using carbon Lennard-Jones parameters from the TraPPe-UA model of carboxylate esters [427] and CM1A optimised partial charges from the LigParGen web server [428]. The simplex algorithm was re-initiated multiple times to check for convergence, each time using the set of molecular parameters from the most recent iteration. The final non-bonded parameters are listed in table 4.5. Radial distribution functions for each of the three models are presented in appendix C, including comparison with the *ab initio* values of Vchirawongkwin et al. [417].

Due to the different weighting of the objective function in equation 4.36 towards volumetric and structural properties, the three bicarbonate models have considerable differences in the obtained standard partial molar volumes. In order to assess the predictive accuracy of the three models against volumetric properties of real alkylammonium salts, tetramethylammonium bicarbonate solutions were simulated across a range of concentrations and the apparent molar volumes calculated using equation 4.34, with the resulting values shown in figure 4.14 for the Final Model. For each model, the simulated values were extrapolated to infinite dilution using a second-order polynomial. The resulting infinite dilution apparent molar volumes were 139.4 $\mathrm{cm^3\,mol^{-1}}$ for Trial Model 1, 126.9 $\mathrm{cm^3\,mol^{-1}}$ for Trial Model 2, and 119.7 $\mathrm{cm^3\,mol^{-1}}$ for the Final Model, compared against the experimental value of 113.0 $\mathrm{cm^3\,mol^{-1}}$ [422]. With estimated deviations of 23% and 12%, Trial Model 1 and Trial Model 2 were precluded from further testing. The Final Model, with an estimated deviation of 6%, was selected for use in simulation of vapour-liquid systems. Simulated apparent molar volumes of tetramethylammonium bicarbonate based on this model are presented in figure 4.14, together with the extrapolation to infinite dilution.

With the primary objective for both alkylammonium and bicarbonate model development being a description of solvent activities in aqueous solutions of alkylammonium bicarbonate, a final test of model performance was made to assess predictive capacity in these systems. As noted for both alkylammonium and bicarbonate, these species are volatile compounds and there are limited data available e.g. for primary amines. Hence, the activity data reported by Abdel-Salam [421] for tetramethylammonium bicarbonate were chosen as a test case. Tetramethylammonium bicarbonate solutions were simulated at 298 K and 100 kPa using the alkylammonium model detailed in section 4.8 together with the bicarbonate model developed here, for concentrations up to 10 $\mathrm{mol\,kg^{-1}}$. The resulting solvent activities are presented in figure 4.15.

The predicted activity of tetramethylammonium bicarbonate based on the models developed in this work

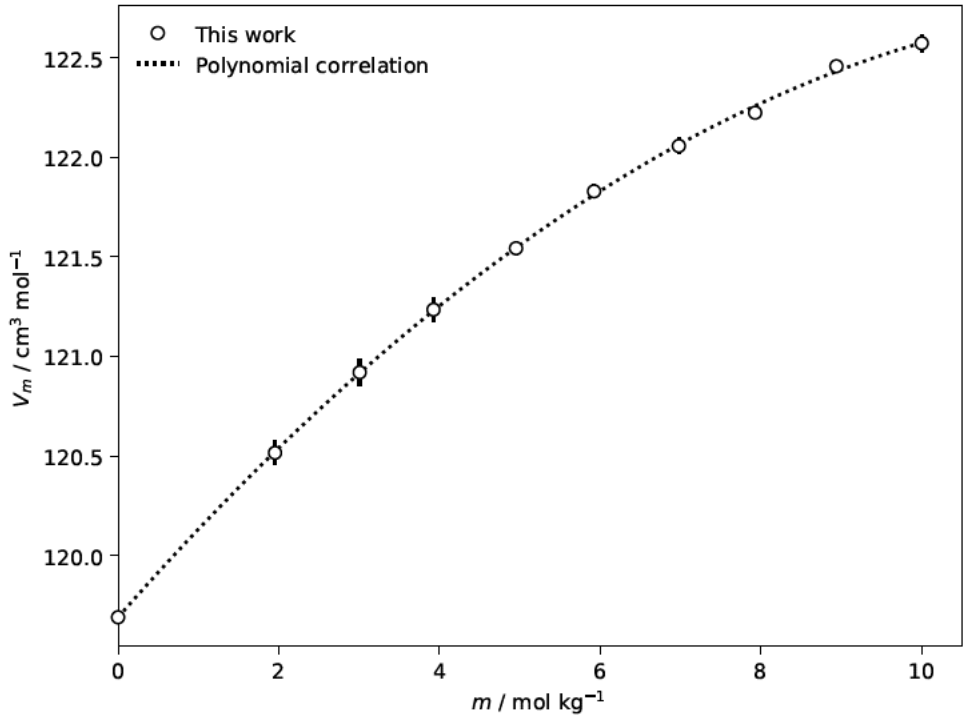

Figure 4.14: Apparent molar volumes of tetramethylammonium bicarbonate in aqueous solution at 298 K. Open symbols indicate simulated values using the model for alkylammonium from table 4.3 and bicarbonate from tables 4.4 and 4.5, together with the TIP4P/2005 water model [128]. Error bars indicate standard deviations calculated from independent sets of simulations. The value at infinite dilution is extrapolated based on a second-order polynomal, indicated by the dotted line.

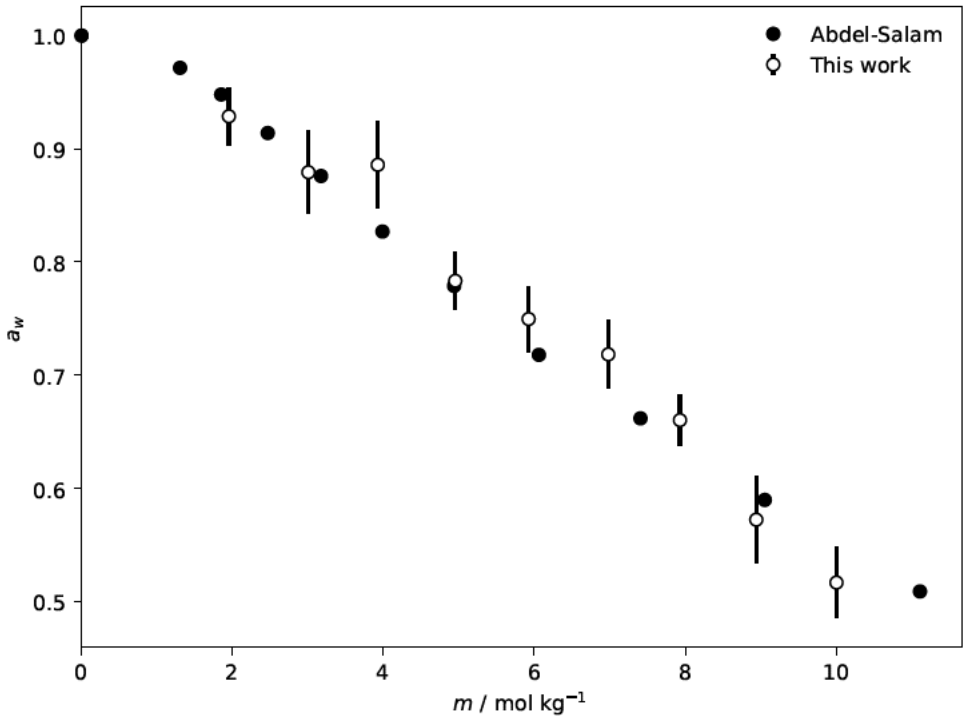

Figure 4.15: Water activity in aqueous trimethylammonium bicarbonate solutions at 298 K. Solid circles indicate experimental values as reported by Abdel-Salam [421]. Open symbols indicate simulated values using the alkylammonium model from table 4.3, together with the bicarbonate model from tables 4.4 and 4.5, together with the TIP4P/2005 water model [128]. Error bars indicate standard deviations calculated from independent sets of simulations.

are in good agreement with those reported by Abdel-Salam [421], with an average deviation of 2.5%. This is well within the statistical uncertainty 4.3% for this set of simulation data. While the last two data points in figure 4.15 taper down somewhat, the statistical precision is not sufficient to suggest a departure from the experimental trend.

4.10 Summary

This chapter started by considering the thermodynamic properties of electrolyte solutions based on a continuum solvent approach. Solubility and solution activities in dilute solutions were found to be well described by the Born and Debye-Hückel theories for ion-solvent and ion-ion interactions, with both relying on prior knowledge of solvent relative permittivity. Semi-empirical approaches were shown to extend the validity range of the continuum solvent approach to higher concentration for simple electrolytes. However, for solutions of complex electrolytes such as the organic ammonium compounds found in reactive CO_2 absorption, continuum solvent models were shown to rapidly fail due to a breakdown of underlying assumptions. As an alternative to continuum solvent models, three contemporary molecular equations of state approaches were considered with different approaches to modelling electrolytes.

- The ePC-SAFT equation of state takes a pragmatic approach, layering Debye-Hückel model on top of the molecular equation of state and requiring prior knowledge of permittivity.
- The eCPA equation of state uses an elaborate geometric framework to estimate solvent permittivity, allowing representation of well-understood solvent mixtures but without clear extension to more complex systems such as polymer solutions.
- Non-primitive models reject the Born and Debye-Hückel models entirely, instead making use of an explicit representation of solvent as dipolar molecules, but have seen less development than continuum-based approaches and are yet to be applied to polymer-electrolyte systems.

With no satisfactory equation of state approach identified to represent facilitated transport systems, explicit molecular models were considered instead. Three key aspects of electrolyte model development were reviewed: selection of target properties, representation of dispersion interactions, and charge scaling. By building on existing models for organic compounds together with a point-particle representation of halide, a generic model for alkylammonium compounds was developed. The proposed model accurately captures solvent activity and liquid densities in aqueous methylammonium solutions, demonstrating the feasibility of representing the thermodynamic properties of complex organic electrolytes based on classical molecular simulation.

In order to study reactive CO_2 absorption by aqueous amine solution, models for both ammonium ions and bicarbonate ions are required. A model for bicarbonate was developed following similar principles as for alkylammonium, but employing *ab initio* radial distribution data instead of solvent activities for parameter

optimisation. The resulting model for bicarbonate, when combined with the previously developed model for tetraalkylammonium, was found to predict the solvent activity in aqueous tetramethylammonium bicarbonate solution with good accuracy. The apparent molar volume of tetramethylammonium bicarbonate was found to be within 6% of the experimental value.

Together, the newly developed models for alkylammonium and bicarbonate permit molecular simulation of the typical species found in reactive CO_2 absorption. In chapter 5, the models for alkylammonium and bicarbonate developed here will be employed to study reactive CO_2 absorption in aqueous amine solution, as well as to calculate physical gas solubility in aqueous amine as a function of HCO_3^- concentration.

The electrolyte models also permits molecular simulation of PVAm at varying states of hydration and CO_2 absorption. Chapter 6 applies the models developed here to facilitated transport membranes, considering the PVAm - H_2O system at varying states of protonation. Additionally, the models presented here for alkylammonium and bicarbonate are applicable to a wide range of amine systems relevant to CO_2 absorption and processing beyond the facilitated transport membranes considered in this work.

Chapter 5

Models of Reactive Solvent Mixtures

5.1 Overview

As discussed in chapter 1, facilitated transport membranes rely on cocurrent pathways of permeation through the polymer, producing an increase in overall CO_2 transport. An important factor contributing to the facilitation effect is the high solubility of CO_2 in hydrated polymer, similar to that seen in amine solutions. Hence, it is important to have the appropriate tools and models to describe the chemical equilibrium of CO_2 in aqueous-organic systems in order to build a predictive molecular model for facilitated transport membranes.

In the preceding chapters we have considered systems of fixed composition, where solvent activity and gas solubility are functions of temperature and pressure. Conversely, in facilitated transport membranes and other aqueous amine systems, system composition is variable in response to CO_2 activity, due to the hydration of CO_2 to form carbonic acid, and its equilibrium with basic organic amines. This chemical reactivity plays a central role for the separation performance of facilitated transport membranes. However, the reactions of CO_2 bring the system from a simple aqueous-organic solution to a complex aqueous-organic electrolyte solution with dependencies between phase equilibrium and reaction equilibrium, presenting challenges for contemporary thermodynamic frameworks.

This chapter aims to identify a molecular modelling framework suitable to describing the reactions of CO_2 in facilitated transport membranes, and develop suitable model parameters for these reactions. We begin by describing the primary reaction pathways present in water - amine - CO_2 solutions in section 5.2. Next, reaction thermodynamics are presented in section 5.3, together with literature approaches to model reactive CO_2 absorption in aqueous amine systems, building from the concept of dilute solution reaction equilibrium. Chemical reactions are also discussed in the context of associating equations of state, with both explicit and implicit schemes for reactions adopted in recent literature. A reaction-implicit SAFT model is shown to give a good representation of CO_2 absorption in aqueous methyldiethanolamine (MDEA), a well-characterised amine absorbent. However, the predictive power of equation of state approaches is limited for systems with high

amine content.

Further, molecular simulation approaches to reactive systems are considered in section 5.4, including reaction ensemble Monte Carlo, reaction ensemble molecular dynamics, and the ReaxFF potential model. An approach similar to reaction ensemble molecular dynamics is developed, suited for simulation of aqueous solutions for which reaction equilibrium data are available for the infinite dilution reference state. Together with the models developed for amines in chapter 3 and electrolytes in 4, this approach allows prediction of reaction equilibrium in systems of arbitrary composition.

The proposed approach for combining molecular simulation and experimental data are tested using the systems MDEA - H_2O - CO_2 and MDEA - H_2O - CO_2 - CH_4, for which vapour-liquid data are available across a range of conditions. The molecular models previously developed for organic ammonium and bicarbonate are employed to describe this mixed solvent system, with additional torsional parameters proposed for amine and ammonium in alkanolamine compounds. The new approach shows promise for the description of acid gas absorption, and is readily extended to other reactive systems.

5.2 CO_2 Absorption in Hydrated Amine Solution

The chemical environment of CO_2 facilitated transport membranes closely resembles that of aqueous amine solutions, with polyamines in place of amine or alkanolamine solvent. Hence, we can expect absorption reactions to be analogous to those observed in amine solvent mixtures. The reaction pathways of CO_2 in aqueous amine mixed solvent are relatively well understood [416], making liquid amines suitable model systems for understand the processes underlying reactive CO_2 absorption. The reaction pathways detailed for CO_2 in aqueous amines are of significant industrial importance for gas sweetening and CO_2 capture applications, forming the basis of the regenerative amine process for acid gas absorption [429]. Amines are known to exhibit a rich family of reactions towards CO_2 in aqueous environments, with the specific reaction mechanisms and kinetics dependent on amine chemistry [416].

The experimental evidence for reactive absorption in amine-based facilitated transport membranes is primarily through attenuated total reflection Fourier transform infrared (ATR-FTIR) measurements prior to and after CO_2 absorption. Yu and Chuang [430] used this technique to study the reaction products of immobilized primary amines in the presence of water vapour, finding predominantly carbamate structures which persisted upon dehydration. Wu et al. [431] studied reactive absorption of both CO_2 and SO_2 in PVAm and other amine-based membranes, finding competing reaction products were generated which modified membrane composition over time, but in each case regenerated upon purging with N_2. Due to the similar FTIR signatures of carbamic and carbonic acid derivatives, the exact form of CO_2 reaction products remains to be conclusively determined, but likely comprises a combination of species depending on the steric environment of the amine and other competing chemical groups (e.g. alcohol in PVA-PVAm hybrid membranes).

Steric hindrance destabilises carbamate and increases free amine in solution [432, 433] hence increasing both loading capacity and reaction kinetics for CO_2 absorption. A number of commercial solvents (e.g. the FLEXSORB® range by ExxonMobil [434]) for CO_2 absorption have adopted sterically hindered amines to improve process performance in separation applications.

Following the same principle of steric hindrance for enhanced absorption, secondary and tertiary amines were investigated by Zhao and Ho [271] for application in a facilitated transport polyallylamine/PVA hybrid membrane. The incorporation of sterically hindered polyallylamine produced an increase in both CO_2 selectivity and permeability. Successful facilitated transport membranes will likely leverage a high fraction of bicarbonate as opposed to carbamate formation, either through steric hindrance or employing amine functionality which otherwise favours this reaction pathway.

Further to amine chemistry and steric hindrance effects, water has been shown to play a key role in the absorption mechanism of CO_2 in immobilized amine solvent by increasing the rate of conversion and promoting the formation of amine-CO_2 reaction products [435]. However, as the presence of water stabilizes the reaction products, it also increases the energy of absorption and consequently inhibits the release of CO_2.

5.2.1 CO_2 Hydration

Upon dissolution in dilute aqueous solutions, CO_2 rapidly reacts with water forming carbonic acid and its conjugate bases. The resulting equilibrium is described according to the reactions

$$CO_2 + H_2O \overset{K_1}{\rightleftharpoons} H_2CO_3 \tag{5.1}$$

$$H_2CO_3 + H_2O \overset{K_2}{\rightleftharpoons} H_3O^+ + HCO_3^- \tag{5.2}$$

$$HCO_3^- + H_2O \overset{K_3}{\rightleftharpoons} H_3O^+ + CO_3^{2-} \tag{5.3}$$

where K_1, K_2 and K_3 are equilibrium constants for each reaction, reported by e.g. Edwards et al. [415]. The formation of carbonic acid and its derivatives is in response to CO_2 activity through the left hand side of reaction 5.1, and hence directly related to CO_2 pressure over the solution. Although the neutral form of carbonic acid can be kinetically stable under certain conditions, it is thermodynamically strongly disfavoured and its deprotonation reaction is catalyzed by water [436]. Hence, in aqueous systems it is only seen in small quantities, and reactions 5.1 and 5.2 are often treated as a one-step process,

$$CO_2 + 2\,H_2O \overset{K_{CO_2}}{\rightleftharpoons} H_3O^+ + HCO_3^- \tag{5.4}$$

describing the formation of bicarbonate from CO_2 in a single reaction. The equilibrium constants are combined as $K_{CO_2} = K_1 K_2$ [415]. Since the concentration of carbonic acid is small under all conditions considered here, we will make use of this approximation for describing reactions in aqueous amine environments.

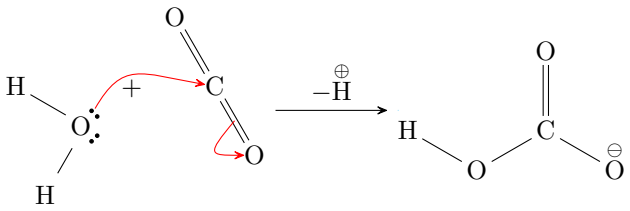

Figure 5.1: Bicarbonate formation from water and CO_2. An oxygen lone pair from water forms a bond to carbon on CO_2, while a hydrogen is lost to solution. Bicarbonate may lose its remaining hydrogen in a second deprotonation step, forming carbonate.

The second deprotonation reaction of carbonic acid leads to the formation of carbonate, with a total stoichiometric ratio of 2:1 against free proton species. The tendency of CO_2 to form carbonate or bicarbonate depends on system composition and acid-base equilibrium stoichiometric ratio. In general, high CO_2 pressures will favour the formation of bicarbonate, as this produces the highest uptake of CO_2 per unit of base in solution. This is true e.g. in the case of CO_2 absorption in aqueous amines [437, 416], where low-pressure conditions produce a combination of carbonate and bicarbonate, while high-pressure conditions produce predominantly bicarbonate.

5.2.2 Amine Protonation

Organic amine compounds act as weak bases in aqueous solution, accepting a proton from water to form organic ammonium compounds. Organic ammonium may remain as a conjugate acid in solution, or form electrolyte compounds together with e.g. strong acids as discussed in chapter 4 for the case of alkylammonium chlorides. The acidity constant pK_a is a key property for amine performance in separation applications [44], being directly correlated with absorption capacity.

Amine protonation is a one-step reaction with water, summarised by its conjugate acid as

$$R_3NH^+ + H_2O \overset{K_a}{\rightleftharpoons} R_3N + H_3O^+ \tag{5.5}$$

where each R group can be either hydrogen or an organic substituent, giving primary, secondary or tertiary amines.

The basicity of amines varies with chemical structure, but follow the general trend primary $>$ secondary $>$ tertiary with conjugate pK_a values typically in the range 9 - 11 for aliphatic amines. However, steric hindrance from organic substituents act to decrease basicity [438], such that e.g. a highly sterically hindered primary amine may show similar basicity to a less hindered secondary amine. Studies of amine basicity distinguish between basicity in solution and gas-phase basicity [438], where the latter is a product of the amine chemical structure and the former additionally includes solvation effects. While solvation effects vary depending on solvent composition, Frenna et al. [439] found a linear correlation between basicity of amines in water and benzene, indicating that free energy contributions from solvation effects to a good approxima-

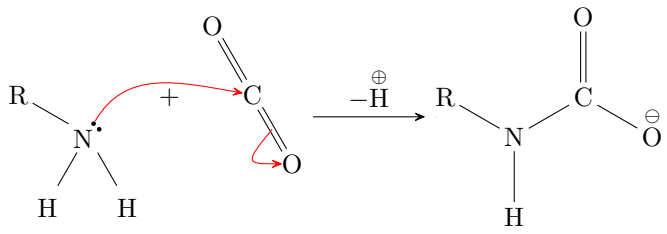

Figure 5.2: Carbamate formation from primary amine and CO_2 following the reaction pathway reported by Kortunov et al. [416]. The nitrogen lone pair forms a bond to carbon on CO_2, while a hydrogen is lost to solution (alternatively migrating to one of the carbamate oxygens).

tion are non-specific between amine compounds. Gas-phase amine basicity have been studied both through theoretical [440, 441, 442] and experimental [438] approaches. However, pK_a values remain challenging to predict accurately based on computational approaches, with Sumon et al. [443] concluding group-contribution empirical approaches outperform *ab initio* methods. Finally, thorough-space strain effects can significantly decrease the basicity of amine compounds [444], although these are most often found in aromatic heterocyclic or small-ring compounds and have little bearing on the systems studied here.

5.2.3 Amine-CO_2 Complexes

Further to the aqueous reaction products described for CO_2 and amines, certain amine-CO_2 reaction products may form in solution depending on the specific amine compound. The most significant of these are carbamates, formed by nucleophilic attack by the nitrogen lone pair towards the CO_2 carbon as illustrated in figure 5.2. Carbamate formation follows the general reaction equilibrium

$$2\,RNH_2 + CO_2 \rightleftharpoons RNHCOO^- + RNH_3^+ \tag{5.6}$$

and unlike the carbonic acid absorption pathway does not consume water as part of the reaction, although it takes part in the proton transfer step. As reaction 5.6 shows carbamate has an absorption capacity of 1 CO_2 per 2 amine, half that of the bicarbonate pathway. For this reason carbamate formation is disfavoured at high CO_2 activity.

Similar to amine conjugate acid pK_a values, the propensity to form carbamate species depends on the steric environment of the amine [445]. It is a major species for primary amines, while tertiary amines including MDEA show no sign of carbamate formation [445]. For polyamines including PVAm there is no conclusive evidence for or against carbamate formation, likely due to the experimental difficulty of distinguishing carbonic acid derivatives and carbamate. However, increased cross-linking and amine alkylation is expected to reduce carbamate formation.

5.2.4 Water Ionization

Further to the protonation reactions shown in equations 5.4, 5.5, and 5.6, the water auto-dissociation reaction influences acid-base equilibrium in aqueous amine solutions. Water ionizes to form H_3O^+ and OH^- according to

$$2\,H_2O \overset{K_w}{\rightleftharpoons} OH^- + H_3O^+ \tag{5.7}$$

where the water auto-dissociation constant K_w varies considerably with temperature. Here, the correlation of Bandura and Lvov [446] is adopted, with K_w represented to within experimental uncertainty in the temperature range 273 K - 1073 K.

5.3 Reaction Thermodynamics and Modelling Approaches

In general, CO_2 solubility in aqueous amines can be described as a combination of a vapour-liquid equilibrium of molecular CO_2 and reactive absorption through chemical equilibrium of CO_2 with amine and water in the liquid phase. As outlined in section 5.2, two primary reaction products may form: the carbamate ion $RNHCOO^-$ favoured for primary amines and low partial pressures of CO_2, and the bicarbonate ion HCO_3^- favoured for tertiary and sterically hindered amines and high partial pressures of CO_2. The stoichiometric ratio of absorbed CO_2 against reacted amine is 1:1 in the case of bicarbonate formation, and 1:2 for carbamate formation. Hence, absorption processes where bicarbonate is the dominant species have the potential for twice the loading for a given pressure, making these amine compounds stronger absorbents for CO_2 separation applications.

Reaction thermodynamics describe the balance between formation of products and reactants in an equilibrium reaction. All reactions are in principle reversible, although some lean so far towards reactants or products that the reverse reaction is not observed. In a regenerative system such as those considered here for CO_2 absorption, all reactions are reversible within the process timescales in response to chemical activities of the system species. The forward or backward movement of a reaction depends on the sign of the reaction free energy $\Delta_r G$, the sum of chemical potential changes for all species involved in the reaction,

$$\Delta_r G = \sum_i \nu_i \mu_i \tag{5.8}$$

where ν is the stoichiometric coefficient for each species. Note that ν is a signed integer, such that it takes on positive values for products and negative values for reactants. When $\Delta_r G$ is negative, the reaction proceeds in the forward direction, and opposite for positive values. The chemical potential is related to activity for each species by equation 3.1. For liquid solutions, activity of solutes is often expressed in terms of activity coefficients γ,

$$a = \gamma \frac{b}{b^\circ} \tag{5.9}$$

where b is the molal concentration and b° the standard molality. Inserting equation 3.1 into equation 5.8 for each species, we obtain

$$\Delta_\mathrm{r}G = \Delta_\mathrm{r}G^\circ + RT\sum_i \nu_i \ln a_i \tag{5.10}$$

where the term $\Delta_\mathrm{r}G^\circ$ contains the sum over μ° for each species. It is worth noting at this point the difference between these two free energies of reaction: $\Delta_\mathrm{r}G$ is the reaction free energy, and can take on positive or negative values depending on the composition of the reactive system. $\Delta_\mathrm{r}G^\circ$ is the standard reaction free energy, and is a fixed quantity describing the net change in formation free energies of reactants and products in the system under standard conditions. Chemical equilibrium is defined by $\Delta_\mathrm{r}G = 0$, i.e. residual chemical potentials exactly balance the standard reaction free energy and the reaction does not proceed in either direction. Under this condition, we can rearrange equation 5.10 as

$$K_\mathrm{eq} \equiv \exp\left[-\frac{\Delta_\mathrm{r}G^\circ}{RT}\right] = \prod_i a_i^{\nu_i} \tag{5.11}$$

defining the equilibrium reaction constant K_eq in terms of the standard reaction free energy $\Delta_\mathrm{r}G^\circ$. While the activity product on the right hand side of equation 5.11 can be evaluated by molecular simulation or molecular equations of state, the left hand term including $\Delta_\mathrm{r}G^\circ$ typically cannot, as formation free energies include the quantum mechanical ground state energy of each species which is outside the scope of molecular models of fluid systems.

For reactions in aqueous solutions, the activities in equation 5.11 are commonly expressed as concentrations referenced against a hypothetical 1 molar solution at infinite dilution (e.g. not accounting for Debye-Hückel effects or other solution non-ideal behaviour). A more robust approach is the use of concentrations corrected by activity coefficients depending on the system composition. Both approaches have been adopted for studying CO_2 solubility in aqueous systems, and are briefly reviewed in the following sections.

5.3.1 Kent-Eisenberg Model

As demonstrated by reactions 5.1 - 5.6, CO_2 absorption in amine solutions can be represented as a system of reactions comprising hydration, acid-base equilibrium, and formation of amine-CO_2 complexes. The balance of each reaction is described by reaction constants of the form given by equation 5.11. If the reaction constants are known, or can be fitted to experimental data, the species activities can be calculated by simultaneously solving each reaction equilibrium in the system.

The Kent-Eisenberg model [447] for acid gas absorption in aqueous amine solutions uses experimental vapour pressure data for ternary water-amine-gas systems to correlate equilibrium constants, allowing calculation of the resulting distribution of species in solution. The activities from equation 5.11, including electrolyte species, are approximated by concentrations without attempting to introduce activity coefficient corrections. Hence, the equilibrium constants correlated from solution data represent an amalgamation of equation 5.11

and other contributions to activities in solution,

$$K_{\mathrm{eq}} = \prod_i a_i^{\nu_i} \approx \prod_i b_i^{\nu_i} \tag{5.12}$$

where b_i is the concentration of species i relative to the reference state. This is a good approximation provided solution properties do not change too much (i.e. activity coefficients remain close to unity for all species). The value of K_{eq} is in turn a function of temperature, regressed based on available data. Kent and Eisenberg [447] used the correlation

$$\ln K = c_0 + \frac{c_1}{T} + c_2 \ln T + c_3 T \tag{5.13}$$

where c_0, c_1, c_2, c_3 are adjustable parameters. The Kent-Eisenberg model has been successfully applied to a number of systems within the field of aqueous amine absorbents. Jou et al. [448] measured the solubility of CO_2 and H_2S in aqueous methyldiethanolamine (MDEA), fitting values for equilibrium constants of amine reactions based on equation 5.13. In addition to variation with temperature, they found systematic concentration-dependent variations in the resulting equilibrium constants. Chakma and Meisen [449] reviewed a comprehensive set of data for CO_2 absorption in aqueous diethanolamine (DEA) and suggested the use of more elaborate correlations for K_{eq}, including system concentrations in addition to temperatures to improve on the Kent-Eisenberg model. Variations in the functional form of correlations for K_{eq} are sometimes denoted modified Kent-Eisenberg models, and while the addition of further model parameters improves agreement with experimental data, it is questionable to what extent the additions provide a physically meaningful description of the real system. Approaches with small adjustments to the treatment of reactions, such as the model by Gabrielsen et al. [450], generally have similar performance and will not be discussed separately.

Applications of Kent-Eisenberg models have been made by Tontlwachwuthikul et al. [451] for CO_2 solubility in 2-amino-2-methyl-1-propanol (AMP), with temperature- and concentration-dependent expressions for K_{eq}. Park et al. [452] considered CO_2 in monoethanolamine (MEA), diethanolamine (DEA), and AMP together with their mixtures, using the a 5-parameter temperature correlation of the form

$$\ln K = \sum_{i=0}^{5} \frac{c_i}{T^i} \tag{5.14}$$

and finding good predictive power for aqueous mixtures of the three amines with up to 30% amine weight fraction. For systems with a narrow range of physical conditions the Kent-Eisenberg model can work well, as illustrated by Le Tourneux et al. [453] for CO_2 absorption in dilute aqueous solutions of 2-amino-2-hydroxymethyl-1,3-propanediol (AHPD, amine weight fraction 0.0015 - 0.025). More recent applications of the Kent-Eisenberg model include Pahlavanzadeh et al. [454] correlating CO_2 solubility in 2-amino-2-methyl-1-propanol (AMP) and Heider et al. [455] in 2(methylamino)ethanol (MAE), both using the 4-parameter expression in equation 5.13. Mondal et al. [456] considered CO_2 solubility in aqueous sodium glycinate, finding

good agreement with experimental data despite not explicitly considering electrolyte interactions in the system. A hybrid approach using the Kent-Eisenberg model in combination with an equation of state approach for predicting species activities was investigated by Suleman et al. [457] for CO_2 solubility in alkanolamine–water systems, based on earlier investigations into equations of state in these systems [458].

Several weaknesses of the Kent-Eisenberg model become evident when considering systems with complexity beyond dilute aqueous solutions. There is no mechanism by which to capture compositional dependence in the system, with model performance generally deteriorating for high amine weight fractions. There is no account of known physical effects, such as those long-range electrostatics described by Debye-Hückel theory, and their influence on the resulting reaction equilibrium. Perhaps most importantly, it is not a predictive model for other properties than speciation, such as solvent activity, heat capacity, or density. The Kent-Eisenberg approach is useful for rapidly evaluating the chemical speciation of a system, but does not provide means by which to calculate other key properties for fluid systems, such as water absorption, non-reactive gas solubility, and the impact of electrolyte concentration on system thermodynamics.

5.3.2 Deshmukh-Mather Model

The limitations of the Kent-Eisenberg model with regards to activities have prompted refinements aiming to incorporate additional effects into the thermodynamic framework to improve model performance. Perhaps the most widely adopted modification is the inclusion of extended Debye-Hückel theory, proposed by Deshmukh and Mather [459]. Extended Debye-Hückel theory describes the activity of ionic species due to long-range electrostatic forces, with mean ion activity coefficients γ for a uni-univalent electrolyte given by

$$\ln \gamma_i = \frac{-A_\phi z_i^2 I^{0.5}}{1 + BI^{0.5}} + 2\sum_j \beta_{ij} b_j \tag{5.15}$$

where A_ϕ is the Debye-Hückel constant (a function of solvent continuum dielectric properties), I is the solution ionic strength, B is a model constant set equal to 1.2 as suggested by Pitzer [315], β_{ij} is a pairwise interaction parameter and b the concentration on molality basis. For further detail about the Debye-Hückel model of electrolyte solutions, see chapter 4. Application of equation 5.15 to equation 5.11 yields the expression

$$K_{\text{eq}} = \prod_i a_i^{\nu_i} \approx \prod_i \gamma_i b_i^{\nu_i} \tag{5.16}$$

where activity coefficients γ are given by equation 5.15, accounting for the stabilisation of electrolyte species due to long-range electrostatics. The initial model by Deshmukh and Mather [459] maintains solvent activity coefficients of unity, despite the Gibbs-Duhem relation implying a concomitant increase in solvent chemical potential. As such it is an inconsistent thermodynamic framework, but nonetheless represents a useful refinement over the Kent-Eisenberg model.

Modifications to the Deshmukh-Mather model were proposed by Roberts and Mather [460] for modelling of mixed solvent systems, with A_ϕ in equation 5.15 adjusted by solvent composition to better capture mixture dielectric properties. MacGregor and Mather [461] adopted these modifications to investigate competitive absorption of CO_2 and H_2S in a MDEA - sulfolane - water mixture, using an empirical correlation for mixed solvent dielectric properties.

The binary parameters in equation 5.15 allows for a large number of adjustable parameters in multi-species systems. Jou et al. [462] measured CO_2 solubility in 30% weight fraction MEA solution and employed the Deshmukh-Mather model for data regression with a binary interaction parameters for all species in solution. They found good agreement with experimental values in the temperature range 273 K - 423 K. Benamor and Aroua [463] employed a similar strategy for binary and ternary aqueous DEA and MDEA mixtures, also incorporating experimental carbamate concentration in fit.

Due to its simplicity and flexibility across amine-like systems, the Deshmukh-Mather model has seen significant adoption in evaluating chemistries for CO_2 absorption in carbon capture applications. Ma'mun et al. [464] investigated a novel amine compound, finding good agreement for CO_2 absorption isotherms and reasonable agreement with composition analysis of liquid phase species. Similarly, Jahangiri et al. [465] employed the Deshmukh-Mather model for CO_2 removal by 2-amino-2-methyl-1-propanol (AMP). A comparison of theoretical models for amine desorber design by Tobiesen et al. [466] found the Deshmukh-Mather model to give the best agreement with experimental data, with mean absolute deviation 6.8% across both high and low loading conditions.

Later work by Li and Mather [467] employs the Clegg-Pitzer equations [468, 469], combining the Pitzer model for electrolyte interactions [315] with a three-suffix Margules expansion for excess Gibbs energy G^{E} describing short-range solvent interactions,

$$\frac{G^{\mathrm{E}}}{RT} = \sum_{i,j} \alpha_{ij} x_i x_j + \sum_{i,j,k} \alpha_{ijk} x_i x_j x_k \tag{5.17}$$

where α_{ij} and α_{ijk} are two- and three-suffix solvent-specific interaction parameters. This model provides explicit activity coefficients for both solvent and electrolyte species, at the cost of additional model parameters. While the model performs well for prediction of mixed solvents the authors identify several weaknesses, most significantly deviations for low- and high-loading systems as well as the ideal gas-phase approximation used for the vapour phase. The Clegg-Pitzer equations are commonly used for multi-electrolyte solutions in mixed solvent, but have seen limited adoption for modelling CO_2 absorption.

The inclusion of electrolyte effects in the Deshmukh-Mather model improves meaningfully on the Kent-Eisenberg model, likely due in part to the increased number of adjustable parameters available. Deshmukh-Mather models have good predictive power for mixed solvent systems and capture concentration dependence without K_{eq} incorporating concentration-dependent terms. However, it suffers from similar weaknesses: with

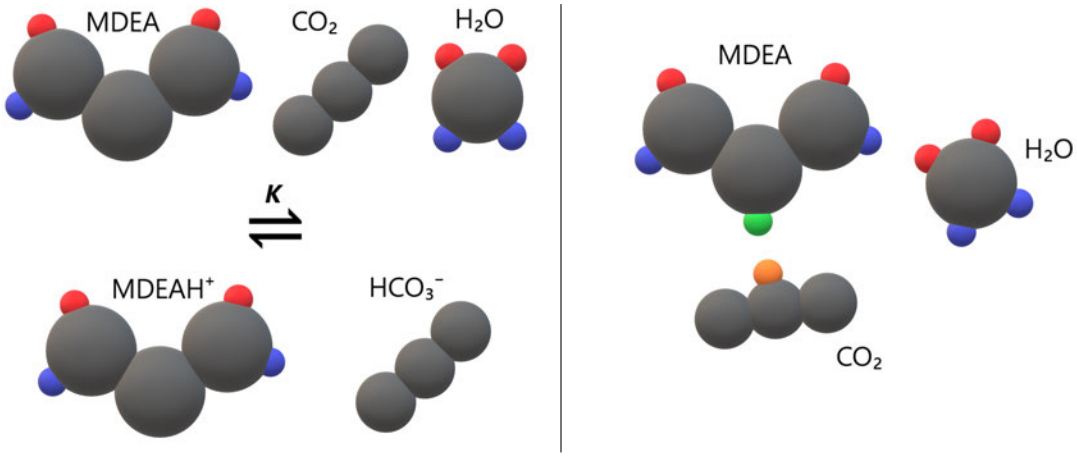

Figure 5.3: Approaches to reaction modelling for reactive H_2O absorption using SAFT molecular equations of state, exemplified by the MDEA-H_2O-CO_2 system. Left panel: Reaction-explicit model for CO_2 absorption, as detailed by Cleeton et al. [47]. Hydrogen bonding is described by association sites A and B (red and blue colour). The reaction products $MDEAH^+$ and HCO_3^- are represented by the molecular parameters of MDEA and CO_2, respectively. Equilibrium composition is calculated using equation 5.11. Right panel: Reaction-implicit model for CO_2 absorption. Hydrogen bonding is described by association sites A and B (red and blue colour) while CO_2 absorption is described by association sites C and D (green and orange colour). Equilibrium composition is calculated by the SAFT free energy expression in equation 2.52.

solvent composition as a dependent variable there is no clear way to calculate water vapour-liquid equilibrium and absorption. Solubility of non-reactive gases is not considered, and require *ad-hoc* models (e.g. Setchenow coefficients, as done by Jou et al. [470] and Schmidt et al. [471] for methane in MDEA solution). Many of these deficiencies may be improved upon by adoption of an equation of state-based modelling framework.

5.3.3 Reaction-Explicit Equation of State Models

The reaction framework outlined in section 5.3 relies on two pieces of information. Firstly, reaction free energy at the chosen reference state, and secondly, a framework for calculating species activities in systems of other compositions of interest. For species activities, both the Kent-Eisenberg and Deshmukh-Mather models of amine absorption estimate activities relative to the reference state - that is, on the assumption of small variations in fluid properties. Conversely, molecular equations of state as detailed in section 2.4 describe solutions at arbitrary compositions, expanding the range where activities can be reasonably obtained.

By combining the equilibrium reaction expression in equation 5.10 with a molecular equation of state, both chemical reactions and fluid properties may be characterised within a consistent thermodynamic framework. This reaction-explicit description of CO_2 absorption is illustrated in figure 5.3.

The use of a reaction-explicit SAFT model to describe CO_2 absorption in aqueous amine solutions was first reported by Nasrifar and Tafazzol [472] for aqueous monoethanolamine (MEA), diethanolamine (DEA), and methyldiethanolamine (MDEA). Using the equilibrium reaction constants by Austgen and Rochelle [473] in combination with the PC-SAFT equation of state, they obtained reasonable agreement with experimental absorption isotherms as well as speciation data. A similar approach was used by Pahlavanzadeh and Bayagi [454]

for aqueous MDEA solutions, exploring different association schemes for hydrogen bonding. Four-site models for both water and MDEA were found to give best results. Later work by Bayagi and Pahlavanzadeh [474] extended the analysis for the MEA - H_2O - CO_2 system, finding a mean average deviation of 36% across the temperature interval 313 K - 413 K and amine weight fractions up to 30%.

For models described so far, the liquid phase is strictly neutral - that is, no charged species are considered when evaluating the liquid phase. However, as discussed in section 5.2 we know that reactive CO_2 absorption produces a variety of electrolyte reaction products. These electrolyte species in turn modulate fluid properties, as discussed in chapter 4.

Electrolyte equations of state, such as ePC-SAFT, may be used in combination with a reaction-explicit framework to improve the description of species activities. The combination of an electrolyte + SAFT equation of state with a reaction-explicit framework for CO_2 absorption was first investigated by Uyan et al. [332] for the MDEA - H_2O - CO_2 system based on acid-base equilibrium reactions in water. The authors obtained a mean average deviation of 34.4% for CO_2 absorption up to 1.3 mole per mole MDEA*. Wangler et al. [333] later considered the same system, fitting binary interaction parameters for electrolyte species present in solution based on experimental osmotic coefficients. The combination of temperature-correlated equilibrium constants and electrolyte-specific binary interaction parameters allowed for a mean average deviation of 19.7%. However, with a total of 29 adjustable parameters used to fit the equation of state model against experimental absorption isotherms, it is unclear to what extent the model performance reflects the predictive capacity.

An approach with a leaner set of parameters, hence lower risk of over-fitting, was explored by Cleeton et al. [47]. The systems MDEA - H_2O - CO_2, MDEA - H_2O - H_2S, and MDEA - H_2O - CO_2 - H_2S were modelled with fixed-value binary interaction parameters obtained from binary systems rather than treated as free optimisation parameters. By considering a wide range of temperatures, amine content, and CO_2 loading, we found the model to provide good agreement for solutions with amine content up to 20%, but drastically reduced performance as amine content increased [47]. This likely reflects a breakdown in the dielectric continuum assumptions of the ePC-SAFT model used, as detailed in chapter 4. Electrolyte equations of state founded on continuum electrostatics have limited predictive power as compositions deviate from the initial fluid system.

5.3.4 Reaction-Implicit SAFT Models

Given the apparent shortcomings of reaction-explicit SAFT models of CO_2 absorption, it is worth considering simplified alternatives which forego the *ad-hoc* machinery of equation 5.11. As seen in the previous sections, the CO_2-amine absorption process can be reasonably approximated as a one-step process where CO_2 reacts with aqueous amines to form either bicarbonate or carbamate products. Using the SAFT framework detailed in section 2.4.3, the CO_2 absorption reaction can be represented as a single association interaction between

*Uyan et al. [332] originally reported a mean average deviation of 19.82%. The revised mean average deviation of 34.4% from Wangler et al. [333] is used here.

i	m	σ / Å	ϵ / k_B^{-1}K	Association	ϵ_{AB} / k_B^{-1}K	κ_{AB}	ϵ_{CD} / k_B^{-1}K	κ_{CD}	Source
MDEA	4.3589	3.3474	237.19	AABBC	1491.60	0.29836	4031.93	0.29334	[47], *
H_2O	2.1945	2.2290	141.66	AABB	1804.04	0.20390	-	-	[127]
CO_2	2.6037	3.7039	151.04	D	-	-	4031.93	0.29334	[51], *

Table 5.1: Molecular parameters for MDEA, H_2O, and CO_2 for the PC-SAFT equation of state with reaction-implicit CO_2 absorption. Note that the association parameters for sites C and D are developed for the amine and not generally transferable for CO_2 in combination with non-amine compounds. *: Parameters for CO_2-amine association developed in this work.

CO_2 and the amine group. This approach significantly simplifies the representation of reactive systems, and provides sufficient flexibility to describe CO_2 absorption in a wide range of aqueous amine systems.

The use of SAFT as an implicit model for CO_2 absorption in aqueous amine solutions was first suggested by Button and Gubbins [475] for the systems MEA - H_2O and DEA - H_2O. In their treatment CO_2-amine associations were not distinguished from hydrogen-bonding associations, with CO_2 represented by a 4-site model. Mean average deviations for CO_2 absorption in MEA - H_2O was 62%, considerably worse performance than the reaction-explicit models discussed previously.

By considering CO_2-amine association separately from hydrogen bonding associations, the parameters for reactive absorption can be optimised specifically for this purpose rather than reflecting a muddled combination of hydrogen bonding and acid-base reactions. This approach was first suggested by Mac Dowel et al. [476], employing SAFT-VR with reaction-specific association parameters to study the MEA - H_2O - CO_2 system. Later work by Mac Dowel et al. [477] included binary parameters for alkylamine - H_2O - CO_2 systems. The proposed parameters appear to have reasonable predictive power for CO_2 absorption, although no quantitative measure is provided.

Reaction-implicit treatments of CO_2 absorption has been applied to a wide range of systems. In a recent quantitative assessment of SAFT models for CO_2 and H_2S capture processes, Alkhatib et al. [478] found this approach to give excellent agreement with experimental absorption isotherms for a wide range of amine compounds. The reaction-implicit SAFT absorption model was found to account for preferential H_2S absorption in these systems. The same approach was also tested for non-aqueous amine - glycol and amine - glyme mixed solvents [479] with good results. This is in contrast with other liquid-phase acid-gas absorption systems such as ionic liquids, where CO_2 and H_2S solubility can be well represented by a non-associative SAFT model as detailed by Al-naish and Lue [480]. Further detail on the reaction-implicit approach to SAFT models for CO_2 absorption is provided in the review by Pereira and Vega [481].

Due to the limited gains of reaction-explicit SAFT representations of CO_2 absorption, a reaction-implicit model is used here to represent reactive CO_2 absorption in amine-water systems. Since no CO_2 absorption data are available for the test system PVAm - H_2O, the system MDEA - H_2O - CO_2, previously characterised using a reaction-explicit ePC-SAFT framework [47], is used to develop CO_2-amine association parameters for the PC-SAFT equation of state, shown in table 5.1. Molecular parameters for MDEA, H_2O, and CO_2 are

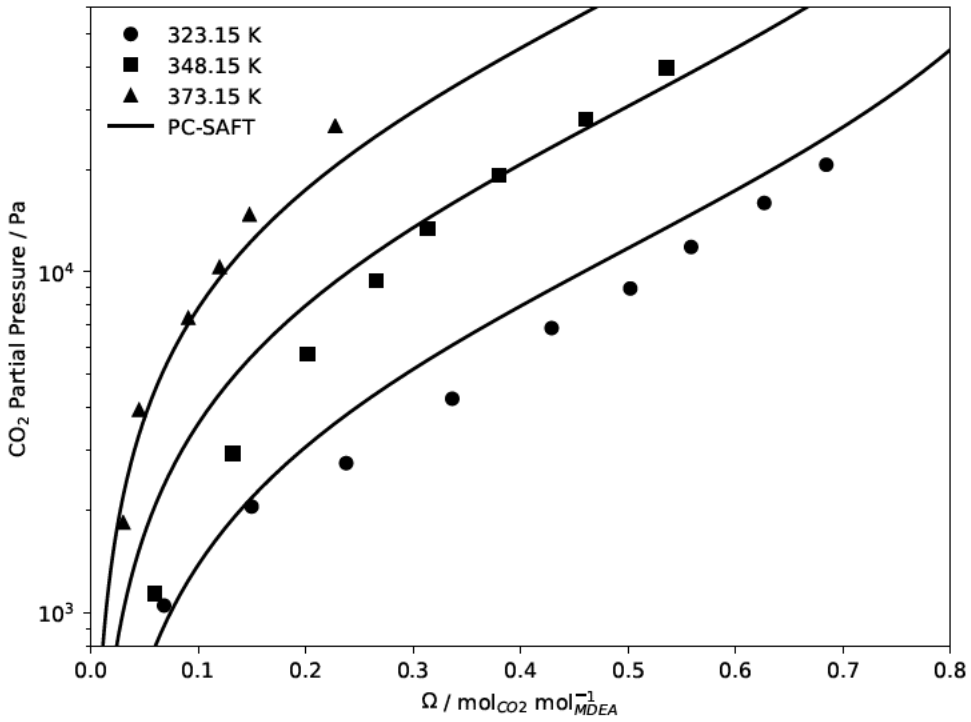

Figure 5.4: CO_2 absorption in 5% amine weight fraction H_2O - MDEA solution at 323 K, 483 K, and 373 K as a function of CO_2 partial pressure. Solid symbols indicate experimental data from Rho et al. [482]. Solid lines indicate PC-SAFT equation of state with model parameters from table 5.1.

regressed against the experimental data from Rho et al. [482] using a least-squares objective function. A comparison of the PC-SAFT model against experimental CO_2 absorption data are shown in figure 5.4, with an absolute mean deviation of 3.5% for CO_2 absorption Ω relative to experimental values at 323 K, 483 K, and 373 K.

5.4 Molecular Simulation of Reactive Systems

The thermodynamic frameworks presented for modelling reactive systems presented in sections 5.3.1 - 5.3.3 are unified by the division of reaction thermodynamics into 'ideal' and 'residual' contributions in line with equation 5.10. The ideal contribution is either represented by explicit reaction constants, or equivalently, implemented as part of the equation of state in the case of SAFT models. In either approach, accurately representing activities of reactive species is essential in order to predict system composition. As seen in chapter 4, equations of state face severe challenges when describing systems beyond the continuum solvent approximation. Aqueous-organic mixtures, such as aqueous amines and facilitated transport membranes, fall into this category due to the composition-dependent dielectric properties and solvent-solute interactions present.

Molecular simulation has a significant advantage over equation of state approaches in the treatment of electrolyte solutions: Solvent dielectric properties (and solvent-solute interactions) are predicted directly

from the molecular parameters through simulation of the target system, without the assumption of a solvent continuum. Hence, molecular simulation can be used to evaluate species activities in equation 5.10 and consequently speciation and loading values at prescribed system compositions. Activities are calculated as

$$a_i = \frac{\rho_i}{\rho_i^\circ} \exp\left[\frac{\Delta_{\mathrm{solv}} G_i - \Delta_{\mathrm{solv}} G_i^\circ}{RT}\right] \tag{5.18}$$

where ρ_i° is the molar density and $\Delta_{\mathrm{solv}} G_i^\circ$ the solvation free energy of the species, both in the chosen reference state. For this work, the reference state used is aqueous solution at the temperature of interest and a pressure of 100 kPa, with solute molecules present at a hypothetical concentration of 1 mol l^{-1} but without solute-solute interactions. The exponential term in equation 5.18 takes the place of activity coefficients in equation 5.16, allowing evaluation of equation 5.11 in the neighbourhood of the simulated conditions – assuming activity coefficients vary smoothly with composition. Values for K_{eq} are taken from experimental sources in the chosen reference state. In this work, the reference state for equilibrium constants is a hypothetical 1 molar solution at at infinite dilution (corrected for the effects of long-range electrostatic interactions).

5.4.1 Reaction Ensemble Monte Carlo

The application of Monte Carlo simulation to study reactive systems was initially proposed by Shaw [483] for N-particle systems, and later independently developed by Johnson et al. [484] for associative systems and by Smith and Triska [485] for generic reactive mixtures. In reaction ensemble Monte Carlo, the deletion and insertion of species according to one or more reactions is a randomly proposed system move, similar to translational, rotational, and volume-change moves seen in isobaric-isothermal Monte Carlo simulations. By accepting or rejecting reaction moves, the system composition converges to minimise the system Gibbs free energy according to the reaction free energy balance in equation 5.8.

The probability $P_{m,n}$ of accepting a reaction move from state m to n is given as [486]

$$P_{m,n} = \min \begin{cases} 1, \\ (\frac{pV}{k_B T})^\sigma K^0 \prod_i \left[\frac{N_i!}{(N_i+\nu_i)!}\right] \exp\left[-\frac{\Delta_{m,n} U}{k_B T}\right] \end{cases} \tag{5.19}$$

where $\sigma = \sum_i \nu_i$ is the net change in molecules for the reaction, K^0 is the vacuum equilibrium constant, and $\Delta_{m,n} U$ is the residual potential energy difference between states m and n. K^0 is analogous to K_{eq} defined in equation 5.11, but instead of an aqueous reference state it refers to an ideal gas reference state at system temperature and 100 kPa. K^0 is defined by

$$\ln K^0 = \frac{\sum_i \nu_i \mu_i^0}{RT} \tag{5.20}$$

where μ_i^0 is the vacuum chemical potential of species i, obtained experimentally or evaluated using quantum

mechanical methods. For further details of the implementation of reaction ensemble Monte Carlo, see the review by Turner et al. [486].

Reaction ensemble Monte Carlo has been employed to study reactive systems across a wide range of physical conditions [486], but only relatively recently in the context of CO_2 absorption and acid-base equilibria. Formation of carbamate, bicarbonate and organic ammonium from CO_2 absorption in aqueous MEA was considered by Balaji et al. [487], giving reasonable agreement with experimental values of speciation as a function of CO_2 loading, although no attempt to estimate CO_2 partial pressure was made.

The limited adoption of reaction ensemble Monte Carlo for CO_2 absorption reactions is likely a combination of two limiting factors: Firstly, molecular models for electrolytes are poorly developed in the context of phase equilibria, giving unreliable estimates of $\Delta_{m,n}U$ in equation 5.19. Secondly, Monte Carlo simulation is inefficient for sampling the dense condensed phase found in electrolyte solutions [488], particularly due to close ion-solvent contacts. While advanced sampling methods such as continuous fractional component [489] can be used to accelerate sampling e.g. for insertion of large molecules and were used by Balaji et al. [487], simulation of electrolyte solutions remains challenging with Monte Carlo techniques and is more readily accessible using molecular dynamics.

5.4.2 Reaction Ensemble Molecular Dynamics

The solution of chemical reaction equilibrium systems based on classical force fields may also be studied by molecular dynamics simulation, as demonstrated by recent work by Smith and Qi [490] and Noroozi and Smith [488, 491]. This approach, denoted reaction ensemble molecular dynamics, aims to minimize total Gibbs free energy for a system of reactive particles through an iterative approach. Gibbs free energy is given by

$$G = \sum_i N_i \mu_{i,\mathbf{X}} \tag{5.21}$$

where $\mu_{i,\mathbf{X}}$ is the chemical potential for species i given system composition $\mathbf{X}$, and N_i is the number of molecules for that species in the system. Chemical potentials are calculated as

$$\mu_{i,\mathbf{X}} = \mu_i^0 + RT \ln \frac{P}{P^0} + RT \ln \frac{x_i}{x^0} + \mu_{i,\mathbf{X}}^{\mathrm{res}} \tag{5.22}$$

where P^0 is the unit pressure and $x^0 = 1$ for the vacuum state. It is important to note that the vacuum chemical potential μ_i^0 includes the free energy of formation for species i, and as such must be obtained through alternative methods such as experimental data or quantum mechanical evaluation of the molecular partition function, as done by Smith and Qi [490]. The residual chemical potential $\mu_{i,\mathbf{X}}^{\mathrm{res}}$ is evaluated for a system of composition $\mathbf{X}$ using a free energy perturbation approach (e.g. the Bennet acceptance ratio method, see section 2.3.2) relative to the vacuum state, such that $\mu_{i,\mathbf{X}}^{\mathrm{res}} = \Delta_{\mathrm{solv}} G_{i,\mathbf{X}}$ which is readily estimated by molecular simulation.

Given chemical potentials for all species obtained through equation 5.22 for a state with composition $\mathbf{X}_0$, chemical potentials are estimated for a new state with composition $\mathbf{X}_1$ based on an ideal mixture assumption, giving

$$\mu_{i,\mathbf{X}_1} = \mu_i^0 + RT \ln \frac{P}{P^0} + RT \ln \frac{x_i}{x^0} + \mu_{i,\mathbf{X}_0}\mathrm{res} \tag{5.23}$$

which allows the Gibbs energy in equation 5.21 to be minimized subject to the usual stoichiometric constraints. Note that the only difference between equations 5.22 and 5.23 is the state labels $\mathbf{X}_0$ and $\mathbf{X}_1$, reflecting the use of one state to estimate chemical potentials for another which allows the reaction ensemble molecular dynamics approach to iteratively converge towards an equilibrium composition.

The scheme proposed by Smith and Qi [490] for reaction ensemble molecular dynamics has the advantage of using efficient molecular dynamics sampling for converging reactive systems at prescribed conditions of temperature, pressure, and initial composition. It is generic in its application to condensed or vapour phase systems, provided adequate molecular models are available for all species. However, the approach is somewhat cumbersome due to a potentially large number of iterations to reach convergence in complex systems, and the need to construct separate simulations at each composition point rather than having system composition converging in a single simulation, as for reaction ensemble Monte Carlo approaches.

Recent work by Noroozi and Smith [488, 491] adapted the reaction ensemble molecular dynamics approach to study CO_2 absorption in aqueous ethanolamine (MEA) solutions. Rather than explicitly considering chemical potentials as function of electrolyte concentration within the reaction ensemble framework the Davies equation [322],

$$\ln \gamma_{\pm} = -A_\phi z^2 \left(\frac{\sqrt{I}}{1+\sqrt{I}} - 0.3I \right) \tag{5.24}$$

is used to calculate electrolyte activities. Solvent activity is obtained by integration of the Gibbs-Duhem equation as

$$a_i^{\mathrm{Davies}} = \frac{M}{1000} A_\phi \left[2\frac{1+2\sqrt{I}}{1+\sqrt{I}} - 4\ln\left(1-\sqrt{I}\right) - 0.3I^2 \right] - \frac{1-x_i}{x_i} \tag{5.25}$$

with the coefficient A_ϕ calculated from the solvent density and dielectric constant, obtained by molecular simulation [488]. This hybrid approach simplifies the reaction ensemble methodology, since solvent composition is essentially fixed and only a single composition needs to be evaluated. Vacuum state chemical potentials μ_i^0 were obtained by Gaussian09 using a number of different basis sets to estimate uncertainties. The authors do not quote comparison values for predicted CO_2 partial pressures against experimental data, but graphically appear to be within 1 - 2 orders of magnitude across the loading range 0.1 $\mathrm{mol_{CO_2}/mol_{MDEA}}$ for absorption in a 30% weight fraction MEA solution at 353 K. Speciation is in reasonable agreement with experimental data for the same system [492, 493, 494, 495], showing the carbamate reaction (equation 5.6) as the primary absorption mechanism up to high loading, where bicarbonate (equation 5.4) becomes the main reaction product due to its more favourable stoichiometric ratio to amine.

Further work based on the reaction ensemble molecular dynamics approach was done for prediction of $\mathrm{p}K_\mathrm{a}$

values across 29 alkanolamines by Noroozi and Smith [491]. In order to study the deprotonation reaction (equation 5.5), solvation free energies for amine and ammonium species together with the H_3O^+ ion are required. However, since no suitable molecular model is available for H_3O^+, the standard value of $-1104.5\,\mathrm{kJ\,mol^{-1}}$ from Tissandier et al. [496] was used rather than attempting to calculate $\Delta_{\mathrm{solv}}G$ by molecular simulation of this species. For ammonium and amines, free energy perturbation approach was used to estimate $\Delta_{\mathrm{solv}}G$. This introduces an additional free energy contribution due to the Galvani potential encountered when transferring a charged species between media of different dielectric properties [497, 498, 499]. Since the Galvani potential is solvent-specific, the solvation of a single ion adds a further possible point of error as the dielectric properties of the model solvent generally deviate from experimental values.

The authors found an AAD of 0.73 pK_{a} units for the best performing set of partial charges considered [491], which is greater than the standard deviation of 0.65 pK_a units for the full set of 29 amines investigated. Hence, it is inconclusive whether the reaction ensemble molecular dynamics approach has significant predictive power for pK_{a} values of alkanolamines. The authors identify poorly developed ion molecular models as the most important area of improvement for prediction of acid-base reactions of aqueous amines, and in particular point to the weaknesses of RESP charges generated under vacuum conditions for the study of condensed phase systems [491].

5.4.3 Reactive Force-Field (ReaxFF)

The approaches to modelling reactive systems discussed so far hinge on the separation of inter- and intramolecular degrees of freedom in the description of molecular species and their interactions. Intermolecular interactions and the resulting residual thermodynamic potentials are assessed through simulation or equations of state, while intramolecular interactions and the resulting ground-state energies are assessed experimentally or through quantum mechanical methods. The reactive force-field (ReaxFF) approach attempts to unify these two aspects, describing both inter- and intramolecular forces through classical potential functions [500, 501]. This allows bond creation or destruction to happen dynamically in a simulated microscopic system.

ReaxFF is constructed similarly to conventional classical potentials described in section 1.5, with an added potential function describing bonded interactions. ReaxFF is based on the notion of bond order, whereby the connectivity of atoms can be determined by the inter-atomic spacing. Bond order (BO) comprises contributions from σ-, π-, and $\pi\pi$-character bonds as

$$BO_{ij} \equiv BO_{ij}^{\sigma} + BO_{ij}^{\pi} + BO_{ij}^{\pi\pi} = \exp\left[p_{bo1}\left(\frac{r_{ij}}{r_0^{\sigma}}\right)^{p_{bo2}}\right] + \exp\left[p_{bo3}\left(\frac{r_{ij}}{r_0^{\pi}}\right)^{p_{bo4}}\right] + \exp\left[p_{bo5}\left(\frac{r_{ij}}{r_0^{\pi\pi}}\right)^{p_{bo6}}\right] \tag{5.26}$$

where p_{bo1} - p_{bo6} and r_0^{σ}, r_0^{π} and $r_0^{\pi\pi}$ are bond-specific parameters [502]. The bond order expression is the basis for calculating energy contributions from reactive potentials, with the primary reactive bonded term

taking the form

$$U_{bond} = -D_e^{\sigma} BO_{ij}^{\sigma} \exp\left[p_{be1}(1 - (BO_{ij}^{\sigma})^{p_{be2}})\right] - D_e^{\pi} BO_{ij}^{\pi} - D_e^{\pi\pi} BO_{ij}^{\pi\pi} \tag{5.27}$$

where D_e^{σ}, D_e^{π}, $D_e^{\pi\pi}$ are adjustable parameters describing bond dissociation energy. Further to equation 5.27, ReaxFF includes potential energy contributions from lone pair formation, over- and under-coordination, valence angles, three- and four-body conjugation effects, hydrogen bond interactions, and species-specific corrections [502].

The ReaxFF approach can give impressive insights to the reaction pathways in applications such as combustion [502] and ion hydration in specific aqueous systems [503]. However, the inordinate number of parameters required significantly limits practical application to new systems, and system-specific parameters have limited transferability as evidenced by the multiple sets of independently developed ReaxFF parameters [501] for different condensed-phase systems. In the context of electrolyte systems, ReaxFF has been employed to study glycine tautomerisation between the neutral and zwitterion forms [504, 505] and hydration of copper ion [503] hydration, but is untested for application to reactive CO_2 absorption.

5.5 MDEA - H_2O - CO_2

The simulation methodologies presented in section section 5.4 offer complementary routes to obtaining species compositions in reactive systems, and either methodology may in theory be employed provided suitable parameters are available. However, practical considerations limit the application of each methodology to characterisation of CO_2 absorption.

Although attractive in principle, the ReaxFF approach to reactive systems is lacking parameters for CO_2 absorption, and faces the same challenges for electrolyte model development as discussed in chapter 4. ReaxFF would require development of a new suite of application-specific parameters, which is incompatible with the model framework employed in chapters 3 and 4.

The similar reaction ensemble Monte Carlo and reaction ensemble molecular dynamics as presented by Smith and Qi [490] both require knowledge of vacuum free energies, which are not generally available and require further *ab initio* studies of each species. Additionally, Monte Carlo simulation of electrolyte solutions is limited by the low acceptance of translational moves for charged species, giving poor sampling of liquid phase configurations.

Here, a hybrid approach is adopted for molecular dynamics simulation of reactive systems, utilising free energy perturbation for residual properties together with experimental reaction constants at well defined reference states. By measuring solvation free energies at both reference state and the system of interest, molecular simulation can be used to evaluate species activities in equation 5.10 and consequently speciation and loading values at prescribed system compositions. Activities are calculated using equation 5.18. Values

Source	Year	T / K	P_{CO_2} / kPa	Weight Fraction / %
Jou et al. [448]	1982	298, 313, 343, 373, 393	0.001 - 6,630	23.8, 51.0
Austgen et al. [473]	1991	313	0.0056 - 93.6	23.8, 51.0
Shen and Li [508]	1992	313, 333, 353, 373	1.1 - 1,979	30.0
Jou et al. [509]	1993	313, 373	0.004 - 236	35.0
Kuranov et al. [445]	1996	313, 333, 373, 393, 413	73.5 - 5,037 ^{a}	23.8, 47.3
Mathonat et al. [510]	1997	313, 353, 393	2,000 - 10,000	30.0
Rho et al. [482]	1997	323, 348, 373	0.775 - 268	5.0, 20.5, 50.0, 75.0
Haji-Sulaiman et al. [511]	1998	303, 313, 323	0.09 - 100	23.8, 47.7
Rogers et al. [512]	1998	313, 323	0.00007 - 1.0018	23.0, 50.0
Silkenbäumer et al. [513]	1998	313	12.0 - 4,080 ^{a}	31.4
Kamps et al. [514]	2001	313, 353, 393	186 - 7,565 ^{a}	48.9
Addicks et al. [515]	2002	313, 353	1,000 - 2,000 ^{a,b}	30.0, 50.0
Huttenhuis et al. [516]	2007	283, 298	0.054 - 351 ^{b}	35.0, 50.0
Dell'Era et al. [517]	2010	298, 303, 313, 323	94.5 - 103.3 ^{a}	10.0, 20.0, 49.0

Table 5.2: Literature studies reporting isothermal CO_2 solubility in aqueous MDEA solution and the physical conditions investigated. a: Total vapour pressure reported. b: Quaternary MDEA - H_2O - CO_2 - CH_4 mixture.

for K_{eq} are taken from experimental sources in the infinite dilution reference state, with pK_{a} values readily available for most common species.

To assess the performance of the reactive system methodology, a prototypical system for CO_2 absorption by sterically crowded amines was selected in the form of aqueous methyldiethanolamine (MDEA) solution. Aqueous MDEA is particularly well suited as a test case because of its unambiguous reaction product with CO_2 and well documented physical properties of both pure and mixed solvents. Bulk properties including density and viscosity of aqueous MDEA solutions have been reported by Rinker et al. [506] and more recently Sobrino et al. [507] under conditions relevant to CO_2 capture applications.

Solubilities of CO_2 and other gases in aqueous MDEA solutions have been reported by numerous authors, with a summary of literature studies for ternary MDEA - H_2O - CO_2 systems provided in table 5.2. Additionally, physical solubility - i.e. solubility of CO_2 in the non-reacted form - in aqueous MDEA solutions has been characterised for methane and ethane [470, 471], together with vapour-liquid equilibrium data by Addicks et al. [515] for the MDEA - H_2O - CO_2 - CH_4 quaternary system. Quaternary VLE data has also been reported for MDEA - H_2O - CO_2 - H_2S by a number of authors, including recent works by Dicko et al. [518] and Haghtalab and Izadi [519]. A review of experimental data for quaternary MDEA - H_2O - CO_2 - H_2S systems is provided by Cleeton et al. [47] and will not be considered further here.

5.5.1 Reaction System

The reaction mechanisms of CO_2 absorption in aqueous MDEA follow those presented in section 5.2 for generic aqueous amines. As a tertiary amine, MDEA only participates in the protonation reaction with water,

$$MDEAH^+ + H_2O \overset{K_{\mathrm{MDEA}}}{\rightleftharpoons} MDEA + H_3O^+ \tag{5.28}$$

	$K_{\mathrm{CO_2}}$	K_{MDEA}
C_1	-12092.1	-819.7
C_2	-36.7816	79.474
C_3	235.482	10.9756
T_{min} - T_{max}	273 K - 498 K	278 K - 368 K

Table 5.3: Parameters and temperature ranges for reference state reaction constants given by equation 5.29 for CO_2 (equation 5.4) and MDEA (equation 5.28) deprotonation reactions. Parameters for CO_2 from Edwards et al. [415] and MDEA from Kamps and Maurer [520]

forming no other significant reaction products with CO_2 or water [416]. The reaction constant for equation 5.28 has been determined experimentally over the temperature range 278 K - 368 K by Kamps and Maurer [520] using electromotive force measurements for dilute aqueous solutions. Their temperature correlation of the form

$$\ln K = \frac{C_1}{T/\mathrm{K}} + C_2 + C_3 \ln(T/\mathrm{K}) \tag{5.29}$$

is used here, with parameters for equation 5.29 listed in table 5.3. The more recent correlation by Hartono et al. [521] is based on potentiometric titration and considers high ionic strength solutions using an extended Debye-Hückel model to describe the influence of other electrolytes on the MDEA deprotonation reaction. These systems go beyond the infinite dilution conditions of interest and were disregarded for the present study, but may be useful for further work.

Absorption of CO_2 in aqueous MDEA solution can be viewed as a conjugate acid-base reaction. Combining equation 5.4 and 5.28 in reverse gives the CO_2 absorption equilibrium reaction

$$\mathrm{CO_2 + H_2O + MDEA} \overset{K_{\mathrm{abs}}}{\rightleftharpoons} \mathrm{MDEAH^+ + HCO_3^-} \tag{5.30}$$

where $K_{\mathrm{abs}} = K_{\mathrm{CO_2}}/K_{\mathrm{MDEA}}$ for the reference state. As for the MDEA dissociation constant K_{MDEA}, values for K_{CO2} can be obtained from literature sources adjusted to infinite dilution. Here, the correlation of Edwards et al. [415] is used, following the functional form in equation 5.29 with parameters listed in table 5.3. The reaction system describing CO_2 absorption in aqueous MDEA is hence given by equations 5.4, 5.7, and 5.30. It is important to note that equation 5.30 contains no OH^- or H_3O^+ species, hence K_{abs} is invariant to changes in activity of these ionized water species.

5.5.2 Simulation Details

Molecular simulations of the $CO_2 - \mathrm{MDEA} - H_2O$ reaction system were performed both in mixed solvent and dilute aqueous systems. As discussed in section 5.3, species activities must be considered in order to correctly assess the free energy of reaction for systems away from the reference state. To assess activities by molecular simulation, solvation free energies $\Delta_{\mathrm{solv}}G$ and number densities ρ_i of both the reference state and system of interest should be simulated. The reference state for the reaction in equation 5.30 is a 1 molar aqueous

solution at infinite dilution for all solutes, while the reference state for water is the saturated liquid state. To calculate activities in a system of interest, CO_2 absorption in a 30% mass fraction solution of MDEA at 353 K was chosen as a test case.

Infinite dilution systems are readily assessed by simulation of a single solute in bulk solvent represented by the usual periodic boundary conditions. Here, a solvent system with approximate size 3.2 nm is used for all solutes, corresponding to 1095 H_2O molecules. Chemical potentials were measured using the Bennett acceptance ratio method discussed in section 2.3.2, allowing 1200 ps of simulation at each λ state with the initial 200 ps discarded as equilibration. The λ states were defined by increments of 0.05 for both λ_{coul} and λ_{disp} with each potential scaled separately, yielding 41 thermodynamic states for each molecule. A comprehensive list of simulation parameters is given in appendix A.

While solvation free energies were measured by direct insertion for CO_2 and H_2O, solvation free energy for MDEA and electrolyte species were considered together in a single step. The perturbation of MDEA, $MDEAH^+$ and HCO_3^- are represented by the pseudo-reaction

$$\mathrm{MDEA} \longrightarrow \mathrm{MDEAH}^+ + \mathrm{HCO}_3^- \tag{5.31}$$

where MDEA is transformed into $MDEAH^+$ by the addition of a hydrogen atom and scaling of atomic charges, while for HCO_3^- both dispersion interactions and charges are scaled as done for single molecules. Rather than corresponding to a single molecule, the resulting solvation free energy represents the net change for all three species;

$$\Delta_{\mathrm{solv}}G = \Delta_{\mathrm{solv}}G_{\mathrm{HCO_3^-}} + \Delta_{\mathrm{solv}}G_{\mathrm{MDEAH^+}} - \Delta_{\mathrm{solv}}G_{\mathrm{MDEA}} \tag{5.32}$$

with the negative sign for $\Delta_{\mathrm{solv}}G_{\mathrm{MDEA}}$ indicating deletion of the species. This approach improves convergence of solvation free energies for the large molecule MDEA, retains system charge neutrality at each step of the transformation, and avoids simulations with species for which there are no suitable molecular models available (i.e. OH^- and H_3O^+).

The MDEA - H_2O mixed solvent system was constructed by 767 H_2O and 50 MDEA molecules, giving a size of approximately 3.2 nm. Maintaining an even size for the two systems avoids any potential bias from finite-size effects, which can be significant particularly for low-concentration electrolyte systems [141]. MDEA protonation states of 0%, 50%, and 100%, were considered, covering the full range of reactive CO_2 absorption. The molecular models for organic ammonium and bicarbonate developed in chapter 4 were employed to represent HCO_3^- and protonated MDEA, with the alcohol groups of MDEA represented by compatible TraPPE-UA potentials [105]. For the O-C-C-N dihedral potential we adopt the analytical expression by Chang et al. [522], with electrostatic and dispersion potentials between the amine and alcohol groups discounted as per the usual united-atom approach for 1-4 interactions.

To improve convergence of mixed solvent systems, 40 ns of simulation in the isothermal-isobaric ensemble

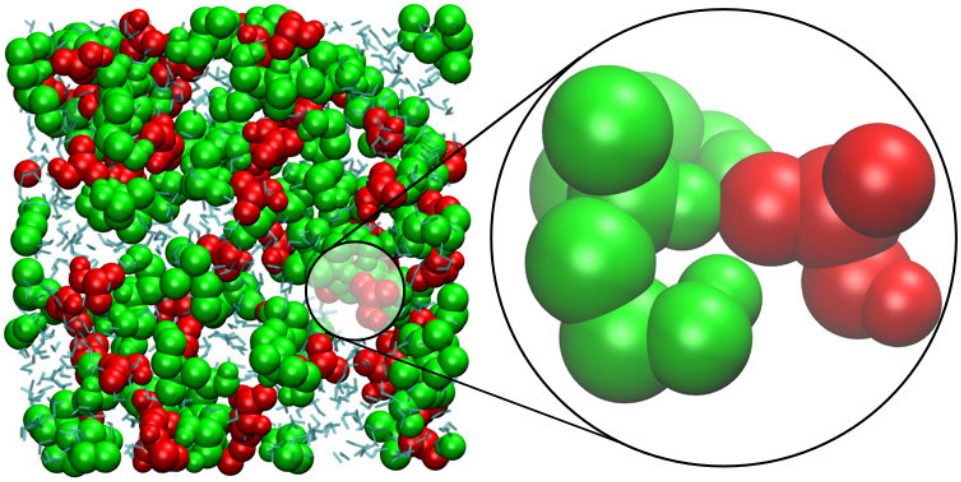

Figure 5.5: Left: Sample system configuration at 100% protonation for reactive CO_2 absorption in MDEA - H_2O solution. Electrolytes are indicated with red for HCO_3^- and green for $MDEAH^+$. Right: Ion pair formation between HCO_3^- and $MDEAH^+$ showing organic ammonium and alcohol hydrogen atoms coordinating with the bicarbonate ion. The right panel is rotated to give a better view of the MDEA-HCO_3^- interaction.

was performed prior to free energy perturbation simulations. Analysis of the system total energy fluctuations using the approach of Chodera [142] indicated convergence of the system to equilibrium conditions within 20 ns for each of the three protonation states considered, as shown in appendix D.

5.5.3 Simulation Results

The resulting solvation free energy changes for H_2O, CO_2, and the pseudo-reaction shown in equation 5.31 are listed in table 5.4. Additionally, the solvation free energy of CH_4 was considered in this system in order to investigate the effect of electrolyte concentration on Henry's law solubility for volatile gases. Aqueous MDEA solutions are known to have a positive salting-in ratio for methane solubility [471], a behaviour which can be accurately captured by molecular simulation as shown in previous work [46]. Solvation free energy for CH_4 was obtained using the same simulation protocol as for the remaining species, except only dispersion interactions are coupled as the TraPPE-UA model for alkanes contains no atomic partial charges [208].

The free energy of solvation for CH_4 and CO_2 together with MDEA molar densities in table 5.4 allows calculation of Henry's law constants for molecular gas solubility in these mixed solvent systems. While Henry's law constant is normally expressed on molarity or mole fraction basis, in aqueous MDEA systems absorption is often quoted in moles per mole amine. Hence, a modified form of Henry's law constant is used, expressed as

$$K_{\mathrm{H}} = \frac{1}{\rho_{\mathrm{MDEA}} RT} \exp\left[\frac{\Delta_{\mathrm{solv}} G_i}{RT}\right] \tag{5.33}$$

where both ρ_{MDEA} and $\Delta_{\mathrm{solv}} G_i$ are functions of total (reactive) CO_2 absorption. The resulting Henry's law constants are shown in figure 5.6. For CO_2, there is no significant variation in Henry's law constant for this system. This is as expected based on the similar values of $\Delta_{\mathrm{solv}} G_{\mathrm{CO_2}}$ across the three protonation states, but

System	H_2O	CO_2	CH_4	MDEA*
		$\Delta_{\mathrm{solv}}G$ / kJ mol^{-1}		
H_2O	-27.3 ± 0.1	4.0 ± 0.2	11.6 ± 0.1	-567 ± 1
0% $MDEAH^+$	-26.5 ± 0.1	3.3 ± 0.1	10.5 ± 0.1	-564 ± 2
50% $MDEAH^+$	-26.1 ± 0.1	3.4 ± 0.1	11.4 ± 0.2	-604 ± 5
100% $MDEAH^+$	-26.3 ± 0.1	3.8 ± 0.1	12.3 ± 0.1	-593 ± 9
		ρ_i / mol m^{-3}		
0% $MDEAH^+$	38710 ± 50	0	0	2528.9 ± 0.2
50% $MDEAH^+$	36750 ± 50	0	0	2402.1 ± 0.1
100% $MDEAH^+$	34970 ± 40	0	0	2284.7 ± 0.1

Table 5.4: Solvation free energy $\Delta_{\mathrm{solv}}G$ and species number densities ρ_i in neat solvent (H_2O) and 0.5 weight fraction methyldiethanolamine (MDEA) solution (solvent basis) at MDEA protonation states 0% $MDEAH^+$, 50% $MDEAH^+$, and 100% $MDEAH^+$. Values obtained by molecular simulation at 353 K and 100 kPa with TraPPE-UA and TIP4P/2005 models as described in the text. A corresponding amount of bicarbonate is added to the 50% $MDEAH^+$ and 100% $MDEAH^+$ protonation systems, representing reactive CO_2 absorption. *: The MDEA excess chemical potential represent simultaneous transformation of MDEA to $MDEAH^+$ and insertion of HCO_3^- to retain system charge neutrality. MDEA number density is the total number density of MDEA and $MDEAH^+$ species.

somewhat at odds with the experimental results of Bishnoi and Rochelle [523] indicating moderate salting-out behaviour for the physical absorption of CO_2 in aqueous MDEA solutions.

For CH_4, there is an approximately 40% reduction in solubility with increasing electrolyte concentration, from 3.8 ± 0.3 mol/mol$_{\mathrm{MDEA}}$/MPa to 2.3 ± 0.2 mol/mol$_{\mathrm{MDEA}}$/MPa with the values obtained for high Ω systems in good agreement with the experimental data from Addicks et al. [515]. The reduction in CH_4 solubility reflects the contraction of the solution due to rising electrolyte concentration, similar to the increase in solvent activity coefficients seen in chapter 4. The good agreement for CH_4 solubility gives confidence in the simulation approach for prediction of physical CO_2 solubility, where experimental data are not available.

Using the free energy of solvation for CO_2, H_2O, and the pseudo-reaction for CO_2 absorption by MDEA, reactive absorption of CO_2 in aqueous MDEA was calculated by solving the equation system defined by equation 5.11 for each of reactions 5.4, 5.7, and 5.30. Activities were calculated using equation 5.18 based on free energies of solvation for CO_2 and H_2O, while the combined activity coefficient for reaction 5.30 is calculated based on $\Delta_{\mathrm{solv}}G$ values for all species involved in the reaction. Additionally, reactive CO_2 absorption was calculated based on the dilute solution approximation in equation 5.12 in combination with Henry's law constant for CO_2 from molecular simulation to assess the impact of simulation-corrected activities on reactive absorption.

The predicted absorption isotherm for CO_2 is shown in figure 5.7, together with experimental values reported by Addicks et al. [515], Shen and Li [508], and Mathonat et al. [510]. Predicted absorption based on simulated values for physical solubility combined with reaction equilibrium calculated based on infinite dilution equilibrium constants is shown by the dotted line, with a mean absolute deviation of 115%. Predicted absorption based on simulated values for physical solubility and reaction equilibrium corrected for species activities (calculated from table 5.4) is shown by the solid line, with a mean average deviation of 60%. Agreement in the

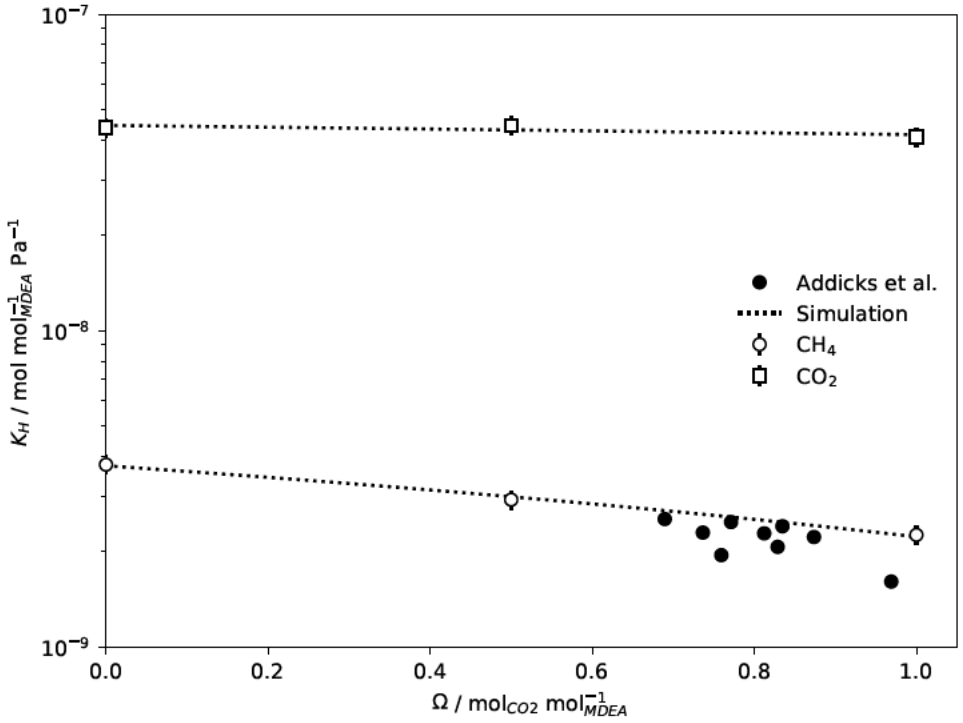

Figure 5.6: Henry's law constant K_H for CH_4 and molecular CO_2 solubility as a function of total CO_2 absorption Ω in 0.3 amine weight fraction H_2O - MDEA solution at 353 K. Open symbols indicate prediction from molecular simulation. Dotted lines indicate linear interpolation of $\Delta_{\text{solv}}G$ and ρ_{MDEA} from simulation data. Experimental values for CH_4 from Addicks et al. [515] are calculated from quaternary H_2O - MDEA - CO_2 - CH_4 vapour-liquid equilibrium data in the pressure range 100 bar - 200 bar.

low-loading regime is worse than the high-loading regime, although with only one experimental source there is limited confidence in this region. While the simulation corrected reactive solubility shows improvement over the dilute solution approximation, agreement with experiment could likely be improved further by additional refinement of the molecular models and simulation methodology. In particular, the numerical uncertainty in $\Delta_{\text{solv}}G$ for MDEA* in dilute solution (right column of table 5.4) produces a corresponding uncertainty in the prediction of initial p_{CO_2} absorption of approximately 40%. This is comparable to the difference between dilute solution approximation and simulation-corrected approach.

For comparison purposes, the reaction-implicit SAFT model from section 5.3.4 is shown in figure 5.7 as a dashed line. While mean absolute deviation at 123% is similar to the dilute solution approximation, absorption at high CO_2 partial pressures deviates significantly from the experimental trend. This reflects the molecular solubility of CO_2 being underestimated by PC-SAFT for $\Omega > 1$, contrary to molecular simulation which correctly describes the physical absorption regime.

5.6 Summary

This chapter has detailed the chemical reactions governing CO_2 absorption in aqueous amine solutions, and established molecular modelling approaches for representing reactive absorption in these systems. The reaction

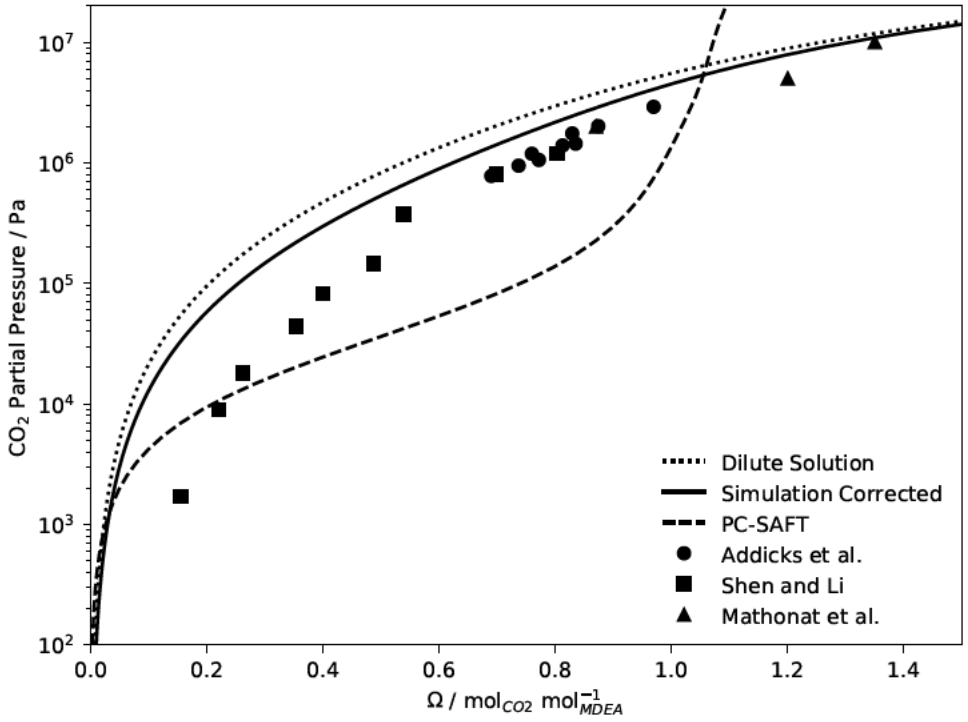

Figure 5.7: Partial pressure of CO_2 as a function of total CO_2 absorption Ω in 0.3 amine weight fraction H_2O - MDEA solution at 353 K. Solid symbols indicate experimental values from Addicks et al. [515], Shen and Li [508], and Mathonat et al. [510]. Dotted line indicates absorption calculated using physical solubility from molecular simulation, combined with a dilute solution assumption for reaction thermodynamics. Solid line indicates absorption calculated using physical solubility from molecular simulation, combined with activity-corrected reaction thermodynamics from molecular simulation. Dashed line indicates prediction by the PC-SAFT model using molecular parameters reported in table 5.1. Molecular simulation is seen to reasonably capture the high-pressure regime, indicating good agreement for physical solubility at high electrolyte concentration, but under-predict loading at low partial pressures. The PC-SAFT model exhibits step-like behaviour with rapid loading near 10^4 Pa indicating saturation of the SAFT association sites beyond this pressure. Physical solubility is poorly predicted by the PC-SAFT model, with little additional loading observed beyond 10^6 Pa.

mechanisms underlying CO_2 absorption were reviewed in section 5.2, and comprise the generation of carbonic acid and subsequent acid-base equilibrium reactions with amine species. Depending on the chemistry of the amine, CO_2 may also attach covalently to the amine group forming carbamate species. These processes drive CO_2 absorption in typical aqueous amine solutions and is likewise expected to be the main driver for CO_2 absorption in facilitated transport membranes.

In section 5.3 a thermodynamic framework was introduced for reactions, connecting reaction free energy to equilibrium composition. This in turn allowed system compositions to be calculated in mixed systems from knowledge of equilibrium constants in dilute aqueous solution together with a description of solution activity as a function of composition. The often used Kent-Eisenberg and Deshmukh-Mather models of CO_2 absorption in aqueous amines were considered together with reaction-explicit SAFT models, each with different approaches to estimating species activities. Finally, a reaction-implicit SAFT model was found to give equivalent performance to reaction-explicit models for systems where absorption is well approximated as a one-step reaction.

Molecular simulation has seen limited application in the study of reactive systems, due to the difficulty in representing reactions using classical interaction potentials. Section 5.4 detailed contemporary approaches to molecular simulation of reactive systems: reaction ensemble Monte Carlo, reaction ensemble molecular dynamics, and the ReaxFF potential family. In this work, an approach similar to reaction ensemble molecular dynamics was developed, using equation 5.18 to calculate species activities from molecular simulation and equation 5.11 to combine these with experimental reaction free energies to predict system compositions.

Using the molecular models developed in chapters 3 and 4, aqueous amine solutions with varying degrees of CO_2 loading may be studied by molecular simulation. In section 5.5, these models were used to simulate aqueous MDEA solutions at varying degrees of CO_2 loading in the form of bicarbonate-ammonium pairs. Aqueous MDEA is a well understood absorption system for CO_2, with a similar chemical environment to facilitated transport membranes. Activities from molecular simulation were in turn used to predict reactive CO_2 absorption in the MDEA - H_2O system as shown in figure 5.5.

The simulation approach developed in this chapter offers a new route to estimating chemical absorption of acid gases, as well as a new framework for combining experimental equilibrium constants with molecular simulation. This approach allows prediction of system compositions for complex reactive systems, provided accurate interaction potentials are available for each species, and equilibrium constants are available at some reference state. In chapter 6, the molecular models developed in chapters 3 and 4 are combined with the reaction-implicit PC-SAFT description from section 5.3.4, in order to predict the behaviour of a model facilitated transport membrane under varying process conditions.

Chapter 6

Application to Facilitated Transport Membranes

6.1 Overview

In the preceding chapters, molecular models were developed for each of the molecular ingredients found in facilitated transport membranes. Chapter 3 developed parameters for simulation of polyamines and an equation of state model for PVAm. Chapter 4 developed models for simulation of alkylammonium and bicarbonate species. Chapter 5 evaluated approaches to reactive CO_2 absorption using both simulation and a PC-SAFT model. This chapter brings these molecular models together to study condensed-phase properties and vapour-liquid equilibrium for facilitated transport membranes.

An overview of the models brought from each chapter is given in section 6.2, together with the description of a model system comprising short PVAm oligomers at 50% protonation with bicarbonate balancing ions. Using both molecular simulation and the PC-SAFT model, liquid densities are predicted for the partially protonated PVAm - H_2O - HCO_3^- system in section 6.3. Further, a qualitative view of the simulation system is presented, and a simple stepping mechanism is proposed to explain the transport of HCO_3^- in facilitated transport membranes.

In section 6.4, the PC-SAFT model is used to calculate solubility for CO_2 and N_2 in a quaternary PVAm - H_2O - CO_2 - N_2 system under post-combustion conditions. Trends with temperature and water activity are discussed for both solubility and solubility-selectivity. Finally, section 6.5 extends the solubility predictions to membrane permeability, using the solution-diffusion assumption and the simple Mackie-Meares model for extrapolating diffusion constants from experimentally obtained values in aqueous solution. Comparison is made with separation performance in real facilitated transport membranes and the Robeson upper bound from chapter 1.

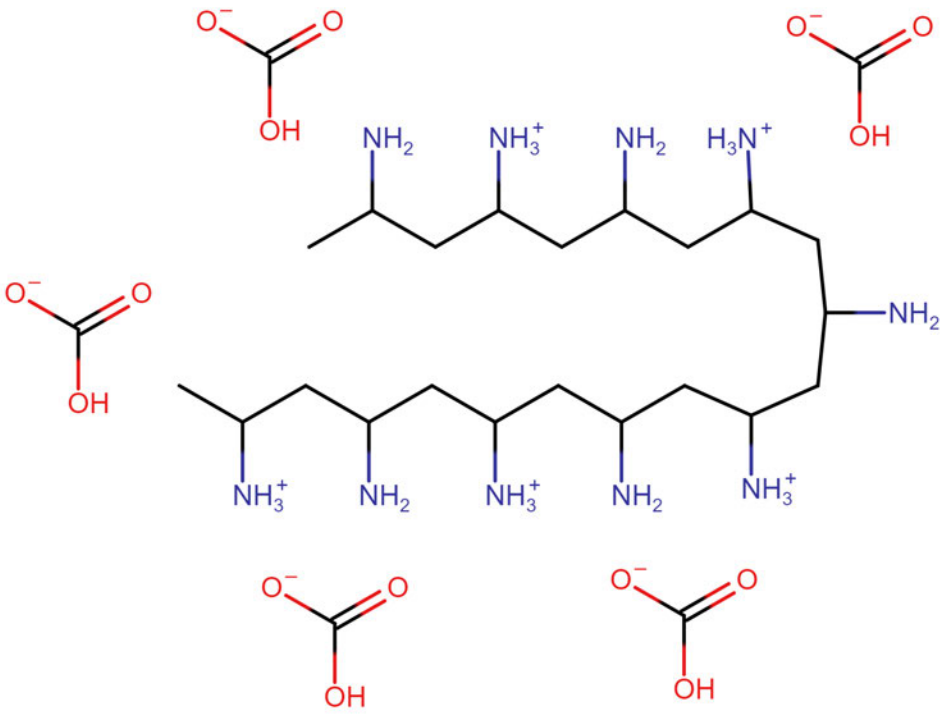

Figure 6.1: Short-chain PVAm with bicarbonate counter-ions used as a model systems to represent facilitated transport membranes. The polyamine backbone is represented using model parameters from chapter 3, while electrolytes are represented using model parameters from chapter 4. Water is represented by the TIP4P/2005 model [128] (not shown).

6.2 Consolidated Model Description

The representation of facilitated transport membranes by molecular models in this work relies on the general principle of group-contribution between similar chemical compounds, and the transferability of molecular models between systems of different compositions and temperatures. The composition of facilitated transport membranes varies depending on exposure to H_2O and CO_2, from the dry polymer studied in section 3.4, to hydrated polymer solution seen in section 3.5, to alkylammonium-bicarbonate electrolyte solutions characterised in sections 4.8 and 4.9. As argued in preceding chapters, molecular simulation and equation of state models play complementary roles in the representation of facilitated transport membranes.

For molecular simulation, the PVAm model presented in section 3 is employed as a base structure. For the real system, the degree of protonation for the amine group will vary depending on temperature, water content, and CO_2 partial pressure. For efficient operation of facilitated transport membranes, a partially protonated state is expected hence a polymer protonation of 50% is chosen here. Every second amine group is protonated and an equivalent density of bicarbonate added to the system, corresponding to a CO_2 loading of $\Omega \approx 0.5$. Based on comparison with aqueous amine systems (e.g. figure 5.7), this degree of CO_2 loading is representative for CO_2 partial pressures near 20 kPa, corresponding to a flue gas stream at near atmospheric pressure. A shorter 10-mer chain is used to decrease correlation times in the strongly associating electrolyte systems, with the resulting oligomer and bicarbonate unit illustrated in figure 6.1.

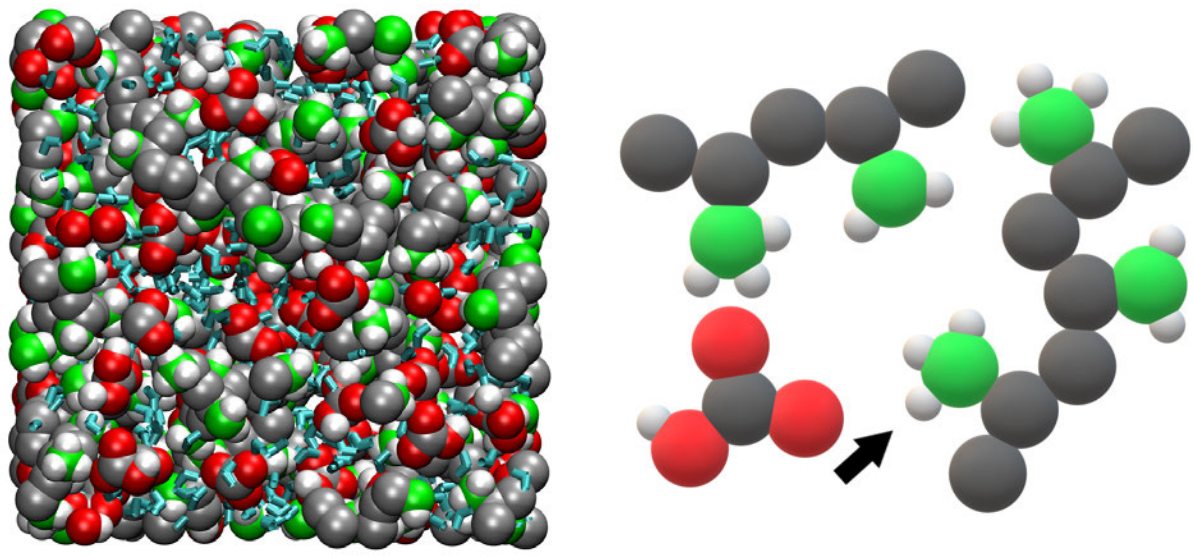

Figure 6.2: Simulation model of the PVAm - H_2O - HCO_3^- system at 0.5 water weight fraction and 50% amine protonation. Left panel: snapshot from molecular simulation at 298 K. The polymer appears fully soluble, with bicarbonate dispersed throughout the liquid state. Right panel: Proposed transport mechanism for bicarbonate ions. Charge-carrying oxygen atoms are seen to coordinate with one or two ammonium groups, allowing the bicarbonate ion to 'walk' along or between polymer strands.

The molecular model for simulation of partially protonated PVAm is the TraPPE-compatible united-atom representation employed in previous chapters, with parameters developed in chapters 3 and 4. As for small-molecule ammonium compounds, dihedral potentials for ammonium species are taken to be the same as equivalent amine dihedral potentials. Nitrogen dispersion interactions are those of primary ammonium, reported in table 4.3. Bicarbonate molecular parameters are those developed in section 4.9 for use together with the united-atom ammonium model. Water is represented by TIP4P/2005 [128] as in previous chapters. The condensed-phase PVAm - H_2O - HCO_3^- system is illustrated in figure 6.2.

For equation of state representation with PC-SAFT, the molecular parameters developed for PVAm in sections 3.4.3 and 3.5.3 form the basis of both protonated and unprotonated systems. Reactive CO_2 absorption in aqueous PVAm solution is represented by the reaction-implicit description from section 5.3.4, using association parameters from table 5.1 with the assumption that CO_2 reactivity is similar for the polyamine solution as in aqueous amine solvent mixtures. The parameters used for simulation of PVAm - H_2O - CO_2 - N_2 systems are summarised in table 6.1. As no vapour-liquid absorption data are available for the PVAm - H_2O - CO_2 system these parameters cannot be validated, but rather represent an informed assumption based on the chemical composition of PVAm.

6.3 Prediction of ρpT Behaviour

The liquid density of partially protonated PVAm solution is an important indicator of model performance, reflecting the total cohesive energy of the system. To evaluate liquid densities of PVAm solution under exposure

i	m	σ / Å	ϵ / k_B^{-1}K	Association	ϵ_{AB} / k_B^{-1}K	κ_{AB}	ϵ_{CD} / k_B^{-1}K	κ_{CD}	Source
PVAm	2.4309	2.8427	285.33	C	1491.60	0.29836	4031.93	0.29334	This work
H_2O	2.1945	2.2290	141.66	AABB	1804.04	0.20390	-	-	[127]
CO_2	2.6037	3.7039	151.04	D	-	-	4031.93	0.29334	[51], *
N_2	1.2053	3.3130	90.96	-	-	-	-	-	[51]

Table 6.1: Molecular parameters for PVAm, H_2O, CO_2, and N_2 for the PC-SAFT equation of state with reaction-implicit CO_2 absorption. Parameters for PVAm developed in chapter 3 with CD association parameters from chapter 5. H_2O parameters from Diamantonis and Economou [127]. CO_2 and N_2 parameters from Gross and Sadowski [51] with added CD association for CO_2 from chapter 5. The binary interaction parameter for PVAm-H_2O is -0.1336.

to CO_2, model systems were constructed using both a molecular simulation and PC-SAFT approach. A PVAm solution with 0.5 water weight fraction on CO_2-free basis was chosen for comparison, reflecting the high-end of water absorption seen for PVA/PVAm hybrid membrane reported by Deng et al. [30] and corresponding to relative humidity in the range 80% - 90% based on experimental data.

For molecular simulation, a system of partially protonated PVAm was constructed using PVAm oligomers with bicarbonate as balancing ions, as shown in figure 6.1. A system size of approximately 3.2 nm was used, corresponding to 21 PVAm oligomers, 105 bicarbonate molecules, and 535 water molecules. A snapshot of the simulation system is shown in the left panel of figure 6.2. As for the polymer-water systems in chapter 3, the replica-exchange method was used to accelerate sampling the isothermal-isobaric ensemble, employing a ladder of 8 temperatures geometrically spaced across the interval 298 K - 373 K and a simulation time of 40 ns with the initial 20 ns discarded as system equilibration. The resulting liquid densities are shown in figure 6.3. A comprehensive list of parameters for simulation in the isothermal-isobaric ensemble is given in appendix A.

Together with evaluation of thermodynamic properties, molecular simulation also allows observation of kinetic properties such as the molecular mechanisms of transport. As outlined in chapter 1, diffusion of CO_2 reaction products in facilitated transport membranes is central to the facilitation effect, and diffusion processes have been investigated by other authors [45]. However, it is worthwhile to consider the transport processes for the new ion models developed in chapter 4. Through observation of HCO_3^- dynamic behaviour in the hydrated PVAm systems, a combination of single and double hydrogen bonding interactions between bicarbonate and the ammonium groups can be identified. While HCO_3^- always remains closely associated with at least one ammonium group, it is nonetheless able to translocate between chains, 'walking' from one ammonium group to the next. This mechanism is illustrated schematically in the right panel of figure 6.2, and supports the site-hopping transport mechanism proposed by Cussler et al. [524].

Liquid density in the PVAm - H_2O - CO_2 system was also predicted using the PC-SAFT model developed in chapters 3 and 5. To ensure the representation of CO_2 absorption in hydrated PVAm using PC-SAFT remained consistent with the molecular system, PVAm, water, and CO_2 weight fractions were fixed at 0.4, 0.4, and 0.2, respectively. The degree of association for CO_2 was calculated using equation 2.50, as required for the reaction-implicit SAFT description of absorption. Liquid densities for this system were calculated across

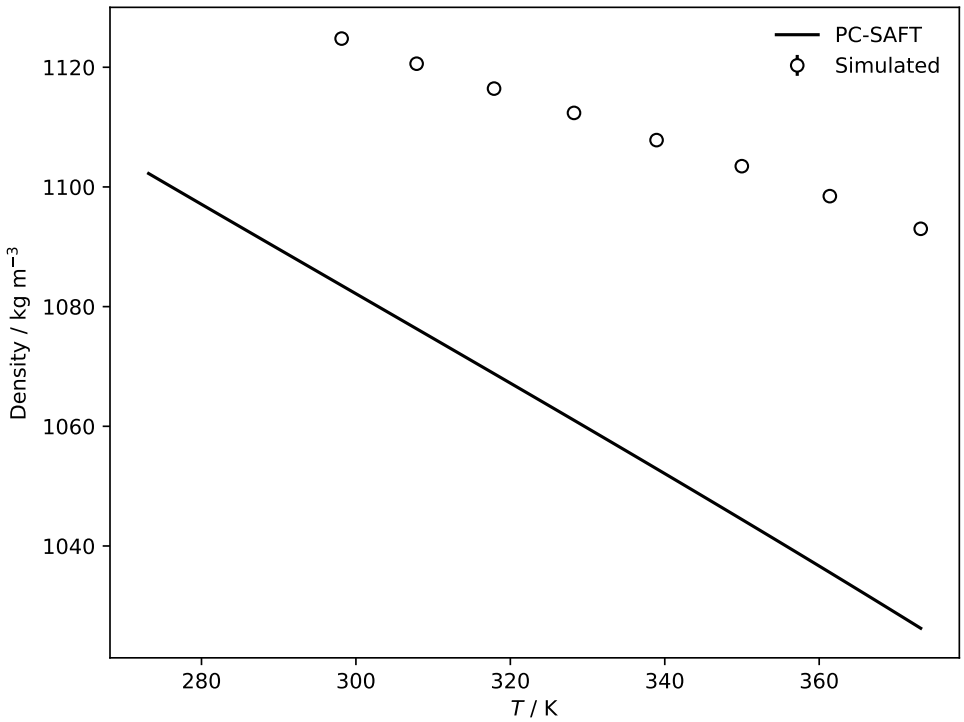

Figure 6.3: Prediction of liquid density as a function of temperature for aqueous PVAm solution with 0.5 water weight fraction (CO_2-free basis) and 50% amine protonation. Open symbols indicate simulated values. Solid line indicates PC-SAFT model. Mean average deviation between the two models is 4.8% across the temperature interval 298 K - 373 K.

the temperature range 298 K - 373 K, with resulting liquid densities shown in figure 6.3. The PC-SAFT model predicts a somewhat lower liquid density compared to the molecular model, with a mean average deviation of 4.8% over the temperature range considered. This likely reflects the absence of electrolyte species with a loss of the corresponding electrostatic interactions, reducing cohesive interactions in the reaction-implicit SAFT model.

6.4 Prediction Physical and Reactive Gas Solubility

While ρpT properties are a useful check of overall system behaviour, they do not inform the use of facilitated transport membranes for separation applications. The consolidated PC-SAFT model also permits estimation of physical and reactive gas solubility, which is more closely associated with process performance through the solution-diffusion model (equation 1.1). Here, we consider the PVAm - H_2O - CO_2 - N_2 ternary vapour-liquid system, comprising the key species found in post-combustion conditions. The physical conditions considered can be varied arbitrarily, such that the impact of e.g. temperature or water content can be investigated. In figure 6.4, we consider a flue gas with CO_2 and N_2 molar fractions of 0.2 and 0.8 respectively on dry basis, and a variable water activity. Temperature is varied over the temperature range 313 K - 373 K while pressure is maintained at 1 atmosphere, reflecting typical post-combustion separation conditions.

The predictions for gas solubility observed in figure 6.4 show clear trends with temperature and water

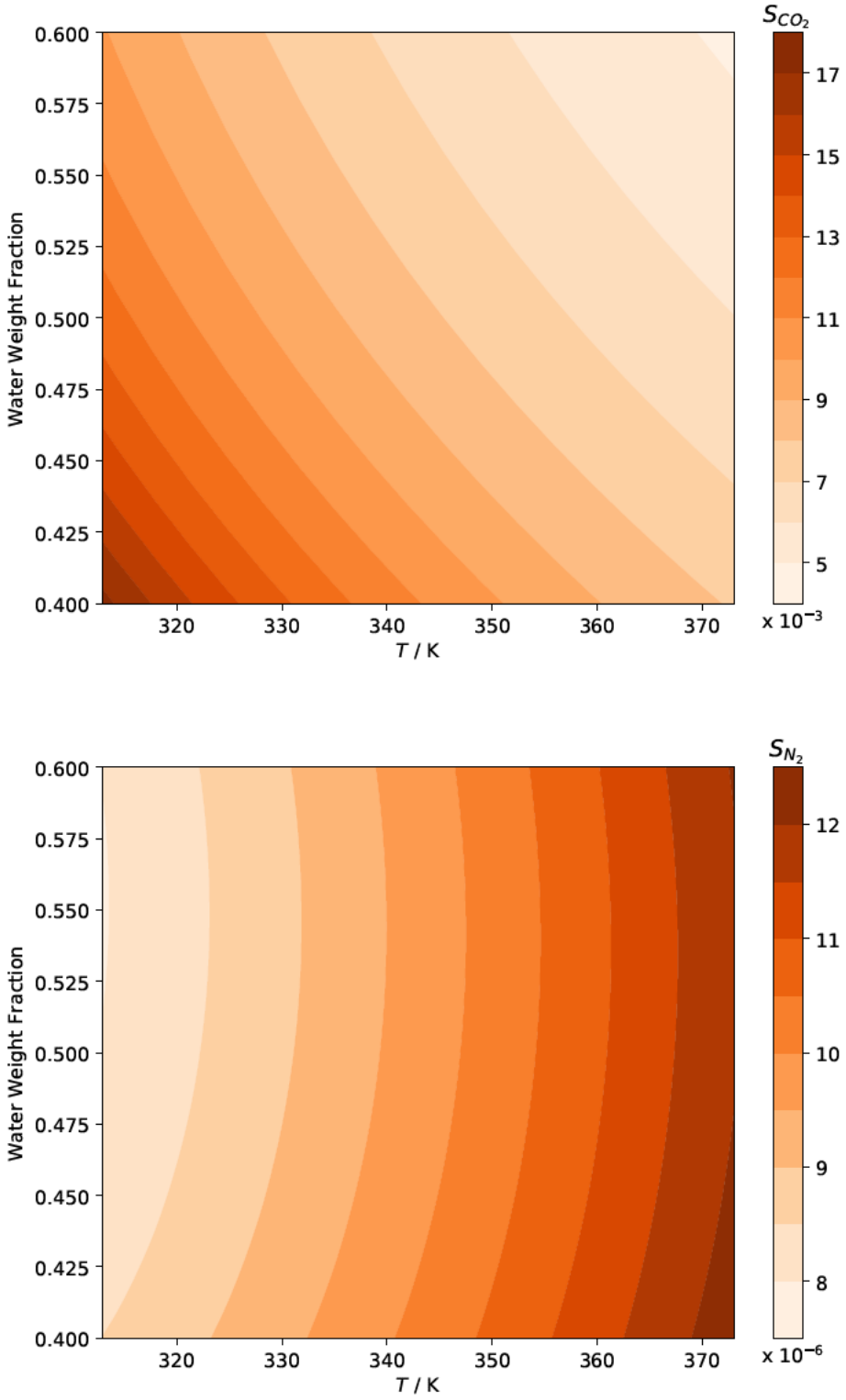

Figure 6.4: Gas solubility in hydrated PVAm calculated using the PC-SAFT equation of state as a function of temperature and water content. Solubility in units of mol m^{-3} Pa^{-1}. Top panel: CO_2 solubility S_{CO_2}, showing increasing solubility at low temperatures and water content. Bottom panel: N_2 solubility S_{N_2}, showing increasing solubility with increasing temperatures.

content for both CO_2 and N_2. The two gases display opposite behaviour with variations in temperature. CO_2 becomes progressively less soluble with increasing temperature, primarily due to the large heat of absorption for CO_2 in amine solvent [525]. Conversely, the solubility of N_2 increases with temperature, consistent with the increasing solubility observed in hydrocarbons and water at elevated temperatures [526]. The small dependence on composition for N_2 also indicates that while relative humidity is an important parameter for CO_2 solubility, it plays a limited role for non-reactive gases. CO_2 solubility shows the largest variation under the conditions considered, from $18 \times 10^{-3}\,\mathrm{mol\,m^{-3}\,Pa^{-1}}$ at 313 K and 0.4 water weight fraction to $4 \times 10^{-3}\,\mathrm{mol\,m^{-3}\,Pa^{-1}}$ at 373 K and 0.6 water weight fraction. CO_2 being more soluble in amine-rich systems conforms to the expectation for aqueous amine solutions.

Using the solubility data in figure 6.4 together with water activities at each composition, the solubility-selectivity between the two gases may be calculated at each system composition. In figure 6.5, solubility-selectivity for the CO_2 / N_2 pair is shown for water activities in the range 80% - 90%, within the experimental range considered by Deng et al. [35]. As evident from figure 6.4, there is a considerable solubility-selectivity factor in favor of CO_2 under all conditions. However, solubility-selectivity is especially pronounced for low-temperature, low-humidity systems, where values in excess of 10^3 can be obtained. This is driven by the strong absorption of CO_2 at low temperatures and high amine content.

6.5 Trends for Gas Separation Applications

The solubility predictions from figures 6.4 and 6.5 provide a connection between process conditions and gas absorption in facilitated transport membranes. The high solubility-selectivity of the model is seemingly in line with the difference in permeability observed in experiment. However, the two are not directly comparable due to the influence of diffusivity as part of the solution-diffusion model in equation 1.1. The PC-SAFT model developed here does not make predictions of kinetic properties. As such, further assumptions are needed for evaluating permeability and process performance.

As outlined by Sarkisov and Fayon [45], diffusion constants in facilitated transport membranes are not easily obtained from simulation methods due to the multiple length scales involved in transport processes and overall slow system dynamics. However, diffusion rates appear to be linked to water dynamics, with diffusion constants in certain cases following the Mackie-Meares model [177, 178] as discussed in section 3.3. In order to provide a speculative view of permeability under varying process conditions, this model is adopted here, together with the experimental aqueous diffusion constants of Cadogan et al. [527]. The resulting predictions for CO_2 and N_2 permeability in hydrated PVAm are shown in figure 6.7.

As a word of caution, we note that the predicted permeability for CO_2 is likely significantly overestimated due to the use of diffusivity values from Cadogan et al. [527] together with the assumptions of the Mackie-Meares model. The ion-ion interactions observed in molecular simulation are likely to significantly retard the

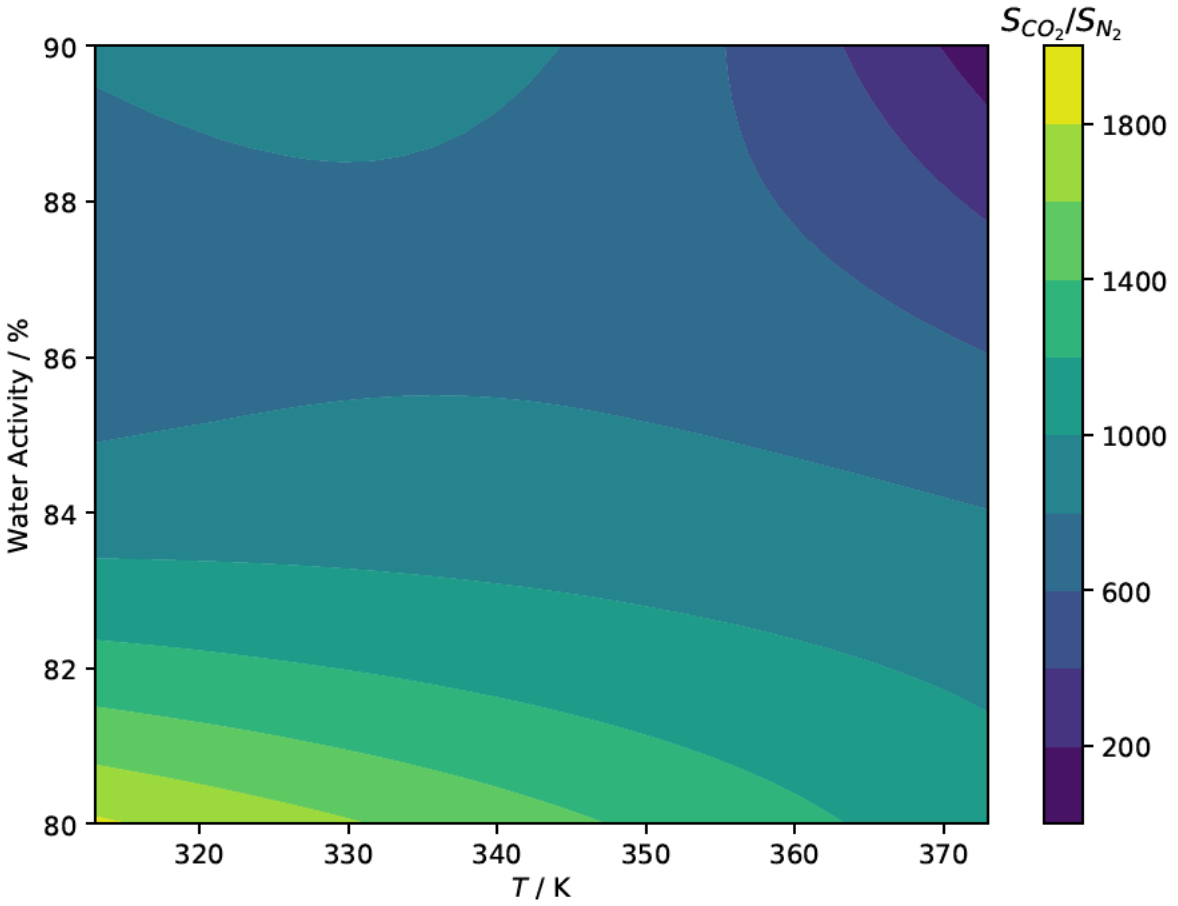

Figure 6.5: Solubility-selectivity for CO_2 and N_2 absorption in hydrated PVAm calculated using the PC-SAFT equation of state as a function of temperature and water activity. Selectivity is highest at low temperatures and humidity due to increased density of amine groups. Selectivity decreases for high-temperature, high-humidity systems.

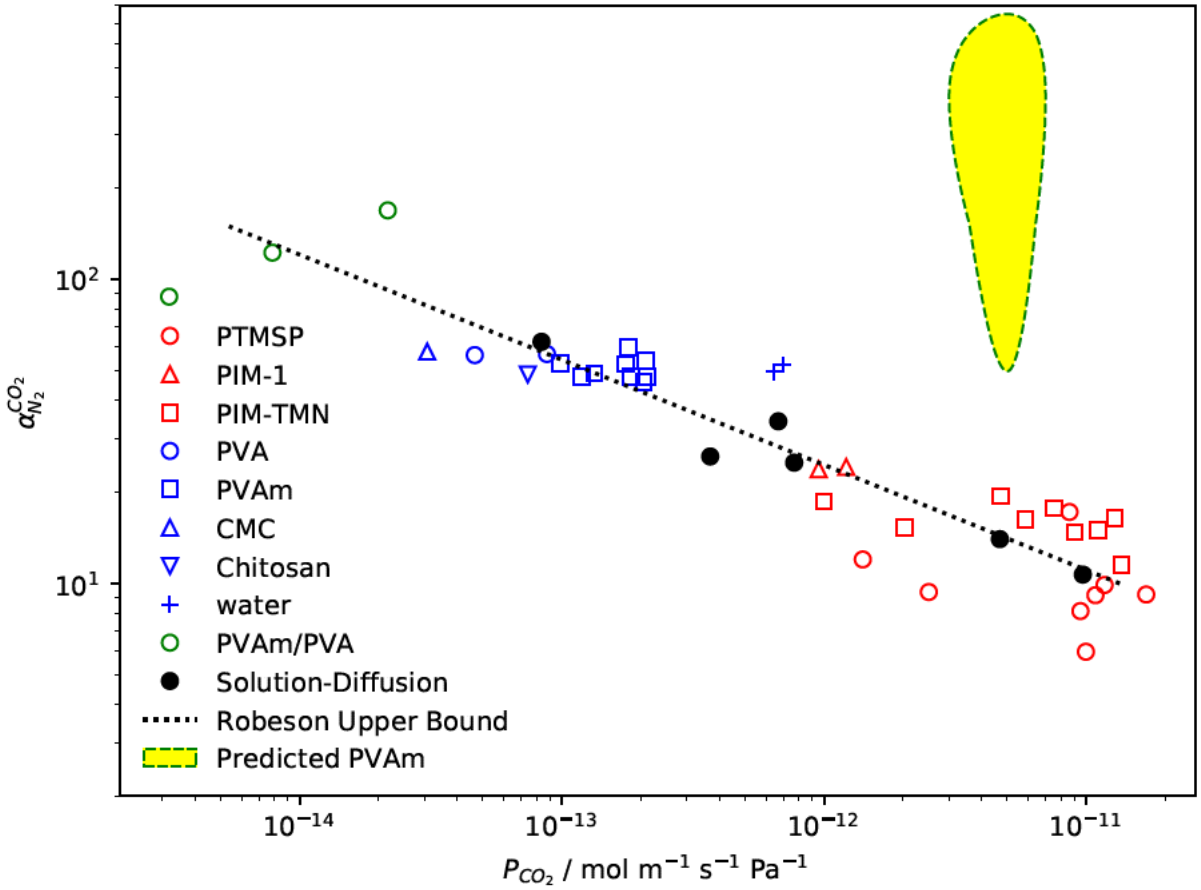

Figure 6.6: Permeability and selectivity for CO_2 / N_2 separation membranes with prediction from molecular model. Black filled circles show conventional solution-diffusion membranes, red open symbols indicate high-porosity materials, blue open symbols show hydrogel membranes, and green open symbols show facilitated transport membranes, as detailed in figure 1.2. The yellow shaded area with green dashed border indicates predicted performance of PVAm based on the molecular model developed in this work, as detailed in the text.

transport of CO_2 reaction products through the membrane, due to association of bicarbonate with relatively immobile organic ammonium. Nonetheless, the predicted permeabilities are of the same magnitude as the high-permeability membranes seen in figure 1.2 for the Robeson upper bound, and a lowering of permeability by 1-2 orders of magnitude would bring model predictions within the same range as seen experimentally for facilitated transport membranes.

Similar to solubility-selectivity, the predicted values for permeability of CO_2 and N_2 allow calculation of selectivity between the two gases under varying process conditions. However, unlike solubility-selectivity these values are comparable against experimentally observed selectivity in facilitated transport membranes. The resulting values are shown in figure 6.8 as a function of temperature and water activity, and display a similar trend as for solubility-selectivity: Under high-temperature, high-water content conditions the membrane begins to lose selectivity, while low-water content systems show high selectivity due to increased CO_2 absorption. Low-temperature, high-water content systems also show high selectivity due to the combination of CO_2 absorption and favourable kinetics; however, this may well be an artifact of using aqueous diffusion constants and extrapolation with the Mackie-Meares model and is unlikely to be observed experimentally.

The observed selectivites range from a factor of 10^2 to over 10^3, with most systems showing a selectivity of 10^3 and above. As shown in figure 1.2, experimentally observed values for selectivity are near 10^2. As for permeability, a reduction in CO_2 diffusivity of 1-2 orders of magnitude would bring the model prediction within the experimentally reported range for facilitated transport membranes, with the discrepancy likely caused by the overly simplistic treatment of kinetic properties.

6.6 Summary

In this chapter, the molecular models developed in chapters 3, 4, and 5 were combined to produce a predictive model for a hydrated PVAm. As a test case, a short-chain PVAm system was considered in sections 6.2 and 6.3, comprising oligomers of 10 monomers. The alkylammonium parameters from table 4.3 were used to assign 50% of amine groups as protonated, with the bicarbonate model from tables 4.5 and 4.4 used to counterbalance formal charges. Comparison of liquid densities between molecular simulation and the PC-SAFT equation of state revealed a somewhat large mean absolute deviation of 4.8%, likely owing to poor treatment of electrostatic interactions in the equation of state.

The PC-SAFT model was subsequently used to predict solubility of CO_2 and N_2 in the ternary PVAm - H_2O - CO_2 - N_2 system. Solubility was found to differ by a factor of approximately 10^3, with CO_2 and N_2 showing differing dependencies on temperature and water content as illustrated in figure 6.4. Further, the simplified Mackie-Meares model [177, 178] from section 3.3 was used to offer a speculative prediction of permeability, shown in figure 6.7. Both permeability and selectivity of CO_2 were significantly overestimated, likely owing to an overly simplistic treatment of system kinetics. Nonetheless, the model provides predictions

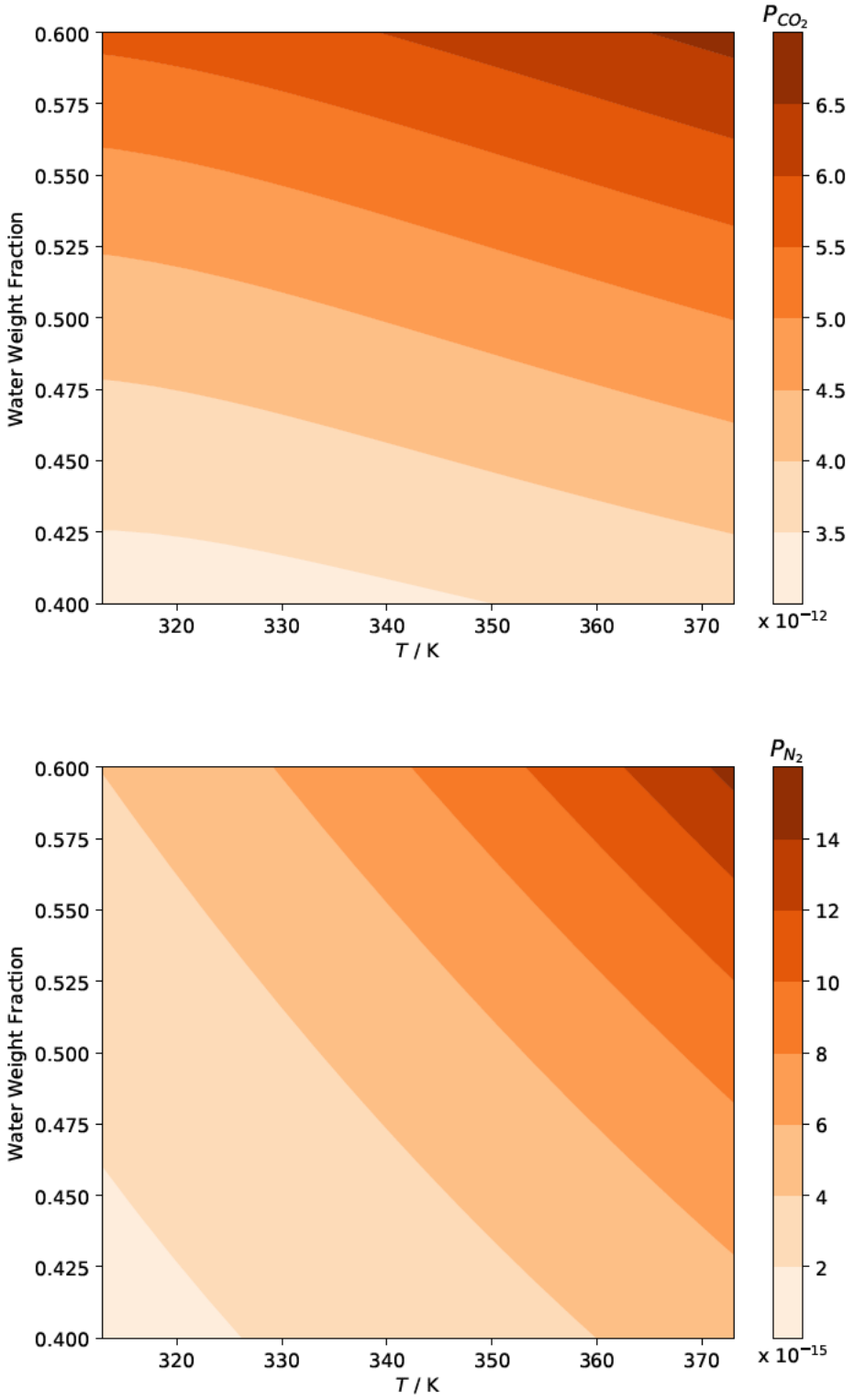

Figure 6.7: Gas permeability in hydrated PVAm calculated using the PC-SAFT equation of state and Mackie-Meares diffusion model [177, 178], as a function of temperature and water content. Permeability in units of $\mathrm{mol\,m^{-1}\,s^{-1}\,Pa^{-1}}$. Top panel: CO_2 permeability $P_{\mathrm{CO_2}}$. Bottom panel: N_2 permeability $P_{\mathrm{N_2}}$. Both gases show increasing permeability with increasing temperature and water content.

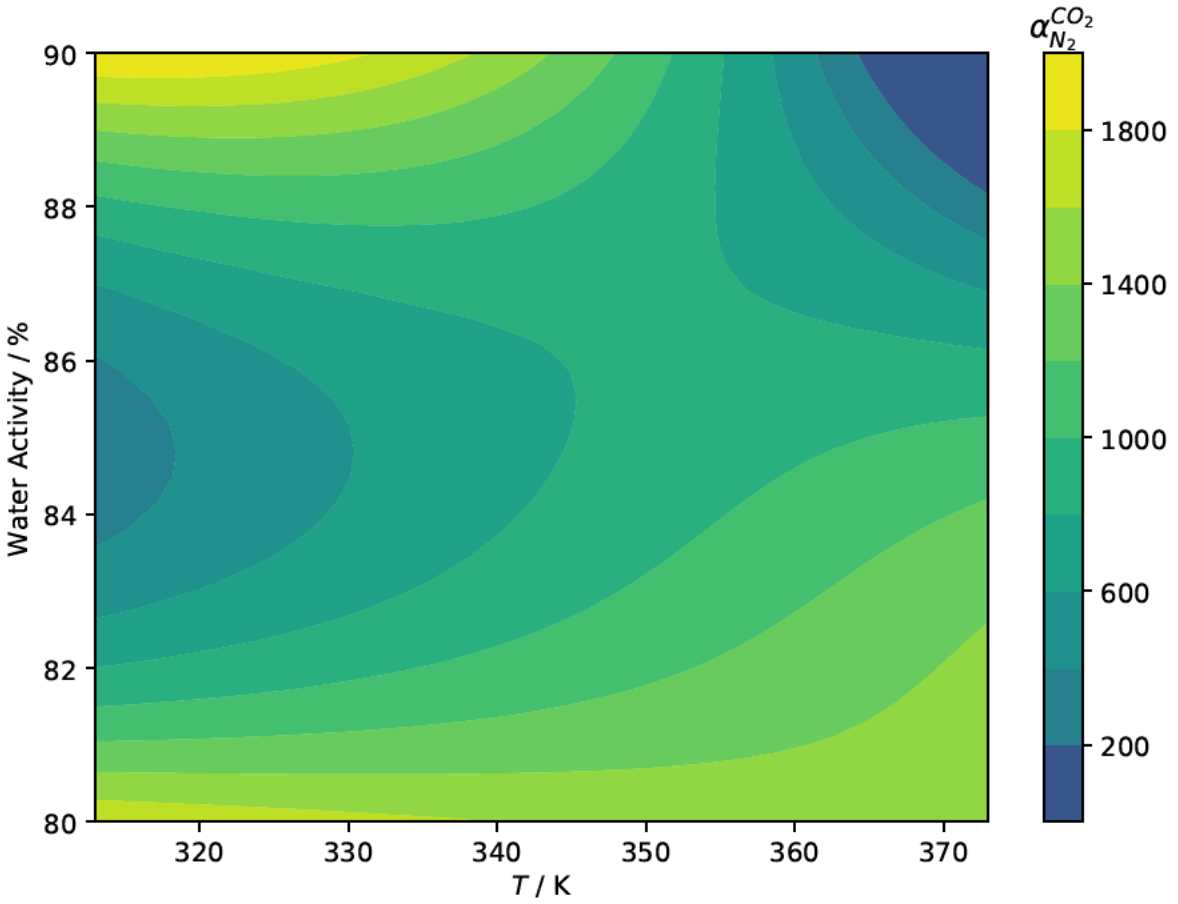

Figure 6.8: Selectivity for CO_2 and N_2 permeability in hydrated PVAm calculated using the PC-SAFT equation of state together with the Mackie-Meares model [177, 178] for diffusion as a function of temperature and water activity. Selectivity decreases for high-temperature, high-humidity systems.

for permeability and selectivity that are near the Robeson upper bound for this system, and offer a view of trends in system performance under varying process conditions.

Chapter 7

Conclusions and Future Work

7.1 Conclusions

This work has detailed the development and application of predictive molecular models to study the process of CO_2 absorption in facilitated transport membranes. By building on model systems for polymer-water, alkylammonium bicarbonate solutions, and reactive solvent mixtures, a predictive model for physical and reactive solubility of CO_2 was established and tested. The model was used to identify the influence of temperature and relative humidity on CO_2 and N_2 absorption, the two gases of primary importance to post-combustion CO_2 capture applications. By providing a quantitative model for the relationship between process conditions and gas solubility, this work has informed future development of facilitated transport membranes and the design of gas separation processes utilising these materials.

Reactive gas solubility and in facilitated transport membranes is a complex process, relying on a balance between polymer-solvent interactions, properties of electrolyte solutions, and reaction thermodynamics. An accurate model for fluid phase properties relies on descriptions of each physical phenomenon and in turn their influence on CO_2 absorption. Hence, this work has been organised according to the physical phenomena encountered in facilitated transport membranes, with the developments in each section contributing to the body of knowledge within the relevant field.

- A hybrid approach for developing equation of state parameters was developed in chapter 3, utilizing molecular simulation to generate ρpT data on which the equation of state model can be trained. The approach was validated on the two well-characterised polymers PEO and PVA, and applied in a predictive manner to PVAm using a united-atom model with additional parameters developed in section 3.3.2.

- The reaction products present in amine-based facilitated transport membranes were identified as alkylammonium and carbonic acid derivatives, and new models were developed for simulation of their aqueous solutions in chapter 4. The thermodynamics of electrolyte solutions were reviewed with the

aim to find a suitable equation of state model for these systems; however, electrolyte extensions to molecular equation of state reported in prior literature were found to offer limited predictive power for aqueous-organic electrolyte solutions.

- A framework for combining empirical reaction constants with molecular simulation data was developed in chapter 5 and employed to study CO_2 absorption in the MDEA - H_2O - CO_2 model system. A variety of thermodynamic frameworks were considered for representing reaction equilibrium within the PC-SAFT equation of state, with a reaction-implicit SAFT model ultimately found to give similar performance to more elaborate schemes.

- The molecular models developed for PVAm, reactive absorption, and the resulting CO_2 reaction products were combined to study reactive absorption in hydrated PVAm as a prototypical facilitated transport membrane. The model predictions allowed for a view of absorption characteristics across different temperatures and hydration levels, informing future experimental work and process optimisation for facilitated transport membranes in commercial applications.

Together, these advancements represent a significant contribution to knowledge in the fields of facilitated transport membranes and molecular modelling of fluid systems. The understanding gained from this work is both directly applicable to facilitated transport membranes, and readily extends to fields such as biophysics and biomolecular simulation, electrochemical systems, and the use of polyelectrolytes as fluid additives. Further, the work on electrolyte models presented here forms part of an ongoing development in the area of molecular simulation to identify the requirements and best practices for representation of electrolytes in fluid systems.

The approaches and models represented in this work reflect a compromise between physical accuracy and model complexity. Any molecular system represented by classical models necessarily loses some of the detail present in the real systems, perhaps most easily recognised by the application of coarse-grained models for polymer in chapter 3 but carrying more gravity for the electrolyte models developed in chapter 4. As discussed in section 4.6.4, there is growing awareness of the deficiencies in conventional electrostatics treatments for molecular simulation, reflecting inherent incongruity between the potential energy and dielectric properties of classical molecular models. Equation of state models for electrolyte solutions face a different range of problems as discussed in section 4.5, but will likely need to overcome the same incongruous behaviour between potential energy and dielectric properties. In this work we recognise the impact of these challenges, but leave it for future researchers to attempt a resolution.

Finally, while the models presented here give predictions for the behaviour of facilitated transport membranes and their gas absorption properties, blind model predictions rarely survive quantitative comparison with real experimental data. Models reflect an incomplete and simplified view of reality, and are created in the hope of capturing behaviour in a way which paints a useful picture of real systems. It is the hope of the author that this work offers such a view, and will prove useful in future explorations of complex fluid systems.

7.2 Future Work

The progress made in this work on molecular modelling approaches as well as the specific molecular models developed in chapters 3, 4, and 5 have immediate relevance to a number of related molecular systems and chemical engineering challenges. Forays into subject areas adjacent to this work have been limited by constraints of time and relevance to the research questions posed in chapter 1, but represent interesting research questions in their own right. A number of possible extensions and applications of this work presented themselves over the course of the research project, the most promising of which are briefly summarised below.

Materials Screening for Reactive CO_2 Absorption

The model parameters developed in this work are readily transferable to generic organic amine compounds, which form the basis for existing chemical CO_2 separation and scrubbing operations. While amine and alkanolamine compounds have been studied extensively by molecular models, their ionic forms have either largely been ignored, or represented by models developed for purposes other than solvent activity calculations. The molecular models presented in chapter 4 allow prediction of fluid properties for solvents at varying states of CO_2 absorption. Further, by developing the reaction approach in chapter 5 to improve numerical convergence, reactive absorption of CO_2 may be predicted in mixed solvent systems based solely on p$K_a$measurements of the amine absorbent.

These advancements together allow for rapid screening of solvents and solvent mixtures of separation applications, allowing performance for CO_2 separation to be reliably predicted. This should in turn be used as input for unit and process simulation, allowing performance optimisation to be vertically integrated from material properties to plant operation. With continued interest in CO_2 absorption technology, molecular simulation promises to be a valuable tool for application-optimized solvents.

Simulation-Driven Polymer Characterisation

The simulation methodology developed in chapter 3 for characterisation of polymer ρpT behaviour may be extended to a wide range of polymers, for which molecular parameters are available or can be developed from small-molecule compounds. This permits rapid prediction of thermodynamics properties as well as development of equation of state parameters for novel polymer compounds, circumventing the need for experimental synthesise and characterisation.

By rapidly evaluating polymers of different chemistry, a virtual screening process can be used to identify polymers with promising thermodynamic properties to be selected for synthesis and experimental characterisation. This process may be applied to facilitated transport membranes, to consider different permutations of amines including alkylations, cross-linking, inclusion of other functional groups, or to investigate other polymer-solvent combinations.

Thermodynamics of Organic Electrolyte Solutions

Organic electrolytes are seen in a wide range of fields, including biological in the form of proteins and DNA, biomedical as bio-compatibility agents, electrochemical systems, and fluid additives in process engineering. The alkylammonium halide and alkylammonium bicarbonate models developed in chapter 4. Perhaps of equal importance, the approach of optimizing electrolyte models based on osmotic behaviour is a straightforward route to development of other electrolyte models with accurate thermodynamic properties.

Of particular importance in the continued development of electrolyte models is the transferability of electrolytes to solvents other than water. Few real-world systems are as simple as binary water-electrolytes. By considering the osmotic properties of electrolyte solutions in solvents such as methanol, acetone, nitrile, and dimethylether, the transferability of electrolyte models to non-aqueous environments can be assessed. This is both a useful test of the model limitations, and can be used as a further criterion to establish realistic and generally applicable electrolyte models.

Transport Processes

As discussed in chapter 1, it is the simultaneous absorption and transport of CO_2 reaction products which produces the facilitated transport effect. This work has been centred on absorption processes, while other authors [45] have detailed the kinetic aspects of ion transport in model polyelectrolyte membranes. The development of new osmotically consistent models for HCO_3^- and alkylammonium in chapter 4 offer an opportunity to revisit simulation of these polyelectrolyte systems with more suitable molecular models, which are likely to produce more physically accurate results for diffusion behaviour.

FTM Process Optimisation

The equation of state models developed for PVAm in chapters 3 and 5 allows prediction of solubility and solubility-selectivity for CO_2 and other gas species across varying process conditions. In practical applications, process conditions are optimised accounting for energy expenditure, product specifications, environmental factors, and other considerations specific for the process at hand. Having a predictive model for process performance allows this optimisation to be done more efficiently than trial-and-error methods. Inversely, a predictive model for process performance allows design of more efficient processes from the drawing board, informing the design next generation gas separation modules.

Acknowledgements

Foremost I would like to thank the my research supervisors, Maria-Chiara Ferrari and Lev Sarkisov, for their unrelenting support throughout this project. Without their initial groundwork this project could never have been conceived, and without their steady guidance it could never have been completed. I am grateful for the opportunity to share a long and interesting journey with two great minds, with many opportunities for both learning and friendship along the way.

This work was supported by the European Union's Horizon 2020 Research and Innovation program [Grant Agreement no. 727734] through the NANOMEMC^2 project. I am thankful for the many researchers within NANOMEMC^2 with which I have had an opportunity to collaborate with and learn from; in particular Riccardo Rea and Maria Grazia de Angelis from University of Bologna, and Conor Cleeton from the University of Edinburgh.

This work was also supported by the UK Engineering and Physical Sciences Research Council (EPSRC) Doctoral Training Partnership [Grant Number EP/W509644/1], administered by The University of Edinburgh. I am thankful for the support from the School of Engineering administrative and academic staff, without whom maintaining the the organisational, logistical, and regulatory aspects of this work would have been a monumental task in its own right.

Additionally, this work has made use of the resources provided by the Edinburgh Compute and Data Facility (ECDF) (http://www.ecdf.ed.ac.uk/). The ECDF Linux Compute Cluster has been employed for molecular simulations, using software compiled specifically for this research project. I am thankful for the assistance of Angela Chitzanidi with regards to practical usage of the Linux Compute Cluster and help with software adaptations.

Finally, I would like to thank the many inspiring and brilliant scientists and researchers I have had the opportunity to meet and share ideas with over the course of the project. In particular, Martin Sweatman and Carole Morrison have provided valuable comments, suggestions, and ideas in the earlier stages of this work. I feel an immense gratitude to all who have shown interest, asked questions, and provided motivation to spur on the completion of this project.

Dissemination

March, 2018 **Molecular Permeability Models for Facilitated Transport Membranes** by Odin Kvam and Pierre Fayon, presented at the NANOMEMC^2 scientific workshop in Sheffield, United Kingdom.

June, 2018 **Mapping Non-Ideal Contributions to Gas Solubility in Multicomponent Aqueous-Organic Systems** by Odin Kvam and Lev Sarkisov, presented at the 20th Symposium on Thermophysical Properties in Boulder, Colerado.

April, 2019 **Solubility prediction in mixed solvents: A combined molecular simulation and experimental approach** by Odin Kvam and Lev Sarkisov, presented in Fluid Phase Equilibria volume 48 DOI:10.1016/j.fluid.2018.11.016

March, 2018 **Molecular Gas Permeation Models for Facilitated Transport Membranes** by Odin Kvam, presented at the University of Edinburgh postgraduate research conference in Edinburgh, United Kingdom.

June, 2019 **Vapor Pressure Depression in Electrolyte Solutions from Direct Gibbs Ensemble Simulation** by Odin Kvam and Lev Sarkisov, presented at Thermodynamics 2019 in Huelva, Spain.

July, 2019 **Modelling Solubility and Diffusivity in Facilitated Transport Membranes: Microscale and Macroscale Approaches** by Odin Kvam and Riccardo Rea, presented at the 3rd Joint EU-South Korea workshop on CCS in Paris, France.

May, 2020 **Competitive H_2S – CO_2 absorption in reactive aqueous methyldiethanolamine solution: Prediction with ePC-SAFT** by Conor Cleeton, Odin Kvam, Riccardo Rea, Lev Sarkisov, and Maria Grazia De Angelis, presented in Fluid Phase Equilibria volume 511 DOI:10.1016/j.fluid.2019.112453

Appendix A

Simulation Parameters

This appendix defines GROMACS parameters for simulation in the canonical and isothermal-isobaric ensembles, as well as parameters for free energy perturbation simulations in the isothermal-isobaric ensemble. Each set of parameters serves as a template for simulations of that type, with variable parameters such as run length, temperature, and pressure. Each variable parameter is denoted by a leading $ followed by a keyword, and is adjusted for the specific conditions of interest.

Listing A.1: GROMACS parameters for simulation in the canonical ensemble. The variable parameter for temperature and run length are indicated by a leading $, and are fixed to a constant value for each simulation. Comments are indicated by a leading semicolon.

```
; RUN CONTROL PARAMETERS
integrator               = sd
; Start time and timestep in ps
tinit                    = 0
dt                       = 0.001
nsteps                   = $N
; mode for center of mass motion removal
comm-mode                = Linear
; number of steps for center of mass motion removal
nstcomm                  = 100

; LANGEVIN DYNAMICS OPTIONS
; Friction coefficient (amu/ps) and random seed
bd-fric                  = 0
ld-seed                  = -1

; OUTPUT CONTROL OPTIONS
; Output frequency for coords (x), velocities (v) and forces (f)
nstxout                  = 1000
nstvout                  = 0
nstfout                  = 0
; Output frequency for energies to log file and energy file
nstlog                   = 1000
nstcalcenergy            = 100
nstenergy                = 1000
; Output frequency and precision for .xtc file
nstxout-compressed       = 0
compressed-x-precision   = 1000

; NEIGHBORSEARCHING PARAMETERS
; cut-off scheme (Verlet: particle based cut-offs, group: using charge groups)
cutoff-scheme            = verlet
```

```
33 ; nblist update frequency
34 nstlist                    = 10
35 ; ns algorithm (simple or grid)
36 ns-type                    = grid
37 ; Periodic boundary conditions: xyz, no, xy
38 pbc                        = xyz
39 periodic-molecules         = no
40 ; Allowed energy error due to the Verlet buffer in kJ/mol/ps per atom,
41 ; a value of -1 means: use rlist
42 verlet-buffer-tolerance    = 0.0001
43 ; nblist cut-off
44 rlist                      = 1
45 ; long-range cut-off for switched potentials
46
47 ; OPTIONS FOR ELECTROSTATICS AND VDW
48 ; Method for doing electrostatics
49 coulombtype               = PME
50 coulomb-modifier          = none
51 rcoulomb-switch           = 0
52 rcoulomb                  = 1.2
53 ; Relative dielectric constant for the medium and the reaction field
54 epsilon-r                 = 1
55 epsilon-rf                = 0
56 ; Method for doing Van der Waals
57 vdwtype                   = cutoff
58 vdw-modifier              = none
59 ; cut-off lengths
60 rvdw-switch               = 0
61 rvdw                      = 1.2
62 ; Apply long range dispersion corrections for Energy and Pressure
63 DispCorr                  = EnerPres
64 ; Extension of the potential lookup tables beyond the cut-off
65 table-extension           = 1
66 ; Separate tables between energy group pairs
67 energygrp-table           =
```

```
68  ; Spacing for the PME/PPPM FFT grid
69  fourierspacing          = 0.1
70  ; FFT grid size, when a value is 0 fourierspacing will be used
71  fourier-nx              = 0
72  fourier-ny              = 0
73  fourier-nz              = 0
74  ; EWALD/PME/PPPM parameters
75  pme-order               = 4
76  ewald-rtol              = 1e-05
77  ewald-rtol-lj           = 0.001
78  lj-pme-comb-rule        = Geometric
79  ewald-geometry          = 3d
80  epsilon-surface         = 0
81
82  ; OPTIONS FOR WEAK COUPLING ALGORITHMS
83  ; Temperature coupling
84  tc-grps                 = system
85  ; Time constant (ps) and reference temperature (K)
86  tau-t                   = 2.0
87  ref-t                   = $T
88  ; pressure coupling
89  pcoupl                  = No
90
91  ; OPTIONS FOR BONDS
92  constraints             = none
93  ; Type of constraint algorithm
94  constraint-algorithm    = LINCS
95  ; Do not constrain the start configuration
96  continuation            = no
97  ; Use successive overrelaxation to reduce the number of shake iterations
98  Shake-SOR               = no
99  ; Relative tolerance of shake
100 shake-tol               = 0.0001
101 ; Highest order in the expansion of the constraint coupling matrix
102 lincs-order             = 6
```

```
103 ; Number of iterations in the final step of LINCS. 1 is fine for
104 ; normal simulations, but use 2 to conserve energy in NVE runs.
105 ; For energy minimization with constraints it should be 4 to 8.
106 lincs-iter                = 1
107 ; Lincs will write a warning to the stderr if in one step a bond
108 ; rotates over more degrees than
109 lincs-warnangle            = 30
110 ; Convert harmonic bonds to morse potentials
111 morse                     = no
```

Listing A.2: GROMACS parameters for simulation in the isobaric-isothermal ensemble. The variable parameters for temperature, pressure, and run length are indicated by a leading $, and are fixed to a constant value for each simulation. Comments are indicated by a leading semicolon.

```
; RUN CONTROL PARAMETERS
integrator               = sd
; Start time and timestep in ps
tinit                    = 0
dt                       = 0.002
nsteps                   = $N
; mode for center of mass motion removal
comm-mode                = Linear
; number of steps for center of mass motion removal
nstcomm                  = 100

; LANGEVIN DYNAMICS OPTIONS
; Friction coefficient (amu/ps) and random seed
bd-fric                  = 0
ld-seed                  = -1

; OUTPUT CONTROL OPTIONS
; Output frequency for coords (x), velocities (v) and forces (f)
nstxout                  = 1000
nstvout                  = 0
nstfout                  = 0
; Output frequency for energies to log file and energy file
nstlog                   = 1000
nstcalcenergy            = 100
nstenergy                = 1000
; Output frequency and precision for .xtc file
nstxout-compressed       = 0
compressed-x-precision   = 1000

; NEIGHBORSEARCHING PARAMETERS
; cut-off scheme (Verlet: particle based cut-offs, group: using charge groups)
cutoff-scheme            = verlet
```

```
33 ; nblist update frequency
34 nstlist                    = 10
35 ; ns algorithm (simple or grid)
36 ns-type                    = grid
37 ; Periodic boundary conditions: xyz, no, xy
38 pbc                        = xyz
39 periodic-molecules         = no
40 ; Allowed energy error due to the Verlet buffer in kJ/mol/ps per atom,
41 ; a value of -1 means: use rlist
42 verlet-buffer-tolerance    = 0.0001
43 ; nblist cut-off
44 rlist                      = 1
45 ; long-range cut-off for switched potentials
46
47 ; OPTIONS FOR ELECTROSTATICS AND VDW
48 ; Method for doing electrostatics
49 coulombtype               = PME
50 coulomb-modifier          = none
51 rcoulomb-switch           = 0
52 rcoulomb                  = 1.2
53 ; Relative dielectric constant for the medium and the reaction field
54 epsilon-r                 = 1
55 epsilon-rf                = 0
56 ; Method for doing Van der Waals
57 vdwtype                   = cutoff
58 vdw-modifier              = none
59 ; cut-off lengths
60 rvdw-switch               = 0
61 rvdw                      = 1.2
62 ; Apply long range dispersion corrections for Energy and Pressure
63 DispCorr                  = EnerPres
64 ; Extension of the potential lookup tables beyond the cut-off
65 table-extension           = 1
66 ; Separate tables between energy group pairs
67 energygrp-table           =
```

```
68  ; Spacing for the PME/PPPM FFT grid
69  fourierspacing          = 0.1
70  ; FFT grid size, when a value is 0 fourierspacing will be used
71  fourier-nx              = 0
72  fourier-ny              = 0
73  fourier-nz              = 0
74  ; EWALD/PME/PPPM parameters
75  pme-order               = 4
76  ewald-rtol              = 1e-05
77  ewald-rtol-lj           = 0.001
78  lj-pme-comb-rule        = Geometric
79  ewald-geometry          = 3d
80  epsilon-surface         = 0
81
82  ; OPTIONS FOR WEAK COUPLING ALGORITHMS
83  ; Groups to couple separately
84  tc-grps                 = system
85  ; Time constant (ps) and reference temperature (K)
86  tau-t                   = 2.0
87  ref-t                   = $T
88  ; pressure coupling
89  pcoupl                  = Parrinello-Rahman
90  pcoupltype              = isotropic
91  nstpcouple              = -1
92  ; Time constant (ps), compressibility (1/bar) and reference P (bar)
93  tau-p                   = 5.0
94  compressibility         = 4.5e-05
95  ref-p                   = 1.0
96  ; Scaling of reference coordinates, No, All or COM
97  refcoord-scaling        = all
98
99  ; OPTIONS FOR BONDS
100 constraints             = none
101 ; Type of constraint algorithm
102 constraint-algorithm     = LINCS
```

```
103 ; Do not constrain the start configuration
104 continuation             = no
105 ; Use successive overrelaxation to reduce the number of shake iterations
106 Shake-SOR                = no
107 ; Relative tolerance of shake
108 shake-tol                = 0.0001
109 ; Highest order in the expansion of the constraint coupling matrix
110 lincs-order               = 6
111 ; Number of iterations in the final step of LINCS. 1 is fine for
112 ; normal simulations, but use 2 to conserve energy in NVE runs.
113 ; For energy minimization with constraints it should be 4 to 8.
114 lincs-iter                = 1
115 ; Lincs will write a warning to the stderr if in one step a bond
116 ; rotates over more degrees than
117 lincs-warnangle           = 30
118 ; Convert harmonic bonds to morse potentials
119 morse                     = no
```

Listing A.3: GROMACS parameters for free energy perturbation simulation in the isobaric-isothermal ensemble. The variable parameters temperature, pressure, and run length are indicated by a leading $, and are fixed to a constant value for each simulation. Comments are indicated by a leading semicolon.

```
; RUN CONTROL PARAMETERS
integrator               = sd
; Start time and timestep in ps
tinit                    = 0
dt                       = 0.002
nsteps                   = $N
; mode for center of mass motion removal
comm-mode                = Linear
; number of steps for center of mass motion removal
nstcomm                  = 100

; LANGEVIN DYNAMICS OPTIONS
; Friction coefficient (amu/ps) and random seed
bd-fric                  = 0
ld-seed                  = -1

; OUTPUT CONTROL OPTIONS
; Output frequency for coords (x), velocities (v) and forces (f)
nstxout                  = 1000
nstvout                  = 0
nstfout                  = 0
; Output frequency for energies to log file and energy file
nstlog                   = 1000
nstcalcenergy            = 100
nstenergy                = 1000
; Output frequency and precision for .xtc file
nstxout-compressed       = 0
compressed-x-precision   = 1000

; NEIGHBORSEARCHING PARAMETERS
; cut-off scheme (Verlet: particle based cut-offs, group: using charge groups)
cutoff-scheme            = verlet
```

```
33 ; nblist update frequency
34 nstlist                   = 10
35 ; ns algorithm (simple or grid)
36 ns-type                   = grid
37 ; Periodic boundary conditions: xyz, no, xy
38 pbc                       = xyz
39 periodic-molecules        = no
40 ; Allowed energy error due to the Verlet buffer in kJ/mol/ps per atom,
41 ; a value of -1 means: use rlist
42 verlet-buffer-tolerance   = 0.0001
43 ; nblist cut-off
44 rlist                     = 1
45 ; long-range cut-off for switched potentials
46
47 ; OPTIONS FOR ELECTROSTATICS AND VDW
48 ; Method for doing electrostatics
49 coulombtype              = PME
50 coulomb-modifier         = none
51 rcoulomb-switch          = 0
52 rcoulomb                 = 1.2
53 ; Relative dielectric constant for the medium and the reaction field
54 epsilon-r                = 1
55 epsilon-rf               = 0
56 ; Method for doing Van der Waals
57 vdwtype                  = cutoff
58 vdw-modifier             = none
59 ; cut-off lengths
60 rvdw-switch              = 0
61 rvdw                     = 1.2
62 ; Apply long range dispersion corrections for Energy and Pressure
63 DispCorr                 = EnerPres
64 ; Extension of the potential lookup tables beyond the cut-off
65 table-extension          = 1
66 ; Separate tables between energy group pairs
67 energygrp-table          =
```

```
68  ; Spacing for the PME/PPPM FFT grid
69  fourierspacing          = 0.1
70  ; FFT grid size, when a value is 0 fourierspacing will be used
71  fourier-nx              = 0
72  fourier-ny              = 0
73  fourier-nz              = 0
74  ; EWALD/PME/PPPM parameters
75  pme-order               = 4
76  ewald-rtol              = 1e-05
77  ewald-rtol-lj           = 0.001
78  lj-pme-comb-rule        = Geometric
79  ewald-geometry          = 3d
80  epsilon-surface         = 0
81
82  ; OPTIONS FOR WEAK COUPLING ALGORITHMS
83  ; Groups to couple separately
84  tc-grps                 = system
85  ; Time constant (ps) and reference temperature (K)
86  tau-t                   = 2.0
87  ref-t                   = $T
88  ; pressure coupling
89  pcoupl                  = Parrinello-Rahman
90  pcoupltype              = isotropic
91  nstpcouple              = -1
92  ; Time constant (ps), compressibility (1/bar) and reference P (bar)
93  tau-p                   = 5.0
94  compressibility         = 4.5e-05
95  ref-p                   = 1.0
96  ; Scaling of reference coordinates, No, All or COM
97  refcoord-scaling        = all
98
99  ; OPTIONS FOR BONDS
100 constraints             = none
101 ; Type of constraint algorithm
102 constraint-algorithm     = LINCS
```

```
103 ; Do not constrain the start configuration
104 continuation             = no
105 ; Use successive overrelaxation to reduce the number of shake iterations
106 Shake-SOR                = no
107 ; Relative tolerance of shake
108 shake-tol                = 0.0001
109 ; Highest order in the expansion of the constraint coupling matrix
110 lincs-order               = 6
111 ; Number of iterations in the final step of LINCS. 1 is fine for
112 ; normal simulations, but use 2 to conserve energy in NVE runs.
113 ; For energy minimization with constraints it should be 4 to 8.
114 lincs-iter                = 1
115 ; Lincs will write a warning to the stderr if in one step a bond
116 ; rotates over more degrees than
117 lincs-warnangle           = 30
118 ; Convert harmonic bonds to morse potentials
119 morse                     = no
120
121 ; Free energy variables
122 free-energy               = yes
123 couple-lambda0            = none
124 couple-lambda1            = vdw-q
125 couple-intramol           = no
126 init-lambda-state         = $LAMBDA
127 fep-lambdas               = $LAMBDA_FEP
128 coul-lambdas              = $LAMBDA_COULOMB
129 vdw-lambdas               = $LAMBDA_VDW
130 calc-lambda-neighbors     = -1
131 sc-alpha                  = 0.5
132 sc-power                  = 1
133 sc-r-power                = 6
134 sc-sigma                  = 0.3
135 sc-coul                   = no
```

Appendix B

Polymer-Water Solution Properties

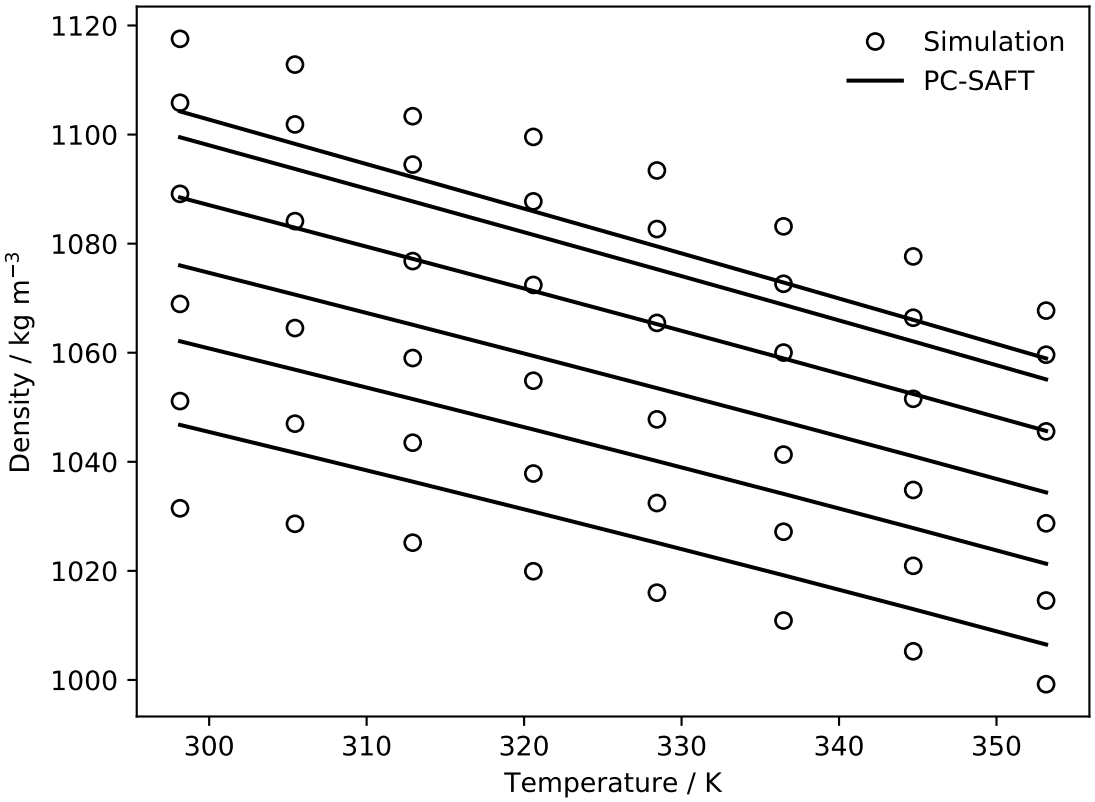

Figure B.1: Density in PEO-H_2O systems at 0.3, 0.4, 0.5, 0.6, 0.7, and 0.8 H_2O mass fraction as a function of temperature. Open circles indicate simulation with the TraPPE-UA model for PEO and TIP4P/2005 model for water, as detailed in chapter 3. Solid lines indicate the PC-SAFT model described in chapter 3. Mean average deviation between simulation and the PC-SAFT model is 0.8%.

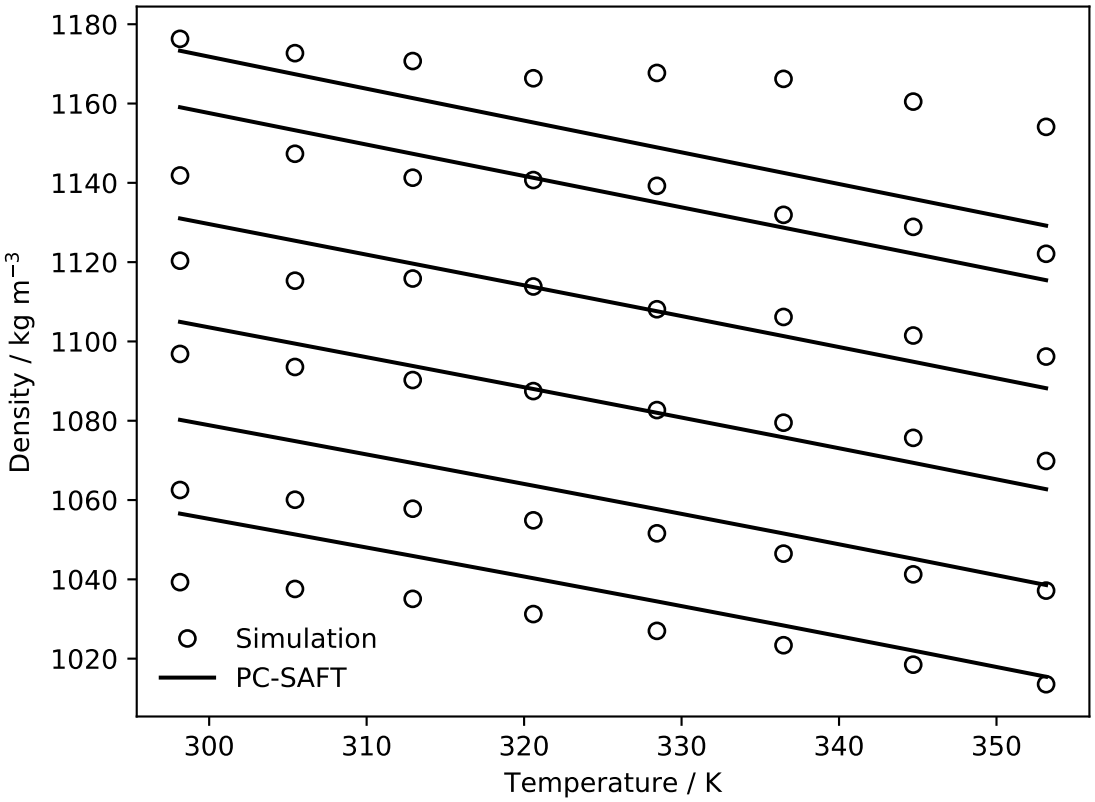

Figure B.2: Density in PVA-H_2O systems at 0.3, 0.4, 0.5, 0.6, 0.7, and 0.8 H_2O mass fraction as a function of temperature. Open circles indicate simulation with the Trappe-UA model for PVA and TIP4P/2005 model for water, as detailed in chapter 3. Solid lines indicate the PC-SAFT model described in chapter 3. Mean average deviation between simulation and PC-SAFT models is 0.9%.

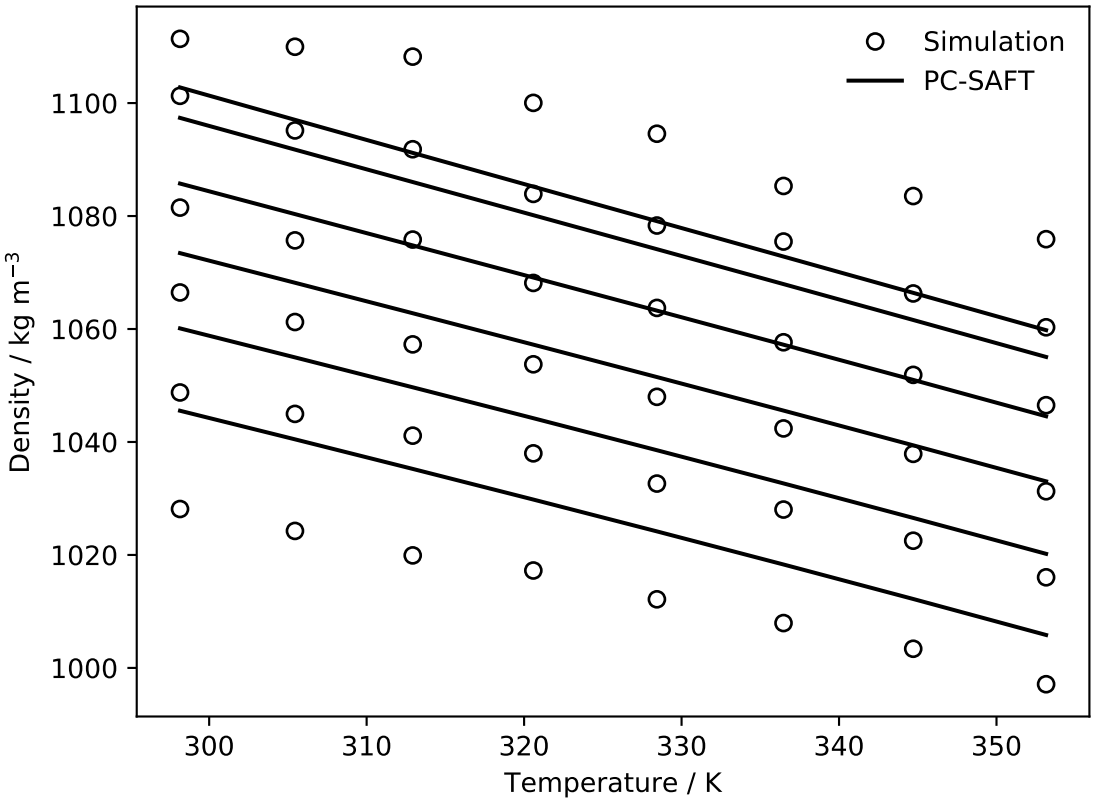

Figure B.3: Density in PVAm-H_2O systems at 0.3, 0.4, 0.5, 0.6, 0.7, and 0.8 H_2O mass fraction as a function of temperature. Open circles indicate simulation with a TraPPE-UA compatible model for PVAm and TIP4P/2005 model for water, as detailed in chapter 3. Solid lines indicate the PC-SAFT model described in chapter 3. Mean average deviation between simulation and the PC-SAFT model is 0.8%.

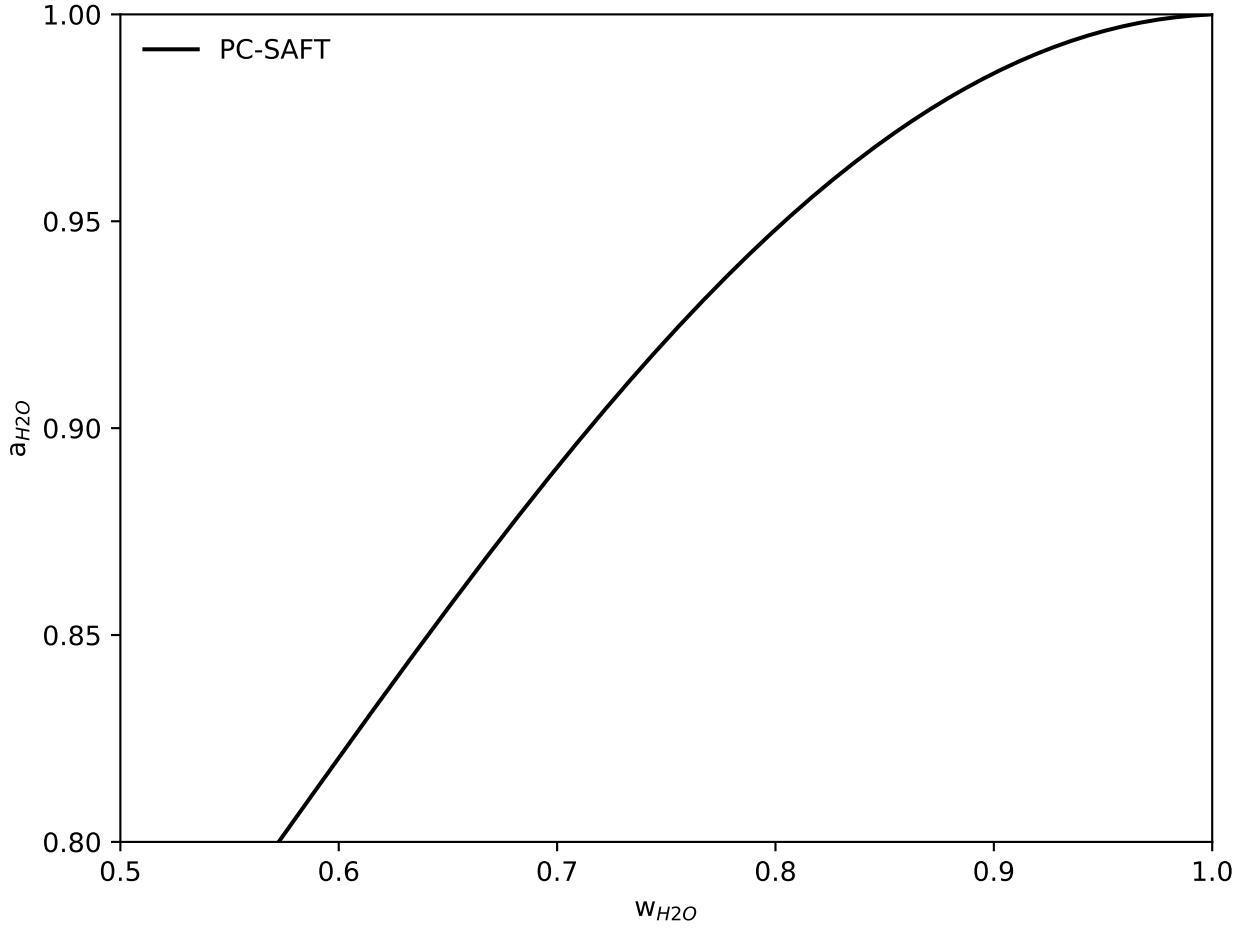

Figure B.4: Water activity in PVAm-H_2O solution as a function of water content at temperature 298 K and pressure 1 atmosphere, predicted by the PC-SAFT equation of state as detailed in chapter:3.

Appendix C

Bicarbonate Radial Distribution Functions

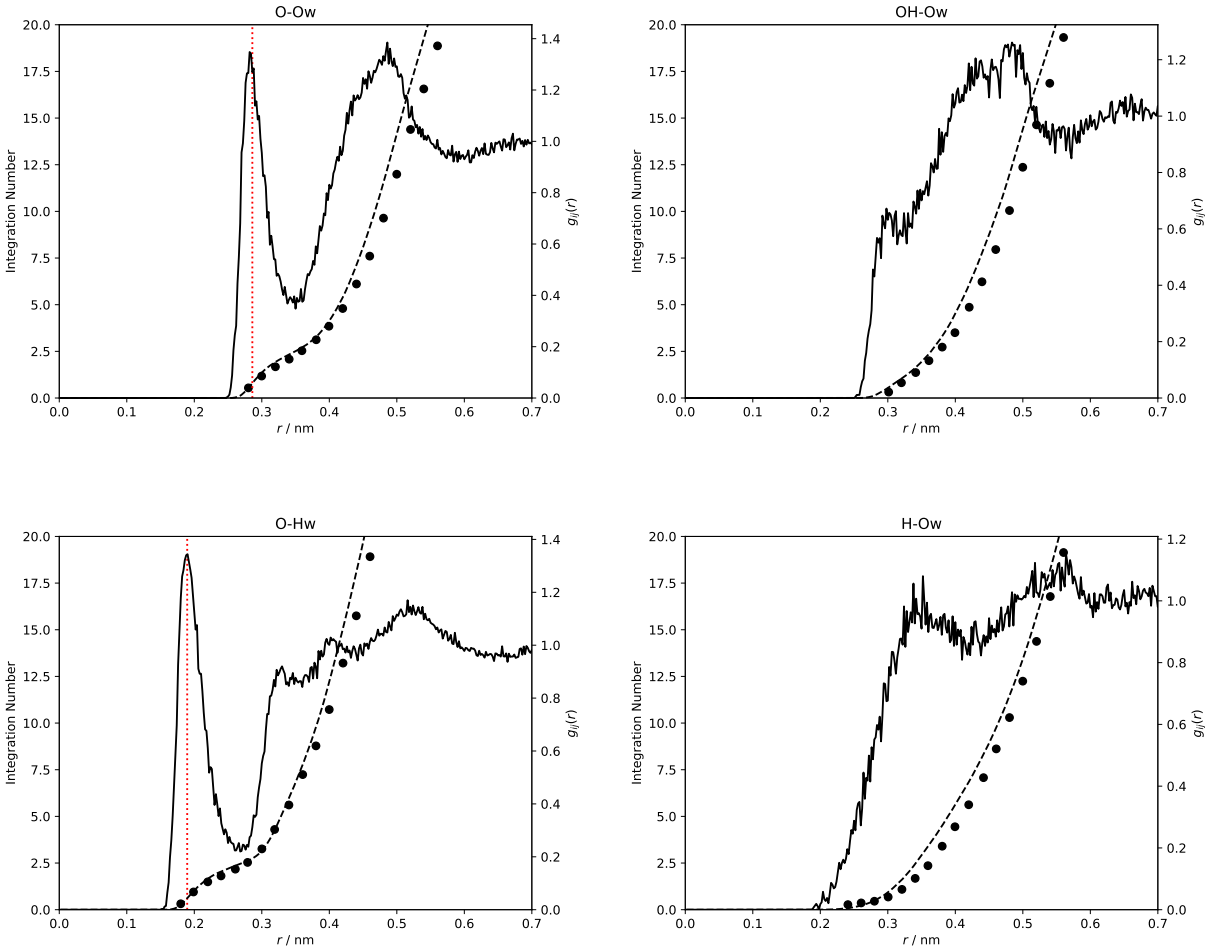

Figure C.1: Radial distribution functions and integration numbers for bicarbonate - water atomic centres, using bicarbonate model 1 (see table X). Solid lines indicate normalised simulated radial distribution functions. Dashed lines indicate simulated integrated radial distribution functions. Circles indicate *ab initio* integrated radial distribution functions reported by Vchirawongkwin et al. [417] for a single hydrated bicarbonate ion. Vertical red dotted lines mark peaks in the radial distribution function reported by Vchirawongkwin et al. [417]. The peaks near 0.2 nm for O-H_w and 0.3 nm for O-O_w indicate formation of hydrogen bonds towards charge-carrying oxygen atoms. This feature is absent from the OH group atoms, suggesting weaker solute-solvent interactions.

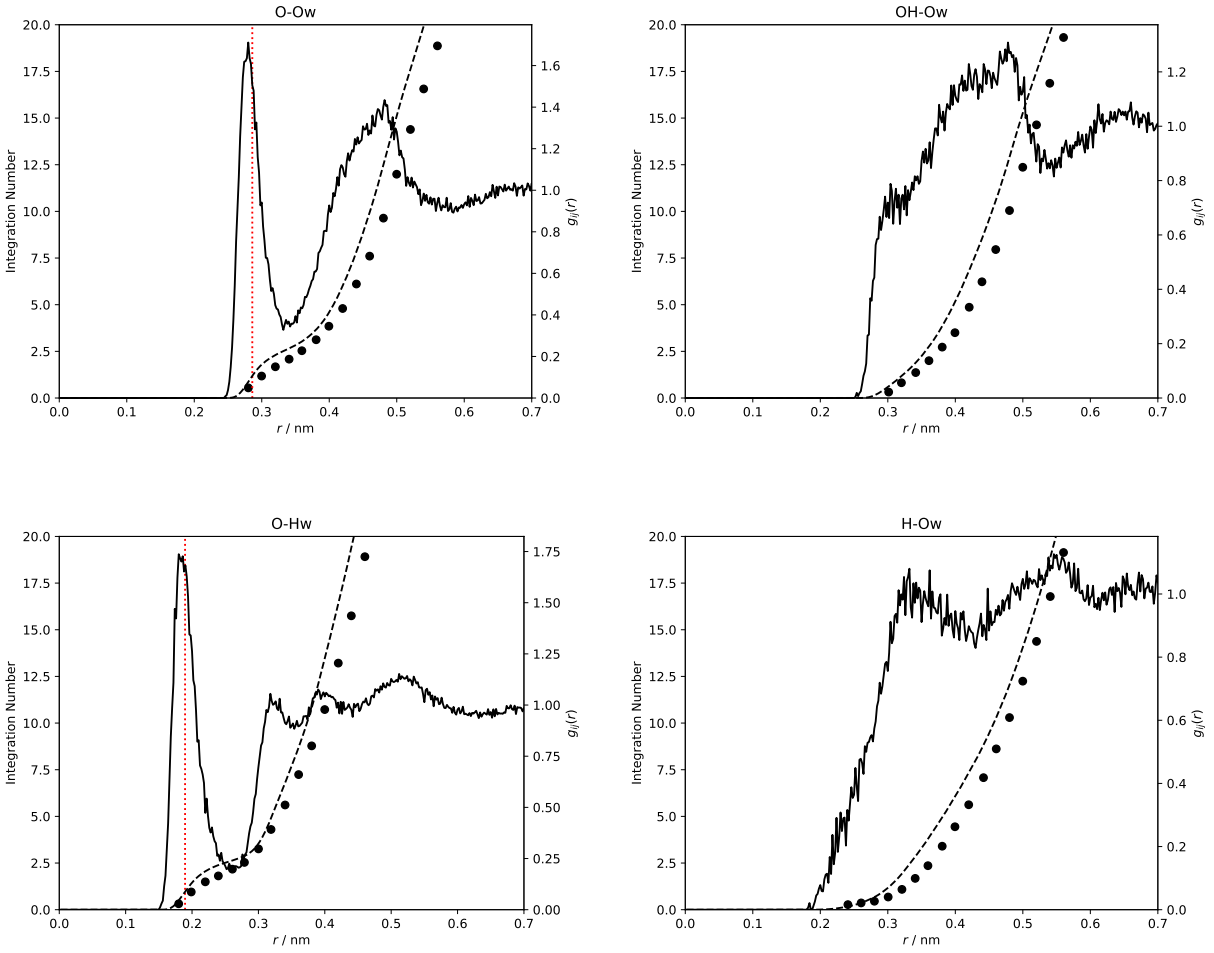

Figure C.2: Radial distribution functions and integration numbers for bicarbonate - water atomic centres, using bicarbonate model 2 (see table X). Solid lines indicate normalised simulated radial distribution functions. Dashed lines indicate simulated integrated radial distribution functions. Circles indicate *ab initio* integrated radial distribution functions reported by Vchirawongkwin et al. [417] for a single hydrated bicarbonate ion. Vertical red dotted lines mark peaks in the radial distribution function reported by Vchirawongkwin et al. [417]. The peaks near 0.2 nm for O-H_w and 0.3 nm for O-O_w indicate formation of hydrogen bonds towards charge-carrying oxygen atoms. This feature is absent from the OH group atoms, suggesting weaker solute-solvent interactions.

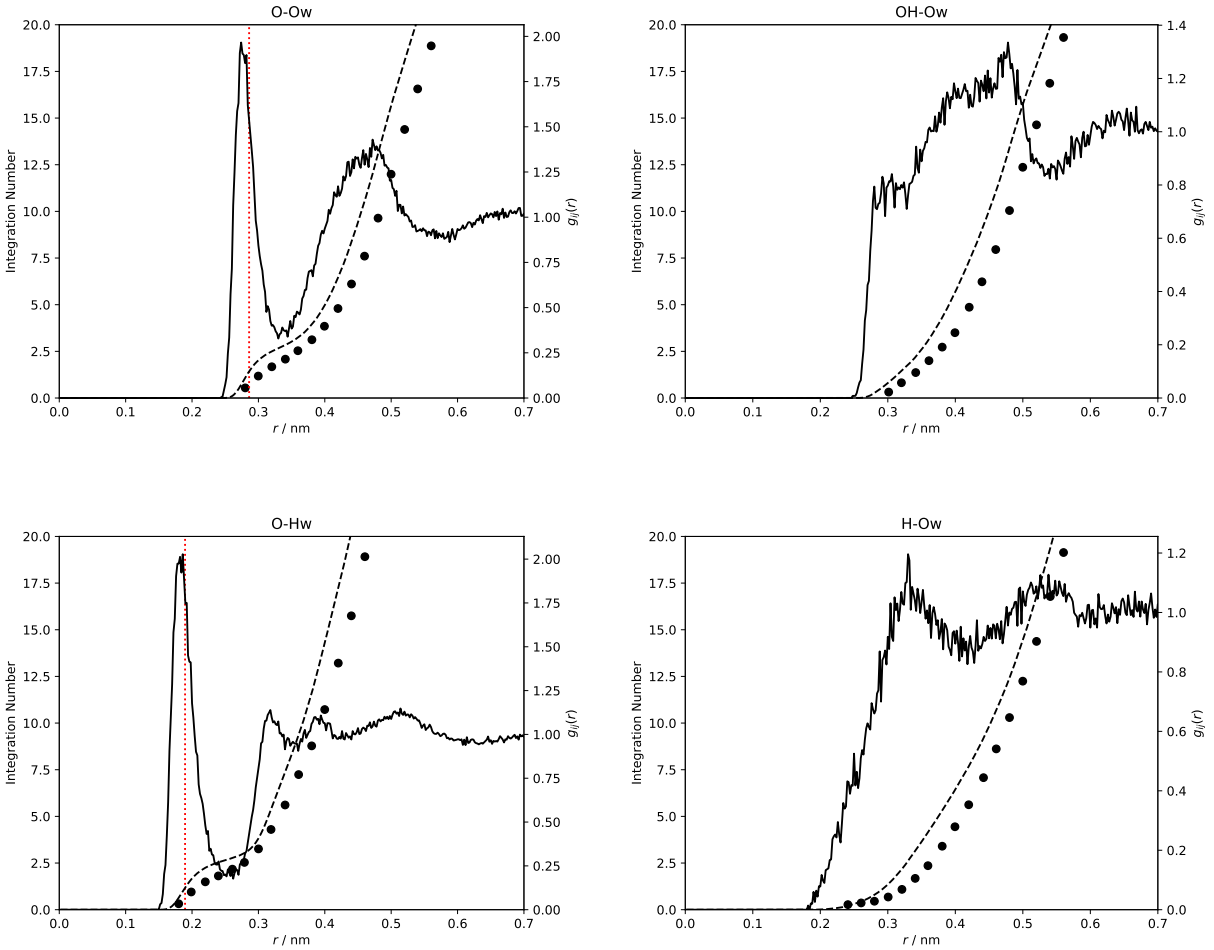

Figure C.3: Radial distribution functions and integration numbers for bicarbonate - water atomic centres, using bicarbonate model 3 (see table X). Solid lines indicate normalised simulated radial distribution functions. Dashed lines indicate simulated integrated radial distribution functions. Circles indicate *ab initio* integrated radial distribution functions reported by Vchirawongkwin et al. [417] for a single hydrated bicarbonate ion. Vertical red dotted lines mark peaks in the radial distribution function reported by Vchirawongkwin et al. [417]. The peaks near 0.2 nm for O-H_w and 0.3 nm for O-O_w indicate formation of hydrogen bonds towards charge-carrying oxygen atoms. This feature is absent from the OH group atoms, suggesting weaker solute-solvent interactions.

Appendix D

MDEA - H_2O - HCO_3^- Convergence

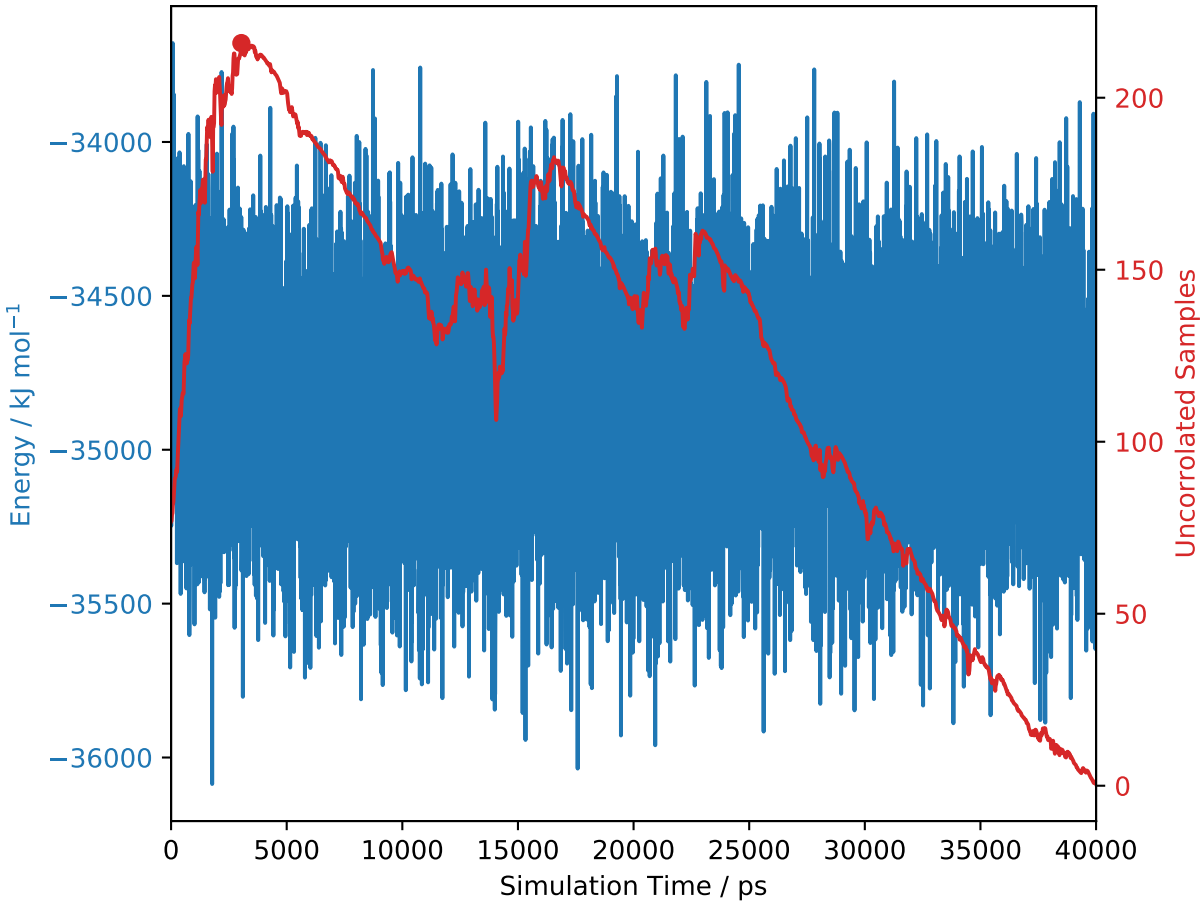

Figure D.1: Time correlation analysis of 0.5 amine weight fraction MDEA-H_2O solution at 0% protonation. Blue: System total energy as a function of simulation time, with values shown on the left axis. Red: Uncorrelated samples calculated using the method of Chodera [142], showing the number of uncorrelated samples remaining as a function of simulation time. The red filled circle indicates the time estimate for the system reaching the equilibrium state.

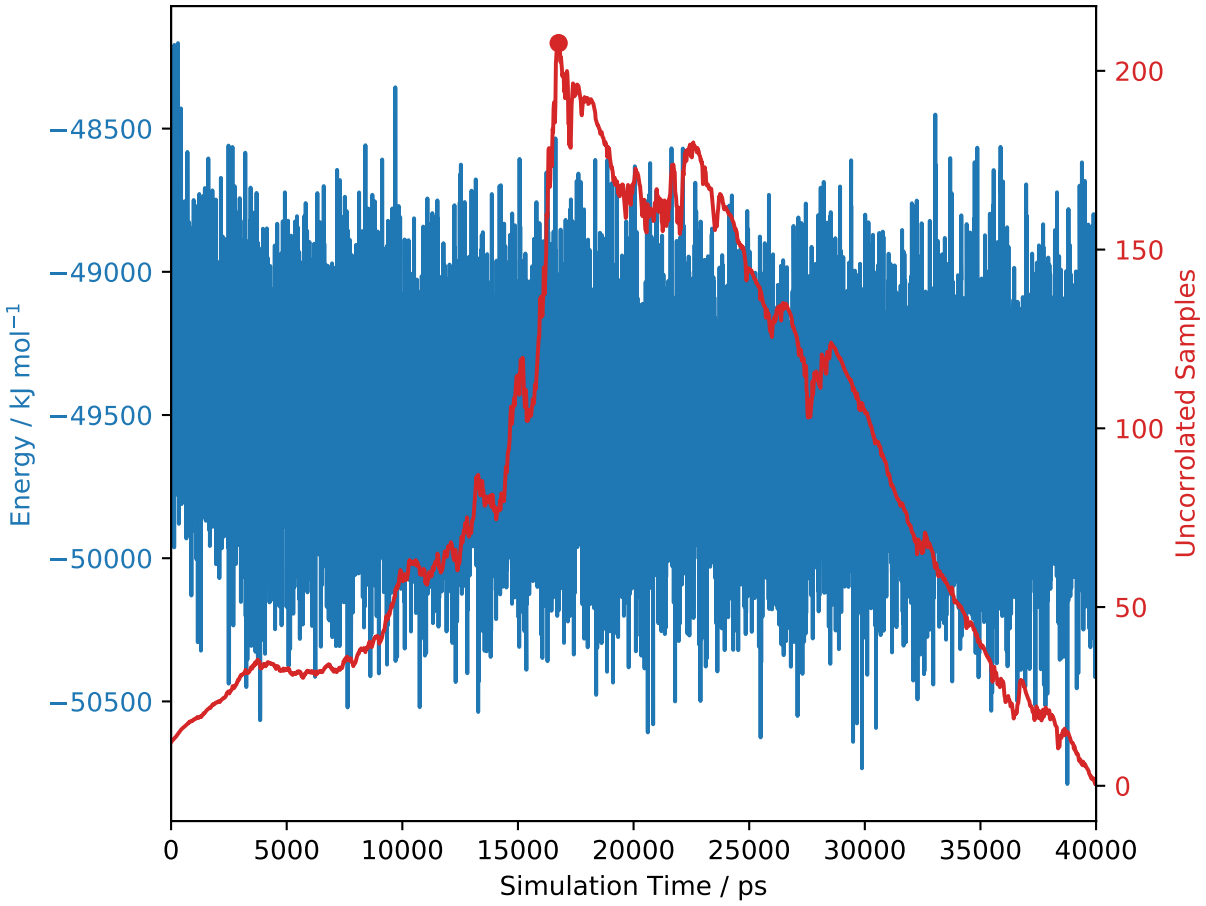

Figure D.2: Time correlation analysis of 0.5 amine weight fraction MDEA-H_2O solution at 50% protonation with HCO_3^- counterions. Blue: System total energy as a function of simulation time, with values shown on the left axis. Red: Uncorrelated samples calculated using the method of Chodera [142], showing the number of uncorrelated samples remaining as a function of simulation time. The red filled circle indicates the time estimate for the system reaching the equilibrium state.

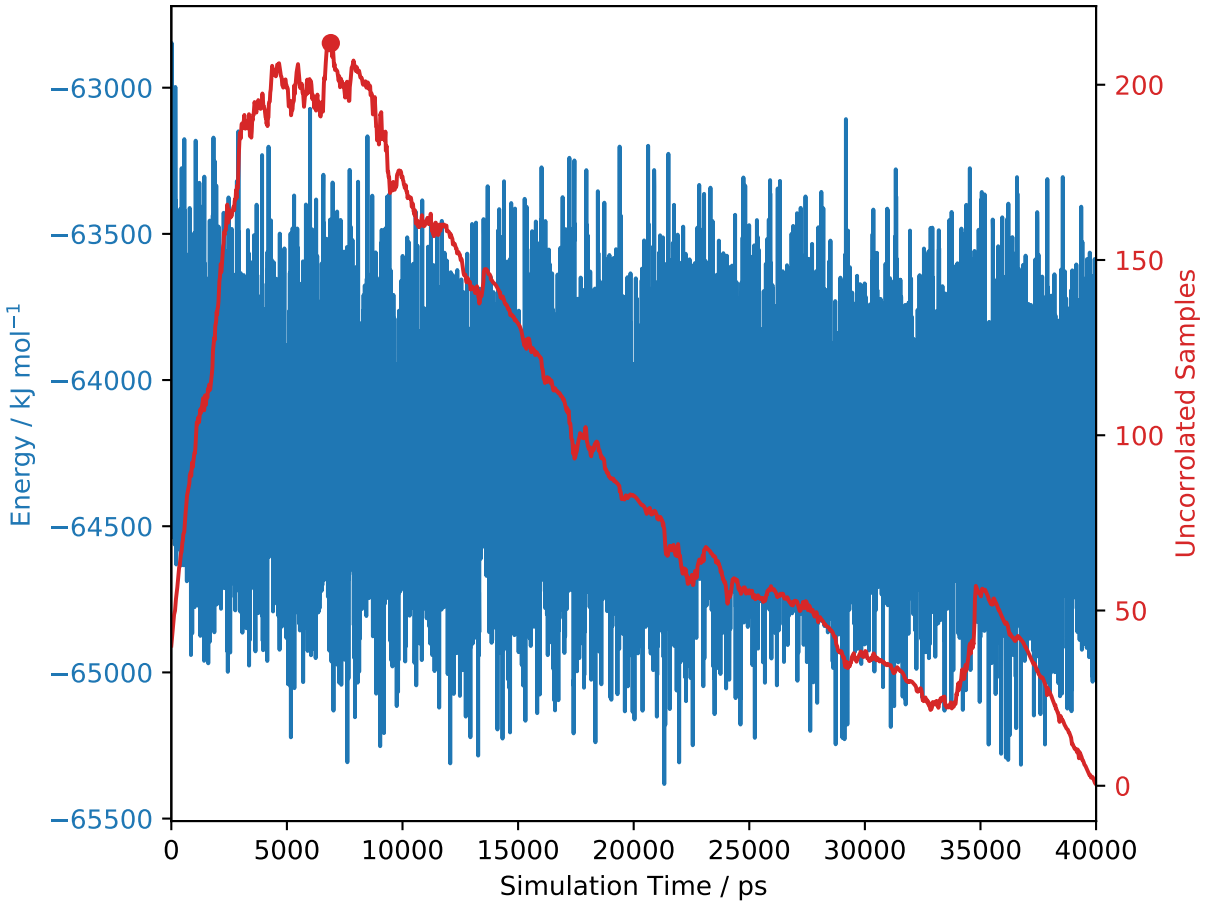

Figure D.3: Time correlation analysis of 0.5 amine weight fraction MDEA-H_2O solution at 100% protonation with HCO_3^- counterions. Blue: System total energy as a function of simulation time, with values shown on the left axis. Red: Uncorrelated samples calculated using the method of Chodera [142], showing the number of uncorrelated samples remaining as a function of simulation time. The red filled circle indicates the time estimate for the system reaching the equilibrium state.

Bibliography

[1] Z. Y. Yeo, T. L. Chew, P. W. Zhu, A. R. Mohamed, and S. P. Chai. *Conventional processes and membrane technology for carbon dioxide removal from natural gas: A review*. 2012. DOI: 10.1016/S1003-9953(11)60366-6.

[2] W. Mazyan, A. Ahmadi, H. Ahmed, and M. Hoorfar. "Market and technology assessment of natural gas processing: A review". In: *Journal of Natural Gas Science and Engineering* 30 (2016), pp. 487–514. DOI: 10.1016/j.jngse.2016.02.010.

[3] K. A. Mumford, Y. Wu, K. H. Smith, and G. W. Stevens. *Review of solvent based carbon-dioxide capture technologies*. 2015. DOI: 10.1007/s11705-015-1514-6.

[4] K. Maqsood, A. Mullick, A. Ali, K. Kargupta, and S. Ganguly. "Cryogenic carbon dioxide separation from natural gas: A review based on conventional and novel emerging technologies". In: *Reviews in Chemical Engineering* 30.5 (2014), pp. 453–477. DOI: 10.1515/revce-2014-0009.

[5] C. A. Grande. "Advances in Pressure Swing Adsorption for Gas Separation". In: *International Scholarly Research Network ISRN Chemical Engineering* 2012 (2012), p. 13. DOI: 10.5402/2012/982934.

[6] A. D. Wiheeb, Z. Helwani, J. Kim, and M. R. Othman. "Pressure Swing Adsorption Technologies for Carbon Dioxide Capture". In: *Separation & Purification Reviews* 45.2 (2016), pp. 108–121. DOI: 10.1080/15422119.2015.1047958.

[7] P. Bernardo, E. Drioli, and G. Golemme. "Membrane gas separation: A review/state of the art". In: *Industrial and Engineering Chemistry Research* 48.10 (2009), pp. 4638–4663. DOI: 10.1021/ie8019032.

[8] P. Bernardo and E. Drioli. "Membrane gas separation progresses for process intensification strategy in the petrochemical industry". In: *Petroleum Chemistry* 50.4 (2010), pp. 271–282. DOI: 10.1134/S0965544110040043.

[9] D. F. Sanders, Z. P. Smith, R. Guo, L. M. Robeson, J. E. McGrath, D. R. Paul, and B. D. Freeman. *Energy-efficient polymeric gas separation membranes for a sustainable future: A review*. 2013. DOI: 10.1016/j.polymer.2013.05.075.

[10] S. Basu, A. L. Khan, A. Cano-Odena, C. Liu, and I. F. Vankelecom. "Membrane-based technologies for biogas separations". In: *Chemical Society Reviews* 39.2 (2010), pp. 750–768. DOI: 10.1039/b817050a.

[11] J. Petisce, M. A. Tapsak, P. C. Simpson, V. Carr-Brendel, and J. H. Brauker. *Oxygen enhancing membrane systems for implantable devices*. 2008.

[12] T. L. Reynolds, T. I. Eklund, and G. A. Haack. *Onboard Inert Gas Generation System/ Onboard Oxygen Gas Generation System (OBIGGS/OBOGS) Study Part II: Gas Separation Technology-State of the Art*. Tech. rep. Cleveland, Ohio: NASA, 2001. URL: https://ntrs.nasa.gov/archive/nasa/casi.ntrs.nasa.gov/20010092198.pdf.

[13] B. Koros. *Three hundred volumes*. 2007. DOI: 10.1016/j.memsci.2007.05.006.

[14] A. I. Stankiewicz and J. A. Moulijn. "Process Intensification: Transforming Chemical Engineering". In: *Chemical Engineering Progress* 96.1 (2000), pp. 22–34.

[15] N. Matsumiya, H. Mano, K. Haraya, H. Matsuyama, and M. Teramoto. "Feasibility study of the application of facilitated transport membrane for separation for CO2 from flue gases". In: *Kagaku Kogaku Ronbunshu* 30.6 (2004), pp. 752–757. DOI: 10.1252/kakoronbunshu.30.752.

[16] A. Hussain and M. B. Hägg. "A feasibility study of CO2 capture from flue gas by a facilitated transport membrane". In: *Journal of Membrane Science* 359.1-2 (2010), pp. 140–148. DOI: 10.1016/j.memsci.2009.11.035.

[17] M. Zhao, A. I. Minett, and A. T. Harris. "A review of techno-economic models for the retrofitting of conventional pulverised-coal power plants for post-combustion capture (PCC) of CO2". In: *Energy and Environmental Science* 6.1 (2013), pp. 25–40. DOI: 10.1039/c2ee22890d.

[18] European Commission. *Horizon 2020 Work Programme 2018-2020*. Tech. rep. 2020. URL: https://ec.europa.eu/research/participants/data/ref/h2020/wp/2018-2020/main/h2020-wp1820-intro_en.pdf.

[19] Cobham Mission Systems. *Nitrogen Inerting, Fuel Tank Inerting*. URL: https://www.cobhammissionsystems.com/nitrogen-inerting/fuel-tank-inerting/.

[20] B. D. Freeman. "Basis of permeability/selectivity tradeoff relations in polymeric gas separation membranes". In: *Macromolecules* 32.2 (1999), pp. 375–380. DOI: 10.1021/ma9814548.

[21] S. Rafiq, L. Deng, and M.-B. Hägg. "Role of Facilitated Transport Membranes and Composite Membranes for Efficient CO2 Capture - A Review". In: *ChemBioEng Reviews* 3.2 (2016), pp. 68–85. DOI: 10.1002/cben.201500013.

[22] Z. Tong and W. S. W. Ho. "Facilitated transport membranes for CO2 separation and capture". In: *Separation Science and Technology* 52.2 (2017), pp. 156–167. DOI: 10.1080/01496395.2016.1217885.

[23] C. F. Wan, T. Yang, G. G. Lipscomb, D. J. Stookey, and T. S. Chung. *Design and fabrication of hollow fiber membrane modules*. 2017. DOI: 10.1016/j.memsci.2017.05.047.

[24] W. Salim, V. Vakharia, Y. Chen, D. Wu, Y. Han, and W. S. Ho. "Fabrication and field testing of spiral-wound membrane modules for CO2 capture from flue gas". In: *Journal of Membrane Science* 556 (2018), pp. 126–137. DOI: 10.1016/j.memsci.2018.04.001.

[25] Y. Ding. "Perspective on Gas Separation Membrane Materials from Process Economics Point of View". In: *Industrial and Engineering Chemistry Research* 59.2 (2020), pp. 556–568. DOI: 10.1021/acs.iecr.9b05975.

[26] L. M. Robeson. "The upper bound revisited". In: *Journal of Membrane Science* 320.1-2 (2008), pp. 390–400. DOI: 10.1016/j.memsci.2008.04.030.

[27] I. Rose, C. G. Bezzu, M. Carta, B. Comesanã-Gándara, E. Lasseuguette, M. C. Ferrari, P. Bernardo, G. Clarizia, A. Fuoco, J. C. Jansen, K. E. Hart, T. P. Liyana-Arachchi, C. M. Colina, and N. B. McKeown. "Polymer ultrapermeability from the inefficient packing of 2D chains". In: *Nature Materials* 16.9 (2017), pp. 932–937. DOI: 10.1038/nmat4939.

[28] C. H. Lau, X. Mulet, K. Konstas, C. M. Doherty, M.-A. Sani, F. Separovic, M. R. Hill, and C. D. Wood. "Hypercrosslinked Additives for Ageless Gas-Separation Membranes". In: *Angewandte Chemie International Edition* 55.6 (2016), pp. 1998–2001. DOI: 10.1002/anie.201508070.

[29] L. Liu, A. Chakma, and X. Feng. "Gas permeation through water-swollen hydrogel membranes". In: *Journal of Membrane Science* 310.1-2 (2008), pp. 66–75. DOI: 10.1016/j.memsci.2007.10.032.

[30] L. Deng, T. J. Kim, and M. B. Hägg. "Facilitated transport of CO2 in novel PVAm/PVA blend membrane". In: *Journal of Membrane Science* 340.1-2 (2009), pp. 154–163. DOI: 10.1016/j.memsci.2009.05.019.

[31] J. Gilron and A. Soffer. "Knudsen diffusion in microporous carbon membranes with molecular sieving character". In: *Journal of Membrane Science* 209.2 (2002), pp. 339–352. DOI: 10.1016/S0376-7388(02)00074-1.

[32] A. J. Burggraaf. "Single gas permeation of thin zeolite (MFI) membranes: Theory and analysis of experimental observations". In: *Journal of Membrane Science* 155.1 (1999), pp. 45–65. DOI: 10.1016/S0376-7388(98)00295-6.

[33] L. M. Robeson. "Correlation of separation factor versus permeability for polymeric membranes". In: *Journal of Membrane Science* 62.2 (1991), pp. 165–185. DOI: 10.1016/0376-7388(91)80060-J.

[34] L. M. Robeson, W. F. Burgoyne, M. Langsam, A. C. Savoca, and C. F. Tien. "High performance polymers for membrane separation". In: *Polymer* 35.23 (1994), pp. 4970–4978. DOI: 10.1016/0032-3861(94)90651-3.

[35] L. Deng and M. B. Hägg. "Swelling behavior and gas permeation performance of PVAm/PVA blend FSC membrane". In: *Journal of Membrane Science* 363.1-2 (2010), pp. 295–301. DOI: 10.1016/j.memsci.2010.07.043.

[36] Y. Zhao and W. S. Ho. "CO2-selective membranes containing sterically hindered amines for CO2/H2 separation". In: *Industrial and Engineering Chemistry Research* 52.26 (2013), pp. 8774–8782. DOI: 10.1021/ie301397m.

[37] Y. Han and W. S. Ho. "Design of Amine-Containing CO2-Selective Membrane Process for Carbon Capture from Flue Gas". In: *Industrial and Engineering Chemistry Research* 59.12 (2020), pp. 5340–5350. DOI: 10.1021/acs.iecr.9b04839.

[38] *NANOMEMC2 Project*. URL: https://www.nanomemc2.eu/.

[39] Q. Yang, G. Puxty, S. James, M. Bown, P. Feron, and W. Conway. "Toward Intelligent CO2 Capture Solvent Design through Experimental Solvent Development and Amine Synthesis". In: *Energy and Fuels* 30.9 (2016), pp. 7503–7510. DOI: 10.1021/acs.energyfuels.6b00875.

[40] M. Minelli and G. C. Sarti. *Modeling mass transport in dense polymer membranes: cooperative synergy among multiple scale approaches*. 2020. DOI: 10.1016/j.coche.2020.01.004.

[41] G. Q. Chen, S. Kanehashi, C. M. Doherty, A. J. Hill, and S. E. Kentish. "Water vapor permeation through cellulose acetate membranes and its impact upon membrane separation performance for natural gas purification". In: *Journal of Membrane Science* 487 (2015), pp. 249–255. DOI: 10.1016/j.memsci.2015.03.074.

[42] B. Jung, H. M. Moon, and G. N. B. Baroña. "Effect of methanol on plasticization and transport properties of a perfluorosulfonic ion-exchange membrane". In: *Journal of Power Sources* 196.4 (2011), pp. 1880–1885. DOI: 10.1016/j.jpowsour.2010.09.030.

[43] R. Rea, M. G. D. Angelis, and M. G. Baschetti. "Models for Facilitated Transport Membranes: A Review". In: *Membranes* 9.2 (2019), p. 26. DOI: 10.3390/membranes9020026.

[44] I. M. Bernhardsen and H. K. Knuutila. *A review of potential amine solvents for CO2 absorption process: Absorption capacity, cyclic capacity and pKa*. 2017. DOI: 10.1016/j.ijggc.2017.03.021.

[45] P. Fayon and L. Sarkisov. "Structure and dynamics of water in molecular models of hydrated polyvinylamine membranes". In: *Physical Chemistry Chemical Physics* 21.48 (2019), pp. 26453–26465. DOI: 10.1039/c9cp05399a.

[46] O. Kvam and L. Sarkisov. "Solubility prediction in mixed solvents: A combined molecular simulation and experimental approach". In: *Fluid Phase Equilibria* 484 (2019), pp. 26–37. DOI: 10.1016/j.fluid.2018.11.016.

[47] C. Cleeton, O. Kvam, R. Rea, L. Sarkisov, and M. G. De Angelis. "Competitive H2S – CO2 absorption in reactive aqueous methyldiethanolamine solution: Prediction with ePC-SAFT". In: *Fluid Phase Equilibria* 511 (2020), p. 112453. DOI: 10.1016/j.fluid.2019.112453.

[48] I. C. Sanchez and R. H. Lacombe. "An elementary molecular theory of classical fluids. Pure fluids". In: *Journal of Physical Chemistry* 80.21 (1976), pp. 2352–2362. DOI: 10.1021/j100562a008.

[49] R. H. Lacombe and I. C. Sanchez. "Statistical thermodynamics of fluid mixtures". In: *Journal of Physical Chemistry* 80.23 (1976), pp. 2568–2580. DOI: 10.1021/j100564a009.

[50] I. C. Sanchez and R. H. Lacombe. "Statistical Thermodynamics of Polymer Solutions". In: *Macromolecules* 11.6 (1978), pp. 1145–1156. DOI: 10.1021/ma60066a017.

[51] J. Gross and G. Sadowski. "Perturbed-chain SAFT: An equation of state based on a perturbation theory for chain molecules". In: *Industrial and Engineering Chemistry Research* 40.4 (2001), pp. 1244–1260. DOI: 10.1021/ie0003887.

[52] J. Gross and G. Sadowski. "Application of the perturbed-chain SAFT equation of state to associating systems". In: *Industrial & Engineering Chemistry Research* 41.22 (2002), pp. 5510–5515. DOI: 10.1021/ie010954d.

[53] J. Gross and G. Sadowski. "Modeling polymer systems using the perturbed-chain statistical associating fluid theory equation of state". In: *Industrial and Engineering Chemistry Research* 41.5 (2002), pp. 1084–1093. DOI: 10.1021/ie010449g.

[54] C. Held, L. F. Cameretti, and G. Sadowski. "Modeling aqueous electrolyte solutions. Part 1. Fully dissociated electrolytes". In: *Fluid Phase Equilibria* 270.1-2 (2008), pp. 87–96. DOI: 10.1016/j.fluid.2008.06.010.

[55] C. Held and G. Sadowski. "Modeling aqueous electrolyte solutions. Part 2. Weak electrolytes". In: *Fluid Phase Equilibria* 279.2 (2009), pp. 141–148. DOI: 10.1016/j.fluid.2009.02.015.

[56] B. Maribo-Mogensen, G. M. Kontogeorgis, and K. Thomsen. "Modeling of dielectric properties of complex fluids with an equation of state". In: *Journal of Physical Chemistry B* 117.12 (2013), pp. 3389–3397. DOI: 10.1021/jp310572q.

[57] B. Maribo-Mogensen, G. M. Kontogeorgis, and K. Thomsen. "Comparison of the Debye-Huckel and the mean spherical approximation theories for electrolyte solutions". In: *Industrial and Engineering Chemistry Research* 51.14 (2012), pp. 5353–5363. DOI: 10.1021/ie2029943.

[58] B. Maribo-Mogensen, G. M. Kontogeorgis, and K. Thomsen. "Modeling of dielectric properties of aqueous salt solutions with an equation of state". In: *Journal of Physical Chemistry B* 117.36 (2013), pp. 10523–10533. DOI: 10.1021/jp403375t.

[59] B. Maribo-Mogensen, K. Thomsen, and G. M. Kontogeorgis. "An electrolyte CPA equation of state for mixed solvent electrolytes". In: *AIChE Journal* 61.9 (2015), pp. 2933–2950. DOI: 10.1002/aic.14829.

[60] J. Wu, Y. Zhou, and E. W. Lemmon. "An Equation of State for the Thermodynamic Properties of Dimethyl Ether". In: *Journal of Physical and Chemical Reference Data* 40.2 (2011), p. 023104. DOI: 10.1063/1.3582533.

[61] L. Piazza and R. Span. "An equation of state for methanol including the association term of SAFT". In: *Fluid Phase Equilibria* 349 (2013), pp. 12–24. DOI: 10.1016/j.fluid.2013.03.024.

[62] W. Wagner and A. Pruß. "The IAPWS formulation 1995 for the thermodynamic properties of ordinary water substance for general and scientific use". In: *Journal of Physical and Chemical Reference Data* 31.2 (2002), pp. 387–535. DOI: 10.1063/1.1461829.

[63] J. C. Slater and J. G. Kirkwood. "The van der waals forces in gases". In: *Physical Review* 37.6 (1931), pp. 682–697. DOI: 10.1103/PhysRev.37.682.

[64] J. E. Lennard-Jones. "On the determination of molecular fields.—I. From the variation of the viscosity of a gas with temperature". In: *Proceedings of the Royal Society of London. Series A, Containing Papers of a Mathematical and Physical Character* 106.738 (1924), pp. 441–462. DOI: 10.1098/rspa.1924.0081.

[65] J. E. Lennard-Jones. "On the determination of molecular fields. —II. From the equation of state of a gas". In: *Proceedings of the Royal Society of London. Series A, Containing Papers of a Mathematical and Physical Character* 106.738 (1924), pp. 463–477. DOI: 10.1098/rspa.1924.0082.

[66] R. A. Buckingham. "The classical equation of state of gaseous helium, neon and argon". In: *Proceedings of the Royal Society of London. Series A. Mathematical and Physical Sciences* 168.933 (1938), pp. 264–283. DOI: 10.1098/rspa.1938.0173.

[67] G. Mie. "Zur kinetischen Theorie der einatomigen Körper". In: *Annalen der Physik* 316.8 (1903), pp. 657–697. DOI: 10.1002/andp.19033160802.

[68] M. P. Allen and D. J. Tildesley. *Computer simulation of liquids*. 2nd. Oxford: Oxford Unitversity Press, 2017.

[69] J. Delhommelle and P. Millié. "Inadequacy of the Lorentz-Berthelot combining rules for accurate predictions of equilibrium properties by molecular simulation". In: *Molecular Physics* 99.8 (2001), pp. 619–625. DOI: 10.1080/00268970010020041.

[70] M. Rouha and I. Nezbeda. "Non-Lorentz-Berthelot Lennard-Jones mixtures: A systematic study". In: *Fluid Phase Equilibria* 277.1 (2009), pp. 42–48. DOI: 10.1016/j.fluid.2008.11.007.

[71] F. Moučka and I. Nezbeda. "Water-methanol mixtures with non-Lorentz-Berthelot combining rules: A feasibility study". In: *Journal of Molecular Liquids*. Vol. 159. 1. Elsevier, 2011, pp. 47–51. DOI: 10.1016/j.molliq.2010.05.005.

[72] A. Y. Toukmaji and J. A. Board. *Ewald summation techniques in perspective: A survey*. 1996. DOI: 10.1016/0010-4655(96)00016-1.

[73] T. Darden, D. York, and L. Pedersen. "Particle mesh Ewald: An N log(N) method for Ewald sums in large systems". In: *The Journal of Chemical Physics* 98.12 (1993), pp. 10089–10092. DOI: 10.1063/1.464397.

[74] B. Hess, H. Bekker, H. J. C. Berendsen, and J. G. E. M. Fraaije. "LINCS: A linear constraint solver for molecular simulations". In: *Journal of Computational Chemistry* 18.12 (1997), pp. 1463–1472. DOI: 10.1002/(SICI)1096-987X(199709)18:12<1463::AID-JCC4>3.0.CO;2-H.

[75] B. Hess. "P-LINCS: A parallel linear constraint solver for molecular simulation". In: *Journal of Chemical Theory and Computation* 4.1 (2008), pp. 116–122. DOI: 10.1021/ct700200b.

[76] W. F. van Gunsteren and H. J. Berendsen. "Computer Simulation of Molecular Dynamics: Methodology, Applications, and Perspectives in Chemistry". In: *Angewandte Chemie International Edition in English* 29.9 (1990), pp. 992–1023. DOI: 10.1002/anie.199009921.

[77] W. F. Van Gunsteren, H. J. Berendsen, and J. A. Rullmann. "Stochastic dynamics for molecules with constraints brownian dynamics of n-alkanes". In: *Molecular Physics* 44.1 (1981), pp. 69–95. DOI: 10.1080/00268978100102291.

[78] M. Parrinello and A. Rahman. "Crystal structure and pair potentials: A molecular-dynamics study". In: *Physical Review Letters* 45.14 (1980), pp. 1196–1199. DOI: 10.1103/PhysRevLett.45.1196.

[79] M. Parrinello and A. Rahman. "Polymorphic transitions in single crystals: A new molecular dynamics method". In: *Journal of Applied Physics* 52.12 (1981), pp. 7182–7190. DOI: 10.1063/1.328693.

[80] S. Nosé and M. L. Klein. "Constant pressure molecular dynamics for molecular systems". In: *Molecular Physics* 50.5 (1983), pp. 1055–1076. DOI: 10.1080/00268978300102851.

[81] R. W. Zwanzig. "High-Temperature Equation of State by a Perturbation Method. I. Nonpolar Gases". In: *Journal of Chemical Physics* 22.8 (1954), pp. 1420–1426. DOI: 10.1063/1.1740409.

[82] W. L. Jorgensen and L. L. Thomas. "Perspective on free-energy perturbation calculations for chemical equilibria". In: *Journal of Chemical Theory and Computation* 4.6 (2008), pp. 869–876. DOI: 10.1021/ct800011m.

[83] M. R. Shirts and V. S. Pande. "Comparison of efficiency and bias of free energies computed by exponential averaging, the Bennett acceptance ratio, and thermodynamic integration". In: *Journal of Chemical Physics* 122.14 (2005), p. 144107. DOI: 10.1063/1.1873592.

[84] C. H. Bennett. "Efficient estimation of free energy differences from Monte Carlo data". In: *Journal of Computational Physics* 22.2 (1976), pp. 245–268. DOI: 10.1016/0021-9991(76)90078-4.

[85] T. P. Straatsma and J. A. McCammon. "Multiconfiguration thermodynamic integration". In: *The Journal of Chemical Physics* 95.2 (1991), pp. 1175–1188. DOI: 10.1063/1.461148.

[86] C. Jarzynski. "Nonequilibrium equality for free energy differences". In: *Physical Review Letters* 78.14 (1997), pp. 2690–2693. DOI: 10.1103/PhysRevLett.78.2690.

[87] J. L. Knight and C. L. Brooks. "λ-dynamics free energy simulation methods". In: *Journal of Computational Chemistry* 30.11 (2009), pp. 1692–1700. DOI: 10.1002/jcc.21295.

[88] A. P. Lyubartsev, A. A. Martsinovski, S. V. Shevkunov, and P. N. Vorontsov-Velyaminov. "New approach to Monte Carlo calculation of the free energy: Method of expanded ensembles". In: *The Journal of Chemical Physics* 96.3 (1992), pp. 1776–1783. DOI: 10.1063/1.462133.

[89] S. Bruckner and S. Boresch. "Efficiency of alchemical free energy simulations. I. A practical comparison of the exponential formula, thermodynamic integration, and Bennett's acceptance ratio method". In: *Journal of Computational Chemistry* 32.7 (2011), pp. 1303–1319. DOI: 10.1002/jcc.21713.

[90] T. Steinbrecher, I. Joung, and D. A. Case. "Soft-core potentials in thermodynamic integration: Comparing one- and two-step transformations". In: *Journal of Computational Chemistry* 32.15 (2011), pp. 3253–3263. DOI: 10.1002/jcc.21909.

[91] T. T. Pham and M. R. Shirts. "Identifying low variance pathways for free energy calculations of molecular transformations in solution phase". In: *The Journal of Chemical Physics* 135.3 (2011), p. 034114. DOI: 10.1063/1.3607597.

[92] T. T. Pham and M. R. Shirts. "Optimal pairwise and non-pairwise alchemical pathways for free energy calculations of molecular transformation in solution phase". In: *The Journal of Chemical Physics* 136.12 (2012), p. 124120. DOI: 10.1063/1.3697833.

[93] M. J. Abraham, T. Murtola, R. Schulz, S. Páll, J. C. Smith, B. Hess, and E. Lindah. "Gromacs: High performance molecular simulations through multi-level parallelism from laptops to supercomputers". In: *SoftwareX* 1-2 (2015), pp. 19–25. DOI: 10.1016/j.softx.2015.06.001.

[94] C. Abrams and G. Bussi. "Enhanced Sampling in Molecular Dynamics Using Metadynamics, Replica-Exchange, and Temperature-Acceleration". In: *Entropy* 16.1 (2013), pp. 163–199. DOI: 10.3390/e16010163.

[95] J. Wereszczynski and J. A. McCammon. "Nucleotide-dependent mechanism of Get3 as elucidated from free energy calculations". In: *Proceedings of the National Academy of Sciences of the United States of America* 109.20 (2012), pp. 7759–7764. DOI: 10.1073/pnas.1117441109.

[96] M. S. Lee and M. A. Olson. "Calculation of absolute protein-ligand binding affinity using path and endpoint approaches". In: *Biophysical Journal* 90.3 (2006), pp. 864–877. DOI: 10.1529/biophysj.105.071589.

[97] K. Hukushima and K. Nemoto. "Exchange Monte Carlo Method and Application to Spin Glass Simulations". In: *Journal of the Physical Society of Japan* 65.6 (1996), pp. 1604–1608. DOI: 10.1143/JPSJ.65.1604.

[98] Y. Sugita and Y. Okamoto. "Replica-exchange molecular dynamics method for protein folding". In: *Chemical Physics Letters* 314.1-2 (1999), pp. 141–151. DOI: 10.1016/S0009-2614(99)01123-9.

[99] M. M. Seibert, A. Patriksson, B. Hess, and D. Van Der Spoel. "Reproducible polypeptide folding and structure prediction using molecular dynamics simulations". In: *Journal of Molecular Biology* 354.1 (2005), pp. 173–183. DOI: 10.1016/j.jmb.2005.09.030.

[100] T. Okabe, M. Kawata, Y. Okamoto, and M. Mikami. "Replica-exchange Monte Carlo method for the isobaric-isothermal ensemble". In: *Chemical Physics Letters* 335.5-6 (2001), pp. 435–439. DOI: 10.1016/S0009-2614(01)00055-0.

[101] S. E. Quiñones-Cisneros and U. K. Deiters. "An efficient algorithm for the calculation of phase envelopes of fluid mixtures". In: *Fluid Phase Equilibria* 329 (2012), pp. 22–31. DOI: 10.1016/j.fluid.2012.05.023.

[102] A. Meurer, C. P. Smith, M. Paprocki, O. Čertík, S. B. Kirpichev, M. Rocklin, A. T. Kumar, S. Ivanov, J. K. Moore, S. Singh, T. Rathnayake, S. Vig, B. E. Granger, R. P. Muller, F. Bonazzi, H. Gupta, S. Vats, F. Johansson, F. Pedregosa, M. J. Curry, A. R. Terrel, Š. Roučka, A. Saboo, I. Fernando, S. Kulal, R. Cimrman, and A. Scopatz. "SymPy: Symbolic computing in python". In: *PeerJ Computer Science* 2017.1 (2017), e103. DOI: 10.7717/peerj-cs.103.

[103] E. A. Guggenheim. "Statistical thermodynamics of mixtures with zero energies of mixing". In: *Proceedings of the Royal Society of London. Series A. Mathematical and Physical Sciences* 183.993 (1944), pp. 203–212. DOI: 10.1098/rspa.1944.0032.

[104] J. M. Stubbs, J. J. Potoff, and J. I. Siepmann. "Transferable potentials for phase equilibria. 6. United-atom description for ethers, glycols, ketones, and aldehydes". In: *Journal of Physical Chemistry B* 108.45 (2004), pp. 17596–17605. DOI: 10.1021/jp049459w.

[105] B. Chen, J. J. Potoff, and J. I. Siepmann. "Monte Carlo calculations for alcohols and their mixtures with alkanes. Transferable potentials for phase equilibria. 5. United-atom description of primary, secondary, and tertiary alcohols". In: *Journal of Physical Chemistry B* 105.15 (2001), pp. 3093–3104. DOI: 10.1021/jp003882x.

[106] J. A. Zollweg and G. W. Mulholland. "On the law of the rectilinear diameter". In: *The Journal of Chemical Physics* 57.3 (1972), pp. 1021–1025. DOI: 10.1063/1.1678352.

[107] K. S. Pitzer. "Ionic fluids. Near-critical and related properties". In: *Journal of physical chemistry* 99.35 (1995), pp. 13070–13077. DOI: 10.1021/j100035a006.

[108] W. G. Chapman, K. E. Gubbins, G. Jackson, and M. Radosz. "SAFT: Equation-of-state solution model for associating fluids". In: *Fluid Phase Equilibria* 52.C (1989), pp. 31–38. DOI: 10.1016/0378-3812(89)80308-5.

[109] W. G. Chapman, K. E. Gubbins, G. Jackson, and M. Radosz. "New reference equation of state for associating liquids". In: *Industrial & Engineering Chemistry Research* 29.8 (1990), pp. 1709–1721. DOI: 10.1021/ie00104a021.

[110] M. S. Wertheim. "Fluids with highly directional attractive forces. I. Statistical thermodynamics". In: *Journal of Statistical Physics* 35.1-2 (1984), pp. 19–34. DOI: 10.1007/BF01017362.

[111] M. S. Wertheim. "Fluids with highly directional attractive forces. II. Thermodynamic perturbation theory and integral equations". In: *Journal of Statistical Physics* 35.1-2 (1984), pp. 35–47. DOI: 10.1007/BF01017363.

[112] M. S. Wertheim. "Fluids with highly directional attractive forces. III. Multiple attraction sites". In: *Journal of Statistical Physics* 42.3-4 (1986), pp. 459–476. DOI: 10.1007/BF01127721.

[113] M. S. Wertheim. "Fluids with highly directional attractive forces. IV. Equilibrium polymerization". In: *Journal of Statistical Physics* 42.3-4 (1986), pp. 477–492. DOI: 10.1007/BF01127722.

[114] M. S. Wertheim. "Fluids of dimerizing hard spheres, and fluid mixtures of hard spheres and dispheres". In: *The Journal of Chemical Physics* 85.5 (1986), pp. 2929–2936. DOI: 10.1063/1.451002.

[115] M. S. Wertheim. "Thermodynamic perturbation theory of polymerization". In: *The Journal of Chemical Physics* 87.12 (1987), pp. 7323–7331. DOI: 10.1063/1.453326.

[116] N. F. Carnahan and K. E. Starling. "Equation of state for nonattracting rigid spheres". In: *The Journal of Chemical Physics* 51.2 (1969), pp. 635–636. DOI: 10.1063/1.1672048.

[117] M. L. Michelsen and E. M. Hendriks. "Physical properties from association models". In: *Fluid Phase Equilibria* 180.1-2 (2001), pp. 165–174. DOI: 10.1016/S0378-3812(01)00344-2.

[118] S. H. Huang and M. Radosz. "Equation of state for small, large, polydisperse, and associating molecules". In: *Industrial & Engineering Chemistry Research* 29.11 (1990), pp. 2284–2294. DOI: 10.1021/ie00107a014.

[119] S. H. Huang and M. Radosz. "Equation of State for Small, Large, Polydisperse, and Associating Molecules: Extension to Fluid Mixtures". In: *Industrial and Engineering Chemistry Research* 30.8 (1991), pp. 1994–2005. DOI: 10.1021/ie00056a050.

[120] F. J. Blas and L. F. Vega. "Thermodynamic behaviour of homonuclear and heteronuclear lennard-jones chains with association sites from simulation and theory". In: *Molecular Physics* 92.1 (1997), pp. 135–150. DOI: 10.1080/002689797170707.

[121] F. J. Blas and L. F. Vega. "Prediction of Binary and Ternary Diagrams Using the Statistical Associating Fluid Theory (SAFT) Equation of State". In: *Industrial & Engineering Chemical Research* 37.2 (1998), pp. 660–674. DOI: 10.1021/IE970449+.

[122] T. Lafitte, A. Apostolakou, C. Avendaño, A. Galindo, C. S. Adjiman, E. A. Müller, and G. Jackson. "Accurate statistical associating fluid theory for chain molecules formed from Mie segments". In: *Journal of Chemical Physics* 139.15 (2013), p. 154504. DOI: 10.1063/1.4819786.

[123] N. I. Diamantonis, G. C. Boulougouris, E. Mansoor, D. M. Tsangaris, and I. G. Economou. "Evaluation of cubic, SAFT, and PC-SAFT equations of state for the vapor-liquid equilibrium modeling of CO2 mixtures with other gases". In: *Industrial and Engineering Chemistry Research* 52.10 (2013), pp. 3933–3942. DOI: 10.1021/ie303248q.

[124] A. G. Perez, C. Coquelet, P. Paricaud, and A. Chapoy. "Comparative study of vapour-liquid equilibrium and density modelling of mixtures related to carbon capture and storage with the SRK, PR, PC-SAFT and SAFT-VR Mie equations of state for industrial uses". In: *Fluid Phase Equilibria* 440 (2017), pp. 19–35. DOI: 10.1016/j.fluid.2017.02.018.

[125] F. Tumakaka, J. Gross, and G. Sadowski. "Thermodynamic modeling of complex systems using PC-SAFT". In: *Fluid Phase Equilibria*. Vol. 228-229. Elsevier, 2005, pp. 89–98. DOI: 10.1016/j.fluid.2004.09.037.

[126] N. I. Diamantonis and I. G. Economou. "Evaluation of statistical associating fluid theory (SAFT) and perturbed chain-SAFT equations of state for the calculation of thermodynamic derivative properties of fluids related to carbon capture and sequestration". In: *Energy & Fuels* 25.7 (2011), pp. 3334–3343. DOI: 10.1021/ef200387p.

[127] N. I. Diamantonis and I. G. Economou. "Modeling the phase equilibria of a H 2 O–CO 2 mixture with PC-SAFT and tPC-PSAFT equations of state". In: *Molecular Physics* 110.11-12 (2012), pp. 1205–1212. DOI: 10.1080/00268976.2012.656721.

[128] J. L. F. Abascal and C. Vega. "A general purpose model for the condensed phases of water: TIP4P/2005". In: *The Journal of Chemical Physics* 123.23 (2005), p. 234505. DOI: 10.1063/1.2121687.

[129] C. Vega, J. L. Abascal, and I. Nezbeda. "Vapor-liquid equilibria from the triple point up to the critical point for the new generation of TIP4P-like models: TIP4P/Ew, TIP4P/2005, and TIP4P/ice". In: *Journal of Chemical Physics* 125.3 (2006), p. 034503. DOI: 10.1063/1.2215612.

[130] T. Boublík. "Hard-sphere equation of state". In: *The Journal of Chemical Physics* 53.1 (1970), pp. 471–472. DOI: 10.1063/1.1673824.

[131] G. A. Mansoori, N. F. Carnahan, K. E. Starling, and T. W. Leland. "Equilibrium Thermodynamic Properties of the Mixture of Hard Spheres". In: *The Journal of Chemical Physics* 54.4 (1971), pp. 1523–1525. DOI: 10.1063/1.1675048.

[132] J. A. Barker and D. Henderson. "Perturbation theory and equation of state for fluids. II. A successful theory of liquids". In: *The Journal of Chemical Physics* 47.11 (1967), pp. 4714–4721. DOI: 10.1063/1.1701689.

[133] J. Gross. "An equation-of-state contribution for polar components: Quadrupolar molecules". In: *AIChE Journal* 51.9 (2005), pp. 2556–2568. DOI: 10.1002/aic.10502.

[134] J. Gross and J. Vrabec. "An equation-of-state contribution for polar components: Dipolar molecules". In: *AIChE Journal* 52.3 (2006), pp. 1194–1204. DOI: 10.1002/aic.10683.

[135] J. Vrabec and J. Gross. "Vapor-liquid equilibria simulation and an equation of state contribution for dipole-quadrupole interactions". In: *Journal of Physical Chemistry B* 112.1 (2008), pp. 51–60. DOI: 10.1021/jp072619u.

[136] R. Span and W. Wagner. "A new equation of state for carbon dioxide covering the fluid region from the triple-point temperature to 1100 K at pressures up to 800 MPa". In: *Journal of Physical and Chemical Reference Data* 25.6 (1996), pp. 1509–1596. DOI: 10.1063/1.555991.

[137] J. J. Potoff and J. I. Siepmann. "Vapor-liquid equilibria of mixtures containing alkanes, carbon dioxide, and nitrogen". In: *AIChE Journal* 47.7 (2001), pp. 1676–1682. DOI: 10.1002/aic.690470719.

[138] X. Tang and J. Gross. "Modeling the phase equilibria of hydrogen sulfide and carbon dioxide in mixture with hydrocarbons and water using the PCP-SAFT equation of state". In: *Fluid Phase Equilibria* 293.1 (2010), pp. 11–21. DOI: 10.1016/j.fluid.2010.02.004.

[139] S. Ahmed, N. Ferrando, J. C. De Hemptinne, J. P. Simonin, O. Bernard, and O. Baudouin. "A New PC-SAFT Model for Pure Water, Water-Hydrocarbons, and Water-Oxygenates Systems and Subsequent Modeling of VLE, VLLE, and LLE". In: *Journal of Chemical and Engineering Data* 61.12 (2016), pp. 4178–4190. DOI: 10.1021/acs.jced.6b00565.

[140] U. Essmann, L. Perera, M. L. Berkowitz, T. Darden, H. Lee, and L. G. Pedersen. "A smooth particle mesh Ewald method". In: *The Journal of Chemical Physics* 103.19 (1995), pp. 8577–8593. DOI: 10.1063/1.470117.

[141] J. M. Young and A. Z. Panagiotopoulos. "System-Size Dependence of Electrolyte Activity Coefficients in Molecular Simulations". In: *Journal of Physical Chemistry B* 122.13 (2018), pp. 3330–3338. DOI: 10.1021/acs.jpcb.7b09861.

[142] J. D. Chodera. "A Simple Method for Automated Equilibration Detection in Molecular Simulations". In: *Journal of Chemical Theory and Computation* 12.4 (2016), pp. 1799–1805. DOI: 10.1021/acs.jctc.5b00784.

[143] C. R. Harris, K. J. Millman, S. J. van der Walt, R. Gommers, P. Virtanen, D. Cournapeau, E. Wieser, J. Taylor, S. Berg, N. J. Smith, R. Kern, M. Picus, S. Hoyer, M. H. van Kerkwijk, M. Brett, A. Haldane, J. F. del Río, M. Wiebe, P. Peterson, P. Gérard-Marchant, K. Sheppard, T. Reddy, W. Weckesser, H. Abbasi, C. Gohlke, and T. E. Oliphant. *Array programming with NumPy*. 2020. DOI: 10.1038/s41586-020-2649-2.

[144] P. Virtanen et al. "SciPy 1.0: fundamental algorithms for scientific computing in Python". In: *Nature Methods* 17.3 (2020), pp. 261–272. DOI: 10.1038/s41592-019-0686-2.

[145] L. Deng, T.-J. Kim, M. Sandru, and M.-B. Hägg. "PVA/PVAm Blend FSC Membrane for Natural Gas Sweetening". In: *Proceedings of the 1st Annual Gas Processing Symposium*. Elsevier, 2009, pp. 247–255. DOI: 10.1016/b978-0-444-53292-3.50032-8.

[146] P. Zoller and D. J. Walsh. *Standard pressure-volume-temperature data for polymers*. Technomic Pub. Co, 1995, p. 412.

[147] C. A. Angell, K. L. Ngai, G. B. McKenna, P. F. McMillan, and S. W. Martin. "Relaxation in glassforming liquids and amorphous solids". In: *Journal of Applied Physics* 88.6 (2000), pp. 3113–3157. DOI: 10.1063/1.1286035.

[148] P. G. Debenedetti and F. H. Stillinger. *Supercooled liquids and the glass transition*. 2001. DOI: 10.1038/35065704.

[149] D. Trache, M. H. Hussin, C. T. Hui Chuin, S. Sabar, M. R. Fazita, O. F. Taiwo, T. M. Hassan, and M. K. Haafiz. *Microcrystalline cellulose: Isolation, characterization and bio-composites application—A review*. 2016. DOI: 10.1016/j.ijbiomac.2016.09.056.

[150] S. F. Edwards and T. A. Vilgis. "The tube model theory of rubber elasticity". In: *Reports on Progress in Physics* 51.2 (1988), p. 243. DOI: 10.1088/0034-4885/51/2/003.

[151] J. Klein. "Evidence for reptation in an entangled polymer melt". In: *Nature* 271.5641 (1978), pp. 143–145. DOI: 10.1038/271143a0.

[152] F. S. Bates. "Polymer-polymer phase behavior". In: *Science* 4996.251 (1991), pp. 898–905. DOI: 10.1126/science.251.4996.898.

[153] A. A. D'souza and R. Shegokar. "Polyethylene glycol (PEG): a versatile polymer for pharmaceutical applications". In: *Expert Opinion on Drug Delivery* 13.9 (2016), pp. 1257–1275. DOI: 10.1080/17425247.2016.1182485.

[154] K. S. Siow, G. Delmas, and D. Patterson. "Cloud-Point Curves in Polymer Solutions with Adjacent Upper and Lower Critical Solution Temperatures". In: *Macromolecules* 5.1 (1972), pp. 29–34. DOI: 10.1021/ma60025a008.

[155] J. Niskanen and H. Tenhu. *How to manipulate the upper critical solution temperature (UCST)?* 2017. DOI: 10.1039/c6py01612j.

[156] P. J. Flory. "Themodynamics of high polymer solutions". In: *The Journal of Chemical Physics* 10.1 (1942), pp. 51–61. DOI: 10.1063/1.1723621.

[157] M. L. Huggins. "Some properties of solutions of long-chain compounds". In: *Journal of Physical Chemistry* 46.1 (1942), pp. 151–158. DOI: 10.1021/j150415a018.

[158] C. E. Bawn, R. F. Freeman, and A. K. Kamaliddin. "High polymer solutions: Part I. - Vapour pressure of polystyrene solutions". In: *Transactions of the Faraday Society* 46.0 (1950), pp. 677–684. DOI: 10.1039/TF9504600677.

[159] J. P. Ryckaert and A. Bellemans. "Molecular dynamics of liquid n-butane near its boiling point". In: *Chemical Physics Letters* 30.1 (1975), pp. 123–125. DOI: 10.1016/0009-2614(75)85513-8.

[160] J. P. Ryckaert and A. Bellemans. "Molecular dynamics of liquid alkanes". In: *Faraday Discussions of the Chemical Society* 66.0 (1978), pp. 95–106. DOI: 10.1039/DC9786600095.

[161] D. C. Rapaport. "Molecular dynamics simulation of polymer chains with excluded volume". In: *Journal of Physics A: Mathematical and General* 11.8 (1978), p. L213. DOI: 10.1088/0305-4470/11/8/008.

[162] D. C. Rapaport. "Molecular dynamics study of a polymer chain in solution". In: *The Journal of Chemical Physics* 71.8 (1979), pp. 3299–3303. DOI: 10.1063/1.438770.

[163] J. J. Pablo, M. Laso, and U. W. Suter. "Simulation of polyethylene above and below the melting point". In: *Journal of Chemical Physics* 96.3 (1992), pp. 2395–2403. DOI: 10.1063/1.462037.

[164] M. Brodeck, F. Alvarez, A. Arbe, F. Juranyi, T. Unruh, O. Holderer, J. Colmenero, and D. Richter. "Study of the dynamics of poly(ethylene oxide) by combining molecular dynamic simulations and neutron scattering experiments". In: *Journal of Chemical Physics* 130.9 (2009). DOI: 10.1063/1.3077858.

[165] A. H. Widmann, M. Laso, and U. W. Suter. "Optimized atomic Lennard-Jones 6-12 parameters for simulating pVT properties of a realistic polymethylene melt". In: *The Journal of Chemical Physics* 102.14 (1995), pp. 5761–5769. DOI: 10.1063/1.469307.

[166] P. V. Krishna Pant, J. Han, G. D. Smith, and R. H. Boyd. "A molecular dynamics simulation of polyethylene". In: *The Journal of Chemical Physics* 99.1 (1993), pp. 597–604. DOI: 10.1063/1.465731.

[167] B. Rosi-Schwartz and G. R. Mitchell. "A complete atomistic model of molten polyethylene from neutron scattering data: a new methodology for polymer structure". In: *Polymer* 35.25 (1994), pp. 5398–5407. DOI: 10.1016/S0032-3861(05)80002-3.

[168] D. Reith, M. Pütz, and F. Müller-Plathe. "Deriving effective mesoscale potentials from atomistic simulations". In: *Journal of Computational Chemistry* 24.13 (2003), pp. 1624–1636. DOI: 10.1002/jcc.10307.

[169] J. J. de Pablo, M. Laso, U. W. Suter, and H. D. Cochran. "Continuum configurational bias Monte-Carlo studies of alkanes and polyethylene". In: *Fluid Phase Equilibria* 83.C (1993), pp. 323–331. DOI: 10.1016/0378-3812(93)87035-Y.

[170] N. F. Van Der Vegt and W. J. Briels. "Efficient sampling of solvent free energies in polymers". In: *Journal of Chemical Physics* 109.17 (1998), pp. 7578–7582. DOI: 10.1063/1.477379.

[171] N. F. Van Der Vegt, W. J. Briels, M. Wessling, and H. Strathmann. "The sorption induced glass transition in amorphous glassy polymers". In: *Journal of Chemical Physics* 110.22 (1999), pp. 11061–11069. DOI: 10.1063/1.479042.

[172] T. Spyriouni, G. C. Boulougouris, and D. N. Theodorou. "Prediction of sorption of co2 in glassy atactic polystyrene at elevated pressures through a new computational scheme". In: *Macromolecules* 42.5 (2009), pp. 1759–1769. DOI: 10.1021/ma8015294.

[173] N. Vergadou and D. N. Theodorou. *Molecular modeling investigations of sorption and diffusion of small molecules in Glassy polymers*. 2019. DOI: 10.3390/membranes9080098.

[174] L. R. Dodd and D. N. Theodorou. "Atomistic Monte Carlo simulation and continuum mean field theory of the structure and equation of state properties of alkane and polymer melts". In: *Advances in Polymer Science* 116 (1994), pp. 248–281. DOI: 10.1007/bfb0080201.

[175] F. Müller-Plathe and W. F. Van Gunsteren. "Solvation of poly(vinyl alcohol) in water, ethanol and an equimolar water-ethanol mixture: Structure and dynamics studied by molecular dynamics simulation". In: *Polymer* 38.9 (1997), pp. 2259–2268. DOI: 10.1016/S0032-3861(96)00773-2.

[176] F. Müller-Plathe. "Diffusion of water in swollen poly(vinyl alcohol) membranes studied by molecular dynamics simulation". In: *Journal of Membrane Science* 141.2 (1998), pp. 147–154. DOI: 10.1016/S0376-7388(97)00289-5.

[177] J. S. Mackie and P. Meares. *The Diffusion of Electrolytes in a Cation-Exchange Resin Membrane. I. Theoretical*. DOI: 10.2307/99826.

[178] J. S. Mackie and P. Meares. *The Diffusion of Electrolytes in a Cation-Exchange Resin Membrane. II. Experimental*. DOI: 10.2307/99827.

[179] F. Müller-Plathe, S. C. Rogers, and W. F. van Gunsteren. "Computational evidence for anomalous diffusion of small molecules in amorphous polymers". In: *Chemical Physics Letters* 199.3-4 (1992), pp. 237–243. DOI: 10.1016/0009-2614(92)80112-0.

[180] A. A. Gusev, S. Arizzi, U. W. Suter, and D. J. Moll. "Dynamics of light gases in rigid matrices of dense polymers". In: *Journal of Chemical Physics* 99.3 (1993), pp. 2221–2227. DOI: 10.1063/1.465283.

[181] B. Amsden. "Modeling solute diffusion in aqueous polymer solutions". In: *Polymer* 43.5 (2002), pp. 1623–1630. DOI: 10.1016/S0032-3861(01)00749-2.

[182] B. Nick and U. W. Suter. "Solubility of water in polymers-atomistic simulations". In: *Computational and Theoretical Polymer Science* 11.1 (2001), pp. 49–55. DOI: 10.1016/S1089-3156(99)00061-6.

[183] C. Wu. "Cooperative behavior of poly(vinyl alcohol) and water as revealed by molecular dynamics simulations". In: *Polymer* 51.19 (2010), pp. 4452–4460. DOI: 10.1016/j.polymer.2010.07.019.

[184] B. Pae, T. Moon, C. Lee, M. Ko, M. Park, L. Lim, J. Kim, and C. Choe. "Phase Behavior in PVA/Water Solution: The Coexistence of UCST and LCST". In: *Korea Polymer Journal* 5.2 (1997), pp. 126–130.

[185] Z. Qiao, Y. Wu, X. Li, and J. Zhou. "Molecular simulation on the separation of water/ethanol azeotropic mixture by poly(vinyl alcohol) membrane". In: *Fluid Phase Equilibria* 302.1-2 (2011), pp. 14–20. DOI: 10.1016/j.fluid.2010.09.045.

[186] E. Chiessi, F. Cavalieri, and G. Paradossi. "Water and polymer dynamics in chemically cross-linked hydrogels of poly(vinyl alcohol): A molecular dynamics simulation study". In: *Journal of Physical Chemistry B* 111.11 (2007), pp. 2820–2827. DOI: 10.1021/jp0671143.

[187] E. E. Dormidontova*. "Influence of End Groups on Phase Behavior and Properties of PEO in Aqueous Solutions". In: (2004). DOI: 10.1021/MA035609+.

[188] Q. G. Zhang, Q. L. Liu, Y. Chen, J. Y. Wu, and A. M. Zhu. "Microstructure dependent diffusion of water-ethanol in swollen poly(vinyl alcohol): A molecular dynamics simulation study". In: *Chemical Engineering Science* 64.2 (2009), pp. 334–340. DOI: 10.1016/j.ces.2008.10.028.

[189] W. L. Jorgensen, J. D. Madura, and C. J. Swenson. "Optimized Intermolecular Potential Functions for Liquid Hydrocarbons". In: *Journal of the American Chemical Society* 106.22 (1984), pp. 6638–6646. DOI: 10.1021/ja00334a030.

[190] O. Berger, O. Edholm, and F. Jähnig. "Molecular dynamics simulations of a fluid bilayer of dipalmitoylphosphatidylcholine at full hydration, constant pressure, and constant temperature". In: *Biophysical Journal* 72.5 (1997), pp. 2002–2013. DOI: 10.1016/S0006-3495(97)78845-3.

[191] S. Toxvaerd. "Molecular dynamics calculation of the equation of state of alkanes". In: *The Journal of Chemical Physics* 93.6 (1990), pp. 4290–4295. DOI: 10.1063/1.458709.

[192] P. Ungerer, C. Beauvais, J. Delhommelle, A. Boutin, B. Rousseau, and A. H. Fuchs. "Optimization of the anisotropic united atoms intermolecular potential for n-alkanes". In: *Journal of Chemical Physics* 112.12 (2000), pp. 5499–5510. DOI: 10.1063/1.481116.

[193] J. Pérez-Pellitero, E. Bourasseau, I. Demachy, J. Ridard, P. Ungerer, and A. D. Mackie. "Anisotropic United-Atoms (AUA) potential for alcohols". In: *Journal of Physical Chemistry B* 112.32 (2008), pp. 9853–9863. DOI: 10.1021/jp802282p.

[194] N. Ferrando, V. Lachet, J. Pérez-Pellitero, A. D. MacKie, P. Malfreyt, and A. Boutin. "A transferable force field to predict phase equilibria and surface tension of ethers and glycol ethers". In: *Journal of Physical Chemistry B* 115.36 (2011), pp. 10654–10664. DOI: 10.1021/jp203278t.

[195] G. A. Orozco, C. Nieto-Draghi, A. D. MacKie, and V. Lachet. "Transferable force field for equilibrium and transport properties in linear, branched, and bifunctional amines I. Primary amines". In: *Journal of Physical Chemistry B* 115.49 (2011), pp. 14617–14625. DOI: 10.1021/jp207601q.

[196] G. A. Orozco, C. Nieto-Draghi, A. D. MacKie, and V. Lachet. "Transferable force field for equilibrium and transport properties in linear and branched monofunctional and multifunctional amines. II. Secondary and tertiary amines". In: *Journal of Physical Chemistry B* 116.21 (2012), pp. 6193–6202. DOI: 10.1021/jp302972p.

[197] G. A. Orozco, V. Lachet, C. Nieto-Draghi, and A. D. Mackie. "A Transferable Force Field for Primary, Secondary, and Tertiary Alkanolamines". In: *Journal of Chemical Theory and Computation* 9.4 (2013), pp. 2097–2103. DOI: 10.1021/ct301098s.

[198] W. L. Jorgensen and C. J. Swenson. "Optimized Intermolecular Potential Functions for Amides and Peptides. Structure and Properties of Liquid Amides". In: *Journal of the American Chemical Society* 107.3 (1985), pp. 569–578. DOI: 10.1021/ja00289a008.

[199] W. L. Jorgensen. "Optimized intermolecular potential functions for liquid alcohols". In: *Journal of Physical Chemistry* 90.7 (1986), pp. 1276–1284. DOI: 10.1021/j100398a015.

[200] W. L. Jorgensen, J. M. Briggs, and M. Leonor Contreras. "Relative partition coefficients for organic solutes from fluid simulations". In: *Journal of Physical Chemistry* 94.4 (1990), pp. 1683–1686. DOI: 10.1021/j100367a084.

[201] W. L. Jorgensen. "Intermolecular potential functions and Monte Carlo simulations for liquid sulfur compounds". In: *Journal of Physical Chemistry* 90.23 (1986), pp. 6379–6388. DOI: 10.1021/j100281a063.

[202] W. L. Jorgensen, D. S. Maxwell, and J. Tirado-Rives. "Development and Testing of the OPLS All-Atom Force Field on Conformational Energetics and Properties of Organic Liquids". In: *Journal of the American Chemical Society* 118.45 (1996), pp. 11225–11236. DOI: 10.1021/JA9621760.

[203] R. C. Rizzo and W. L. Jorgensen. "OPLS All-Atom Model for Amines: Resolution of the Amine Hydration Problem". In: *Journal of the American Chemical Society* 121.20 (1999), pp. 4827–4836. DOI: 10.1021/JA984106U.

[204] G. A. Kaminski, R. A. Friesner, J. Tirado-Rives, and W. L. Jorgensen. "Evaluation and reparametrization of the OPLS-AA force field for proteins via comparison with accurate quantum chemical calculations on peptides". In: *Journal of Physical Chemistry B* 105.28 (2001), pp. 6474–6487. DOI: 10.1021/jp003919d.

[205] S. W. Siu, K. Pluhackova, and R. A. Böckmann. "Optimization of the OPLS-AA force field for long hydrocarbons". In: *Journal of Chemical Theory and Computation* 8.4 (2012), pp. 1459–1470. DOI: 10.1021/ct200908r.

[206] M. J. Robertson, J. Tirado-Rives, and W. L. Jorgensen. "Improved treatment of nucleosides and nucleotides in the OPLS-AA force field". In: *Chemical Physics Letters* 683 (2017), pp. 276–280. DOI: 10.1016/j.cplett.2017.02.049.

[207] M. G. Martin. "Comparison of the AMBER, CHARMM, COMPASS, GROMOS, OPLS, TraPPE and UFF force fields for prediction of vapor-liquid coexistence curves and liquid densities". In: *Fluid Phase Equilibria* 248.1 (2006), pp. 50–55. DOI: 10.1016/j.fluid.2006.07.014.

[208] M. G. Martin and J. I. Siepmann. "Transferable Potentials for Phase Equilibria. 1. United-Atom Description of n-Alkanes". In: *Journal of Physical Chemistry B* 102.14 (1998), pp. 2569–2577. DOI: 10.1021/JP972543+.

[209] M. G. Martin and J. I. Siepmann. "Novel configurational-bias Monte Carlo method for branched molecules. Transferable potentials for phase equilibria. 2. United-atom description of branched alkanes". In: *Journal of Physical Chemistry B* 103.21 (1999), pp. 4508–4517. DOI: 10.1021/jp984742e.

[210] B. Chen and J. I. Siepmann. "Transferable Potentials for Phase Equilibria. 3. Explicit-Hydrogen Description of Normal Alkanes". In: *Journal of Physical Chemistry B* 103.25 (1999), pp. 5370–5379. DOI: 10.1021/JP990822M.

[211] C. D. Wick, M. G. Martin, and J. I. Siepmann. "Transferable Potentials for Phase Equilibria. 4. United-Atom description of linear and branched alkenes and alkylbenzenes". In: *Journal of Physical Chemistry B* 104.33 (2000), pp. 8008–8016. DOI: 10.1021/jp001044x.

[212] C. D. Wick, J. M. Stubbs, N. Rai, and J. I. Siepmann. "Transferable potentials for phase equilibria. 7. Primary, secondary, and tertiary amines, nitroalkanes and nitrobenzene, nitriles, amides, pyridine, and pyrimidine". In: *Journal of Physical Chemistry B* 109.40 (2005), pp. 18974–18982. DOI: 10.1021/jp0504827.

[213] N. Lubna, G. Kamath, J. J. Potoff, N. Rai, and J. I. Siepmann. "Transferable potentials for phase equilibria. 8. United-atom description for thiols, sulfides, disulfides, and thiophene". In: *Journal of Physical Chemistry B* 109.50 (2005), pp. 24100–24107. DOI: 10.1021/jp0549125.

[214] N. Rai and J. I. Siepmann. "Transferable Potentials for Phase Equilibria. 9. Explicit Hydrogen Description of Benzene and Five-Membered and Six-Membered Heterocyclic Aromatic Compounds". In: *The Journal of Physical Chemistry B* 111.36 (2007), pp. 10790–10799. DOI: 10.1021/jp0735861.

[215] J. Wang, R. M. Wolf, J. W. Caldwell, P. A. Kollman, and D. A. Case. "Development and testing of a general amber force field". In: *Journal of Computational Chemistry* 25.9 (2004), pp. 1157–1174. DOI: 10.1002/jcc.20035.

[216] C. Oostenbrink, A. Villa, A. E. Mark, and W. F. Van Gunsteren. "A biomolecular force field based on the free enthalpy of hydration and solvation: The GROMOS force-field parameter sets 53A5 and 53A6". In: *Journal of Computational Chemistry* 25.13 (2004), pp. 1656–1676. DOI: 10.1002/jcc.20090.

[217] C. Oostenbrink, T. A. Soares, N. F. Van Der Vegt, and W. F. Van Gunsteren. "Validation of the 53A6 GROMOS force field". In: *European Biophysics Journal* 34.4 (2005), pp. 273–284. DOI: 10.1007/s00249-004-0448-6.

[218] N. Schmid, A. P. Eichenberger, A. Choutko, S. Riniker, M. Winger, A. E. Mark, and W. F. Van Gunsteren. "Definition and testing of the GROMOS force-field versions 54A7 and 54B7". In: *European Biophysics Journal* 40.7 (2011), pp. 843–856. DOI: 10.1007/s00249-011-0700-9.

[219] X. Periole and S.-J. Marrink. "The Martini Coarse-Grained Force Field". In: Humana Press, Totowa, NJ, 2013, pp. 533–565. DOI: 10.1007/978-1-62703-017-5{_}20.

[220] H. Lee, A. H. De Vries, S. J. Marrink, and R. W. Pastor. "A coarse-grained model for polyethylene oxide and polyethylene glycol: Conformation and hydrodynamics". In: *Journal of Physical Chemistry B* 113.40 (2009), pp. 13186–13194. DOI: 10.1021/jp9058966.

[221] F. Grunewald, G. Rossi, A. H. De Vries, S. J. Marrink, and L. Monticelli. "Transferable MARTINI Model of Poly(ethylene Oxide)". In: *Journal of Physical Chemistry B* 122.29 (2018), pp. 7436–7449. DOI: 10.1021/acs.jpcb.8b04760.

[222] H. Sun. "Compass: An ab initio force-field optimized for condensed-phase applications - Overview with details on alkane and benzene compounds". In: *Journal of Physical Chemistry B* 102.38 (1998), pp. 7338–7364. DOI: 10.1021/jp980939v.

[223] H. Sun. *Ab Initio Characterizations of Molecular Structures, Conformation Energies, and Hydrogen-Bonding Properties for Polyurethane Hard Segments*. Tech. rep. 1993, pp. 5924–5936.

[224] H. Sun, S. J. Mumby, J. R. Maple, and A. T. Hagler. "An ab Initio CFF93 All-Atom Force Field for Polycarbonates". In: *Journal of the American Chemical Society* 116.7 (1994), pp. 2978–2987. DOI: 10.1021/ja00086a030.

[225] H. Sun. "Force field for computation of conformational energies, structures, and vibrational frequencies of aromatic polyesters". In: *Journal of Computational Chemistry* 15.7 (1994), pp. 752–768. DOI: 10.1002/jcc.540150708.

[226] H. Sun. "Ab Initio Calculations and Force Field Development for Computer Simulation of Polysilanes". In: *Macromolecules* 28.3 (1995), pp. 701–712. DOI: 10.1021/ma00107a006.

[227] H. Sun, S. J. Mumby, J. R. Maple, and A. T. Hagler. "Ab initio calculations on small molecule analogues of polycarbonates". In: *Journal of Physical Chemistry* 99.16 (1995), pp. 5873–5882. DOI: 10.1021/j100016a022.

[228] P. Y. Morgantini and P. A. Kollman. "Solvation Free Energies of Amides and Amines: Disagreement between Free Energy Calculations and Experiment". In: *Journal of the American Chemical Society* 117.22 (1995), pp. 6057–6063. DOI: 10.1021/ja00127a019.

[229] Y. Ding, D. N. Bernardo, K. Krogh-Jespersen, and R. M. Levy. "Solvation free energies of small amides and amines from molecular dynamics/free energy perturbation simulations using pairwise additive and many-body polarizable potentials". In: *Journal of Physical Chemistry* 99.29 (1995), pp. 11575–11583. DOI: 10.1021/j100029a040.

[230] E. C. Meng, J. W. Caldwell, and P. A. Kollman. "Investigating the anomalous solvation free energies of amines with a polarizable potential". In: *Journal of Physical Chemistry* 100.6 (1996), pp. 2367–2371. DOI: 10.1021/jp952463a.

[231] B. Marten, K. Kim, C. Cortis, R. A. Friesner, R. B. Murphy, M. N. Ringnalda, D. Sitkoff, and B. Honig. "New model for calculation of solvation free energies: Correction of self-consistent reaction field continuum dielectric theory for short-range hydrogen-bonding effects". In: *Journal of Physical Chemistry* 100.28 (1996), pp. 11775–11788. DOI: 10.1021/jp953087x.

[232] H. Hesske and K. Gloe. "Hydration behavior of alkyl amines and their corresponding protonated forms. 1. Ammonia and methylamine". In: *Journal of Physical Chemistry A* 111.39 (2007), pp. 9848–9853. DOI: 10.1021/jp073154a.

[233] C. Oostenbrink, D. Juchli, and W. F. van Gunsteren. "Amine Hydration: A United-Atom Force-Field Solution". In: *ChemPhysChem* 6.9 (2005), pp. 1800–1804. DOI: 10.1002/cphc.200400542.

[234] D. S. Maxwell, J. Tirado-Rives, and W. L. Jorgensen. "A comprehensive study of the rotational energy profiles of organic systems byab initio MO theory, forming a basis for peptide torsional parameters". In: *Journal of Computational Chemistry* 16.8 (1995), pp. 984–1010. DOI: 10.1002/jcc.540160807.

[235] N. L. Allinger, U. Burkert, and S. Profeta. "Ab initio calculations of the rotational potential functions for propylamine and ethylmethylamine". In: *Journal of Computational Chemistry* 1.3 (1980), pp. 281–284. DOI: 10.1002/jcc.540010310.

[236] D. Zeroka, J. O. Jensen, and A. C. Samuels. "Rotation/inversion study of the amino group in ethylamine". In: *Journal of Physical Chemistry A* 102.32 (1998), pp. 6571–6579. DOI: 10.1021/jp982031a.

[237] L. A. de Carvalho and J. J. Teixeira-Dias. "Ab initio MO conformational study of ethylmethylamine". In: *Journal of Molecular Structure: THEOCHEM* 282.3 (1993), pp. 199–209. DOI: 10.1016/0166-1280(93)85003-H.

[238] L. A. de Carvalho and J. J. Teixeira-Dias. "Conformational analysis of dimethylethylamine: an ab initio MO study and comparison with ethylamine and ethylmethylamine". In: *Journal of Molecular Structure: THEOCHEM* 282.3 (1993), pp. 211–221. DOI: 10.1016/0166-1280(93)85004-I.

[239] C. Wohlfarth. *CRC handbook of phase equilibria and thermodynamic data of aqueous polymer solutions*. Taylor & Francis, 2012.

[240] P. M. Budd, N. B. McKeown, B. S. Ghanem, K. J. Msayib, D. Fritsch, L. Starannikova, N. Belov, O. Sanfirova, Y. Yampolskii, and V. Shantarovich. "Gas permeation parameters and other physicochemical properties of a polymer of intrinsic microporosity: Polybenzodioxane PIM-1". In: *Journal of Membrane Science* 325.2 (2008), pp. 851–860. DOI: 10.1016/j.memsci.2008.09.010.

[241] F. T. Peters, F. S. Laube, and G. Sadowski. "Development of a group contribution method for polymers within the PC-SAFT model". In: *Fluid Phase Equilibria* 324 (2012), pp. 70–79. DOI: 10.1016/j.fluid.2012.03.009.

[242] F. T. Peters, M. Herhut, and G. Sadowski. "Extension of the PC-SAFT based group contribution method for polymers to aromatic, oxygen- and silicon-based polymers". In: *Fluid Phase Equilibria* 339 (2013), pp. 89–104. DOI: 10.1016/j.fluid.2012.11.031.

[243] C. Wohlfarth. *CRC Handbook of Phase Equilibria and Thermodynamic Data of Aqueous Polymer Solutions*. Boca Raton: CRC Press, 2019.

[244] S. L. Liu, L. Shao, M. L. Chua, C. H. Lau, H. Wang, and S. Quan. "Recent progress in the design of advanced PEO-containing membranes for CO2 removal". In: *Progress in Polymer Science* 38.7 (2013), pp. 1089–1120. DOI: 10.1016/j.progpolymsci.2013.02.002.

[245] A. Car, C. Stropnik, W. Yave, and K. V. Peinemann. "PEG modified poly(amide-b-ethylene oxide) membranes for CO2 separation". In: *Journal of Membrane Science* 307.1 (2008), pp. 88–95. DOI: 10.1016/j.memsci.2007.09.023.

[246] J. E. Shin, S. K. Lee, Y. H. Cho, and H. B. Park. "Effect of PEG-MEA and graphene oxide additives on the performance of Pebax®1657 mixed matrix membranes for CO2 separation". In: *Journal of Membrane Science* 572 (2019), pp. 300–308. DOI: 10.1016/j.memsci.2018.11.025.

[247] A. C. French, A. L. Thompson, and B. G. Davis. "High-Purity Discrete PEG-Oligomer Crystals Allow Structural Insight". In: *Angewandte Chemie International Edition* 48.7 (2009), pp. 1248–1252. DOI: 10.1002/anie.200804623.

[248] H. S. Byun and B. S. Lee. "Liquid-liquid equilibrium of hydrogen bonding polymer solutions". In: *Polymer* 121 (2017), pp. 1–8. DOI: 10.1016/j.polymer.2017.06.012.

[249] N. R. Nannan, C. M. De Servi, T. Van Der Stelt, P. Colonna, and A. Bardow. "An equation of state based on PC-SAFT for physical solvents composed of polyethylene glycol dimethylethers". In: *Industrial and Engineering Chemistry Research* 52.51 (2013), pp. 18401–18412. DOI: 10.1021/ie401456q.

[250] F. Gao and L. Han. "Implementing the Nelder-Mead simplex algorithm with adaptive parameters". In: *Computational Optimization and Applications* 51.1 (2012), pp. 259–277. DOI: 10.1007/s10589-010-9329-3.

[251] T. S. Gaaz, A. B. Sulong, M. N. Akhtar, A. A. H. Kadhum, A. B. Mohamad, A. A. Al-Amiery, and D. J. McPhee. *Properties and applications of polyvinyl alcohol, halloysite nanotubes and their nanocomposites*. 2015. DOI: 10.3390/molecules201219884.

[252] J. Torstensen, R. M. Helberg, L. Deng, Ø. W. Gregersen, and K. Syverud. "PVA/nanocellulose nanocomposite membranes for CO2 separation from flue gas". In: *International Journal of Greenhouse Gas Control* 81 (2019), pp. 93–102. DOI: 10.1016/j.ijggc.2018.10.007.

[253] R. Xing and W. S. Ho. "Synthesis and characterization of crosslinked polyvinylalcohol/polyethyleneglycol blend membranes for CO2/CH4 separation". In: *Journal of the Taiwan Institute of Chemical Engineers* 40.6 (2009), pp. 654–662. DOI: 10.1016/j.jtice.2009.05.004.

[254] M. Barooah and B. Mandal. "Enhanced CO 2 separation performance by PVA/PEG/silica mixed matrix membrane". In: *Journal of Applied Polymer Science* 135.28 (2018), p. 46481. DOI: 10.1002/app.46481.

[255] L. Deng and M. B. Hägg. "Carbon nanotube reinforced PVAm/PVA blend FSC nanocomposite membrane for CO2/CH4 separation". In: *International Journal of Greenhouse Gas Control* 26 (2014), pp. 127–134. DOI: 10.1016/j.ijggc.2014.04.018.

[256] M. Omidkhah. "Facilitated Transport of CO2 through EA-Mediated Poly(Vinyl alcohol)Membrane Cross-Linked by Formaldehyde". In: *Journal of Membrane Science & Technology* 03.01 (2013), pp. 1–6. DOI: 10.4172/2155-9589.1000119.

[257] M. Krumova, D. López, R. Benavente, C. Mijangos, and J. M. Pereña. "Effect of crosslinking on the mechanical and thermal properties of poly(vinyl alcohol)". In: *Polymer* 41.26 (2000), pp. 9265–9272. DOI: 10.1016/S0032-3861(00)00287-1.

[258] K. A. M. Abd El-Kader and S. F. Abdel Hamied. "Preparation of poly(vinyl alcohol) films with promising physical properties in comparison with commercial polyethylene film". In: *Journal of Applied Polymer Science* 86.5 (2002), pp. 1219–1226. DOI: 10.1002/app.11068.

[259] P. Song, Z. Xu, Y. Lu, and Q. Guo. "Bioinspired strategy for tuning thermal stability of PVA via hydrogen-bond crosslink". In: *Composites Science and Technology* 118 (2015), pp. 16–22. DOI: 10.1016/j.compscitech.2015.08.006.

[260] A. Katchalsky, J. Mazur, and P. Spitnik. "SECTION II: Polybase properties of polyvinylamine". In: *Journal of Polymer Science* 23.104 (1957), pp. 513–532. DOI: 10.1002/pol.1957.1202310401.

[261] R. K. Pinschmidt. "Polyvinylamine at last". In: *Journal of Polymer Science Part A: Polymer Chemistry* 48.11 (2010), pp. 2257–2283. DOI: 10.1002/pola.23992.

[262] R. Pelton. "Polyvinylamine: A tool for engineering interfaces". In: *Langmuir* 30.51 (2014), pp. 15373–15382. DOI: 10.1021/la5017214.

[263] T. J. Kim, L. I. Baoan, and M. B. Hägg. "Novel fixed-site-carrier polyvinylamine membrane for carbon dioxide capture". In: *Journal of Polymer Science, Part B: Polymer Physics* 42.23 (2004), pp. 4326–4336. DOI: 10.1002/polb.20282.

[264] M. Sandru, T. J. Kim, and M. B. Hägg. "High molecular fixed-site-carrier PVAm membrane for CO2 capture". In: *Desalination* 240.1-3 (2009), pp. 298–300. DOI: 10.1016/j.desal.2008.01.053.

[265] M. Washim Uddin and M. B. Hägg. "Effect of monoethylene glycol and triethylene glycol contamination on CO 2/CH 4 separation of a facilitated transport membrane for natural gas sweetening". In: *Journal of Membrane Science* 423-424 (2012), pp. 150–158. DOI: 10.1016/j.memsci.2012.08.011.

[266] T. J. Kim, H. Vrålstad, M. Sandru, and M. B. Hägg. "Separation performance of PVAm composite membrane for CO2 capture at various pH levels". In: *Journal of Membrane Science* 428 (2013), pp. 218–224. DOI: 10.1016/j.memsci.2012.10.009.

[267] L. Deng and M. B. Hägg. "Fabrication and Evaluation of a Blend Facilitated Transport Membrane for CO2/CH4 Separation". In: *Industrial and Engineering Chemistry Research* 54.44 (2015), pp. 11139–11150. DOI: 10.1021/acs.iecr.5b02971.

[268] C. Dong, Z. Wang, C. Yi, and S. Wang. "Preparation of polyvinylamine/polysulfone composite hollow-fiber membranes and their CO2/CH4 separation performance". In: *Journal of Applied Polymer Science* 101.3 (2006), pp. 1885–1891. DOI: 10.1002/app.23342.

[269] Z. Qiao, Z. Wang, S. Yuan, J. Wang, and S. Wang. "Preparation and characterization of small molecular amine modified PVAm membranes for CO2/H2 separation". In: *Journal of Membrane Science* 475 (2015), pp. 290–302. DOI: 10.1016/j.memsci.2014.10.034.

[270] J. Liao, Z. Wang, C. Gao, M. Wang, K. Yan, X. Xie, S. Zhao, J. Wang, and S. Wang. "A high performance PVAm-HT membrane containing high-speed facilitated transport channels for CO2 separation". In: *Journal of Materials Chemistry A* 3.32 (2015), pp. 16746–16761. DOI: 10.1039/C5TA03238E.

[271] Y. Zhao and W. S. Winston Ho. "Steric hindrance effect on amine demonstrated in solid polymer membranes for CO 2 transport". In: *Journal of Membrane Science* 415-416 (2012), pp. 132–138. DOI: 10.1016/j.memsci.2012.04.044.

[272] R. Rea and S. Ligi. *Personal communication*. 2018.

[273] J. N. Spencer, W. S. Wolbach, J. W. Hovick, L. Ansel, and K. J. Modarress. "Hydrogen bonding by alcohols and amines". In: *Journal of Solution Chemistry* 14.11 (1985), pp. 805–814. DOI: 10.1007/BF00646002.

[274] Y. C. Bae, S. M. Lambert, D. S. Soane, and J. M. Prausnitz. "Cloud-Point Curves of Polymer Solutions from Thermooptical Measurements". In: *Macromolecules* 24 (1991), pp. 4403–4407.

[275] S. A. Deshmukh, S. K. Sankaranarayanan, K. Suthar, and D. C. Mancini. "Role of solvation dynamics and local ordering of water in inducing conformational transitions in poly(N -isopropylacrylamide) oligomers through the LCST". In: *Journal of Physical Chemistry B* 116.9 (2012), pp. 2651–2663. DOI: 10.1021/jp210788u.

[276] J. R. Espinosa, E. Sanz, C. Valeriani, and C. Vega. "Homogeneous ice nucleation evaluated for several water models". In: *Journal of Chemical Physics* 141.18 (2014), pp. 18–529. DOI: 10.1063/1.4897524.

[277] V. Crupi, M. P. Jannelli, S. Magazu', G. Maisano, D. Majolino, P. Migliardo, and R. Ponterio. "Raman spectroscopic study of water in the poly(ethylene glycol) hydration shell". In: *Journal of Molecular Structure* 381.1-3 (1996), pp. 207–212. DOI: 10.1016/0022-2860(96)09308-8.

[278] C. Branca, S. Magazù, G. Maisano, F. Migliardo, P. Migliardo, and G. Romeo. "Hydration study of PEG/water mixtures by quasi elastic light scattering, acoustic and rheological measurements". In: *Journal of Physical Chemistry B* 106.39 (2002), pp. 10272–10276. DOI: 10.1021/jp014345v.

[279] S. P. Teng and T. T. Teng. "Measurement and Prediction of the Density of Aqueous Multicomponent Solutions Involving Polyethylene Glycol 2000". In: *Journal of Chemical Engineering of Japan* 37.1 (2004), pp. 40–44. DOI: 10.1252/jcej.37.40.

[280] M. Mohsen-Nia, H. Modarress, and H. Rasa. "Measurement and modeling of density, kinematic viscosity, and refractive index for poly(ethylene glycol) aqueous solution at different temperatures". In: *Journal of Chemical and Engineering Data* 50.5 (2005), pp. 1662–1666. DOI: 10.1021/je050130t.

[281] T. Murugesan and M. Perumalsamy. "Densities and viscosities of polyethylene glycol 2000 + salt + water systems from (298.15 to 318.15) K". In: *Journal of Chemical and Engineering Data* 50.4 (2005), pp. 1290–1293. DOI: 10.1021/je050035k.

[282] S. K. Kushare, S. S. Terdale, D. H. Dagade, and K. J. Patil. "Compressibility and volumetric studies of polyethylene-glycols in aqueous, methanolic, and benzene solutions at T = 298.15 K". In: *Journal of Chemical Thermodynamics* 39.8 (2007), pp. 1125–1131. DOI: 10.1016/j.jct.2007.01.006.

[283] S. Trivedi, C. Bhanot, and S. Pandey. "Densities of {poly(ethylene glycol) + water} over the temperature range (283.15 to 363.15) K". In: *Journal of Chemical Thermodynamics* 42.11 (2010), pp. 1367–1371. DOI: 10.1016/j.jct.2010.06.001.

[284] A. Salabat and A. Mehrdad. "Viscometric and volumetric study of dilute aqueous solutions of binary and ternary poly(ethylene glycol)/poly(vinyl alcohol) systems at different temperatures". In: *Journal of Molecular Liquids* 157.1 (2010), pp. 57–60. DOI: 10.1016/j.molliq.2010.08.009.

[285] K. Zhang, J. Yang, X. Yu, J. Zhang, and X. Wei. "Densities and viscosities for binary mixtures of poly(ethylene glycol) 400 + dimethyl sulfoxide and poly(ethylene glycol) 600 + water at different temperatures". In: *Journal of Chemical and Engineering Data* 56.7 (2011), pp. 3083–3088. DOI: 10.1021/je200148u.

[286] R. Sadeghi, R. Hosseini, and B. Jamehbozorg. "Effect of sodium phosphate salts on the thermodynamic properties of aqueous solutions of poly(ethylene oxide) 6000 at different temperatures". In: *Journal of Chemical Thermodynamics* 40.9 (2008), pp. 1364–1377. DOI: 10.1016/j.jct.2008.05.007.

[287] A. Eliassi and H. Modarress. "Excess volume of polymer/solvent mixtures and proposed model for prediction of activity of solvents based on excess volume data". In: *Journal of Applied Polymer Science* 95.5 (2005), pp. 1219–1227. DOI: 10.1002/app.21314.

[288] M. Herskowltz and M. Gottlieb. "Vapor-Liquid Equilibrium in Aqueous Solutions of Various Glycols and Poly (ethylene glycols). 3. Poly (ethylene glycols)". In: *Journal of Chemical and Engineering Data* 30.2 (1985), pp. 233–234. DOI: 10.1021/je00040a033.

[289] M. Herskowltz and M. Gottlieb. "Vapor-Liquid Equilibrium in Aqueous Solutions of Various Glycols and Poly (ethylene glycols). 2. Tetraethylene Glycol and Estimation of UNIFAC Parameters". In: *Journal of Chemical and Engineering Data* 29.4 (1984), pp. 450–452. DOI: 10.1021/je00038a025.

[290] R. Sadeghi and Y. Shahebrahimi. "Vapor pressure osmometry determination of solvent activities of different aqueous and nonaqueous polymer solutions at 318.15 K". In: *Journal of Chemical and Engineering Data* 56.6 (2011), pp. 2946–2954. DOI: 10.1021/je200176t.

[291] R. Sadeghi and Y. Shahebrahimi. "Vapor-liquid equilibria of aqueous polymer solutions from vapor-pressure osmometry and isopiestic measurements". In: *Journal of Chemical and Engineering Data* 56.4 (2011), pp. 789–799. DOI: 10.1021/je100178s.

[292] R. Sadeghi and F. Ziamajidi. "Water activities of ternary mixtures of poly(ethylene glycol), NaCl and water over the temperature range of 293.15 K to 313.15 K". In: *Journal of Chemical Thermodynamics* 38.11 (2006), pp. 1335–1343. DOI: 10.1016/j.jct.2006.02.003.

[293] M. T. Zafarani-Moattar, S. Hamzehzadeh, and S. Hosseinzadeh. "Phase diagrams for liquid-liquid equilibrium of ternary poly(ethylene glycol) + di-sodium tartrate aqueous system and vapor-liquid equilibrium of constituting binary aqueous systems at T = (298.15, 308.15, and 318.15) K Experiment and correlation". In: *Fluid Phase Equilibria* 268.1-2 (2008), pp. 142–152. DOI: 10.1016/j.fluid.2008.03.010.

[294] L. Ninni, M. S. Camargo, and A. J. Meirelles. "Water activity in poly(ethylene glycol) aqueous solutions". In: *Thermochimica Acta* 328.1-2 (1999), pp. 169–176. DOI: 10.1016/s0040-6031(98)00638-8.

[295] R. Sadeghi and F. Ziamajidi. "Thermodynamic properties of aqueous polypropylene oxide 400 solutions from isopiestic measurements over a range of temperatures". In: *Fluid Phase Equilibria* 249.1-2 (2006), pp. 165–172. DOI: 10.1016/j.fluid.2006.09.028.

[296] N. A. Peppas. "Infrared spectroscopy of semicrystalline poly(vinyl alcohol) networks". In: *Die Makromolekulare Chemie* 178.2 (1977), pp. 595–601. DOI: 10.1002/macp.1977.021780228.

[297] R. Iwamoto, M. Miya, and S. Mima. "Determination of crystallinity of swollen poly(vinyl alcohol) by laser Raman spectroscopy". In: *Journal of Polymer Science: Polymer Physics Edition* 17.9 (1979), pp. 1507–1515. DOI: 10.1002/pol.1979.180170904.

[298] R. M. Hodge, G. H. Edward, and G. P. Simon. "Water absorption and states of water in semicrystalline poly(vinyl alcohol) films". In: *Polymer* 37.8 (1996), pp. 1371–1376. DOI: 10.1016/0032-3861(96)81134-7.

[299] A. Molisso, G. Mangiapia, G. D'Errico, and R. Sartorio. "Interaction of Poly(vinyl alcohol) with Poly(acrylic acid) and with Sodium Polyacrylate in Aqueous Solutions: A Volumetric Study at 25°C". In: *Journal of Solution Chemistry* 39.11 (2010), pp. 1627–1635. DOI: 10.1007/s10953-010-9615-9.

[300] J. Kim, K. C. Joung, S. Hwang, W. Huh, C. S. Lee, and K. P. Yoo. "Measurement of vapor sorption equilibria of polymer solutions and comparative correlation by GE-models and lattice equations of state". In: *Korean Journal of Chemical Engineering* 15.2 (1998), pp. 199–210. DOI: 10.1007/BF02707073.

[301] C. Panayiotou and J. H. Vera. "Statistical thermodynamics of r-mer fluids and their mixtures". In: *Polymer Journal* 14.9 (1982), pp. 681–694. DOI: 10.1295/polymj.14.681.

[302] A. Striolo and J. M. Prausnitz. "Vapor-liquid equilibria for some concentrated aqueous polymer solutions". In: *Polymer* 41.3 (2000), pp. 1109–1117. DOI: 10.1016/S0032-3861(99)00256-6.

[303] T. Hino, S. M. Lambert, D. S. Soane, and J. M. Prausnitz. "Lattice thermodynamics for binary closed-loop equilibria: Ordinary and polymer systems". In: *AIChE Journal* 39.5 (1993), pp. 837–845. DOI: 10.1002/aic.690390512.

[304] J. E. Palamara, J. M. Zielinski, M. Hamedi, J. L. Duda, and R. P. Danner. "Vapor-liquid equilibria of water, methanol, and methyl acetate in poly(vinyl acetate) and partially and fully hydrolyzed poly(vinyl alcohol)". In: *Macromolecules* 37.16 (2004), pp. 6189–6196. DOI: 10.1021/ma049666u.

[305] K. F. Csáki, M. Nagy, and F. Csempesz. "Influence of the chain composition on the thermodynamic properties of binary and ternary polymer solutions". In: *Langmuir* 21.2 (2005), pp. 761–766. DOI: 10.1021/la047827h.

[306] E. E. Shafee and H. F. Naguib. "Water sorption in cross-linked poly(vinyl alcohol) networks". In: *Polymer* 44.5 (2003), pp. 1647–1653. DOI: 10.1016/S0032-3861(02)00865-0.

[307] K.-D. Suh, Y.-C. Bae, J.-W. Kim, and S. Kobayashi. "Swelling of poly(vinyl amine) gels: applicability of the Donnan theory". In: *Journal of Macromolecular Science, Part A* 36.4 (1999), pp. 507–516. DOI: 10.1081/MA-100101545.

[308] P. W. Atkins and A. J. MacDermott. "The born equation and ionic solvation". In: *Journal of Chemical Education* 59.4 (1982), pp. 359–360. DOI: 10.1021/ed059p359.

[309] J. Burgess. *Metal Ions in Solution*. 1st ed. John Wiley & Sons, 1978.

[310] E. Hückel and P. Debye. "Zur theorie der elektrolyte. I. gefrierpunktserniedrigung und verwandte erscheinungen". In: *Physikalische Zeitschrift. 24: 185–206.* 24 (1923), pp. 185–206.

[311] P. Debye and P. Hückel. "Zur theorie der elektrolyte. II. Das Grenzgesetz für die elektrische Leitfähigkeit". In: *Physikalische Zeitschrift* 24 (1923), pp. 305–325.

[312] G. M. Kontogeorgis, B. Maribo-Mogensen, and K. Thomsen. "The Debye-Hückel theory and its importance in modeling electrolyte solutions". In: *Fluid Phase Equilibria* 462 (2018), pp. 130–152. DOI: 10.1016/j.fluid.2018.01.004.

[313] F. Moučka, I. Nezbeda, and W. R. Smith. "Molecular simulation of aqueous electrolytes: Water chemical potential results and Gibbs-Duhem equation consistency tests". In: *Journal of Chemical Physics* 139.12 (2013), p. 124505. DOI: 10.1063/1.4821153.

[314] W. J. Hamer and Y. Yung chi. "Osmotic Coefficients and Mean Activity Coefficients of Uni univalent Electrolytes in Water at 25°C". In: *Journal of Physical and Chemical Reference Data* 1.4 (1972), pp. 1047–1100. DOI: 10.1063/1.3253108.

[315] K. S. Pitzer. "Thermodynamics of electrolytes. I. Theoretical basis and general equations". In: *The Journal of Physical Chemistry* 77.2 (1973), pp. 268–277. DOI: 10.1021/j100621a026.

[316] K. S. Pitzer and G. Mayorga. "Thermodynamics of electrolytes. II. Activity and osmotic coefficients for strong electrolytes with one or both ions univalent". In: *The Journal of Physical Chemistry* 77.19 (1973), pp. 2300–2308. DOI: 10.1021/j100638a009.

[317] K. S. Pitzer and G. Mayorga. "Thermodynamics of Electrolytes. III. Activity and Osmotic Coefficients for 2-2 Electrolytes". In: *Journal of Solution Chemistry* 3.7 (1974).

[318] K. S. Pitzer and J. J. Kim. "Thermodynamics of Electrolytes.: IV. Activity and Osmotic Coefficients for Mixed Electrolytes". In: (1993), pp. 413–419. DOI: 10.1142/9789812795960{_}0060.

[319] K. S. Pitzer. "Thermodynamics of Electrolytes. V. Effects of Higher-Order Electrostatic Terms". In: *Journal of Solution Chemistry* 4.3 (1975).

[320] K. S. Pitzer and L. F. Silvester. " Thermodynamics of Electrolytes.: VI. Weak Electrolytes Including H 3 PO 4 ". In: (1993), pp. 437–446. DOI: 10.1142/9789812795960{_}0062.

[321] S. Lindenbaum and G. E. Boyd. "Osmotic and Activity Coefficients for the Symmetrical Tetraalkyl Ammonium Halides in Aqueous Solution at 25° 1". In: *The Journal of Physical Chemistry* 68.4 (1964), pp. 911–917. DOI: 10.1021/j100786a038.

[322] C. W. Davies. "397. The extent of dissociation of salts in water. Part VIII. An equation for the mean ionic activity coefficient of an electrolyte in water, and a revision of the dissociation constants of some sulphates". In: *Journal of the Chemical Society (Resumed)* 0 (1938), pp. 2093–2098. DOI: 10.1039/JR9380002093.

[323] E. A. Guggenheim and J. C. Turgeon. "Specific interaction of ions". In: *Transactions of the Faraday Society* 51.0 (1955), pp. 747–761. DOI: 10.1039/tf9555100747.

[324] D. Rowland, E. Königsberger, G. Hefter, and P. M. May. "Aqueous electrolyte solution modelling: Some limitations of the Pitzer equations". In: *Applied Geochemistry* 55 (2015), pp. 170–183. DOI: 10.1016/j.apgeochem.2014.09.021.

[325] L. F. Cameretti, G. Sadowski, and J. M. Mollerup. "Modeling of aqueous electrolyte solutions with perturbed-chain statistical associated fluid theory". In: *Industrial and Engineering Chemistry Research* 44.9 (2005), pp. 3355–3362. DOI: 10.1021/ie0488142.

[326] C. Held, T. Reschke, S. Mohammad, A. Luza, and G. Sadowski. "ePC-SAFT revised". In: *Chemical Engineering Research and Design* 92.12 (2014), pp. 2884–2897. DOI: 10.1016/j.cherd.2014.05.017.

[327] W. B. Floriano and M. A. C. Nascimento. "Dielectric constant and density of water as a function of pressure at constant temperature". In: *Brazilian Journal of Physics* 34.1 (2004), pp. 38–41. DOI: 10.1590/S0103-97332004000100006.

[328] W. Yan, S. Huang, and E. H. Stenby. "Measurement and modeling of CO2 solubility in NaCl brine and CO2-saturated NaCl brine density". In: *International Journal of Greenhouse Gas Control* 5.6 (2011), pp. 1460–1477. DOI: 10.1016/j.ijggc.2011.08.004.

[329] C. Held, A. Prinz, V. Wallmeyer, and G. Sadowski. "Measuring and modeling alcohol/salt systems". In: *Chemical Engineering Science* 68.1 (2012), pp. 328–339. DOI: 10.1016/j.ces.2011.09.040.

[330] M. Sadeghi, C. Held, A. Samieenasab, C. Ghotbi, M. J. Abdekhodaie, V. Taghikhani, and G. Sadowski. "Thermodynamic properties of aqueous salt containing urea solutions". In: *Fluid Phase Equilibria* 325 (2012), pp. 71–79. DOI: 10.1016/j.fluid.2012.04.003.

[331] C. Held, T. Reschke, R. Müller, W. Kunz, and G. Sadowski. "Measuring and modeling aqueous electrolyte/amino-acid solutions with ePC-SAFT". In: *Journal of Chemical Thermodynamics* 68 (2014), pp. 1–12. DOI: 10.1016/j.jct.2013.08.018.

[332] M. Uyan, G. Sieder, T. Ingram, and C. Held. "Predicting CO2solubility in aqueous N-methyldiethanolamine solutions with ePC-SAFT". In: *Fluid Phase Equilibria* 393 (2015), pp. 91–100. DOI: 10.1016/j.fluid.2015.02.026.

[333] A. Wangler, G. Sieder, T. Ingram, M. Heilig, and C. Held. "Prediction of CO2 and H2S solubility and enthalpy of absorption in reacting N-methyldiethanolamine /water systems with ePC-SAFT". In: *Fluid Phase Equilibria* 461 (2018), pp. 15–27. DOI: 10.1016/j.fluid.2017.12.033.

[334] J. G. Kirkwood. "On the theory of dielectric polarization". In: *The Journal of Chemical Physics* 4.9 (1936), pp. 592–601. DOI: 10.1063/1.1749911.

[335] J. G. Kirkwood. "The dielectric polarization of polar liquids". In: *The Journal of Chemical Physics* 7.10 (1939), pp. 911–919. DOI: 10.1063/1.1750343.

[336] G. Oster and J. G. Kirkwood. "The influence of hindered molecular rotation on the dielectric constants of water, alcohols, and other polar liquids". In: *The Journal of Chemical Physics* 11.4 (1943), pp. 175–178. DOI: 10.1063/1.1723823.

[337] L. Sun, X. Liang, N. von Solms, and G. M. Kontogeorgis. "Modeling Tetra-n-butyl ammonium halides aqueous solutions with the electrolyte cubic plus association equation of state". In: *Fluid Phase Equilibria* 486 (2019), pp. 37–47. DOI: 10.1016/j.fluid.2018.12.033.

[338] L. Sun, X. Liang, N. von Solms, and G. M. Kontogeorgis. "Thermodynamic modeling of gas solubility in aqueous solutions of quaternary ammonium salts with the e-CPA equation of state". In: *Fluid Phase Equilibria* 507 (2020), p. 112423. DOI: 10.1016/j.fluid.2019.112423.

[339] J. K. Percus and G. J. Yevick. "Hard-core insertion in the many-body problem". In: *Physical Review* 136.1B (1964), B290. DOI: 10.1103/PhysRev.136.B290.

[340] J. L. Lebowitz and J. K. Percus. "Mean spherical model for lattice gases with extended hard cores and continuum fluids". In: *Physical Review* 144.1 (1966), pp. 251–258. DOI: 10.1103/PhysRev.144.251.

[341] L. Blum. "Solution of the mean spherical approximation for hard ions and dipoles of arbitrary size". In: *Journal of Statistical Physics* 18.5 (1978), pp. 451–474. DOI: 10.1007/BF01014518.

[342] L. Blum and D. Q. Wei. "Analytical solution of the mean spherical approximation for an arbitrary mixture of ions in a dipolar solvent". In: *The Journal of Chemical Physics* 87.1 (1987), pp. 555–565. DOI: 10.1063/1.453604.

[343] D. Wei and L. Blum. "The mean spherical approximation for an arbitrary mixture of ions in a dipolar solvent: Approximate solution, pair correlation functions, and thermodynamics". In: *The Journal of Chemical Physics* 87.5 (1987), pp. 2999–3007. DOI: 10.1063/1.453036.

[344] L. Blum, F. Vericat, and W. R. Fawcett. "On the mean spherical approximation for hard ions and dipoles". In: *The Journal of Chemical Physics* 96.4 (1992), pp. 3039–3044. DOI: 10.1063/1.462001.

[345] W. B. Liu, Y. G. Li, and J. F. Lu. "A new equation of state for real aqueous ionic fluids based on electrolyte perturbation theory, mean spherical approximation and statistical associating fluid theory". In: *Fluid Phase Equilibria* 158-160 (1999), pp. 595–606. DOI: 10.1016/s0378-3812(99)00082-5.

[346] B. S. Lee and K. C. Kim. "Modeling of aqueous electrolyte solutions based on perturbed-chain statistical associating fluid theory incorporated with primitive mean spherical approximation". In: *Korean Journal of Chemical Engineering* 26.6 (2009), pp. 1733–1747. DOI: 10.1007/s11814-009-0286-4.

[347] S. Herzog, J. Gross, and W. Arlt. "Equation of state for aqueous electrolyte systems based on the semirestricted non-primitive mean spherical approximation". In: *Fluid Phase Equilibria* 297.1 (2010), pp. 23–33. DOI: 10.1016/j.fluid.2010.05.024.

[348] J. Li, C. He, C. Peng, H. Liu, Y. Hu, and P. Paricaud. "Modeling of the thermodynamic properties of aqueous ionic liquid solutions with an equation of state for square-well chain fluid with variable range". In: *Industrial and Engineering Chemistry Research* 50.11 (2011), pp. 7027–7040. DOI: 10.1021/ie102156m.

[349] G. Das, S. Hlushak, and C. McCabe. "A SAFT-VR+DE equation of state based approach for the study of mixed dipolar solvent electrolytes". In: *Fluid Phase Equilibria* 416 (2016), pp. 72–82. DOI: 10.1016/j.fluid.2015.11.027.

[350] D. K. Eriksen, G. Lazarou, A. Galindo, G. Jackson, C. S. Adjiman, and A. J. Haslam. "Development of intermolecular potential models for electrolyte solutions using an electrolyte SAFT-VR Mie equation of state". In: *Molecular Physics* 114.18 (2016), pp. 2724–2749. DOI: 10.1080/00268976.2016.1236221. URL: https://www.tandfonline.com/doi/full/10.1080/00268976.2016.1236221.

[351] S. Reiser, M. Horsch, and H. Hasse. "Density of Methanolic Alkali Halide Salt Solutions by Experiment and Molecular Simulation". In: *Journal of Chemical and Engineering Data* 60.6 (2015), pp. 1614–1628. DOI: 10.1021/je5009944.

[352] S. Reiser, M. Horsch, and H. Hasse. "Density of ethanolic alkali halide salt solutions by experiment and molecular simulation". In: *Fluid Phase Equilibria* 408 (2016), pp. 141–150. DOI: 10.1016/j.fluid.2015.08.005.

[353] E. Hawlicka and D. Swiatla-Wojcik. "Effect of sodium halides on the structure of methanol-water mixture - MD simulation studies". In: *Journal of Molecular Liquids* 98-99 (2002), pp. 357–367. DOI: 10.1016/s0167-7322(01)00338-5.

[354] E. Hawlicka and D. Swiatla-Wojcik. "Aggregation of ions in methanol-water solutions of sodium halides". In: *Journal of Chemical Physics* 119.4 (2003), pp. 2206–2213. DOI: 10.1063/1.1583676.

[355] A. Sarkar, M. K. Dixit, and B. L. Tembe. "Solvation structures of lithium halides in methanol-water mixtures". In: *Chemical Physics* 447 (2015), pp. 76–85. DOI: 10.1016/j.chemphys.2014.11.019.

[356] M. Kohns, M. Horsch, and H. Hasse. "Partial molar volume of NaCl and CsCl in mixtures of water and methanol by experiment and molecular simulation". In: *Fluid Phase Equilibria* 458 (2018), pp. 30–39. DOI: 10.1016/j.fluid.2017.10.034.

[357] I. Nezbeda, F. Moučka, and W. R. Smith. "Recent progress in molecular simulation of aqueous electrolytes: force fields, chemical potentials and solubility". In: *Molecular Physics* 114.11 (2016), pp. 1665–1690. DOI: 10.1080/00268976.2016.1165296.

[358] W. R. Smith, I. Nezbeda, J. Kolafa, and F. Moučka. "Recent progress in the molecular simulation of thermodynamic properties of aqueous electrolyte solutions". In: *Fluid Phase Equilibria* 466 (2018), pp. 19–30. DOI: 10.1016/j.fluid.2018.03.006.

[359] M. B. Gee, N. R. Cox, Y. Jiao, N. Bentenitis, S. Weerasinghe, and P. E. Smith. "A Kirkwood-Buff Derived Force Field for Aqueous Alkali Halides". In: *Journal of Chemical Theory and Computation* 7.5 (2011), pp. 1369–1380. DOI: 10.1021/ct100517z.

[360] I. S. Joung and T. E. Cheatham. "Determination of alkali and halide monovalent ion parameters for use in explicitly solvated biomolecular simulations". In: *Journal of Physical Chemistry B* 112.30 (2008), pp. 9020–9041. DOI: 10.1021/jp8001614.

[361] I. S. Joung and T. E. Cheatham. "Molecular dynamics simulations of the dynamic and energetic properties of alkali and halide ions using water-model-specific ion parameters". In: *Journal of Physical Chemistry B* 113.40 (2009), pp. 13279–13290. DOI: 10.1021/jp902584c.

[362] D. Horinek, S. I. Mamatkulov, and R. R. Netz. "Rational design of ion force fields based on thermodynamic solvation properties". In: *The Journal of Chemical Physics* 130.12 (2009), p. 124507. DOI: 10.1063/1.3081142.

[363] S. Reiser, S. Deublein, J. Vrabec, and H. Hasse. "Molecular dispersion energy parameters for alkali and halide ions in aqueous solution". In: *Journal of Chemical Physics* 140.4 (2014), p. 044504. DOI: 10.1063/1.4858392.

[364] H. J. C. Berendsen, J. R. Grigera, and T. P. Straatsma. "The Missing Term in Effective Pair Potentials". In: *J. Phys. Chem* 91 (1987), pp. 6269–6271.

[365] M. Soniat and S. W. Rick. "The effects of charge transfer on the aqueous solvation of ions". In: *Journal of Chemical Physics* 137.4 (2012), pp. 6146–6952. DOI: 10.1063/1.4736851.

[366] F. G. Fumi and M. P. Tosi. "Ionic sizes and born repulsive parameters in the NaCl-type alkali halides-I. The Huggins-Mayer and Pauling forms". In: *Journal of Physics and Chemistry of Solids* 25.1 (1964), pp. 31–43. DOI: 10.1016/0022-3697(64)90159-3.

[367] M. P. Tosi and F. G. Fumi. "Ionic sizes and born repulsive parameters in the NaCl-type alkali halides-II. The generalized Huggins-Mayer form". In: *Journal of Physics and Chemistry of Solids* 25.1 (1964), pp. 45–52. DOI: 10.1016/0022-3697(64)90160-X.

[368] J. E. Mayer. "Dispersion and polarizability and the van der waals potential in the alkali halides". In: *The Journal of Chemical Physics* 1.4 (1933), pp. 270–279. DOI: 10.1063/1.1749283.

[369] M. L. Huggins and J. E. Mayer. "Interatomic distances in crystals of the alkali halides". In: *The Journal of Chemical Physics* 1.9 (1933), pp. 643–646. DOI: 10.1063/1.1749344.

[370] M. Ferrario, G. Ciccotti, E. Spohr, T. Cartailler, and P. Turq. "Solubility of KF in water by molecular dynamics using the Kirkwood integration method". In: *Journal of Chemical Physics* 117.10 (2002), pp. 4947–4953. DOI: 10.1063/1.1498820.

[371] E. Sanz and C. Vega. "Solubility of KF and NaCl in water by molecular simulation". In: *Journal of Chemical Physics* 126.1 (2007), p. 014507. DOI: 10.1063/1.2397683.

[372] J. L. Aragones, E. Sanz, and C. Vega. "Solubility of NaCl in water by molecular simulation revisited". In: *Journal of Chemical Physics* 136.24 (2012), p. 244508. DOI: 10.1063/1.4728163.

[373] A. L. Benavides, J. L. Aragones, and C. Vega. "Consensus on the solubility of NaCl in water from computer simulations using the chemical potential route". In: *Journal of Chemical Physics* 144.12 (2016), p. 124504. DOI: 10.1063/1.4943780.

[374] P. T. Kiss and A. Baranyai. *A new polarizable force field for alkali and halide ions*. 2014. DOI: 10.1063/1.4895129.

[375] S. Weerasinghe and P. E. Smith. "A Kirkwood-Buff derived force field for sodium chloride in water". In: *Journal of Chemical Physics* 119.21 (2003), pp. 11342–11349. DOI: 10.1063/1.1622372.

[376] B. Jönsson, O. Edholm, and O. Teleman. "Molecular dynamics simulations of a sodium octanoate micelle in aqueous solution". In: *The Journal of Chemical Physics* 85.4 (1986), pp. 2259–2271. DOI: 10.1063/1.451122.

[377] I. V. Leontyev and A. A. Stuchebrukhov. "Electronic continuum model for molecular dynamics simulations". In: *Journal of Chemical Physics* 130.8 (2009), p. 085102. DOI: 10.1063/1.3060164.

[378] I. V. Leontyev and A. A. Stuchebrukhov. "Electronic Polarizability and the Effective Pair Potentials of Water". In: *Journal of Chemical Theory and Computation* 6.10 (2010), pp. 3153–3161. DOI: 10.1021/ct1002048.

[379] I. Leontyev and A. Stuchebrukhov. *Accounting for electronic polarization in non-polarizable force fields*. 2011. DOI: 10.1039/c0cp01971b.

[380] I. V. Leontyev and A. A. Stuchebrukhov. "Polarizable mean-field model of water for biological simulations with AMBER and CHARMM force fields". In: *Journal of Chemical Theory and Computation* 8.9 (2012), pp. 3207–3216. DOI: 10.1021/ct300011h.

[381] I. V. Leontyev and A. A. Stuchebrukhov. "Polarizable molecular interactions in condensed phase and their equivalent nonpolarizable models". In: *Journal of Chemical Physics* 141.1 (2014), p. 014103. DOI: 10.1063/1.4884276.

[382] Z. R. Kann and J. L. Skinner. "A scaled-ionic-charge simulation model that reproduces enhanced and suppressed water diffusion in aqueous salt solutions". In: *Journal of Chemical Physics* 141.10 (2014), p. 104507. DOI: 10.1063/1.4894500.

[383] C. J. Tainter, P. A. Pieniazek, Y. S. Lin, and J. L. Skinner. "Robust three-body water simulation model". In: *Journal of Chemical Physics* 134.18 (2011), p. 184501. DOI: 10.1063/1.3587053.

[384] F. Wang, O. Akin-Ojo, E. Pinnick, and Y. Song. "Approaching post-Hartree-Fock quality potential energy surfaces with simple pair-wise expressions: Parameterising point-charge-based force fields for liquid water using the adaptive force matching method". In: *Molecular Simulation* 37.7 (2011), pp. 591–605. DOI: 10.1080/08927022.2011.565759.

[385] J. Li and F. Wang. "Pairwise-additive force fields for selected aqueous monovalent ions from adaptive force matching". In: *Journal of Chemical Physics* 143.19 (2015), p. 194505. DOI: 10.1063/1.4935599.

[386] O. Akin-Ojo, Y. Song, and F. Wang. "Developing ab initio quality force fields from condensed phase quantum-mechanics/molecular-mechanics calculations through the adaptive force matching method". In: *Journal of Chemical Physics* 129.6 (2008), p. 064108. DOI: 10.1063/1.2965882.

[387] R. Fuentes-Azcatl and M. C. Barbosa. "Sodium Chloride, NaCl/e: New Force Field". In: *Journal of Physical Chemistry B* 120.9 (2016), pp. 2460–2470. DOI: 10.1021/acs.jpcb.5b12584.

[388] A. L. Benavides, M. A. Portillo, V. C. Chamorro, J. R. Espinosa, J. L. F. Abascal, and C. Vega. "A potential model for sodium chloride solutions based on the TIP4P/2005 water model". In: *The Journal of Chemical Physics* 147.10 (2017), p. 104501. DOI: 10.1063/1.5001190.

[389] I. M. Zeron, J. L. Abascal, and C. Vega. "A force field of Li+, Na+, K+, Mg2+, Ca2+, Cl-, and S O 4 2 - In aqueous solution based on the TIP4P/2005 water model and scaled charges for the ions". In: *Journal of Chemical Physics* 151.13 (2019), p. 134504. DOI: 10.1063/1.5121392.

[390] I. V. Vorobyov, V. M. Anisimov, and A. D. MacKerell. "Polarizable empirical force field for alkanes based on the classical Drude oscillator model". In: *Journal of Physical Chemistry B* 109.40 (2005), pp. 18988–18999. DOI: 10.1021/jp053182y.

[391] M. Jorge and L. Lue. "The dielectric constant: Reconciling simulation and experiment". In: *Journal of Chemical Physics* 150.8 (2019), p. 084108. DOI: 10.1063/1.5080927.

[392] S. Lindenbaum. "Thermodynamics of aqueous solutions of tetrabutylammonium carboxylates. Model systems for the hydrophobic interaction in proteins". In: *The Journal of Physical Chemistry* 75.24 (1971), pp. 3733–3737. DOI: 10.1021/j100693a017.

[393] K. Ghandi. "A Review of Ionic Liquids, Their Limits and Applications". In: *Green and Sustainable Chemistry* 04.01 (2014), pp. 44–53. DOI: 10.4236/gsc.2014.41008.

[394] Sigma-Aldrich. *Ammonium Based Ionic Liquids*. 2020. URL: https://www.sigmaaldrich.com/chemistry/chemistry-products.html?TablePage=16255867.

[395] J. B. Macaskill and R. G. Bates. "Osmotic and activity coefficients of monomethyl-, dimethyl-, and trimethylammonium chlorides at 25°C". In: *Journal of Solution Chemistry* 15.4 (1986), pp. 323–330. DOI: 10.1007/BF00648886.

[396] J. Turner, A. K. Soper, and J. L. Finney. "A neutron-diffraction study of tetramethylammonium chloride in aqueous solution". In: *Molecular Physics* 70.4 (1990), pp. 679–700. DOI: 10.1080/00268979000102661.

[397] J. Turner, A. K. Soper, and J. L. Finney. "Water structure in aqueous solutions of tetramethylammonium chloride". In: *Molecular Physics* 77.3 (1992), pp. 411–429. DOI: 10.1080/00268979200102521.

[398] A. K. Soper, J. Turner, and J. L. Finney. "Solute-solute correlations in aqueous solutions of tetramethylammonium chloride". In: *Molecular Physics* 77.3 (1992), pp. 431–437. DOI: 10.1080/00268979200102531.

[399] J. Z. Turner, A. K. Soper, and J. L. Finney. "Ionic versus apolar behavior of the tetramethylammonium ion in water". In: *The Journal of Chemical Physics* 102.13 (1995), pp. 5438–5443. DOI: 10.1063/1.469271.

[400] G. N. James Port and A. Pullman. "An ab initio study of the hydration of alkylammonium groups". In: *Theoretica Chimica Acta* 31.3 (1973), pp. 231–237. DOI: 10.1007/BF00526513.

[401] J. Koller and D. Hadzi. "Ab initio and semiempirical calculations on the interaction of tetramethylammonium with a water molecule". In: *Journal of Molecular Structure: THEOCHEM* 279.C (1993), pp. 311–319. DOI: 10.1016/0166-1280(93)90079-Q.

[402] S. S. Wee, S. Kim, M. S. Jhon, and H. A. Scheraga. "Analytical intermolecular potential functions from ab initio SCF calculations for hydration of methylamine and methylammonium ion". In: *The Journal of Physical Chemistry* 94.4 (1990), pp. 1656–1660. DOI: 10.1021/j100367a079.

[403] D. D. Kemp and M. S. Gordon. "Theoretical study of the solvation of fluorine and chlorine anions by water". In: *Journal of Physical Chemistry A* 109.34 (2005), pp. 7688–7699. DOI: 10.1021/jp058086b.

[404] J. K. Buckner and W. L. Jorgensen. "Energetics and Hydration of the Constituent Ion Pairs of Tetramethylammonium Chloride". In: *Journal of the American Chemical Society* 111.7 (1989), pp. 2507–2516. DOI: 10.1021/ja00189a023.

[405] E. Hawlicka and T. Dlugoborski. "Molecular dynamics simulations of the aqueous solution of tetramethylammonium chloride". In: *Chemical Physics Letters* 268.5-6 (1997), pp. 325–330. DOI: 10.1016/S0009-2614(97)00229-7.

[406] S. Garde, G. Hummer, and M. E. Paulaitis. "Free energy of hydration of a molecular ionic solute: Tetramethylammonium ion". In: *Journal of Chemical Physics* 108.4 (1998), pp. 1552–1561. DOI: 10.1063/1.475526.

[407] L. García-Tarrés and E. Guàrdia. "Hydration and dynamics of a tetramethylammonium ion in water: A computer simulation study". In: *Journal of Physical Chemistry B* 102.38 (1998), pp. 7448–7454. DOI: 10.1021/jp981427j.

[408] J. B. MacAskill and A. D. Pethybridge. "Osmotic coefficients and activity coefficients of methyl-substituted ammonium chlorides and ammonium methyl sulphates in water at 25°C". In: *Journal of the Chemical Society, Faraday Transactions 1: Physical Chemistry in Condensed Phases* 71.0 (1975), pp. 1465–1468. DOI: 10.1039/F19757101465. URL: https://pubs.rsc.org/en/content/articlelanding/1975/f1/f19757101465.

[409] O. D. Bonner. "Osmotic and activity coefficients of methyl-substituted ammonium chlorides". In: *Journal of the Chemical Society, Faraday Transactions 1: Physical Chemistry in Condensed Phases* 77.10 (1981), pp. 2515–2518. DOI: 10.1039/F19817702515.

[410] A. Losurdo and H. E. Wirth. "The temperature dependence of the apparent and partial molal volumes of concentrated aqueous electrolyte solutions of tetraalkylammonium bromides, cetyltrimethylammonium bromide, and ammonium and lithium bromides". In: *The Journal of Physical Chemistry* 76.9 (1972), pp. 1333–1338. DOI: 10.1021/j100653a020.

[411] P.-A. Leduc and J. E. Desnoyers. "Apparent Molal Heat Capacities and Volumes of Tetrabutylammonium Carboxylates and Related Solutes in Water at 25 °C". In: *Canadian Journal of Chemistry* 51.17 (1973), pp. 2993–2998. DOI: 10.1139/v73-445.

[412] G. Perron, N. Desrosiers, and J. E. Desnoyers. "Thermodynamic properties of tetraalkylammonium halides: volumes, heat capacities, and expansibilities in H2O, D2O and urea–water mixtures from 278 to 328 K". In: *Canadian Journal of Chemistry* 54.14 (1976), pp. 2163–2183. DOI: 10.1139/v76-309.

[413] W. L. Jorgensen and J. Gao. "Monte Carlo simulations of the hydration of ammonium and carboxylate ions". In: *The Journal of Physical Chemistry* 90.10 (1986), pp. 2174–2182. DOI: 10.1021/j100401a037.

[414] P. Cremaschi and M. Simonetta. "Barmer to internal rotation in the methylammonium ion". In: *Journal of Molecular Structure* 29.1 (1975), pp. 39–45. DOI: 10.1016/0022-2860(75)88005-7.

[415] T. J. Edwards, G. Maurer, J. Newman, and J. M. Prausnitz. "Vapor-liquid equilibria in multicomponent aqueous solutions of volatile weak electrolytes". In: *AIChE Journal* 24.6 (1978), pp. 966–976. DOI: 10.1002/aic.690240605.

[416] P. V. Kortunov, M. Siskin, M. Paccagnini, and H. Thomann. "CO2 Reaction Mechanisms with Hindered Alkanolamines: Control and Promotion of Reaction Pathways". In: *Energy & Fuels* 30.2 (2016), pp. 1223–1236. DOI: 10.1021/acs.energyfuels.5b02582.

[417] V. Vchirawongkwin, A. B. Přibil, and B. M. Rode. "Ab initio quantum mechanical charge field study of hydrated bicarbonate ion: Structural and dynamical properties". In: *Journal of Computational Chemistry* 31.2 (2010), pp. 249–257. DOI: 10.1002/jcc.21308.

[418] R. L. Sass and R. F. Scheuerman. "The crystal structure of sodium bicarbonate". In: *Acta Crystallographica* 15.1 (1962), pp. 77–81. DOI: 10.1107/s0365110x62000158.

[419] P. George, C. W. Bock, and M. Trachtman. "An ab initio study of the geometry, energy, and selected force constants for the three planar conformers of carbonic acid, and the bicarbonate ion; and of the energy for the reaction H2O CO2 H2CO3". In: *Journal of Computational Chemistry* 3.3 (1982), pp. 283–296. DOI: 10.1002/jcc.540030303.

[420] G. Herzberg. *Electronic spectra and electronic structure of polyatomic molecules*. New York: Van Nostrand, 1966.

[421] O. E. Abdel-Salam. "Activity Coefficients of Tetramethylammonium Carbonate, Bicarbonate & Hydroxide in Aqueous Medium". In: *Indian Journal of Chemistry* 21 (1982), pp. 785–787.

[422] Y. Marcus. "Thermodynamics of solvation of ions. Part 6. - The standard partial molar volumes of aqueous ions at 298.15 K". In: *Journal of the Chemical Society, Faraday Transactions* 89.4 (1993), pp. 713–718. DOI: 10.1039/FT9938900713.

[423] G. Levitin, D. Bush, C. A. Eckert, and D. W. Hess. "Phase behavior and modeling of CO 2/methanol/tetramethylammonium bicarbonate and CO 2/methanol/tetramethylammonium bicarbonate/water mixtures at high pressures". In: *Journal of Chemical and Engineering Data* 49.3 (2004), pp. 599–606. DOI: 10.1021/je0302351.

[424] C. Yang, S. Ma, and X. Yin. "Organic salt effect of tetramethylammonium bicarbonate on the vapor-liquid equilibrium of the methanol-water system". In: *Journal of Chemical and Engineering Data* 56.10 (2011), pp. 3747–3751. DOI: 10.1021/je200341c.

[425] C. Yang, X. Yin, and S. Ma. "Organic salt effect of tetramethylammonium bicarbonate on the vapor-liquid equilibrium of the dimethyl carbonate + methanol system". In: *Journal of Chemical and Engineering Data* 57.1 (2012), pp. 66–71. DOI: 10.1021/je200697m.

[426] G. Kamath, F. Cao, and J. J. Potoff. "An improved force field for the prediction of the vapor-liquid equilibria for carboxylic acids". In: *Journal of Physical Chemistry B* 108.37 (2004), pp. 14130–14136. DOI: 10.1021/jp048581s.

[427] G. Kamath, J. Robinson, and J. J. Potoff. "Application of TraPPE-UA force field for determination of vapor-liquid equilibria of carboxylate esters". In: *Fluid Phase Equilibria* 240.1 (2006), pp. 46–55. DOI: 10.1016/j.fluid.2005.11.034.

[428] L. S. Dodda, I. Cabeza De Vaca, J. Tirado-Rives, and W. L. Jorgensen. "LigParGen web server: an automatic OPLS-AA parameter generator for organic ligands". In: *Nucleic Acids Research* 45 (2017), pp. 331–336. DOI: 10.1093/nar/gkx312.

[429] M. Wang, A. Lawal, P. Stephenson, J. Sidders, and C. Ramshaw. "Post-combustion CO2 capture with chemical absorption: A state-of-the-art review". In: *Chemical Engineering Research and Design* 89.9 (2011), pp. 1609–1624. DOI: 10.1016/j.cherd.2010.11.005.

[430] J. Yu and S. S. Chuang. "The structure of adsorbed species on immobilized amines in CO2 capture: An in situ IR study". In: *Energy and Fuels* 30.9 (2016), pp. 7579–7587. DOI: 10.1021/acs.energyfuels.6b01423.

[431] D. Wu, C. Sun, P. K. Dutta, and W. S. Winston Ho. "SO2 interference on separation performance of amine-containing facilitated transport membranes for CO2 capture from flue gas". In: *Journal of Membrane Science* 534 (2017), pp. 33–45. DOI: 10.1016/j.memsci.2017.04.003.

[432] G. Sartorl and D. W. Savage. "Sterically Hindered Amines for CO2 Removal from Gases". In: *Industrial and Engineering Chemistry Fundamentals* 22.2 (1983), pp. 239–249. DOI: 10.1021/i100010a016.

[433] S. Wiechert, W. S. Ho, and D. W. Savage. "Sterically-Hindered amines for acid-gas absorption". In: *Separation & Purification Reviews* 16.2 (1987), pp. 171–200. DOI: 10.1080/03602548708058543.

[434] *FLEXSORB Gas Treating Technology — ExxonMobil Chemical*. URL: https://www.exxonmobilchemical.com/en/catalysts-and-technology-licensing/gas-treating.

[435] J. Yu and S. S. Chuang. "The Role of Water in CO2 Capture by Amine". In: *Industrial and Engineering Chemistry Research* 56.21 (2017), pp. 6337–6347. DOI: 10.1021/acs.iecr.7b00715.

[436] T. Loerting, C. Tautermann, R. T. Kroemer, I. Kohl, A. Hallbrucker, E. Mayer, and K. R. Liedl. "On the Surprising Kinetic Stability of Carbonic Acid (H2CO3)". In: *Angewandte Chemie International Edition* 39.5 (2000), pp. 891–894. DOI: 10.1002/(SICI)1521-3773(20000303)39:5<891::AID-ANIE891>3.0.CO;2-E.

[437] G. Richner and G. Puxty. "Assessing the chemical speciation during CO 2 absorption by aqueous amines using in situ FTIR". In: *Industrial and Engineering Chemistry Research* 51.44 (2012), pp. 14317–14324. DOI: 10.1021/ie302056f.

[438] J. I. Brauman, J. M. Riveros, and L. K. Blair. "Gas-Phase Basicities of Amines". In: *Journal of the American Chemical Society* 93.16 (1971), pp. 3914–3916. DOI: 10.1021/ja00745a016.

[439] V. Frenna, N. Vivona, G. Consiglio, and D. Spinelli. "Amine basicities in benzene and in water". In: *Journal of the Chemical Society, Perkin Transactions 2* 12 (1985), pp. 1865–1868. DOI: 10.1039/P29850001865.

[440] W. Yang and W. J. Mortier. "The Use of Global and Local Molecular Parameters for the Analysis of the Gas-Phase Basicity of Amines". In: *Journal of the American Chemical Society* 108.19 (1986), pp. 5708–5711. DOI: 10.1021/ja00279a008.

[441] K. Zhang, D. M. Zimmerman, A. Chung-Phillips, and C. J. Cassady. "Experimental and ab Initio Studies of the Gas-Phase Basicities of Polyglycines". In: *Journal of the American Chemical Society* 115.23 (1993), pp. 10812–10822. DOI: 10.1021/ja00076a044.

[442] E. F. Da Silva and H. F. Svendsen. "Prediction of the pKa values of amines using ab initio methods and free-energy perturbations". In: *Industrial and Engineering Chemistry Research* 42.19 (2003), pp. 4414–4421. DOI: 10.1021/ie020808n.

[443] K. Z. Sumon, A. Henni, and A. L. East. "Predicting pK a of amines for CO 2 capture: Computer versus pencil-and-paper". In: *Industrial and Engineering Chemistry Research* 51.37 (2012), pp. 11924–11930. DOI: 10.1021/ie301033p.

[444] R. W. Alder. "Strain Effects on Amine Basicities". In: *Chemical Reviews* 89.5 (1989), pp. 1215–1223. DOI: 10.1021/cr00095a015.

[445] G. Kuranov, B. Rumpf, N. A. Smirnova, and G. Maurer. "Solubility of Single Gases Carbon Dioxide and Hydrogen Sulfide in Aqueous Solutions of N-Methyldiethanolamine in the Temperature Range 313-413 K at Pressures up to 5 MPa". In: *Industrial & Engineering Chemistry Research* 35.6 (1996), pp. 1959–1966. DOI: 10.1021/ie950538r.

[446] A. V. Bandura and S. N. Lvov. "The ionization constant of water over wide ranges of temperature and density". In: *Journal of Physical and Chemical Reference Data* 35.1 (2006), pp. 15–30. DOI: 10.1063/1.1928231.

[447] R. L. Kent and B. Elsenberg. "Better Data for Amine Treating". In: *Hydrocarbon Processing* 55.2 (1976), pp. 87–90.

[448] F. Y. Jou, A. E. Mather, and F. D. Otto. "Solubility of hydrogen sulfide and carbon dioxide in aqueous methyldiethanolamine solutions". In: *Industrial & Engineering Chemistry Process Design and Development* 21.4 (1982), pp. 539–544. DOI: 10.1021/i200019a001.

[449] A. Chakma and A. Meisen. "Improved Kent-Eisenberg model for predicting CO2 solubilities in aqueous diethanolamine (DEA) solutions". In: *Gas Separation and Purification* 4.1 (1990), pp. 37–40. DOI: 10.1016/0950-4214(90)80025-G.

[450] J. Gabrielsen, M. L. Michelsen, E. H. Stenby, and G. M. Kontogeorgis. "A model for estimating CO2 solubility in aqueous alkanolamines". In: *Industrial and Engineering Chemistry Research* 44.9 (2005), pp. 3348–3354. DOI: 10.1021/ie048857i.

[451] P. Tontlwachwuthikul, A. Meisen, and C. J. Llm. "Solubility of CO2 in 2-Amino-2-methyl-1-propanol Solutions". In: *Journal of Chemical and Engineering Data* 36.1 (1991), pp. 130–133. DOI: 10.1021/je00001a038.

[452] S. H. Park, K. B. Lee, J. C. Hyun, and S. H. Kim. "Correlation and prediction of the solubility of carbon dioxide in aqueous alkanolamine and mixed alkanolamine solutions". In: *Industrial and Engineering Chemistry Research* 41.6 (2002), pp. 1658–1665. DOI: 10.1021/ie010252o.

[453] D. Le Tourneux, I. Iliuta, M. C. Iliuta, S. Fradette, and F. Larachi. "Solubility of carbon dioxide in aqueous solutions of 2-amino-2- hydroxymethyl-1,3-propanediol". In: *Fluid Phase Equilibria* 268.1-2 (2008), pp. 121–129. DOI: 10.1016/j.fluid.2008.04.003.

[454] H. Pahlavanzadeh, A.R.Jahangiri, and I. Noshadi. "Modeling of CO2 Removal from Gas Mixtureby 2-amino-2-methyl-1-propanol (AMP) Using the Modified Kent Eisenberg Model". In: (2010). DOI: 10.5281/ZENODO.1063310.

[455] H. A. Haider, R. Yusoff, and M. K. Aroua. "Equilibrium solubility of carbon dioxide in 2(methylamino)ethanol". In: *Fluid Phase Equilibria* 303.2 (2011), pp. 162–167. DOI: 10.1016/j.fluid.2011.01.016.

[456] B. K. Mondal, S. S. Bandyopadhyay, and A. N. Samanta. "VLE of CO2 in aqueous sodium glycinate solution - New data and modeling using Kent-Eisenberg model". In: *International Journal of Greenhouse Gas Control* 36 (2015), pp. 153–160. DOI: 10.1016/j.ijggc.2015.02.010.

[457] H. Suleman, A. S. Maulud, and Z. Man. "A hybrid equation of state and Kent-Eisenberg model for accurate prediction of carbon dioxide separation by aqueous alkanolamines". In: *Separation Science and Technology* 51.17 (2016), pp. 2744–2755. DOI: 10.1080/01496395.2016.1217241.

[458] H. Suleman, Q. Nasir, A. S. Maulud, and Z. Man. "Comparative Study of Electrolyte Thermodynamic Models for Carbon Dioxide Solubility in Water at High Pressure". In: *Chemical Engineering Transactions* 45 (2015). DOI: 10.3303/CET1545099.

[459] R. D. Deshmukh and A. E. Mather. "A mathematical model for equilibrium solubility of hydrogen sulfide and carbon dioxide in aqueous alkanolamine solutions". In: *Chemical Engineering Science* 36.2 (1981), pp. 355–362. DOI: 10.1016/0009-2509(81)85015-4.

[460] B. E. Roberts and A. E. Mather. "Solubility of C02 and H2S in a Mixed Solvent". In: *Chemical Engineering Communications* 72.1 (1988), pp. 201–211. DOI: 10.1080/00986448808940017.

[461] R. J. Macgregor and A. E. Mather. "Equilibrium solubility of H2S and CO2 and their mixtures in a mixed solvent". In: *The Canadian Journal of Chemical Engineering* 69.6 (1991), pp. 1357–1366. DOI: 10.1002/cjce.5450690618.

[462] F.-Y. Jou, A. E. Mather, and F. D. Otto. "The solubility of CO 2 in a 30 mass percent monoethanolamine solution". In: *The Canadian Journal of Chemical Engineering* 73.1 (1995), pp. 140–147. DOI: 10.1002/cjce.5450730116.

[463] A. Benamor and M. K. Aroua. "Modeling of CO2 solubility and carbamate concentration in DEA, MDEA and their mixtures using the Deshmukh-Mather model". In: *Fluid Phase Equilibria* 231.2 (2005), pp. 150–162. DOI: 10.1016/j.fluid.2005.02.005.

[464] S. Ma'mun, J. P. Jakobsen, H. F. Svendsen, and O. Juliussen. "Experimental and modeling study of the solubility of carbon dioxide in aqueous 30 mass% 2-((2-aminoethyl)amino)ethanol solution". In: *Industrial and Engineering Chemistry Research*. Vol. 45. 8. American Chemical Society, 2006, pp. 2505–2512. DOI: 10.1021/ie0505209.

[465] A. Jahangiri, H. Pahlavanzadeh, and A. Mohammadi. "Modeling of CO2 Removal From Gas Mixture by 2-amino-2-methyl-1-propanol (AMP) Using the Deshmakh-Mather Model". In: *Petroleum Science and Technology* 32.16 (2014), pp. 1921–1931. DOI: 10.1080/10916466.2011.592893.

[466] F. A. Tobiesen, O. Juliussen, and H. F. Svendsen. "Experimental validation of a rigorous desorber model for CO2 post-combustion capture". In: *Chemical Engineering Science* 63.10 (2008), pp. 2641–2656. DOI: 10.1016/j.ces.2008.02.011.

[467] Y. G. Lif and A. E. Mather. "Correlation and Prediction of the Solubility of Carbon Dioxide in a Mixed Alkanolamine Solution". In: *Industrial and Engineering Chemistry Research* 33.8 (1994), pp. 2006–2015. DOI: 10.1021/ie00032a017.

[468] S. L. Clegg, K. S. Pitzer, and P. Brimblecombe. "Thermodynamics of multicomponent, miscible, ionic solutions. 2. Mixtures including unsymmetrical electrolytes". In: *Journal of Physical Chemistry* 96.23 (1992), pp. 9470–9479. DOI: 10.1021/j100202a074.

[469] S. L. Clegg and K. S. Pitzer. "Thermodynamics of multicomponent, miscible, ionic solutions: Generalized equations for symmetrical electrolytes". In: *Journal of Physical Chemistry* 96.8 (1992), pp. 3513–3520. DOI: 10.1021/j100187a061.

[470] F.-Y. Jou, J. J. Carrol, A. E. Mather, and F. D. Otto. "Solubility of Methane and Ethane in Aqueous Solutions of Methyldiethanolamine". In: *Journal of Chemical & Engineering Data* 43.5 (1998), pp. 781–784. DOI: 10.1021/JE980003F.

[471] K. A. G. Schmidt, F. Y. Jou, and A. E. Mather. "Solubility of methane in an aqueous methyldiethanolamine solution (mass fraction 50 %)". In: *Journal of Chemical & Engineering Data* 53.8 (2008), pp. 1725–1727. DOI: 10.1021/je700734p.

[472] K. Nasrifar and A. H. Tafazzol. "Vapor- liquid equilibria of acid gas- aqueous ethanolamine solutions using the PC-SAFT equation of state". In: *Industrial & Engineering Chemistry Research* 49.16 (2010), pp. 7620–7630. DOI: 10.1021/ie901181n.

[473] D. M. Austgen, G. T. Rochelle, and C. C. Chen. "Model of vapor-liquid equilibria for aqueous acid gas-alkanolamine systems. 2. Representation of H2S and CO2 solubility in aqueous MDEA and CO2 solubility in aqueous mixtures of MDEA with MEA or DEA". In: *Industrial and Engineering Chemistry Research* 30.3 (1991), pp. 543–555. DOI: 10.1021/ie00051a016.

[474] S. Fakouri Baygi and H. Pahlavanzadeh. "Application of the perturbed chain-SAFT equation of state for modeling CO2 solubility in aqueous monoethanolamine solutions". In: *Chemical Engineering Research and Design* 93 (2015), pp. 789–799. DOI: 10.1016/j.cherd.2014.07.017.

[475] J. Button and K. Gubbins. "SAFT prediction of vapour-liquid equilibria of mixtures containing carbon dioxide and aqueous monoethanolamine or diethanolamine". In: *Fluid Phase Equilibria* 158-160 (1999), pp. 175–181. DOI: 10.1016/S0378-3812(99)00150-8.

[476] N. Mac Dowell, F. Llovell, C. S. Adjiman, G. Jackson, and A. Galindo. "Modeling the fluid phase behavior of carbon dioxide in aqueous solutions of monoethanolamine using transferable parameters with the SAFT-VR approach". In: *Industrial & Engineering Chemistry Research* 49.4 (2010), pp. 1883–1899. DOI: 10.1021/ie901014t.

[477] N. Mac Dowell, F. E. Pereira, F. Llovell, F. J. Blas, C. S. Adjiman, G. Jackson, and A. Galindo. "Transferable SAFT-VR models for the calculation of the fluid phase equilibria in reactive mixtures of carbon dioxide, water, and n-alkylamines in the context of carbon capture". In: *Journal of Physical Chemistry B* 115.25 (2011), pp. 8155–8168. DOI: 10.1021/jp107467s.

[478] I. I. Alkhatib, L. M. Pereira, and L. F. Vega. "110th Anniversary: Accurate Modeling of the Simultaneous Absorption of H 2 S and CO 2 in Aqueous Amine Solvents". In: *Industrial and Engineering Chemistry Research* 58.16 (2019), pp. 6870–6886. DOI: 10.1021/acs.iecr.9b00862.

[479] I. I. Alkhatib, L. M. Pereira, A. Alhajaj, and L. F. Vega. "Performance of non-aqueous amine hybrid solvents mixtures for CO2 capture: A study using a molecular-based model". In: *Journal of CO2 Utilization* 35 (2020), pp. 126–144. DOI: 10.1016/j.jcou.2019.09.010.

[480] H. Al-fnaish and L. Lue. "Modelling the solubility of H2S and CO2 in ionic liquids using PC-SAFT equation of state". In: *Fluid Phase Equilibria* 450 (2017), pp. 30–41. DOI: 10.1016/j.fluid.2017.07.008.

[481] L. M. Pereira and L. F. Vega. "A systematic approach for the thermodynamic modelling of CO2-amine absorption process using molecular-based models". In: *Applied Energy* 232 (2018), pp. 273–291. DOI: 10.1016/j.apenergy.2018.09.189.

[482] S. W. Rho, K. P. Yoo, J. S. Lee, S. C. Nam, J. E. Son, and B. M. Min. "Solubility of CO2 in aqueous methyldiethanolamine solutions". In: *Journal of Chemical and Engineering Data* 42.6 (1997), pp. 1161–1164. DOI: 10.1021/je970097d.

[483] M. S. Shaw. "Monte Carlo simulation of equilibrium chemical composition of molecular fluid mixtures in the Natoms PT ensemble". In: *The Journal of Chemical Physics* 94.11 (1991), pp. 7550–7553. DOI: 10.1063/1.460188.

[484] J. K. Johnson, A. Z. Panagiotopoulos, and K. E. Gubbins. "Reactive canonical monte carlo a new simulation technique for reacting or associating fluids". In: *Molecular Physics* 81.3 (1994), pp. 717–733. DOI: 10.1080/00268979400100481.

[485] W. R. Smith and B. Triska. "The reaction ensemble method for the computer simulation of chemical and phase equilibria. I. Theory and basic examples". In: *The Journal of Chemical Physics* 100.4 (1994), pp. 3019–3027. DOI: 10.1063/1.466443.

[486] C. Heath Turner, J. K. Brennan, M. Lísal, W. R. Smith, J. Karl Johnson, and K. E. Gubbins. "Simulation of chemical reaction equilibria by the reaction ensemble Monte Carlo method: a review". In: *Molecular Simulation* 34.2 (2008), pp. 119–146. DOI: 10.1080/08927020801986564.

[487] S. P. Balaji, S. Gangarapu, M. Ramdin, A. Torres-Knoop, H. Zuilhof, E. L. Goetheer, D. Dubbeldam, and T. J. Vlugt. "Simulating the reactions of CO2 in aqueous monoethanolamine solution by reaction ensemble Monte Carlo using the continuous fractional component method". In: *Journal of Chemical Theory and Computation* 11.6 (2015), pp. 2661–2669. DOI: 10.1021/acs.jctc.5b00160.

[488] J. Noroozi and W. R. Smith. "An Efficient Molecular Simulation Methodology for Chemical Reaction Equilibria in Electrolyte Solutions: Application to CO2 Reactive Absorption". In: *Journal of Physical Chemistry A* 123.18 (2019), pp. 4074–4086. DOI: 10.1021/acs.jpca.9b00302.

[489] W. Shi and E. J. Maginn. "Continuous fractional component Monte Carlo: An adaptive biasing method for open system atomistic simulations". In: *Journal of Chemical Theory and Computation* 3.4 (2007), pp. 1451–1463. DOI: 10.1021/ct7000039.

[490] W. R. Smith and W. Qi. "Molecular Simulation of Chemical Reaction Equilibrium by Computationally Efficient Free Energy Minimization". In: *ACS Central Science* 4.9 (2018), pp. 1185–1193. DOI: 10.1021/acscentsci.8b00361.

[491] J. Noroozi and W. R. Smith. "Prediction of Alkanolamine pKa Values by Combined Molecular Dynamics Free Energy Simulations and ab Initio Calculations". In: *Journal of Chemical and Engineering Data* 65.3 (2020), pp. 1358–1368. DOI: 10.1021/acs.jced.9b00927.

[492] J. P. Jakobsen, J. Krane, and H. F. Svendsen. "Liquid-phase composition determination in CO2-H 2O-alkanolamine systems: An NMR study". In: *Industrial and Engineering Chemistry Research* 44.26 (2005), pp. 9894–9903. DOI: 10.1021/ie048813+.

[493] W. Böttinger, M. Maiwald, and H. Hasse. "Online NMR spectroscopic study of species distribution in MEA-H2O-CO2 and DEA-H2O-CO2". In: *Fluid Phase Equilibria* 263.2 (2008), pp. 131–143. DOI: 10.1016/j.fluid.2007.09.017.

[494] N. S. Matin, J. E. Remias, J. K. Neathery, and K. Liu. "Facile method for determination of amine speciation in CO 2 capture solutions". In: *Industrial and Engineering Chemistry Research* 51.19 (2012), pp. 6613–6618. DOI: 10.1021/ie300230k.

[495] L. J. Du Preez, N. Motang, L. H. Callanan, and A. J. Burger. "Determining the Liquid Phase Equilibrium Speciation of the CO 2 -MEA-H 2 O System Using a Simplified in Situ Fourier Transform Infrared Method". In: *Industrial and Engineering Chemistry Research* 58.1 (2019), pp. 469–478. DOI: 10.1021/acs.iecr.8b04437.

[496] M. D. Tissandier, K. A. Cowen, W. Y. Feng, E. Gundlach, M. H. Cohen, A. D. Earhart, J. V. Coe, and T. R. Tuttle. "The proton's absolute aqueous enthalpy and Gibbs free energy of solvation from cluster-ion solvation data". In: *Journal of Physical Chemistry A* 102.40 (1998), pp. 7787–7794. DOI: 10.1021/jp982638r.

[497] D. Asthagiri, L. R. Pratt, and H. S. Ashbaugh. "Absolute hydration free energies of ions, ion-water clusters, and quasichemical theory". In: *Journal of Chemical Physics* 119.5 (2003), pp. 2702–2708. DOI: 10.1063/1.1587122.

[498] C. P. Kelly, C. J. Cramer, and D. G. Truhlar. "Aqueous solvation free energies of ions and ion-water clusters based on an accurate value for the absolute aqueous solvation free energy of the proton". In: *Journal of Physical Chemistry B* 110.32 (2006), pp. 16066–16081. DOI: 10.1021/jp063552y.

[499] T. L. Beck. "The influence of water interfacial potentials on ion hydration in bulk water and near interfaces". In: *Chemical Physics Letters* 561-562 (2013), pp. 1–13. DOI: 10.1016/j.cplett.2013.01.008.

[500] A. C. Van Duin, S. Dasgupta, F. Lorant, and W. A. Goddard. "ReaxFF: A reactive force field for hydrocarbons". In: *Journal of Physical Chemistry A* 105.41 (2001), pp. 9396–9409. DOI: 10.1021/jp004368u.

[501] T. P. Senftle, S. Hong, M. M. Islam, S. B. Kylasa, Y. Zheng, Y. K. Shin, C. Junkermeier, R. Engel-Herbert, M. J. Janik, H. M. Aktulga, T. Verstraelen, A. Grama, and A. C. Van Duin. "The ReaxFF reactive force-field: Development, applications and future directions". In: *npj Computational Materials* 2.1 (2016), pp. 1–14. DOI: 10.1038/npjcompumats.2015.11.

[502] K. Chenoweth, A. C. Van Duin, and W. A. Goddard. "ReaxFF reactive force field for molecular dynamics simulations of hydrocarbon oxidation". In: *Journal of Physical Chemistry A* 112.5 (2008), pp. 1040–1053. DOI: 10.1021/jp709896w.

[503] A. C. Van Duin, V. S. Bryantsev, M. S. Diallo, W. A. Goddard, O. Rahaman, D. J. Doren, D. Raymand, and K. Hermansson. "Development and validation of a ReaxFF reactive force field for Cu cation/water interactions and copper metal/metal oxide/metal hydroxide condensed phases". In: *Journal of Physical Chemistry A* 114.35 (2010), pp. 9507–9514. DOI: 10.1021/jp102272z.

[504] O. Rahaman, A. C. Van Duin, W. A. Goddard, and D. J. Doren. "Development of a ReaxFF reactive force field for glycine and application to solvent effect and tautomerization". In: *Journal of Physical Chemistry B* 115.2 (2011), pp. 249–261. DOI: 10.1021/jp108642r.

[505] S. Monti, A. C. Van Duin, S. Y. Kim, and V. Barone. "Exploration of the conformational and reactive dynamics of glycine and diglycine on TiO 2: Computational investigations in the gas phase and in solution". In: *Journal of Physical Chemistry C* 116.8 (2012), pp. 5141–5150. DOI: 10.1021/jp2121593.

[506] E. B. Rinker, D. W. Oelschlager, A. T. Colussi, K. R. Henry, and O. C. Sandall. "Viscosity, Density, and Surface Tension of Binary Mixtures of Water and N-Methyldiethanolamine and Water and Diethanolamine and Tertiary Mixtures of These Amines with Water over the Temperature Range 20–100°C". In: *Journal of Chemical and Engineering Data* 39.2 (1994), pp. 392–395. DOI: 10.1021/je00014a046.

[507] M. Sobrino, E. I. Concepción, Á. Gómez-Hernández, M. C. Martín, and J. J. Segovia. "Viscosity and density measurements of aqueous amines at high pressures: MDEA-water and MEA-water mixtures for CO2 capture". In: *Journal of Chemical Thermodynamics* 98 (2016), pp. 231–241. DOI: 10.1016/j.jct.2016.03.021.

[508] K. P. Shen and M. H. Li. "Solubility of Carbon Dioxide in Aqueous Mixtures of Monoethanolamine with Methyldiethanolamine". In: *Journal of Chemical and Engineering Data* 37.1 (1992), pp. 96–100. DOI: 10.1021/je00005a025.

[509] F. Y. Jou, J. J. Carroll, A. E. Mather, and F. D. Otto. "Solubility of Mixtures of Hydrogen Sulfide and Carbon Dioxide in Aqueous N-Methyldiethanolamine Solutions". In: *Journal of Chemical and Engineering Data* 38.1 (1993), pp. 75–77. DOI: 10.1021/je00009a018.

[510] C. Mathonat, V. Majer, A. E. Mather, and J. P. Grolier. "Enthalpies of absorption and solubility of CO2 in aqueous solutions of methyldiethanolamine". In: *Fluid Phase Equilibria* 140.1-2 (1997), pp. 171–182. DOI: 10.1016/s0378-3812(97)00182-9.

[511] M. Z. Haji-Sulaiman. "Analysis of equilibrium data of CO2 in aqueous solutions of diethanolamine (DEA), methyldiethanolamine (MDEA) and their mixtures using the modified Kent Eisenberg model". In: *Chemical Engineering Research and Design* 76.8 A8 (1998), pp. 961–968. DOI: 10.1205/026387698525603.

[512] W. J. Rogers, J. A. Bullin, and R. R. Davison. "FTIR measurements of acid-gas–methyldiethanolamine systems". In: *AIChE Journal* 44.11 (1998), pp. 2423–2430. DOI: 10.1002/aic.690441110.

[513] D. Silkenbäumer, B. Rumpf, and R. N. Lichtenthaler. "Solubility of carbon dioxide in aqueous solutions of 2-amino-2-methyl-1-propanol and N-methyldiethanolamine and their mixtures in the temperature range from 313 to 353 K and pressures up to 2.7 MPa". In: *Industrial and Engineering Chemistry Research* 37.8 (1998), pp. 3133–3141. DOI: 10.1021/ie970925w.

[514] Á. P.-S. Kamps, A. Balaban, M. Jödecke, G. Kuranov, N. A. Smirnova, and G. Maurer. "Solubility of Single Gases Carbon Dioxide and Hydrogen Sulfide in Aqueous Solutions of N -Methyldiethanolamine at Temperatures from 313 to 393 K and Pressures up to 7.6 MPa: New Experimental Data and Model Extension". In: *Industrial & Engineering Chemistry Research* 40.2 (2001), pp. 696–706. DOI: 10.1021/ie000441r.

[515] J. Addicks, G. A. Owren, A. O. Fredheim, and K. Tangvik. "Solubility of carbon dioxide and methane in aqueous methyldiethanolamine solutions". In: *Journal of Chemical and Engineering Data* 47.4 (2002), pp. 855–860. DOI: 10.1021/je010292z.

[516] P. Huttenhuis, N. Agrawal, J. Hogendoorn, and G. Versteeg. "Gas solubility of H2S and CO2 in aqueous solutions of N-methyldiethanolamine". In: *Journal of Petroleum Science and Engineering* 55.1-2 (2007), pp. 122–134. DOI: 10.1016/J.PETROL.2006.04.018.

[517] C. Dell'Era, P. Uusi-Kyyny, J. P. Pokki, M. Pakkanen, and V. Alopaeus. "Solubility of carbon dioxide in aqueous solutions of diisopropanolamine and methyldiethanolamine". In: *Fluid Phase Equilibria* 293.1 (2010), pp. 101–109. DOI: 10.1016/j.fluid.2010.02.035.

[518] M. Dicko, C. Coquelet, C. Jarne, S. Northrop, and D. Richon. "Acid gases partial pressures above a 50 wt% aqueous methyldiethanolamine solution: Experimental work and modeling". In: *Fluid Phase Equilibria* 289.2 (2010), pp. 99–109. DOI: 10.1016/j.fluid.2009.11.012.

[519] A. Haghtalab and A. Izadi. "Simultaneous measurement solubility of carbon dioxide+hydrogen sulfide into aqueous blends of alkanolamines at high pressure". In: *Fluid Phase Equilibria* 375 (2014), pp. 181–190. DOI: 10.1016/j.fluid.2014.05.017.

[520] Á. P.-S. Kamps and G. Maurer. "Dissociation Constant of N-Methyldiethanolamine in Aqueous Solution at Temperatures from 278 K to 368 K". In: *Journal of Chemical & Engineering Data* 41.6 (1996), pp. 1505–1513. DOI: 10.1021/JE960141+.

[521] A. Hartono, M. Saeed, I. Kim, and H. F. Svendsen. "Protonation constant (pKa) of MDEA in water as function of temperature and ionic strength". In: *Energy Procedia* 63 (2014), pp. 1122–1128. DOI: 10.1016/j.egypro.2014.11.121.

[522] Y. P. Chang, T. M. Su, T. W. Li, and I. Chao. "Intramolecular hydrogen bonding, Gauche interactions, and thermodynamic functions of 1,2-ethanediamine, 1,2-ethanediol, and 2-aminoethanol: A global conformational analysis". In: *Journal of Physical Chemistry A* 101.34 (1997), pp. 6107–6117. DOI: 10.1021/jp971022j.

[523] S. Bishnoi and G. T. Rochelle. "Physical and chemical solubility of carbon dioxide in aqueous methyldiethanolamine". In: *Fluid Phase Equilibria* 168.2 (2000), pp. 241–258. DOI: 10.1016/S0378-3812(00)00303-4.

[524] E. L. Cussler, R. Aris, and A. Bhown. "On the limits of facilitated diffusion". In: *Journal of Membrane Science* 43.2-3 (1989), pp. 149–164. DOI: 10.1016/S0376-7388(00)85094-2.

[525] A. V. Rayer and A. Henni. "Heats of absorption of CO2 in aqueous solutions of tertiary amines: N -methyldiethanolamine, 3-dimethylamino-1-propanol, and 1-dimethylamino-2-propanol". In: *Industrial and Engineering Chemistry Research* 53.12 (2014), pp. 4953–4965. DOI: 10.1021/ie4041324.

[526] R. Wiebe, V. L. Gaddy, and C. Heins. "The Solubility of Nitrogen in Water at 50, 75 and 100° from 25 to 1000 Atmospheres". In: *Journal of the American Chemical Society* 55.3 (1933), pp. 947–953. DOI: 10.1021/ja01330a011.

[527] S. P. Cadogan, G. C. Maitland, and J. P. M. Trusler. "Diffusion Coefficients of CO2 and N2 in Water at Temperatures between 298.15 K and 423.15 K at Pressures up to 45 MPa". In: (2014). DOI: 10.1021/je401008s.